Dissertation zur Erlangung des Doktorgrades
der Fakultät für Chemie und Pharmazie
der Ludwig-Maximilians-Universität München

Synthesis of Immunoreactive Cyclic Dinucleotides for Cancer Immunotherapy and Treatment of Chronic Inflammation

Aikaterini Pappa

aus

Ioannina, Griechenland

2024

Erklärung

Diese Dissertation wurde im Sinne von §7 der Promotionsordnung vom 28. November 2011 von Herrn Prof. Dr. Thomas Carell betreut.

Eidesstattliche Versicherung

Diese Dissertation wurde selbstständig und ohne unerlaubte Hilfe erarbeitet.

München, 03.05.2024

Aikaterini Pappa

Dissertation eingereicht am: 03.05.2024

1. Gutachter: Prof. Dr. Thomas Carell

2. Gutachter: Dr. Pavel Kielkowski

Mündliche Prüfung am: 10.06.2024

For my family

Acknowledgments

First and foremost, I would like to cordially thank my PhD supervisor Professor *Thomas Carell*. Since arriving in your lab in 2018 as an Erasmus student, you were instantly so greatly inviting and approachable but at the same time created an environment of trust and a feeling of scientific liberty that you passed down to all of your students. When you accepted me as a PhD student you allowed me to fulfill my greatest ambitions so far, working in a state-of-the-art laboratory surrounded by fantastic people, constantly stimulating my mind and gathering more and more experiences. You always made clear how much you valued that you have an international group and to me this was always such an uplifting statement, especially since moving to Germany from Greece was a huge but also uncertain step in my life. Lastly, I am grateful for giving me the opportunity to experience how a leading university functions and for allowing me to develop as a chemist and a scientist. This has been one of the greatest chapters of my personal Odyssey.

I would also like to thank *Dr. Markus Müller* whose commitment to the lab organization and scientific guidance of the group is indispensable. From biological assays to movie recommendations, discussions with you over a Jever were always a pleasure. I am very grateful for the highly insightful comments on my thesis and for always looking for the deeper meaning.

Dear *Frau Gärtner* and *Nada Raddaoui*, thank you for all your help and organizational support through these years, I will always recall your kindness. Dearest *Kerstin Kurz*, our job would be nearly impossible without you. Thank you for your compassion and warm heart.

I would like to especially thank the group members/friends who I initiated this journey with in room F4.004: *Eva Korytiakova* - from supervisor to friend, thank you for all your support; guidance and converting the lab into a party; *Markus Hillmeier* – I couldn't ask for a better lab mate; *Lukas Zeisel* – your passion for science is continuously inspiring; and of course *Andreas Reichl* - working side by side with you while listening to the most random music is something I will forever cherish.

I would like to give my warmest appreciation to the people that formed the STING subgroup from its early days until now. *Clemens Dialer, Samuele Stazzoni, Simon Veth, Dilara Özdemir, Giacomo Ganazzoli, Fabian Hernichel, Yasmin Gärtner, Anna-Lena Halbritter , Jahongir Nabiev* and, most importantly, dearest *Johann DeGraaff* thank you for the fruitful collaboration, for all those problem-solving sessions that we had together over iced coffee and for keeping up the determination and motivation throughout these years.

My thankful regards go to all the past and current group members that I got to meet during these years and shaped me as a person in their own ways. In addition, I want to especially thank *Annika Tölke, Felix Xu, Chun Yin (Jamie) Chan, Alex Pichler, Stelios Xefteris, Luis Montiel* and *Eva Schönegger* who will always remind me of the good times, the dinner dates, the Mensa walks, the billiard evenings. Without your friendship and compassion the path would be full of darkness.

I need to also thank my former Master thesis supervisor and Professor *Ioannis Lykakis* who was the person that paved the way for me to pursue my PhD in Germany and for always being the kindest and most warm-hearted person.

Thank you to *Dr. Markus Müller, Andreas Reichl, Johann DeGraaff and Christina Pappa* who invested their time to read and correct this dissertation. Thank you for all the scientific comments and talks.

Finally, my most heartfelt and grateful thanks go to the people that I dedicate this dissertation to, my family. To my parents, *Agni and Pericles*, who are always going the extra mile for their loved ones, who believe in me and never set a limit to my dreams and ambitions. Especially to my father, who inspired me to become a chemist like him and always urged me to forge my own path. To my sisters, *Christina* and *Ioanna*, who are always there for me, supporting me even when I become the annoying big sister. Σας αγαπώ.

Last but certainly not least, I want to thank the most important person in my life right now, my loving partner *Dimitris*. You are the biggest motivating force I have ever met, the voice of reason and the clearest mind. You guided me through dark times, led me through every obstacle and made me appreciate each day I am next to you. Σ' ευχαριστώ και σ' αγαπώ.

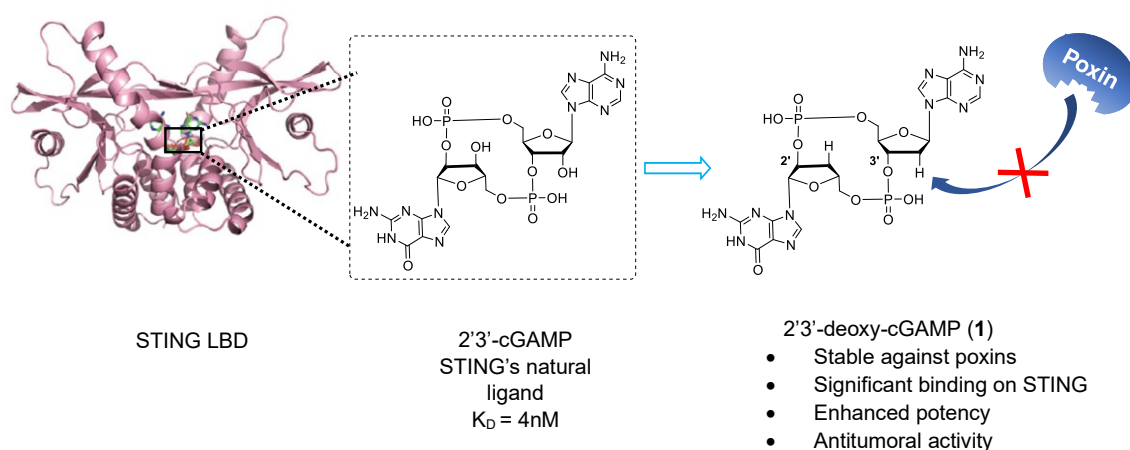Katerina Pappa

Munich, 2023

Table of Contents

1 Abstract

The cGAS-STING pathway is a fundamental part of the innate immune system, recognizing the presence of double stranded DNA in the cytosol as a danger signal. The recognition is independent of the DNA's origin, whether from pathogens or from damaged host nuclei and mitochondria. 2'3'-cGAMP is the second messenger that is produced by the DNA-recognizing enzyme cGAS and is responsible for binding and activating STING protein. Activation of STING is essential for the production of type I interferons and other pro-inflammatory cytokines that stimulate the protective immune responses against pathogens and even against the development of cancer by promoting antitumoral activities.
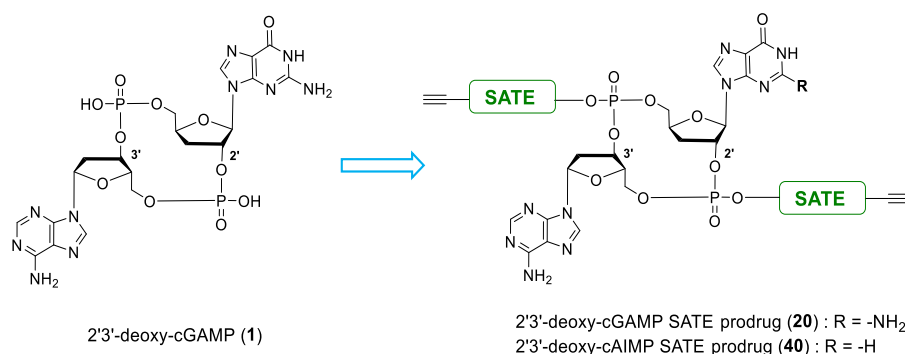
Starting from 2'3'-cGAMP's structure and developing novel bioactive compounds based on it, scientists can effectively regulate the cGAS-STING pathway and, thus, target aberrant inflammation and cancer. Generally, potent STING agonists shows remarkable capability as efficient antitumor agents especially when combined with immune checkpoint inhibitors or tumor irradiation. On the other hand, STING inhibitors are equally important as they manage to regulate abnormal STING signaling that is responsible for chronic inflammation and autoimmune diseases.

In the first part of this dissertation, we designed and synthesized a 2'3'-cGAMP-based agonist (**1**) that does not contain the 2'- and 3'- OH groups on its ribose. We first established and optimized the synthesis and then evaluated the compound's ability to bind and activate STING. Moreover, we performed stability studies of the compound against poxvirus nucleases (poxins) and we assessed its antitumoral activity using a murine hepatocellular carcinoma xenograft.

STING LBD

2'3'-cGAMP
STING's natural ligand
K_D = 4nM

2'3'-deoxy-cGAMP (**1**)
- Stable against poxins
- Significant binding on STING
- Enhanced potency
- Antitumoral activity

The pharmaceutical properties of 2'3'-cGAMP pose challenges largely caused by its negative charge that limits cellular permeability. Subsequently, we showed our synthetic approaches towards a 2'3'-cGAMP prodrug that carries two biologically labile S-acyl-2-thioester (SATE) groups, which mask its negative charges. The SATE groups also bear a terminal alkyne that can be further utilized at a later stage by attaching specific molecules through click-chemistry and provide targeted delivery.

Abstract

2'3'-deoxy-cGAMP (**1**)

2'3'-deoxy-cGAMP SATE prodrug (**20**) : R = -NH$_2$
2'3'-deoxy-cAIMP SATE prodrug (**40**) : R = -H

In the second chapter, I demonstrate the development of three cyclic dinucleotide conjugates that can act as STING inhibitors. Compound **75** is a hybrid molecule that consists of two species that are bonded via a flexible linker, a STING-targeting cyclic dinucleotide (CDN) and a small molecule which recruits thioesterase LYPLAL1. The small molecule is supposed to bring the esterase into close contact with STING to cleave the palmitate tag from STING residues Cys88 and 91. By using this "proximity inducing" conjugate we can target and block STING's palmitoylation, a modification which is essential for immune signaling.

We also designed compounds **83** and **84** to exhibit improved cellular uptake through the folate transporter SLC19A1, which imports folates but also certain CDNs, but at the same time act as inhibitors of STING. We anticipated that by ligating a CDN with a folate moiety we will provide the proper parameters for preferred SLC19A1-mediated cellular delivery of the conjugate. We counted on **83** and **84** having an inhibitory activity due to the bulky folate which, after STING binding, might not allow STING's lid closure or a proper conformational change that promotes STING activation. Finally, we performed some initial in vitro assays which showed that these compounds do not trigger the production of type I interferons.

Recruitment of depalmitoylating enzyme LYPLAL1

75

2'3'-deoxy-cGAMP (**1**)

83 : R$_1$= -OH, R$_2$= -NH$_2$
84 : R$_1$= -NH$_2$, R$_2$= -H

Improved cell permeability through transporter SLC19A1
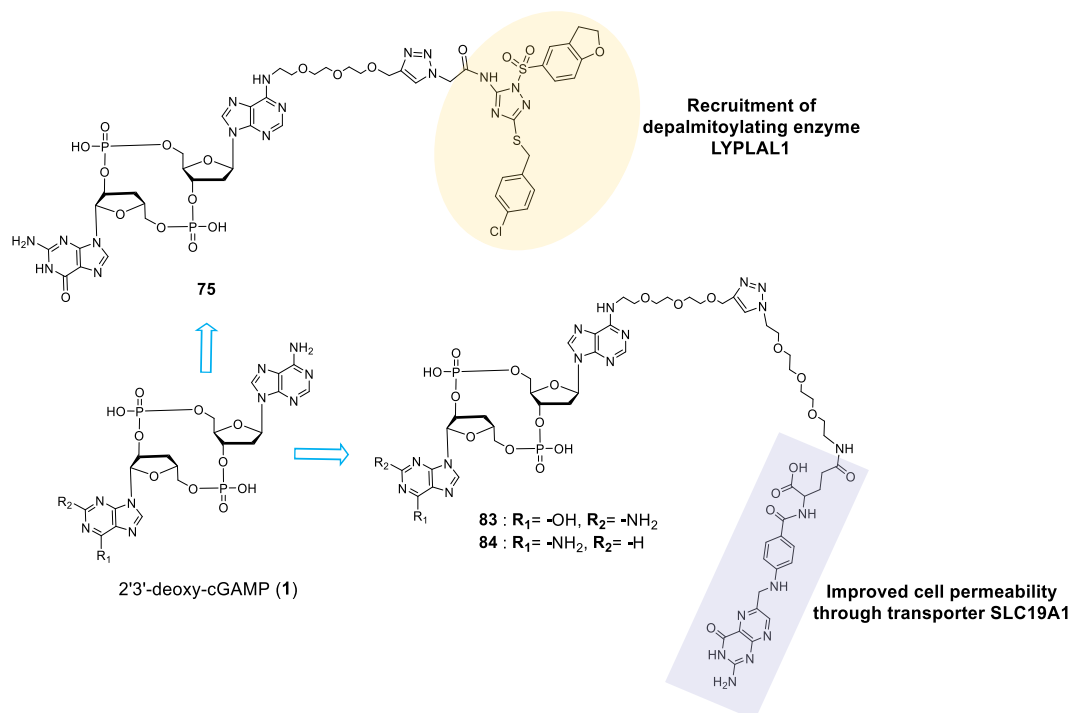
2 Introduction

2.1 The cGAS-STING pathway

Surveillance and detection of foreign DNA play a pivotal role in immunity across various organisms. In normal functioning eukaryotic cells, DNA is strictly packed in the nucleus and mitochondria and, if released, is rapidly degraded by nucleases in the cytosol and endosomes. Various pathological states can however induce the presence of DNA inside the cell which is promptly received by the innate immune system as a danger signal. In the metazoan organisms, the cGAS-STING pathway is on the forefront of immunological responses.[2-5] Aberrantly released or mislocalized double stranded DNA (dsDNA) in the cytosol (>20 bp) is sensed by the enzyme cGAS (cGAMP synthase) which in turn activates the stimulator of interferon genes (STING) protein.[6-8] After stimulation, the cGAS-STING pathway has a significant impact, primarily leading to the production of antiviral cytokines of the type I interferon family (type I IFNs) through the activation of TANK-binding kinase 1 (TBK1) and, subsequently, of the transcription factor IFN regulatory factor 3 (IRF3) and nuclear factor kappa B (NF-κB).[9-12] These cytokines, in a cascading way, stimulate the expression of numerous interferon-related genes (IRGs) and initiate a wide range of antiviral activities and other immune responses. Moreover, STING promotes cell autophagy and restricts viral propagation in a cell autonomous way.[13] Overall, the cGAS-STING pathway combines the recognition of cytosolic dsDNA with the activation of innate immunity (Figure 1).
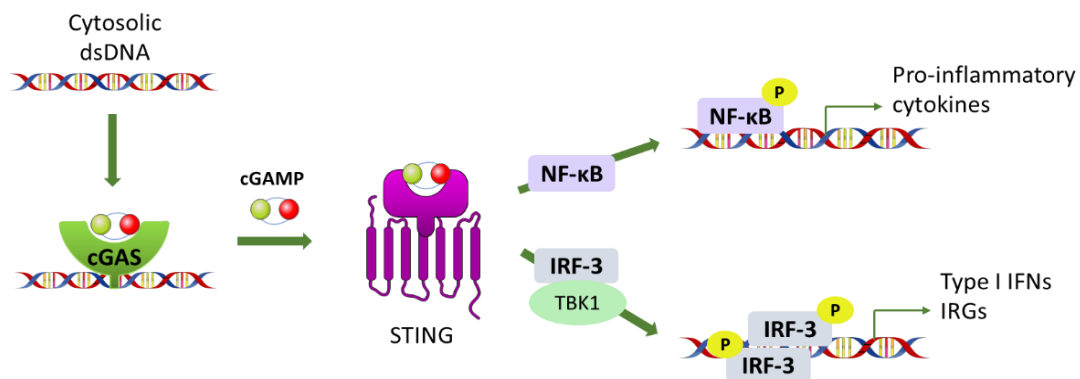

Figure 1. Overview of the cGAS-STING pathway and its downstream activation pathway. cGAMP (cyclic 2'3'-cyclic guanosine monophosphate-adenosine monophosphate), cGAS (cyclic-cGAMP synthase), STING (STimulator of INterferon Genes), TBK1 (TANK-binding kinase 1), IRF3 (IFN regulatory factor 3), NF-κB (nuclear factor kappa B), IFNs (Interferons), IRGs (Immunity Related Genes).

STING (also known as TMEM173, MITA, ERIS and MPYS) is a 40kDa dimeric transmembrane protein comprised of 379 amino acids (aa) which in its resting mode resides on the surface of the endoplasmatic reticulum (ER) and after activation translocates to the Golgi compartment (Figure 2A). It is expressed in various endothelial and epithelial cells, as well as in haematopoietic cells, such as T-cells, macrophages and dendritic cells and acts as a master regulator of type I interferon (IFN) production.[11, 14, 15] STING functions as an indirect cytoplasmic dsDNA sensor and as a direct immunosensor of endo- and exogenously synthesized cyclic dinucleotides (CDNs).[16] CDNs are known to be inherently synthesized by bacterial and mammalian cells and are very important signaling molecules as they influence a multitude of functional and immune responses.[16]

Introduction

The determining step to activate STING and initiate the cGAS-STING pathway is the binding of the self-derived CDN 2'3'-cyclic guanosine monophosphate-adenosine monophosphate (2'3'-cGAMP).[17] In order to activate STING, 2'3'-cGAMP is produced by cGAS which freely accumulates in the cytosol. [18-20] cGAS catalyzes the production of 2'3'-cGAMP from intracellular adenosine triphosphate (ATP) and guanosine triphosphate (GTP). Initially, DNA binds to cGAS and causes a conformational change in order for the enzyme to start catalyzing the phosphodiester bond formation.[21, 22] 2'3'-cGAMP's phosphate groups connect the two nucleosides from positions 2'- and 5'- of guanosine and from the 3'- and 5'- positions of adenosine leading to the formation of a non-canonical 2'-5' phosphodiester bond (Figure 2B).[8] This bond is unique in nature and so far is only encountered on cGAMP, while the well-known bacterial derived messenger CDNs cyclic di-GMP (c-di-GMP) and cyclic di-AMP (c-di-AMP) contain two 3'-5' phosphodiester linkages.[16] Since it always contains the 2'-5' and 3'-5' phosphodiester linkages that are naturally produced by cGAS, 2'3'-cGAMP is from here on referred to as "cGAMP".
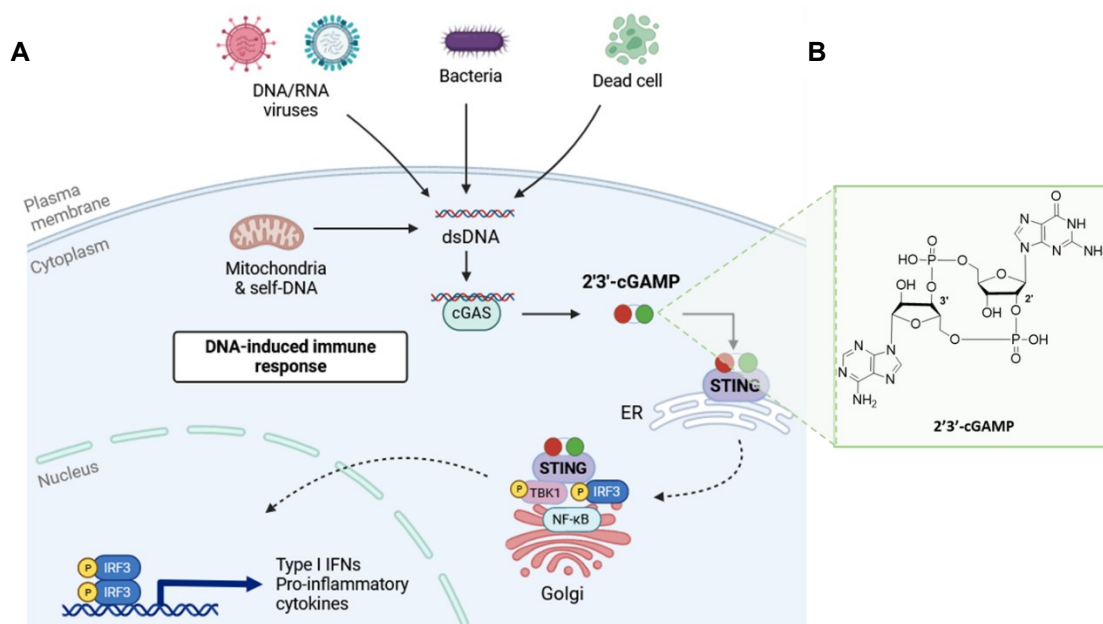

Figure 2. A) General depiction of the cGAS-STING signaling pathway. Upon detection of dsDNA, cGAS ligates on it, resulting in the synthesis of cGAMP. cGAMP then binds on STING that localizes on the endoplasmatic reticulum (ER) causing a conformational change on its structure. STING translocates to the Golgi compartment where it recruits TANK-binding kinase 1 (TBK1) promoting TBK1 autophosphorylation, STING phosphorylation and interferon regulatory factor 3 (IRF3) recruitment. IRF3 gets phosphorylated by TBK1 and travels to the nucleus where it activates the transcription of type I IFN genes and activation of the NF-κB pathway. Created with BioRender.com. B) Chemical structure of 2'3'-cGAMP.

After formation, cGAMP acts as a second messenger and can be recognized by STING on the ER. Second messengers are small, rapidly diffusing molecules that act as signal transmitters when cells are stimulated. These second messengers propagate the initial signal that is created when a ligand binds to a receptor or protein in order to initiate a cellular response.[16] In the case of the cGAS-STING pathway, the triggering ligand is the dsDNA and the surveilling protein is cGAS. Once dsDNA is situated in the cytosol it gets detected by cGAS, regardless of whether it originates from the host organism or from a pathogen. External dsDNA sources are DNA and RNA viruses and bacteria and phagocytosed DNA fragments that escape from the lysosomal compartment. Besides that, aberrantly released and insufficiently degraded host DNA is also a triggering factor. That includes leaked genomic DNA from

ruptured nuclei and micronuclei due to cell damage or senescence and DNA from damaged mitochondria (Figure 2A).

2.1.1 STING's downstream activation mechanism

A monomer of STING is comprised of a short N-terminal cytosolic domain and four transmembrane (TM) helices (TM1-4) that together consist of the first 154 amino acids, as well as a cytosolic ligand-binding domain (LBD, aa 155-341) on which a C-terminal tail (CTT, aa 342-379) is attached (Figure 3A). [23, 24] The TM domains and the CTT are connected via a connector helix and a connector loop. The LBD is the active component that binds cGAMP and related CDNs. When no ligand is attached (apo-state), the LBD domain forms a symmetrical dimer that adopts a V-shaped conformation resembling a butterfly with its head towards the ER. [25] When cGAMP binds on the LBD, STING undergoes an extensive conformational change. This includes a 180° rotation of the LBD and the formation of a β-sheet that resembles a "lid" that closes above the LBD and covers it (Figure 3B).
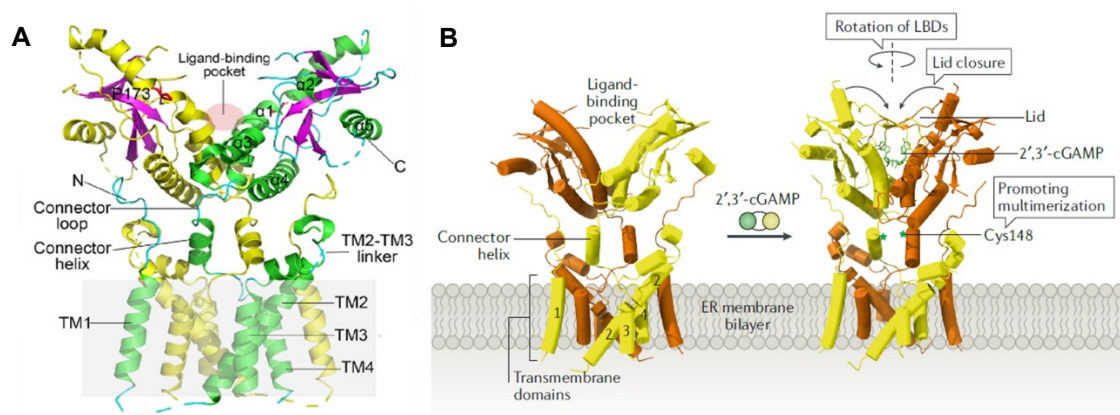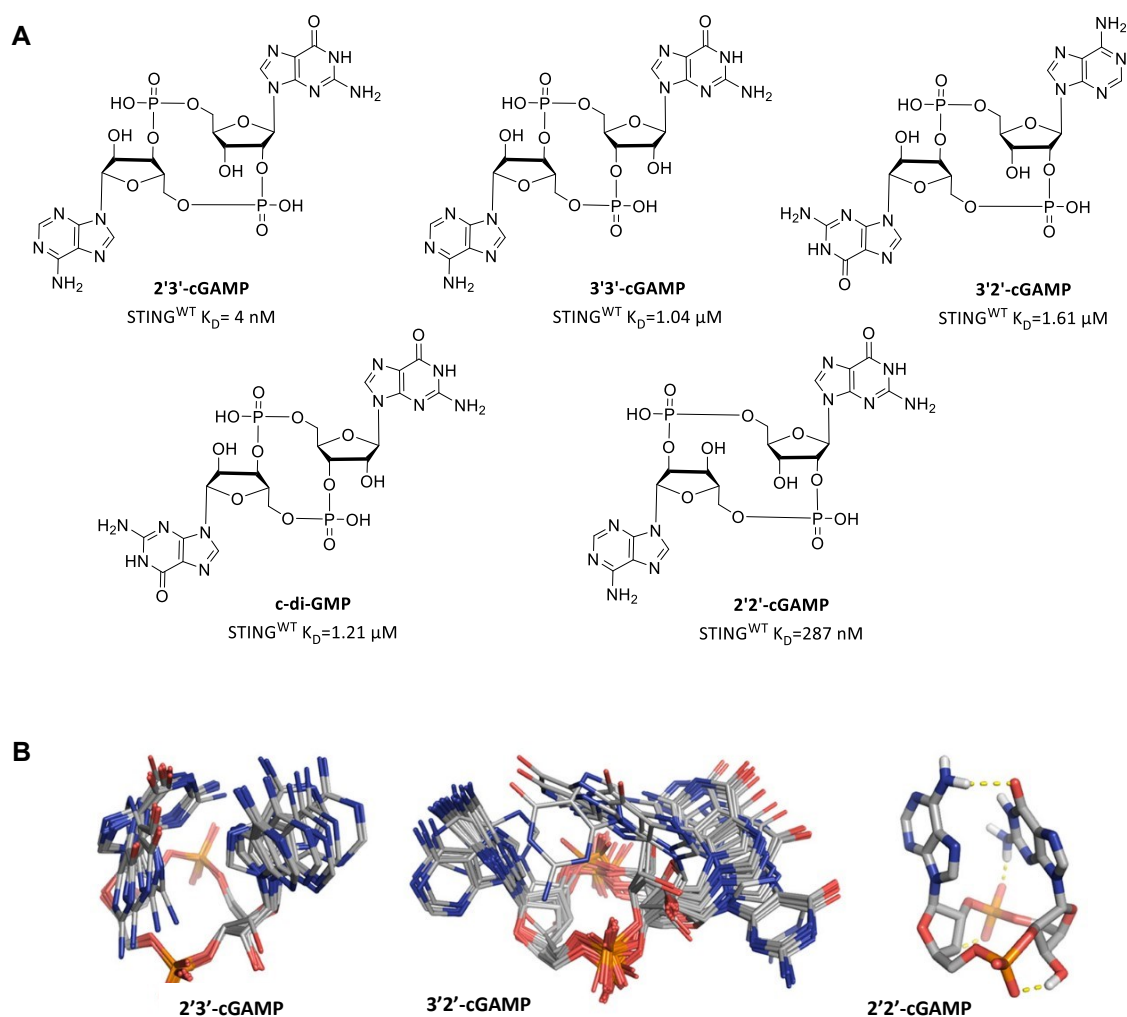

Figure 3. A) Cryo-EM structure of full-length hSTING in the front view (PDB: 6NT5). Figure adapted from *Zhang et al.*[26] B) Mechanism of STING activation. Cryo-EM structure of the ligand-free chicken STING (PDB: 6NT6) and the cGAMP bind dimer (PDB: 6NT7). cGAMP binding leads to lid closure and rotation of the LBD. This promotes STING oligomerization that is stabilized by disulfide bonds formed on Cys148. Figure adapted from *Hopfner et al.*[27]

These actions are generating a proper surface geometry on which STING oligomerizes and forms side-by-side clusters. The oligomerization is stabilized by formation of disulfide bonds on Cys148 of the connector helix and is very crucial for the downstream signaling of STING. The binding of cGAMP - and other CDNs- promotes the translocation of STING to the Golgi compartment via the trans-ER-Golgi intermediate compartment (ERGIC). There, STING recruits TBK1 via the CTT, TBK1 autophosphorylates and then phosphorylates STING's tails. [12, 28] Phosphorylated tails then recruit IRF3, which is subsequently phosphorylated by TBK1. It is proposed that clustering of STING at the lipid rafts of the Golgi compartment brings TBK1 and IRF3 into close proximity, so that IRF3 phosphorylation takes place. [29, 30] The phosphorylated IRF3 dimerizes, enters the nucleus and activates the transcription of IFNs and inflammatory cytokine genes (Figure 2). In addition, cGAS-STING signaling also leads to the expression of pro-inflammatory cytokines like IL-1, IL-6, TNFα through the NF-κB pathway.

2.2 Overview of STING's structure and cGAMP binding mechanism

cGAMP, although asymmetric, binds to human STING with higher affinity and induces stronger IFN production compared to its linkage isomers 2'2'-cGAMP, 3'2'-cGAMP and bacterial CDNs 3'3'-cGAMP and c-di-GMP (Figure 4A).[18, 21, 31] The differences in binding of different ligands on STING was determined by structural studies that measured thermodynamic factors[21]. cGAMP adopts a closed conformation that is very similar to the STING-bound conformation (Figure 4C). Despite being asymmetric, while STING's LBD is symmetric, the conversion of cGAMP's conformation from free-state to bound-state is energetically much more favorable than for the other CDNs in terms of entropy and enthalpy shifts. 3'2'-cGAMP and bacterial CDNs 3'3'-cGAMP and c-di-GMP need to pay a much higher entropic cost in order to fit ideally to the LBD because they attain a more open conformation, with higher degrees of freedom, that requires a significant conformational change[21] (Figure 4B,C). On the contrary, 2'2'-cGAMP is presenting a more tightly folded conformation due to intramolecular purine-base derived hydrogen bonds and π-π stacking interactions between the purine bases that require a higher enthalpy input to unfold and bind.[21] Thus, cGAMP achieves a precise equilibrium between conformational flexibility and stability, making it highly favorable and preferential for binding with STING over other CDNs.

A

2'3'-cGAMP
STING^{WT} K_D= 4 nM

3'3'-cGAMP
STING^{WT} K_D=1.04 μM

3'2'-cGAMP
STING^{WT} K_D=1.61 μM

c-di-GMP
STING^{WT} K_D=1.21 μM

2'2'-cGAMP
STING^{WT} K_D=287 nM

B

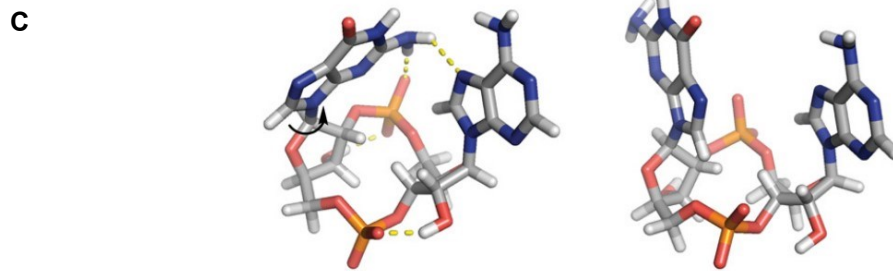**2'3'-cGAMP**   **3'2'-cGAMP**   **2'2'-cGAMP**

C

Figure 4. A) Structures and binding affinities of cGAMP, its linkage isomers 3'3'-cGAMP, 3'2'-cGAMP, 2'2'-cGAMP and c-di-GMP. B) cGAMP adopts an organized free-ligand conformation that resembles the STING-bound conformation and pays low entropy and enthalpy costs to convert into the active form. On the contrary, 3'2'-cGAMP has high degrees of freedom and needs to undergo a large conformational change to bind. 2'2'-cGAMP is locked in a rigid, closed conformation that needs significant energy to rotate and favorably bind on STING. C) (left) cGAMP's equilibrium geometry in solution resembles the STING-bound active conformation (right). Figures adapted from *Chen*[22] and *Shi et al.*[21]

Since 2012, at least four different laboratories have managed to crystalize and characterize STING's LBD domain in the apo-state or in c-di-GMP-bound states. [32-35] Some crystal structures are of the WT (R232 allelic variant) while others are of the minor allele H232 where residue 232 is a histidine instead of an arginine. The crystal structures show that c-di-GMP inserts in a U-shaped conformation in the deep crevice of the LBD. However, when bound to c-di-GMP, STING adopts an open conformation with the two STING dimers having a 55 Å distance between them (Figure 5C). Later on, the structures of hSTING's LBD (truncated STING) bound to cGAMP were determined.[18, 19] For these studies, the two major STING variants, R232 and H232, were used and, although different, they demonstrated almost identical crystal structures and also very similar to the c-di-GMP-bound complex. As seen in Figure 5B, when cGAMP is bound on STING it occupies the deep cleft of the LBD which is then covered with the β-sheet that acts as a "lid" and additionally brings the two STING clefts in close proximity.[36]
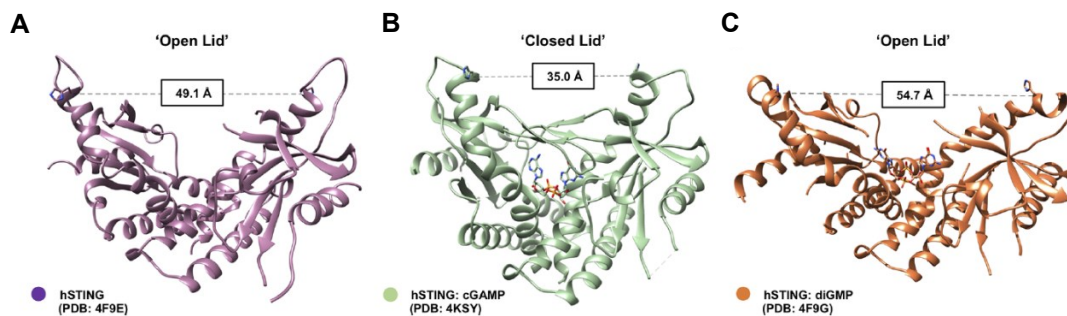

Figure 5. Crystal structures of STING LBDs. A) Apo-state STING in the inactive conformation (unbound) (PDB: 4F9E). B) cGAMP-bound STING with the two STING dimers are brought in close proximity and a β-sheet "lid" is formed (PDB: 4KSY). C) The open conformation of STING when c-di-GMP is bound (PDB: 4F9G). Figure adapted from *Garland et al.*[37]

It is very important to note that not all STING agonists induce a closed lid conformation. In fact, while the bacterial c-di-GMP binds with far weaker affinity than cGAMP and does not cause obvious conformational changes on STING (Figure 5C), it still promotes STING's oligomerization and further downstream signaling.[25, 33] In other words, it appears that the ability of a STING agonist to induce lid closure is necessary for high potency but not for STING activation itself.

Introduction

In 2019, *Zhang et al.* managed to solve the structure of full-length human STING via cryo-electron microscopy (cryo-EM).[23] The structures reveal that cGAMP's binding on the LBD is a result of the combination of two major factors: first, the formation of binding site interactions like hydrogen bonds, π-π stacking interactions and purine base stacking interactions and, second, the establishment of ligand-binding pocket shape complementarity.[18, 25] When bound, cGAMP adopts a U-shaped conformation. This structure prompts the phosphate and ribose moieties to sit in the bottom of the crevice, whereas the two bases are placed above and oriented almost parallel to each other. The free 3'-OH of the guanosine points towards the two Ser162 side chains at the bottom of the pocket (Figure 6A). [19] The purine bases form π-π stacking interactions with Tyr167 from both sides of the dimer. The α-phosphate groups are stabilized by electrostatic interactions with Arg238 (Figure 6A, B).

Figure 6. A) Intermolecular interactions between STING allele R232 and cGAMP (PDB: 4KSY). Interacting residues are in blue and yellow. Salt bridges are shown in orange and direct interactions are shown in green. B) Intermolecular interactions between STING allele H232 and cGAMP (PDB: 4LOH). The interacting residues are colored magenta and yellow. Water molecules are red spheres and hydrogen bonds are colored green. Figures adapted from *Zhang et al.*[26]

Figure 7. 2D intermolecular interactions between cGAMP and STING H232 residues (PDB: 4LOH). Figure made using BIOVIA Discovery Studio™ 2021.

Introduction

Even though STING R232 and H232 variants adopt almost identical structures, they present subtle differences in cGAMP binding. In the STING H232 variant, the guanine base is mainly coordinated through a network of water-mediated hydrogen bonds and adenine seems to not participate in this system (Figure 6B). However, in the STING R232 variant guanine directly contacts with the Glu260 and Thr263 residues and adenine with Val239 (Figure 6A). Finally, *Gao et al.* managed to pinpoint that residues S162, T263 but also Y167 and R238 of the STING H232 LBD are indispensable for effective cGAMP binding (Figure 7).[19]

2.3 cGAMP regulation and inter-cellular signaling

Binding of cGAMP to STING leads to the activation of transcription factors IRF3 and NF-κB to promote antiviral and pro-inflammatory activities. One of the undoubting advantages of second messengers like cGAMP is the ability to boost and expand the danger message. Indeed, besides activating immunity within the cell of origin, cGAMP can act as an immunotrasmitter and trigger antiviral responses in neighboring cells as well. It can directly diffuse into nearby cells either through connexin-dependent gap junctions or by being packaged into viral particles (Figure 8).[38-40] cGAMP can also be released into the microenvironment due to pathological reasons like cell damage or cell death and this extracellular cGAMP can then enter bystander cells via transport proteins and ion channels.
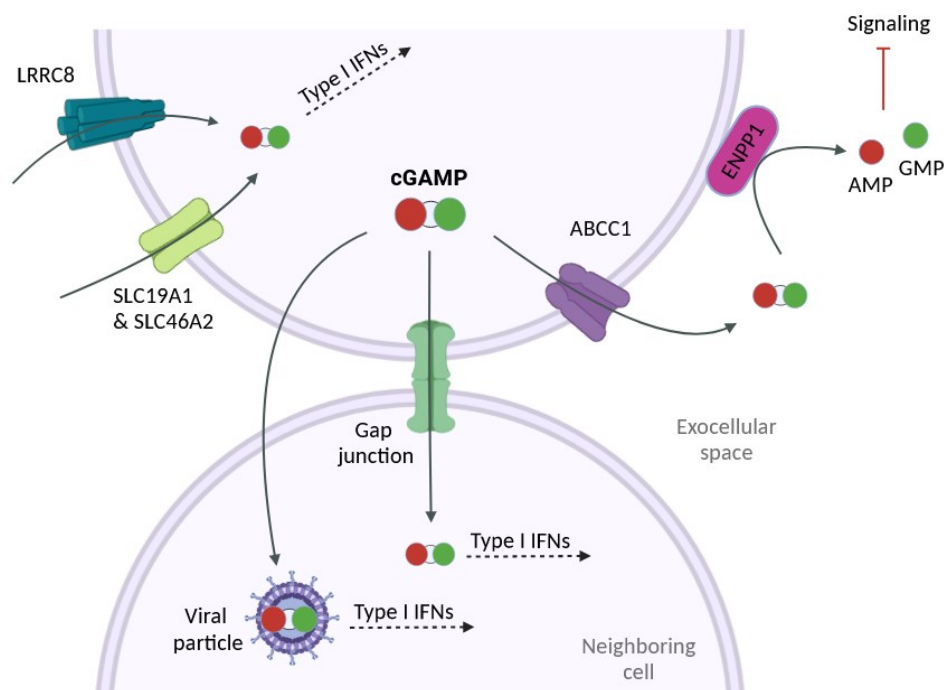

Figure 8. Extracellular cGAMP transport. In order to promote immune signaling and further transmit the danger message, cGAMP can be transported into nearby cells through gap junctions or packaged into viral particles. Additionally, it can be imported into the cytoplasm via anion channels (LRRC8) and transporters (SLC19A1 and SLC46A2). cGAMP gets excreted from the cytoplasm to the microenvironment via the ABCC1 transporter where it can be degraded by the phosphodiesterase ENPP1 to AMP and GMP as a way to inhibit immune signaling. Created with BioRender.com.

The mechanism by which cGAMP can re-enter cells was not clear until very recently when a number of membrane transport proteins were identified as gatekeepers that provide cell entrance of cGAMP and

other CDNs. Among them are the folate transporters SLC19A1 and SLC46A2 that showed preference in importing cGAMP and some CDNs and are found in many primary human monocytic cell lines (Figure 8). [41-43] Volume-regulated anion channels (VRACs) like LRRC8 are also identified as potential indirect cGAMP importers although their contribution is probably tissue specific and may be affected by osmotic disruption. [44-46] Besides importing, ATP-binding cassette ABCC1 has been identified as a mediator for direct cGAMP export. [47] ABCC1 export of cGAMP was shown to negatively regulate interferon production thus it can have a direct regulatory role in diminishing autoinflammation and autoimmunity.

Extracellular cGAMP that accumulates in the microenvironment is degraded by a specific mammalian phosphodiesterase, ENPP1 (ecto-nucleotide pyrophosphatase phosphodiesterase), thereby controlling the uptake of cGAMP from neighboring cells. [48, 49] ENPP1 shows selectivity towards cGAMP and is not active against other CDNs, like 3'3'-cGAMP. [50] It cleaves cGAMP's 2'-5' phosphodiester bond, initially producing the linear 5'-pApG intermediate and eventually leading to the release of 5'-AMP and 5'-GMP (Figure 8). [51] As ENPP1 can only degrade cGAMP at the extracellular space, so far no intracellular phosphodiesterase has been identified that degrades cGAMP and its metabolic fate inside cells is still unclear. Regardless, the regulation and secretion of cGAMP into the microenvironment has many systemic roles that reaches out to many aspects of the immune activation and especially cancer immunity. For instance, *Carozza et al.* [52] demonstrated that cancer cells actively excrete cGAMP into the tumor microenvironment. Certain cancers upregulate ENPP1 in the TME and that way they exploit its cGAMP-degrading function in order to evade immunosurveillance and continue to develop and cause tumor metastasis. [53, 54] Notably, ENPP1 inhibitors represent an exceptional therapeutic strategy as it allows for the cGAMP localization in the TME and, thus, the amplification of the danger signaling for antitumor responses.

2.4 STING-related diseases

The levels and tenacity at which cGAMP is able to spread and activate STING in nearby cells has a crucial role in disease pathogenesis. In this chapter, the known STING-related diseases and their correlation with deregulated cGAMP are demonstrated.

2.4.1 STING allelic variants

Single nucleotide polymorphisms are responsible for the existence of five different STING allelic variants in humans that exhibit variable activities in inducing downstream signaling. [32] The R232 variant is the most prominent one and, thus, considered to be the wild-type (WT), followed by R71H-G230A-R293Q (HAQ), R232H (REF), Q230A-R293Q (AQ) and R293Q (Q). These variants are activated by 2'3'-cGAMP to a similar extent, but have different affinities to the bacterial CDNs (c-di-GMP, c-di-AMP and 3'3'-cGAMP). When new compounds are designed to target STING, either agonists or antagonists, the respective STING variants must always be considered, since the therapeutic uptake and compatibility can change. [55, 32, 56, 57] Moreover, STING's protein sequence differs depending on the species. For example, mouse and human STING share 81% amino acid sequence similarity with 61% identity in the LBD and

exhibit similar structural conformation.[5, 6, 58] Despite those similarities, the residue differences between mSTING and hSTING can have fundamental effects and, when overlooked, in vivo studies could lead to unreliable conclusions or misleading results.

2.4.2 STING drives autoinflammation and autoimmunity

The cGAS-STING pathway has arisen as a key factor for the initiation and pathogenesis of autoimmune and autoinflammatory diseases (Figure 9).[59] Rare mutations on STING1 gene can lead to pediatric onset of severe autoinflammatory syndrome named STING-associated vasculopathy with onset in infancy (SAVI)[60]. These mutations trigger ligand-independent activation of STING leading to increased type I interferon production in primary patient cells. Furthermore, dominant negative mutations in the coatomer subunit-α (COPA) of the coatomer complex I (COPI) result in abnormal STING trafficking. COPI vesicles are involved in retrograde Golgi to ER vesicular transport of STING, which is essential for maintaining immunological homeostasis. Disruption of Golgi apparatus to ER trafficking, due to mutations in COPA, results in the trapping of STING in the Golgi apparatus and an immune response equivalent to that observed in SAVI (COPA syndrome).[61]

Loss of function mutations in the endolysosomal DNA endonuclease DNase II or the cytosolic DNA exonuclease TREX1 result in the overactivation of cGAS-STING pathway due to increased availability of DNA in the cytosol. This results in developing an autoinflammatory condition called Aicardi-Goutières syndrome.[62] Additionally, heterozygous mutations in TREX1 lead to less severe and heterogeneous phenotypes, such as lupus erythematosus.[63] These pathogenic states are commonly referred to as type I interferonopathies.[59] Moreover, leakage of nuclear DNA that can accumulate within senescent cells can also aberrantly activate the cGAS-STING pathway. As a consequence, many ageing cells present a state of "inflammageing" that creates a constant inflammatory state in senescent cells which, consequently, display a senescence-associated secretory phenotype (SASP) which can result in cell and tissue damage.[64-66]
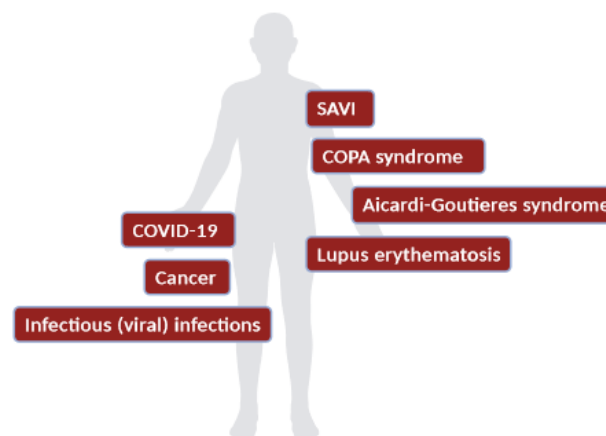

Figure 9. Examples of diseases that are associated with STING. Image made using BioRender.com.

On the basis of these findings, a lot of efforts are underway to develop inhibitors that antagonize the cGAS-STING pathway, either by deactivating cGAS or by inhibiting STING using small molecule modulators as will be discussed in detail later on.

2.4.3 STING on the forefront of antimicrobial responses

STING's involvement in the antimicrobial defense is already established and well-reviewed.[10, 14, 67, 68] In many antigen-presenting cells like macrophages and dendritic cells the induction of interferons after infection with viruses like HSV-1 virus and other bacteria was shown to be entirely dependent on STING.[14, 69-71] Furthermore, STING has been confirmed as a critical component of the host's immune defense against retroviruses like HIV, SIV, and MLV.[70, 72, 73]

Very recently, the cGAS-STING pathway was directly linked to COVID-19 (caused by SARS-CoV-2), a respiratory coronavirus disease that is characterized by upper and lower respiratory tract infections and, since 2020, has caused a global pandemic leading to unprecedented rates of pneumonia and death. *Domizio et al.*[74] managed to demonstrate that in severely damaged lung cells of patients the cGAS-STING pathway signaling is very prominent. Moreover, complementary to the work of *Neufeldt et al.*[75], they show that cGAS-STING pathway-induced IFNs and NF-κB-related pro-inflammatory cytokines are produced at a late stage of the infection and promote severe lung tissue damage. By inhibiting STING in a COVID-susceptible mouse model, they demonstrated improved disease severity and better survival. Overall, targeting STING and diminishing hyperinflammation seems to be very beneficial for severe COVID even at a late stage of the infection.

In the opposite direction, microbes can be protected against host antimicrobial defense by taking advantage of the signal transduction of the cGAS-STING pathway. One way of bypassing the host's defense is by destroying the danger message itself. Poxvirus nucleases (poxins) are employing this clever way of flying under the immunosurveillance radar by selectively degrading cGAMP. Poxins degrade cGAMP by cleaving its 3'-5' linkage, promoted by the nucleophilic attack of the adenosine 2'-OH by Lys142 of the active site, and leads to the linear 5'-pG(2',5')pA molecule (Figure 10). [76] Notably, poxins have a very specific and selective way of action and they only target cGAMP and not other CDNs like c-di-GMP. cGAMP is positioned in a deep crevice of the poxin's ligand binding domain in a way that the 3'-5' linkage is exposed to the active site. Here, adenosine is rotated and its 2'-OH acts as a reacting nucleophile initializing the acid-base reaction with the catalytic triad of the active site (Figure 10). Thus, the inactive linear molecule results and the virus can continue to replicate and spread in neighboring cells.
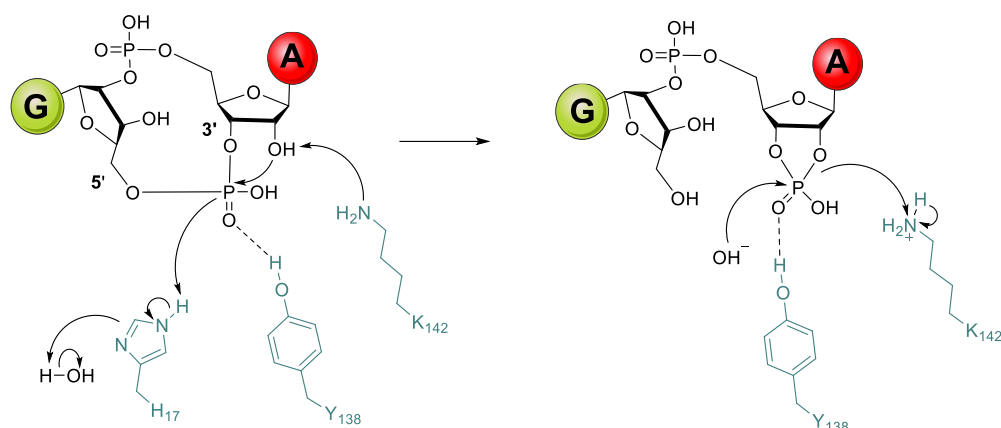

Figure 10. Proposed mechanism that poxins use to degrade cGAMP [76]. Poxins cleave the 3'-5' bond, catalyzed by the deprotonation of the 2'-OH of adenosine by the lysine of the catalytic active site. The active site of the poxvirus nuclease contains a catalytic triad that consists of a lysine (K142), a tyrosine (Y138) and a histidine (H17) (depicted in blue). A: adenine, G: guanine.

The African swine fever virus is another example of viral immune evasion as it encodes two proteins (C129R and EP364R) that are able to degrade cGAMP in infected cells by cleaving its phosphate bonds.[77] In conclusion, the activation of the STING pathway holds substantial promise for preventing and treating infectious diseases. cGAMP and other CDN STING agonists have already shown potential as vaccine adjuvants, enhancing the generation of pathogen-specific antibodies and strengthening T cell responses in mouse models.[78] Furthermore, modified CDNs can be designed and synthesized to avoid virus detection and degradation while still activating an antiviral response.

2.4.4 STING and the cancer immunity cycle

Cancer antigens are being produced during cancer cell death. Antigen-presenting cells (APCs) process and capture antigens and present them to T cells in order to activate them. Following systemic T cell trafficking to reach the tumor site, the T cells are infiltrated into the tumor allowing for the immune recognition of the cancer cells. Then, cytotoxic T lymphocytes identify and kill the cancer cells. Dead cancer cells release more antigens, thus continuing the cycle. This cyclic process is defined as the cancer immunity cycle and is a subject of major significance for the scientific community as it comprises the basis for tumor immunotherapy.[79] Numerous studies have shown that the expression of type I IFNs and interferon genes in cancer cells lead to tumor T-cell infiltration in the tumor microenvironment (TME) and to the control of tumors both in vivo and in vitro.[80, 81] Hence, STING, as a stimulator of type I IFN production, has been demonstrated as a master regulator of the cancer immunity cycle.
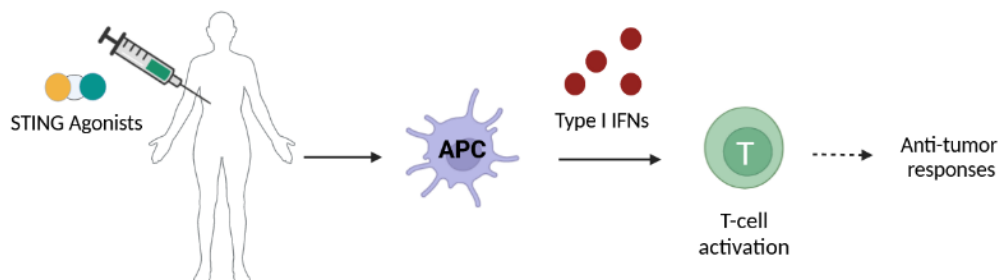

Figure 11. Antitumor responses of STING agonists. After administration, STING-induced type I IFNs stimulate antigen presenting cells (APCs) and promote the presentation of tumor antigens to T cells in order to "heat up" non-inflamed "cold" tumors and initiate antitumor immune responses.

Notably, wild-type mice with functional STING signaling exhibited attenuated tumor growth relative to mice that were deficient in various STING pathway components.[82, 83] Indeed, in response to STING agonist treatment, regression in murine tumor models was attributed to antitumor immunity caused by type I IFNs and other pro-inflammatory cytokines that are characteristic of STING activation[83-85] and, in addition, this effect majorly contributes to the anti-tumor effects of supportive treatments like radiation therapy. In accordance to the cancer immunity cycle, the antitumor activity of STING signaling has been pinpointed to enhanced tumor antigen-specific T cell responses and T-cell tumor infiltration.

Introduction

A survival strategy of tumors is the activation of immune homeostasis-associated negative regulatory pathways (checkpoints) in order to deregulate the STING pathway and evade deletion. In fact, one of the most prominent cancer immunotherapies is the treatment with immune checkpoint inhibitors (ICIs) that directly target the adaptive immune system by restoring its activity and strengthening T cell activity. [86, 87] For instance, the immune checkpoints programmed death receptor 1 (PD-1) and ligand 1 (PD-L1) restrain innate immune responses and help tumor progression and tumor immunity evasion, while cytotoxic T lymphocyte associated protein 4 (CTLA-4) downregulates anti-tumor T-cell activation. Inhibition of these checkpoints leads to the reactivation of T cells and the effective elimination of cancer cells. In 2014, cancer treatment methods were revolutionized by the FDA approval of the PD-1/PD-L1 antibodies pembrolizumab[88] and nivolumab[89, 90] and the first CTLA-4 inhibitory antibody ipilimumab[91, 92] some years before. Motivated by these antibodies, significant research attempts were focusing at better, more potent and selective next-generation ICIs with many of them having reached clinical trials.[93-96] However, the clinical application of ICIs is limited as a big number of patients does not successfully respond and even suffer from severe side effects.[86, 87]
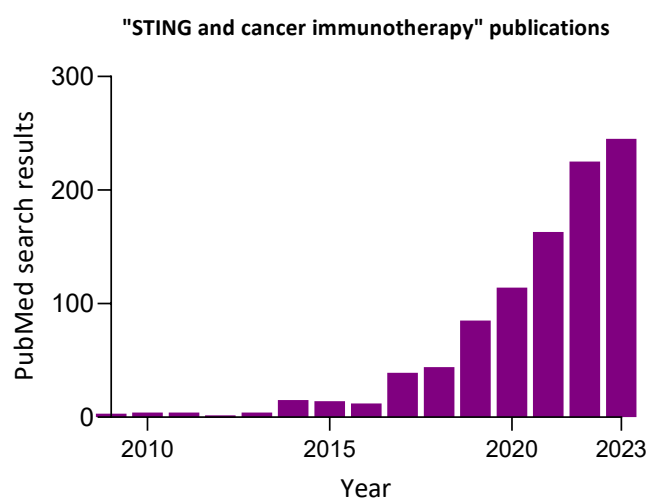

Figure 12. Number of publications for "STING and cancer immunology" for each year between 2009 and 2023. Search results derived from NCBI.

Additionally, in order for the ICIs to work successfully the tumors have to present an already pre-existing T-cell immunity in the tumor (called "hot" tumors). "Cold" tumors are unresponsive to checkpoint inhibitors. They present lack of T-cell infiltration and feature no chemokine expression, thus they are characterized as immunologically non-inflamed.[97] The activation of the cGAS-STING pathway was proposed to play a key role in treating "cold" tumors and turning them into "hot", especially in combination with ICIs like anti-PD-1 antibodies and tumor irradiation. These observations suggest that direct activation of the STING pathway in the TME by intratumoral injection of STING agonists is an effective therapeutic strategy to promote broad T-cell priming and infiltration responses in tumors (Figure 11). [2, 5, 98] Indeed, as indicated by the rate of publications about the correlation of STING and cancer immunotherapy (Figure 12) the interest of academic and pharmaceutical research groups for STING agonists has escalated, creating what is called nowadays "STING fever", as well as the number of

compounds that have reached clinical trials. More about STING agonists that target cancer immunotherapy is explored in the next chapter.

2.5 STING agonists

Over the last years, the rapid development of many potential STING agonists is being witnessed and a number of them have shown promising clinical benefits. Synthetic STING agonists are separated into two categories based on their structures: cyclic dinucleotides that mimic the natural cGAMP's structural aspects and small molecules.

2.5.1 Cyclic dinucleotide analogues

In order to design and synthesize improved STING agonists, chemists have targeted their efforts towards modifying and optimizing cGAMP's structure to create novel compounds. Aiming to improve principles like potency, selectivity and stability these modifications were mainly employing (1) the use of different nucleobases[99-102], (2) structural alterations of the ribose[103, 104] and (3) phosphodiester linkage modifications.[105, 106] A lot of research effort has been focused on the establishment of suitable synthetic methodologies for these compounds. These include enzymatic approaches (biocatalysis)[107, 108] and the use of phosphoramidite/phosphate or H-phosphonate organic synthesis employing oligonucleotide chemistry. The superiority of cyclic nucleotide analogues versus small molecules relies on their structural similarity with the self-derived cGAMP. It is already known that cGAMP has a definitive selectivity for STING, that means that its CDN analogues will possibly share this selectivity and target only STING with no additional off-target effects. Furthermore, their identical manner of action could possibly mean that their activity will be favorable and well-tolerated across species and different STING alleles.

Aduro Biotech, created a series of CDNs where they exchanged the phosphodiester bonds with phosphorothioate ones.[109] This type of bond shows increased resistance to hydrolysis by nucleases and phosphodiesterases and is widely employed for oligonucleotide synthesis.[110, 111] However, arising from the stereogenic nature of phosphorothioate linkers, the CDNs that carry these bonds are obtained as mixtures of four P-diastereomers (R_PR_P, R_PS_P, S_PR_P, S_PS_P) and each stereoisomer elicit different activity levels. Thus, each isomer needs to be isolated from the mixture and requires separate evaluation. The compound ADU-S100 (Figure 13) arised as the R_PR_P stereoisomer from a series of 2'3'-cAAMP phosphorothioate analogues and was proven to be the most effective to withstand ENPP1 degradation. It also demonstrated superior half-life and antitumor activity in mouse models. Based on these results, ADU-S100 was launched into phase I and phase II clinical trials in combination with anti-PD-1 antibodies for patients that present solid tumors or lymphomas with modest clinical benefits.[112, 113] Accordingly, *Li et al.*[48] synthesized a number of phosphorothioate analogues through enzymatic synthesis and resulted with bisphosphorothioate 2'3'-cG^{S}A^{S}MP (Figure 13) that showed significantly increased resistance to ENPP1 hydrolysis in comparison to natural cGAMP. Furthermore, 2'3'-cG^{S}A^{S}MP exhibited a similar affinity for hSTING as cGAMP and was notably more potent in inducing IFN-β expression in human THP-1 monocytes.
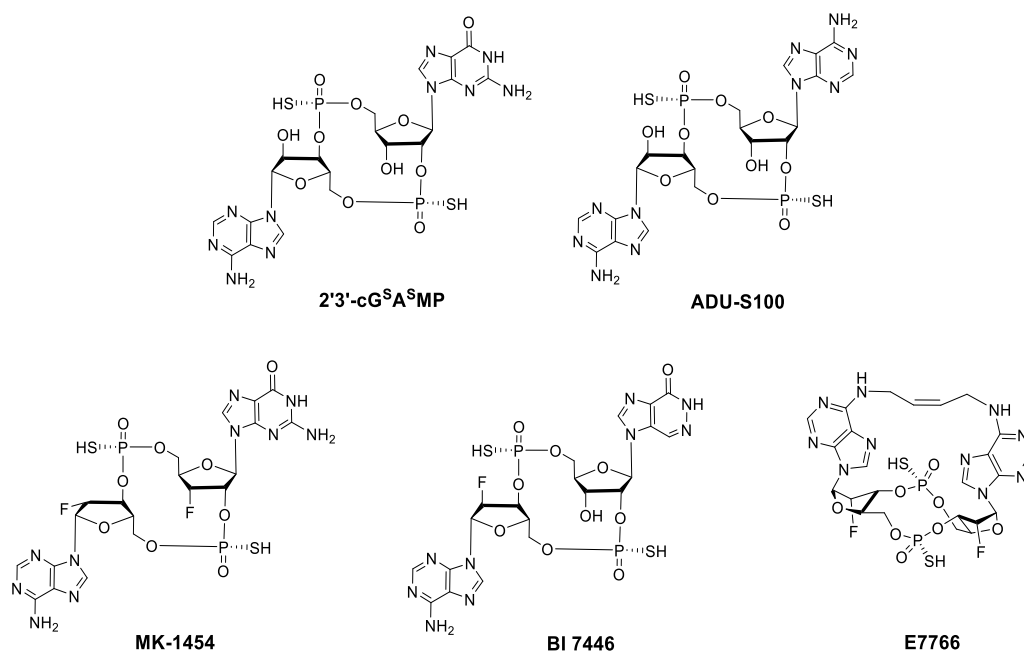
Figure 13. Chemical structures of known cyclic dinucleotide STING agonists that entered clinical trials.

Later, researchers at Merck developed a synthetic CDN agonist named MK-1454 that consists of two fluorinated adenosine and guanosine nucleotides connected via two phosphorothioate linkages ($R_P R_P$ stereoisomer) in order to introduce improved metabolic stability against degrading enzymes.[114] MK-1454 binds to STING in a similar way as cGAMP and its intratumoral administration resulted in tumor regression, enhanced by anti-PD-1 therapy. MK-1454 is currently studied in phase I clinical studies alone or in combination with antibodies for patients with advanced or metastatic tumors or lymphomas[115]. The most recent CDN-based approach was pursued by Boehringer-Ingelheim who developed a CDN (named BI 7446, Figure 13) that features a non-canonical imidazopyridazinone base in combination with 2'-fluoro-adenosine and phosphorothioate linkages.[116] This compound showed increased potency and selectivity across different STING alleles and is currently being administered to clinical trial patients for the treatment of solid tumors.

Apart from aiming for improved stability, efforts to design novel CDN agonists were made to pursuit structural pre-organization of the compound. Eisai company developed E7766, the first bridged bisphosphorothioate macrocycle targeting STING that contained two adenosine nucleotides and was designed to lock its structure in the STING active conformation.[117] This favorable conformation leads to promising antitumor results and pan-genotypic activity, hence, E7766 is also being evaluated in clinical trials.

As a way to enhance selectivity and bioavailability of next-generation STING agonists, many groups are working towards establishing alternative delivery platforms. ImmuneSensor Therapeutics developed a STING agonist, IMSA172 (Figure 14), which can be conjugated to a tumor-targeting antibody against EGFR, a tumor-associated antigen.[118] Using mouse models, they show that this antibody can be used for systemic administration, in contrast to the more common but clinically less beneficial intra-tumoral injections. Moreover, they provide proof that the antibody activated antitumor responses and suggest

that IMSA172 can in the future be conjugated to diverse antibodies so as to target different types of tumors.

Figure 14. Chemical structures of STING agonist IMSA 172 and antibody-drug conjugate anti-EGFR-172.

2.5.1.a Cyclic dinucleotide prodrugs as STING agonists

Although CDN analogues provide a very suitable and nature mimicking model for STING agonists, at the same time they hold the drawback of high polarity. The nucleotidic nature and negative charges on the phosphoric oxygen or sulfur restricts their cytosolic availability as their passive diffusion of the cell membrane is limited. One way to overcome this is the employment of prodrugs, which are bio-labile chemical moieties that can be synthetically attached on the anionic sites of the molecule and thereby shield the negative charge. Once the prodrug enters the cell, enzymes like nucleases or esterases cleave the prodrug moiety resulting in the accumulation of the active free phosphate parent analogue (Figure 15). As a result, the CDN can better diffuse in the cell and demonstrate increased potency.

Figure 15. Schematic illustration of the prodrug approach mechanism. The prodrug-masked CDN can penetrate the cellular membrane due to the shielding of its negative charges. When it reaches the cytosol the labile prodrug groups are enzymatically cleaved off and the free active CDN can activate STING and initiate immune responses.

Several prodrug strategies were developed to improve the transport of polar nucleoside phosphates and phosphonates across the cell membrane and many of the resulting prodrugs were clinically validated and FDA-approved. Standout examples are adefovir dipivoxil[119] and sofosbuvir[120] used for the treatment of hepatitis as well as remdesivir[121] for the treatment of COVID-19 infections. The first CDN-based prodrug for STING was developed by the group of Gabriel Birkuš[122] (Figure 16). They managed to synthesize 3',3'-c-di(2'-F, 2'-AMP) and then mask its phosphate negative charge using pivaloyloxymethyl (POM) groups. The prodrug was very promising, demonstrating increased cellular uptake, greater efficiency compared to the parent CDN and that the POM groups were rapidly cleaved off inside the cells. Future studies are planned to evaluate its potential as an anticancer drug. Later, *Xie et al.*[123] synthesized a number of deoxyribose-prodrugs for STING that featured S-acylthioalkyl (SATE) groups as masking species. The prodrug that bears two adenines connected via a 3'-3' phosphodiester bond demonstrated the highest activity towards STING-induced antitumor responses and had better efficiency and stability than cGAMP.

3'3'-c-di(2'-F, 2'-AMP)-POM prodrug   **3'3'-dideoxy-cdiAMP-SATE prodrug**
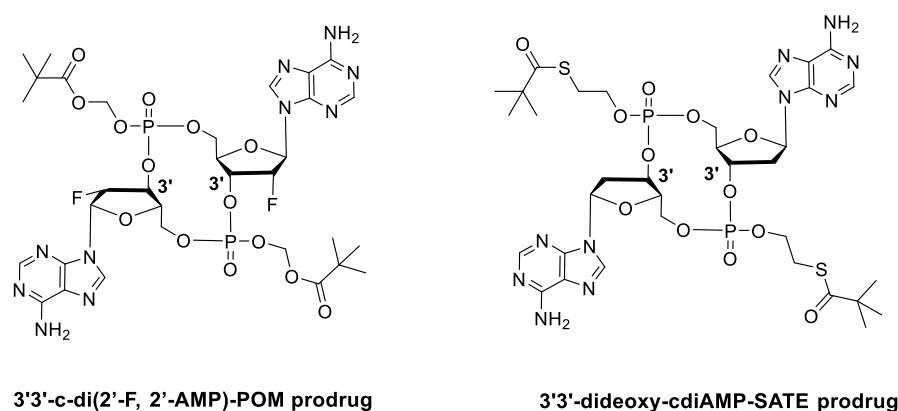
Figure 16. Chemical structures of known CDN-based prodrugs as STING agonists.

2.5.2 Small molecule STING agonists

Apart from CDN-based compounds many non-nucleotide small molecules were synthesized as STING agonists. The xanthenone derivative DMXAA (Figure 17) was one of the first STING agonists to be developed and initial preclinical anticancer results were very promising.[19] Despite its activity, DMXAA was discontinued as it was later verified that it binds only on murine STING and not on the human protein.[124]

DMXAA   **SNX281**   **di-ABZI derivative**
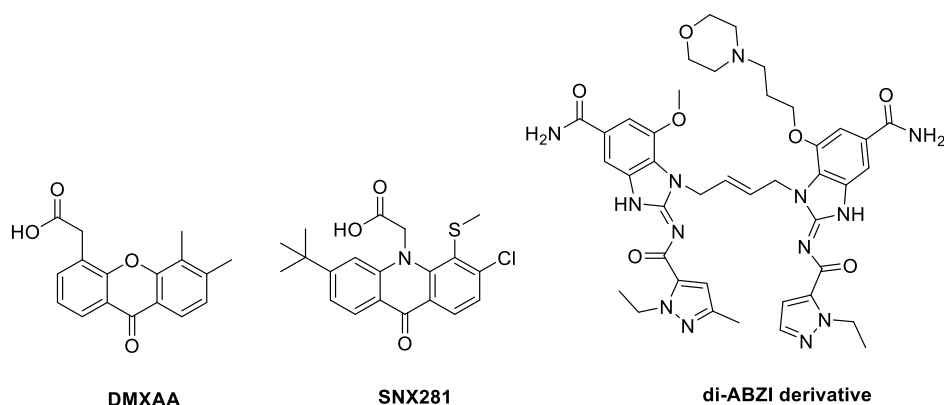
Figure 17. Chemical structures of known non-nucleotide STING agonists.

Later, computationally-driven approaches directed to the optimization of DMXAA's structure and led to the discovery of SNX281.[125] This compound exhibits potent antitumor activity both on murine and human STING. *Ramanjulu et al.* from GSK discovered a number of amidobenzimidazole derivatives (di-ABZI) that showed effective antitumor activity[126]. These derivatives initiated signaling even though STING maintained an open apo-state, corroborating to the fact that STING's lid closure may not be critical for STING activation.

2.6 STING inhibitors

As previously discussed, aberrant STING activation and signaling leads to autoinflammation and autoimmune pathogenesis. Constant states of inflammation need to be effectively treated using pharmaceutical methods and, indeed, the research for STING inhibitors is currently on the rise.[127, 128] A number of small molecule inhibitors has been developed already and they can be sorted into two categories based on their mechanism of action: competitive antagonists of STING that bind and occupy the CDN binding site and covalent inhibitors that target STING's palmitoylation.

2.6.1 Inhibitors targeting the LBD

The peptide Astin C was one of the first compounds that were identified to inhibit STING. *Liu et al.* suggested that Astin C could specifically target STING and create a conformational change that blocked other CDNs from binding.[129] Additionally, it was shown to inhibit STING by blocking its recruitment to IRF3 and, thus, inhibited IFN expression.
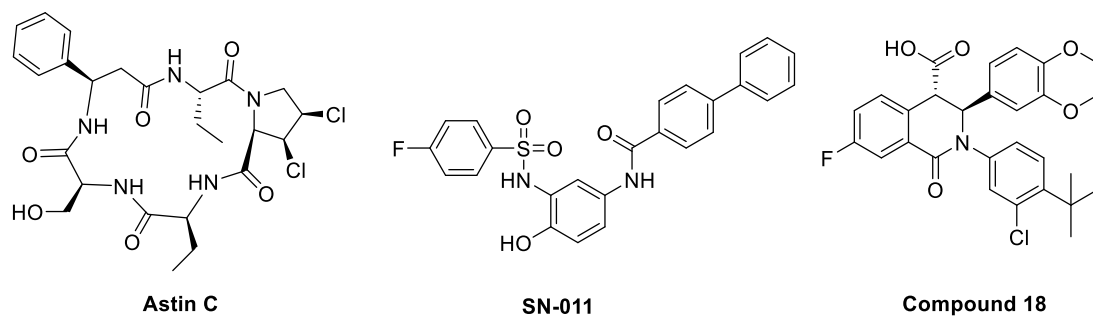
Figure 18. Chemical structures of reported inhibitors that occupy STING's ligand binding site.

Later on, *Siu et al.* from Merck identified Compound 18 (Figure 18) as a STING antagonist that inhibits interferon gene expression with an IC_{50} of 11μM. This molecule binds on STING at a 2:1 binding ratio (molecule of Compound 18 : STING monomer) and keeps STING in the inactive "open lid" conformation while lying in the bottom of the cleft of the LBD.[130] In comparison, *Hong et al.* recently discovered SN-011 with an IC_{50} of 76nM that locks STING in an inactive open conformation and binds on the LBD in a 1:1 binding ratio[131].

2.6.2 Inhibitors targeting palmitoylation

Palmitoylation is a post-translational lipid modification of proteins catalyzed by palmitoyltransferases that target and modify cysteine residues.[132] In particular, palmitoylation is the reversible covalent attachment of a long-chain fatty acid (palmitic acid) to a cysteine residue via a thioester bond (Figure 19).
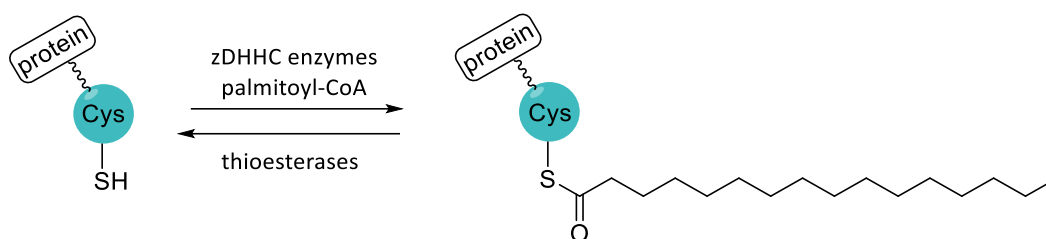

Figure 19. Palmitoylation is the reversible attachment of palmitic acid on cysteine residues catalyzed by palmitoyl-transferases. Thioesterases catalyze the removal of the palmitate tag.

Palmitoylation in mammalian cells is catalyzed by 23 zinc finger DHHC-type palmitoyltransferases (zDHHCs), meanwhile a number of thioesterases are controlling the removal of the palmitoylation.[133] Notably, palmitoylation is essential for proteins to be able to stably settle on membranes that are important for their function and for trafficking.[134] It has recently been demonstrated that STING undergoes palmitoylation[29] and this happens at the Golgi compartment, right after STING's translocation from the ER. However, preventing or blocking palmitoylation does not interfere with the exit of STING from the ER, which in turn means that STING's trafficking is not dependent on palmitoylation.[29]

On the other hand, palmitoylation is absolutely vital for the expression of interferon genes (IFN-β, IRF3 and NF-κB genes) and downstream signaling.[29] In fact, palmitoylation is most likely helping STING to form tight clusters on the Golgi membrane that subsequently allows it to bring TBK1 and IRF3 into close proximity so that IRF3 can be phosphorylated. Additionally, residues Cys88 and 91 were recognized as the target residues for STING palmitoylation. These reside adjacent to the STING's oligomerization interface with Cys88 buried into the TM2-TM3 linker and Cys91 more exposed to the cytosol and, therefore, more prone to palmitoylation.[23] Although it is known that S-palmitoylation is a reversible modification, STING carries the palmitate tag all the way to its degradation in the lysosomes.[29]
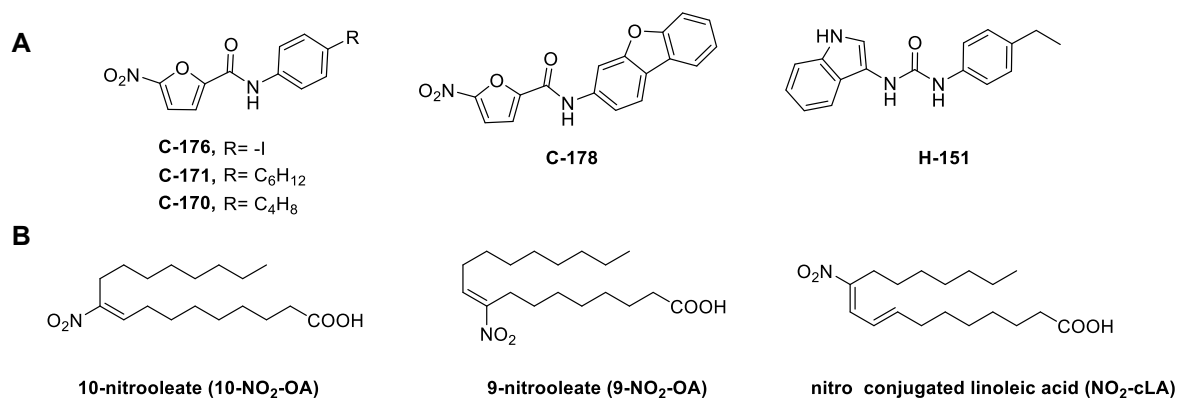
Figure 20. Chemical structures of reported STING palmitoylation inhibitors on Cys88/91.

Introduction

It is safe to say that STING palmitoylation could be exploited as a very operant pharmaceutical target for the inhibition of abnormal STING signaling. Indeed, successful steps were made towards that goal by the groups of *Christian K. Holm* and *Andrea Ablasser*.[135, 136] The former group discovered that endogenously formed nitro-fatty acids can successfully nitro-alkylate both Cys88 and 91 via reversible *Michael* addition reactions and effectively block palmitoylation (Figure 20B and 22). *Ablasser et al.* identified a series of nitrofuran derivatives (C-176, C-178, C-170, C-171) and a 3-acylamino indole compound (H-151) that irreversibly bind only to Cys91 (Figure 20A and 21). Nonetheless, they showed that they can successfully inhibit STING downstream signaling in vivo for both human and murine STING.
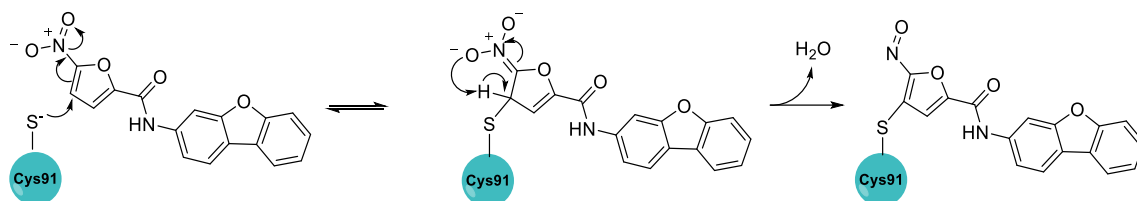
Figure 21. Proposed mechanism of the nitro-*Michael* reaction of the electrophilic nitrofuran with Cys91 of STING.
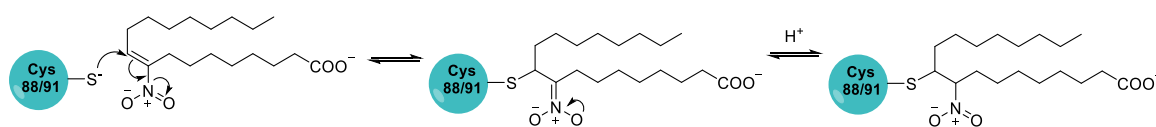
Figure 22. Proposed mechanism for the reversible nitro-fatty acid acylation of cysteines 88 and 91 of STING.

2.7 Aim of the project

The detection of foreign DNA is an essential first step and a triggering point to kick off host defense responses. The discovery of cGAS-STING pathway has provided remarkable insights into the mechanism of this detection and allowed researchers to comprehend the causes of irregular inflammation noticed in autoinflammatory diseases. Moreover, it was soon after demonstrated that STING has an essential role in antitumor responses and the generation of effective antitumor immunity. Thus, STING and the cGAS-STING pathway is an exceptional druggable target for therapeutic intervention.

Since the elucidation of cGAMP's structure, many attempts were made to modify it in order to produce novel CDN-based drug candidates that act as agonists for STING. From a medicinal chemistry point of view, these modifications mainly aim at improving stability, binding affinity and potency. The first aim of this project is the design and synthesis of a CDN analogue whose structure resembles that of natural cGAMP, using straightforward organic chemistry approaches (Chapter 3.1.1). We also conduct biological and binding assays in order to evaluate its activity and its binding on STING and facilitate a comparison with natural cGAMP. Finally, we perform a stability study against poxviruses and evaluate the compound's anticancer activity in vivo.

Despite the fact that CDNs are natural ligands for STING, their anionic nature impairs their cellular permeability. In Chapter 3.1.2 we explore the design and synthetic attempts towards a cGAMP-based prodrug which contains two biologically labile groups that mask the negative charge of the compound's phosphate moieties. Prodrug synthesis is nowadays on the rise and many clinical drugs are being administered in their prodrug form. Therefore, the synthesis of a cGAMP-based prodrug is of prominent importance.

While activated STING produces inflammatory responses to battle pathogen invasions, sustained or uncontrolled inflammatory signaling is the cause of many autoinflammatory diseases. Following this idea, in Chapter 3.2 we demonstrate the synthesis of novel cGAMP-based compounds that can act as STING competitive inhibitors. In the first part, we target palmitoylation of STING which is a post-translational modification that is indispensable for STING-mediated signaling. We demonstrate the mindset behind the design process of a hybrid molecule that consists of a cGAMP-based CDN linked with a depalmitoylating enzyme recruiter. Our goal is the synthesis of an inhibitor that not only is selective for STING but can also compete with the endogenous cGAMP.

In the second part of the inhibitor chapter, we establish the synthesis of two CDNs, each conjugated to a folate moiety. The purpose is to leverage the recently discovered folate transporter SLC19A1, which is nowadays known to be the main importer for CDNs and folates in monocytic cells. By conjugating CDNs with a folate moiety, we aim to combine favorable cell penetration with STING selectivity without regard to the CDN's limiting negative charges. Due to the ligation to the bulky folate, the CDNs can potentially bind on STING while keeping it in the inactive "open-lid" state and, thus, block STING signaling. After establishing the synthetic methodology, our future goal is to conduct in vitro assays in order to determine their efficiency in deactivating IFN production and ultimately whether they could act as a treatment in the context of immunopathology.

3 Results and discussion

3.1 STING agonists

3.1.1 2'3'-deoxy-cGAMP: A poxin-resistant STING agonist

cGAMP and STING constitute a crucial starting point from which innate immunity gets activated. Binding of cGAMP on STING is only one part of the major cGAS-STING pathway but it determines not only the successful initiation of immune responses but also the degree of activation for these signals. In this part of the dissertation, we established and optimized an innovative and reliable synthetic route towards 2'3'-deoxy-cGAMP (**1**). For this, we employed phosphoramidite/phosphate approaches according to typical oligonucleotide chemistry. First, the guanosine part of the molecule was synthesized starting from 1,2-isopropylidene-a-D-xylofuranose which was deoxygenated at the 3'-position of the ribose and then coupled with guanine via a *Vorbrüggen*-type base coupling. After the 5'-O-DMT protection of the ribose, the guanosine nucleoside precursor was turned into a phosphotriester which was coupled with a commercially available adenosine phosphoramidite. Consequently, the resulting linear molecule was cyclized furnishing our desired 2'3'-deoxy-cGAMP (**1**). Furthermore, **1** was evaluated for its binding affinity for STING using Isothermal Titration Calorimetry (ITC) and nano-Differential Scanning Fluorimetry (nano-DSF) which gave us valuable insights into the chemical thermodynamics of 2'3'-deoxy-cGAMP's favorable binding. Next, we demonstrated its potency at inducing type-I IFN gene expression in vitro by feeding reporter THP-1 monocytes and then measuring its half-maximal effective concentration (EC_{50}). Motivated by STING's involvement in the battle against foreign microorganisms, we decided to test **1**'s stability against a type of poxvirus nucleases (poxins). **1** was incubated in protein lysates containing poxins and its exact mass was measured by HPLC-HESI-MS spectrometry and quantified via its UV absorption. We noticed that **1** was completely resistant to poxin degradation whereas cGAMP had almost immediately completely degraded. This stability feature is attributed to the absence of the crucial 2'-OH that is essential for poxin degrading activity and is evidence that compound **1** can be used as an antiviral drug candidate or as a vaccine adjuvant against poxviruses. Since STING-mediated antitumor activity is by now well recognized, we evaluated **1** for its in vivo anti-cancer response in a murine hepatocellular carcinoma xenograph. Indeed, **1** had in fact a strong antitumor activity and showed superior results in delaying tumor size progression compared to natural cGAMP. These findings represent an important discovery that launches further research attempts in the field of STING-targeting modified cyclic dinucleotides.

Novel Poxin Stable cGAMP-Derivatives Are Remarkable STING Agonists

S. Stazzoni, D. F. R. Böhmer, F. Hernichel, D. Özdemir, **A. Pappa**, D. Drexler, S. Bauernfried, G. Witte, M. Wagner, S. Veth, K.-P. Hopfner, V. Hornung, L. M. König, T. Carell

Author contribution

In this work I was responsible for the design, synthesis and purification of the compound 2'3'-deoxy-cGAMP (**1**) and also for its subsequent analysis and characterization. Furthermore, I analyzed and evaluated the mass spectrometry data derived from the poxin stability study for compound **1**. Compounds **2** and **3** (2'3'-deoxy-cAAMP and 2'3'-deoxy-cAGMP) were designed and synthesized by *Dr. Samuele Stazzoni* as part of his PhD thesis. *Daniel Böhmer* conducted the mice intratumoral injection studies and analyzed and evaluated the xenographic data. *Fabian Hernichel* was responsible for resynthesizing compounds **2** and **3** and analyzing and evaluating the mass spectrometry data for their stability against poxins. *Dr. Dilara Özdemir* conducted the cellular experiments and analyzed the data for establishing the EC_{50} values for **1,2** and **3**.

Authorization

VIP | **Medicinal Chemistry** *Very Important Paper*

Novel Poxin Stable cGAMP-Derivatives Are Remarkable STING Agonists

Samuele Stazzoni[+], Daniel F. R. Böhmer[+], Fabian Hernichel[+], Dilara Özdemir,
Aikaterini Pappa, David Drexler, Stefan Bauernfried, Gregor Witte, Mirko Wagner,
Simon Veth, Karl-Peter Hopfner, Veit Hornung,* Lars M. König,* and Thomas Carell*

Abstract: 2′,3′-cGAMP is a cyclic A- and G-containing dinucleotide second messenger, which is formed upon cellular recognition of foreign cytosolic DNA as part of the innate immune response. The molecule binds to the adaptor protein STING, which induces an immune response characterized by the production of type I interferons and cytokines. The development of STING-binding molecules with both agonistic as well as antagonistic properties is currently of tremendous interest to induce or enhance antitumor or antiviral immunity on the one hand, or to treat autoimmune diseases on the other hand. To escape the host innate immune recognition, some viruses encode poxin endonucleases that cleave 2′,3′-cGAMP. Here we report that dideoxy-2′,3′-cGAMP (**1**) and analogs thereof, which lack the secondary ribose-OH groups, form a group of poxin-stable STING agonists. Despite their reduced affinity to STING, particularly the compound constructed from two A nucleosides, dideoxy-2′,3′-cAAMP (**2**), features an unusually high antitumor response in mice.

The innate immune system is the first line of defense against pathogens. It is triggered by dedicated sensor proteins that recognize specific pathogen features as non-self.[1,2] Bacterial and viral infections, but also ruptured nuclear and mitochondrial membranes of damaged cells, generate double-stranded DNA (dsDNA) in the cytosol of the corresponding cell.[3] This creates a pathogenic state that is sensed by the enzyme cyclic-GMP-AMP-synthase (cGAS), which cyclizes GTP and ATP to generate the second messenger 2′,3′-cyclic-GMP-AMP (2′,3′-cGAMP) (Figure 1a).[4–7] Binding of 2′,3′-cGAMP to the endoplasmic reticulum transmembrane protein stimulator of interferon genes (STING) leads to its oligomerization, which finally stimulates the expression of type I interferons (IFNs) and pro-inflammatory cytokines with potent anti-viral and anti-bacterial effects.[8] To circumvent the cGAS/STING host defense system, vaccinia viruses encode poxvirus immune nucleases (poxins), which were shown to specifically hydrolyze the 3′-5′-linkage of the mediator molecule 2′,3′-cGAMP, leading to its degradation (Figure 1a).[9] This is achieved by the metal ion-free catalysis of an auto-degradation process, in which the poxin activates the free 2′-OH of 2′,3′-cGAMP with an active site lysine residue (K142) to promote an intramolecular attack on the 3′-5′ phosphodiester linkage, to generate an adenosine-2′,3′-cyclophosphate intermediate. According to this mechanism, removing the 2′-OH group of 2′,3′-cGAMP would potentially provide a powerful agonist that would be resistant to this viral escape pathway. However, removing the ribose OH group has consequences regarding binding to STING. It is proposed that the 3′-OH group establishes a key interaction with Ser162 of the human STING (hSTING) active site.[10] This is supposed to allow hSTING to differentiate 2′,3′-cGAMP from 3′,3′-cGAMP, which is a key bacterial second messenger (Figure 1a).

In the context of antiviral therapies, the cGAS/STING-pathway is a key component of innate immunity against DNA viruses and retroviruses such as HIV.[11–15] Activation of STING can consequently increase antiviral responses. In

[*] Dr. S. Stazzoni[+]
New address: Monoclonal Antibody Discovery (MAD) Lab, Fondazione Toscana Life Sciences
53100 Siena (Italy)

Dr. S. Stazzoni,[+] MSc. F. Hernichel,[+] MSc. D. Özdemir,
MSc. A. Pappa, Dr. M. Wagner, Dr. S. Veth, Prof. Dr. T. Carell
Department of Chemistry, Ludwig-Maximilians-Universität
München
Butenandtstr. 5–13, 81377 Munich (Germany)
E-mail: Thomas.carell@lmu.de

Dr. D. F. R. Böhmer,[+] Dr. L. M. König
Division of Clinical Pharmacology, University Hospital, Ludwig-Maximilians-Universität München
Lindwurmstr. 2a, 80337 Munich (Germany)
E-mail: lars.koenig@med.uni-muenchen.de

Dr. D. Drexler, Dr. S. Bauernfried, Dr. G. Witte,
Prof. Dr. K.-P. Hopfner, Prof. Dr. V. Hornung
Gene Center and Department of Biochemistry, Ludwig-Maximilians-Universität München
Feodor-Lynen-Str. 25, 81377 Munich (Germany)
E-mail: hornung@genzentrum.lmu.de

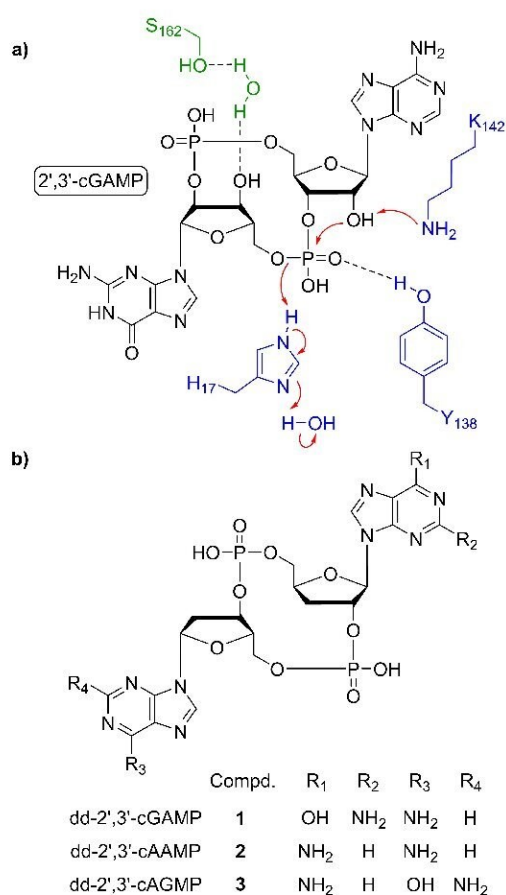[+] These authors contributed equally to this work.

Figure 1. a) Depiction of important 2′,3′-cGAMP interactions. Green: Interaction of 3′-OH with S162 of hSTING according to Zhang et al.[10] Blue: Mechanism of cleavage performed by vaccinia virus poxins, adapted from Eaglesham et al.[9] b) Structures of the synthesized dideoxy-2′,3′-cGAMP derivatives.

addition, STING activation can stimulate antitumor immune responses, which makes STING also a prime target for cancer immunotherapy.[16–19] The first STING agonists have recently entered clinical trials.[20–22] Here we present a new and concise synthesis of dideoxy-2′,3′-cyclic-dinucleotides (dd-2′,3′-CDNs) such as **1**, **2** and **3** (Figure 1b) and data about poxin-mediated degradation. Furthermore, we benchmark the synthesized compounds to natural 2′,3′-cGAMP in a preclinical mouse model of hepatocellular carcinoma.

The synthesis of dd-2′,3′-CDNs **1–3** started from protected xylofuranose **4** (Scheme 1). Dimethoxytrityl (DMTr) protected 3′-deoxyribonucleotides **5** and **6** were obtained over seven steps via Barton-McCombie deoxygenation, acetolysis and subsequent Vorbrüggen glycosylation, according to literature procedures.[23–25] The key 2′-phosphotriester precursors **7** and **8** were prepared in a four-step one-pot reaction by first converting **5** and **6** into the respective 2′-phosphoramidites, then condensing them with allyl alcohol, followed by oxidation with *tert*-butyl hydroperoxide (*t*BuOOH) and deprotection with dichloroacetic acid (DCA). Precursors **7** and **8** were subsequently coupled with commercially available adenosine and guanosine phosphoramidites **9** and **10** to give the 2′-5′ linked dinucleotides **11**, **12**

and **13**. Next, the allyl protecting group was removed with sodium iodide in refluxing acetone to provide the dinucleotides **14**, **15** and **16**. After precipitation and product isolation, 1-(mesitylene-2-sulfonyl)-3-nitro-1*H*-1,2,4-triazole (MSNT) was added to solutions containing **14–16** to activate the free phosphate for the cyclization key step, which established the 3′-5′ linkage. The raw cyclization products were not isolated, but directly subjected to a deprotection step with 33 % *v/v* methylamine in ethanol. We obtained the final compounds **1**, **2** and **3** after precipitation from cold acetone and purification by reverse-phase HPLC in the form of white powders.

The binding properties of dd-2′,3′-CDNs **1–3** were evaluated with nano differential scanning fluorimetry (nDSF) thermal shift experiments. To this end, we added increasing amounts of the compounds to recombinant hSTING and measured the protein melting curves. Binding of the ligand stabilizes the protein, which increases the T_m-value. As shown in Table 1 all our dd-2′,3′-CDNs stabilize hSTING. Natural 2′,3′-cGAMP generated the largest stabilization (ΔT_m) by 16.2 °C, followed by dd-2′,3′-cGAMP (**1**), which stabilized by 13.1 °C. This shows that the OH groups indeed influence the binding to STING but that they are not essential. In contrast dd-2′,3′-cAAMP (**2**) and dd-2′,3′-cAGMP (**3**) showed a significantly smaller stabilization effect of $\Delta T_m = 2$ °C. For dd-2′,3′-cAAMP (**2**) this is less than half compared to the OH-containing reference compound 2′,3′-cAAMP with $\Delta T_m = 5.5$ °C. These data suggest that the nucleoside exchange from G to A has a much more dramatic influence on binding than the OH groups.

We next performed isothermal titration calorimetry (ITC) to gain deeper insight into the binding event (Table 1). Indeed, the lack of the two OH groups reduced the affinity, but binding was still observed in the submicromolar regime. For dd-2′,3′-cGAMP (**1**) we determined a K_D of 445 nM, mostly because of a loss of enthalpic stabilization. dd-2′,3′-cAAMP (**2**) showed reduced binding compared

Table 1: EC$_{50}$ and affinity data of dd-2′,3′-CDNs **1–3**.[a]

Compound	EC$_{50}$ [µM][b]	ΔT_m [°C] (nDSF)[c]	K$_D$ [µM] (ITC)[d]
dd-2′,3′-cGAMP (**1**)	7.4 ± 1.7	13.1	0.45 ± 0.23
dd-2′,3′-cAAMP (**2**)	74.4 ± 4.6	1.90 ± 0.04	15.1 ± 14.5
dd-2′,3′-cAGMP (**3**)	>110	2.30 ± 0.02	42.9 ± 35.1
2′,3′-cAAMP	26.6 ± 4.9	5.50 ± 0.01	4.98 ± 0.82
2′,3′-cGAMP	10.6[e]	16.2 ± 0.1	0.004[f]

[a] Green: Synthesized dd-2′,3′-CDNs **1–3**. Blue: OH-containing reference compounds. [b] EC$_{50}$ values were measured in THP-1-Dual monocytic cells in three independent experiments. [c] Thermal shift temperatures are obtained from nDSF experiments. The temperature represents the difference in melting temperature between 5 µM hSTING incubated with 100 µM of the respective ligand and 5 µM hSTING without ligand. The results are mean values from three independent experiments. [d] K_D values are calculated from ITC experiments with an error from the individual fit of the binding model to the experimental data. [e] A single-replicate experiment was conducted to confirm literature known EC$_{50}$ values of 2′,3′-cGAMP.[27] [f] K_D value published by Zhang et al.[10]
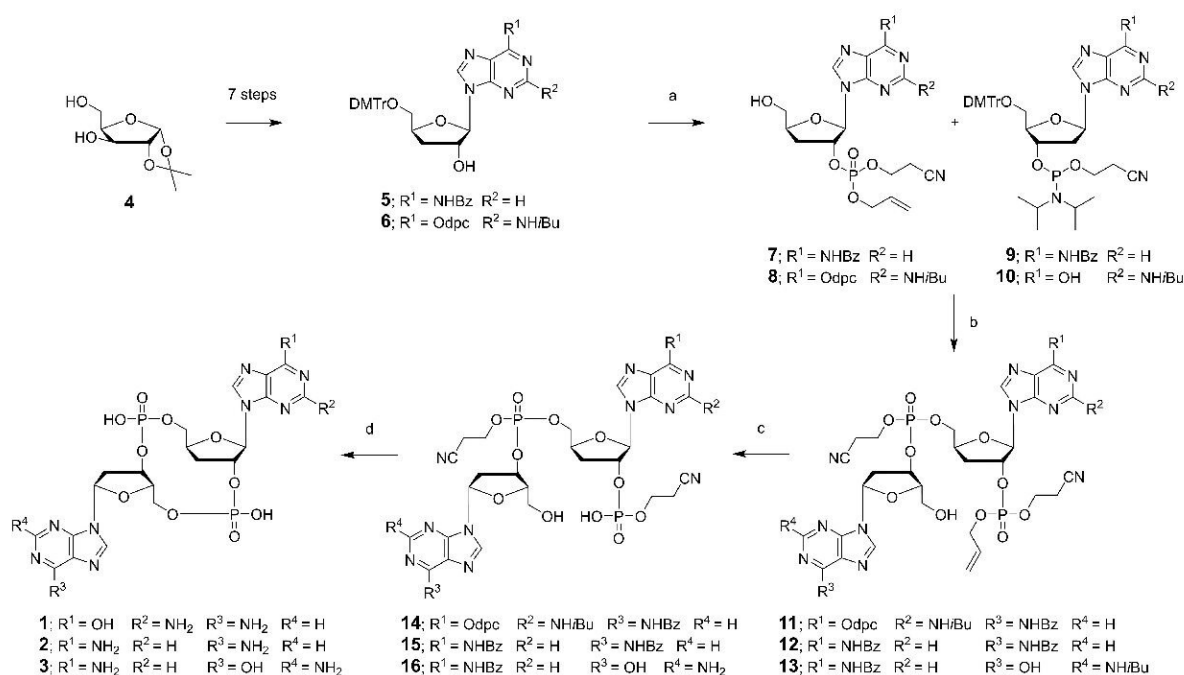
Scheme 1. Synthesis of dd-2′,3′-cGAMP derivatives **1**, **2** and **3**. Conditions: a) 1. 2-Cyanoethyl *N,N,N′,N′*-tetraisopropylphosphorodiamidite, pyridine trifluoroacetate, DCM, RT, 3 h; 2. BTT, allyl alcohol, RT, 1 h; 3. *t*BuOOH, RT, 40 min; 4. 3% *v/v* DCA in DCM, RT, 15 min; b) 1. BTT, MeCN, RT, 1 h; 2. *t*BuOOH, RT, 40 min; 3. 3% *v/v* DCA in DCM, RT, 10 min; c) NaI in acetone, reflux, 3 h; d) 1. MSNT, pyridine, RT, 18 h; 2. 33% *v/v* MeNH₂ in EtOH, RT, 4 h.

to reference compound 2′,3′-cAAMP by a factor of 3, while for dd-2′,3′-cAGMP (**3**) binding shifted to a higher micromolar value. Most importantly, all compounds, particularly dd-2′,3′-cGAMP (**1**) with a K_D of 0.5 µM, have a higher binding affinity to STING compared to other recently reported nucleoside agonists.[26]

To investigate the in cellulo activity of the prepared dd-2′,3′-CDNs **1**, **2** and **3**, we next measured their ability to induce an interferon response in immune cells (Table 1). For this purpose, we used a THP-1 monocytic reporter cell line containing a Lucia luciferase gene under the control of a promoter that is stimulated by 5 IFN-stimulated response elements. This allows to study the activation of the interferon pathway by measuring luminescence intensities. For control studies we used a THP-1 reporter cell line with STING being knocked out (STING-KO). For dd-2′,3′-cGAMP (**1**) and dd-2′,3′-cAAMP (**2**) ($c = 200$–300 µM, 37°C, 24 h) we did not detect luminescence in the STING-KO control cell line, showing that both compounds operate as expected in a strictly STING-dependent fashion. In contrast, STING-competent THP-1 cells showed a strong luminescence response upon 2′,3′-cGAMP treatment. Concentration-dependent studies allowed us to determine an EC₅₀ of 10.6 µM for 2′,3′-cGAMP, which is in good agreement with literature data.[27] When performing the measurements using dd-2′,3′-cGAMP (**1**) we again determined a strictly STING-dependent response with an EC₅₀ of 7.4 µM, which is even slightly lower compared to natural 2′,3′-cGAMP itself. This is surprising given that the lack of 3′-OH groups reduces the affinity to STING. One possible explanation could be a different cellular uptake triggered by the lacking two OH

groups. For reference compound 2′,3′-cAAMP we measured an EC₅₀ of 27 µM and for dd-2′,3′-cAAMP (**2**) an EC₅₀ of 74 µM was determined. The dd-2′,3′-cAGMP (**3**) derivative gave an EC₅₀ of >110 µM. These results show that all dideoxy compounds show in cellulo STING activation. In the case of dd-2′,3′-cGAMP (**1**) it goes even beyond the capability of parent compound 2′,3′-cGAMP.

To test the stability of dd-2′,3′-CDNs **1** and **2** towards poxin degradation and compare it with 2′,3′-cGAMP, BHK-21 cells were infected with vaccinia virus WR ($\approx 1 \times 10^7$ PFUs) for one hour and subsequently incubated for another 14 hours to allow expression of viral particles and poxin enzymes. Cell lysates were prepared in a lysis buffer providing suitable conditions for maintaining the enzymatic activity of the poxins.[9] After removal of cell debris and protein quantification, 30 ng of total protein lysate per sample were incubated either with 2′,3′-cGAMP or with compounds **1** and **2** for up to 24 hours, thereby establishing a time course experiment with increasing sampling time intervals. Upon sampling, enzymes were inactivated by addition of a phenol: chloroform mixture (1:1). The aqueous fractions of the samples were purified and subsequently analyzed by LC–MS. Here, all compounds were unequivocally identified via their exact mass and quantified via their UV absorption at 260 nm. The resulting data is depicted in Figure 2. Our data show that the OH- containing reference compound 2′,3′-cGAMP is quickly hydrolyzed by the viral poxins. This is not the case for the dideoxy compounds. Indeed, our data show that dd-2′,3′-CDNs **1** and **2** are stable towards poxin degradation and therefore able to evade the viral degradation response. Taken together, dd-
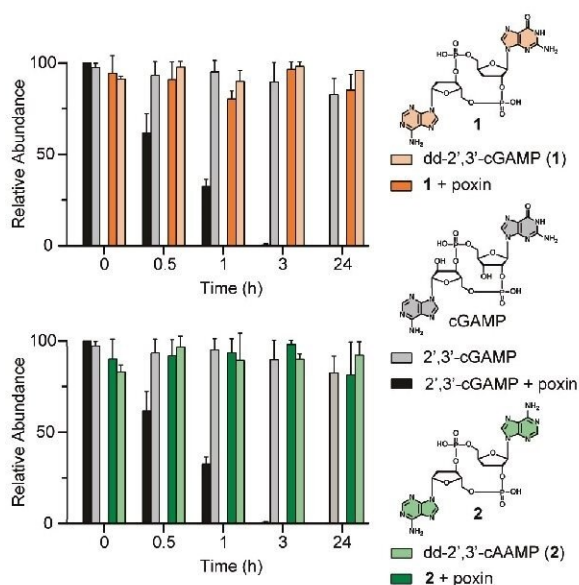
Figure 2. Stability of the dd-2′,3′-CDNs 1 and 2 and of the reference compound 2′,3′-cGAMP against poxin catalyzed degradation. ▨ = 1, ▨ = 1 + poxin; ▨ = 2′,3′-cGAMP, ■ = 2′,3′-cGAMP + poxin; ▨ = 2, ▨ = 2 + poxin. All values are normalized to the amount of compound present at $t = 0$ h, which was set to 100%. Error bars represent the standard deviation of three independent experimental replicates.
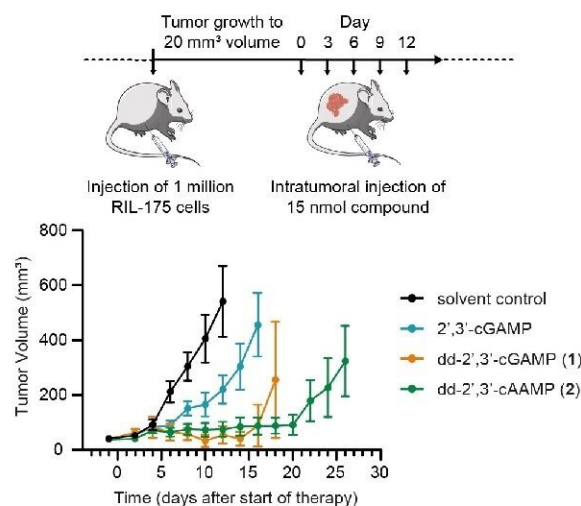

Figure 3. Schematic presentation of the in vivo xenograft tumor mouse model and the in vivo data, which show a dramatic control of the tumor growth particularly with dd-2′,3′-cAAMP (2): Top: Treatment scheme. Mice were subcutaneously inoculated with RIL-175 tumor cells (hepatocellular carcinoma cells). Once tumors reached a mean volume of 20 mm³, intratumoral therapy on every third day was initiated. Solvent control or 15 nmol of 2′,3′-cGAMP, dd-2′,3′-cGAMP (1) or dd-2′,3′-cAAMP (2) were used for up to five treatments as depicted. Bottom: Tumor growth of CDN-treated tumors ($n = 11$ for solvent control, $n = 12$ for 2′,3′-cGAMP and dd-2′,3′-cAAMP (2) and $n = 6$ for dd-2′,3′-cGAMP (1)). Mean tumor volume $+/-$ SEM is shown. Pooled data from two independent experiments are shown.

2′,3′-cGAMP (1) and dd-2′,3′-cAAMP (2) are stable STING agonists with reduced affinity but with remarkable EC_{50} values.

In order to finally clarify how compounds 1 and 2 would behave in a tumor model, we examined their therapeutic efficacy in a mouse model of hepatocellular carcinoma (HCC) targeting mouse STING (mSTING). Analysis of published crystal structures and active site sequences shows that the interaction of mSTING and hSTING with the 3′-OH group should be similar.[7,28] For the study, 1×10^6 RIL-175 tumor cells were subcutaneously injected into C57BL/6 mice. The mice were treated five times by intratumoral injections of solvent control ($n = 11$), 2′,3′-cGAMP ($n = 12$), dd-2′,3′-cAAMP (2) ($n = 12$) and dd-2′,3′-cGAMP (1) ($n = 6$). The data together with a schematic representation of the experiment are shown in Figure 3. The data show that intratumoral injection of 2′,3′-cGAMP into RIL-175 tumors led to a significant delay in tumor growth (Figure 3 and Figure SI-5). Unexpectedly, we observed with dd-2′,3′-CDNs 1 and 2 a superior delay in tumor growth compared to parent compound 2′,3′-cGAMP (Figure 3 and Figure SI-5). At this point we believe that one reason for the better in vivo effect could be an improved cellular uptake of the dideoxy compounds as already hypothesized for the exceptional EC_{50} values. In addition, the "less is more" paradigm could be at work here, which argues that a lower affinity of the compounds to the STING adaptor protein could result in a decreased T-cell toxicity, which has been described for high concentration of STING agonists.[29,30] Certainly, the surprisingly high EC_{50} values and the strong in vivo tumor growth control require deeper mechanistic investigation.

In conclusion, we described the synthesis of 2′,3′-cGAMP dideoxy derivatives with superior in vivo characteristics for potential use as anti-viral and anti-tumoral therapeutics. The 2′- and 3′-OH groups of 2′,3′-cGAMP, which is the natural ligand for the adaptor protein STING, have been discussed as key elements that allow STING binding and enable STING to differentiate the 2′,3′-linked cGAMP derivative from 3′,3′-linked cyclic dinucleotides, of which the latter are key bacterial second messengers. The OH groups do affect binding of the ligands in two ways: first the 3′-OH group is known to establish a H-bond with Ser162 of the protein; second, the OH groups change and define the pucker of the ribose unit.[10] In deoxyribonucleotides it is known that the ribose can exist both in the C2′-endo and C3′-endo conformation, while for the ribonucleotides containing a free 2′-OH groups, a clear conformational preference for the C3′-endo conformation is reported as needed for binding.[31] The synthesis of the key compounds dd-2′,3′-cGAMP (1) and of dd-2′,3′-cAAMP (2) were possible using a new and concise synthetic combination of phosphoramidite and phosphotriester chemistry. ITC measurements show that the OH groups have only a minor enthalpic effect, but they make binding entropically more unfavorable because of the less preorganized structure of the ribose unit (Figure SI-3 and Table SI-1). Despite this effect, all prepared dideoxy-compounds show specific STING binding and STING pathway activation. Due to the lack of the 2′-OH groups, which is exploited by poxins to initiate 2′,3′-cGAMP hydrolysis, our compounds resist poxin degradation. Unexpectedly, we

observe in a preclinical tumor model that particularly dd-2′,3′-cAAMP (**1**) is able to control the tumor growth far better than the parent compound and natural ligand 2′,3′-cGAMP.

Conflict of Interest

The authors declare no conflict of interest.

Data Availability Statement

The data that support the findings of this study are available from the corresponding author upon reasonable request.

[1] X. Tan, L. Sun, J. Chen, Z. J. Chen, *Annu. Rev. Microbiol.* **2018**, *72*, 447–478.

[2] G. P. Amarante-Mendes, S. Adjemian, L. M. Branco, L. C. Zanetti, R. Weinlich, K. R. Bortoluci, *Front. Immunol.* **2019**, *9*, 2379.

[3] K. N. Miller, S. G. Victorelli, H. Salmonowicz, N. Dasgupta, T. Liu, J. F. Passos, P. D. Adams, *Cell* **2021**, *184*, 5506–5526.

[4] A. Ablasser, M. Goldeck, T. Cavlar, T. Deimling, G. Witte, I. Röhl, K.-P. Hopfner, J. Ludwig, V. Hornung, *Nature* **2013**, *498*, 380–384.

[5] L. Sun, J. Wu, F. Du, X. Chen, Z. J. Chen, *Science* **2013**, *339*, 786–791.

[6] J. Wu, L. Sun, X. Chen, F. Du, H. Shi, C. Chen, Z. J. Chen, *Science* **2013**, *339*, 826–830.

[7] P. Gao, M. Ascano, Y. Wu, W. Barchet, B. L. Gaffney, T. Zillinger, A. A. Serganov, Y. Liu, R. A. Jones, G. Hartmann, T. Tuschl, D. J. Patel, *Cell* **2013**, *153*, 1094–1107.

[8] C. Zhang, G. Shang, X. Gui, X. Zhang, X.-C. Bai, Z. J. Chen, *Nature* **2019**, *567*, 394–398.

[9] J. B. Eaglesham, Y. Pan, T. S. Kupper, P. J. Kranzusch, *Nature* **2019**, *566*, 259–263.

[10] X. Zhang, H. Shi, J. Wu, X. Zhang, L. Sun, C. Chen, Z. J. Chen, *Mol. Cell* **2013**, *51*, 226–235.

[11] D. Gao, J. Wu, Y.-T. Wu, F. Du, C. Aroh, N. Yan, L. Sun, J. Chen Zhijian, *Science* **2013**, *341*, 903–906.

[12] M. Moriyama, T. Koshiba, T. Ichinohe, *Nat. Commun.* **2019**, *10*, 4624.

[13] X.-D. Li, J. Wu, D. Gao, H. Wang, L. Sun, J. Chen Zhijian, *Science* **2013**, *341*, 1390–1394.

[14] J. Paijo, M. Döring, J. Spanier, E. Grabski, M. Nooruzzaman, T. Schmidt, G. Witte, M. Messerle, V. Hornung, V. Kaever, U. Kalinke, *PLoS Pathog.* **2016**, *12*, e1005546.

[15] B. Sun, K. B. Sundström, J. J. Chew, P. Bist, E. S. Gan, H. C. Tan, K. C. Goh, T. Chawla, C. K. Tang, E. E. Ooi, *Sci. Rep.* **2017**, *7*, 3594.

[16] Y. Wang, J. Luo, A. Alu, X. Han, Y. Wei, X. Wei, *Mol. Cancer* **2020**, *19*, 136.

[17] L. T. Khoo, L.-Y. Chen, *EMBO Rep.* **2018**, *19*, e46935.

[18] J. Kwon, S. F. Bakhoum, *Cancer Discovery* **2020**, *10*, 26–39.

[19] A. Amouzegar, M. Chelvanambi, J. N. Filderman, W. J. Storkus, J. J. Luke, *Cancers* **2021**, *13*, 2695.

[20] D.-S. Kim, A. Endo, F. G. Fang, K.-C. Huang, X. Bao, H.-W. Choi, U. Majumder, Y. Y. Shen, S. Mathieu, X. Zhu, K. Sanders, T. Noland, M.-H. Hao, Y. Chen, J. Y. Wang, S. Yasui, K. TenDyke, J. Wu, C. Ingersoll, K. A. Loiacono, J. E. Hutz, N. Sarwar, *ChemMedChem* **2021**, *16*, 1741–1744.

[21] W. Chang, M. D. Altman, C. A. Lesburg, S. A. Perera, J. A. Piesvaux, G. K. Schroeder, D. F. Wyss, S. Cemerski, Y. Chen, E. DiNunzio, A. M. Haidle, T. Ho, I. Kariv, I. Knemeyer, J. E. Kopinja, B. M. Lacey, J. Laskey, J. Lim, B. J. Long, Y. Ma, M. L. Maddess, B.-S. Pan, J. P. Presland, E. Spooner, D. Steinhuebel, Q. Truong, Z. Zhang, J. Fu, G. H. Addona, A. B. Northrup, E. Parmee, J. R. Tata, D. J. Bennett, J. N. Cumming, T. Siu, B. W. Trotter, *J. Med. Chem.* **2022**, *65*, 5675–5689.

[22] J. Le Naour, L. Zitvogel, L. Galluzzi, E. Vacchelli, G. Kroemer, *Oncoimmunology* **2020**, *9*, 1777624–1777624.

[23] F. Hulpia, S. Van Calenbergh, G. Caljon, L. Maes, Universiteit Gent, Universiteit Antwerpen, WO2019076633, **2019**.

[24] A. Kumar, S. I. Khan, A. Manglani, Z. K. Khan, S. B. Katti, *Nucleosides Nucleotides Nucleic Acids* **1994**, *13*, 1049–1058.

[25] C. Meier, J. M. Neumann, F. Andre, Y. Henin, T. Huynh Dinh, *J. Org. Chem.* **1992**, *57*, 7300–7308.

[26] C. Ding, Z. Song, A. Shen, T. Chen, A. Zhang, *Acta Pharm. Sin. B* **2020**, *10*, 2272–2298.

[27] B. Novotná, L. Vaneková, M. Zavřel, M. Buděšínský, M. Dejmek, M. Smola, O. Gutten, Z. A. Tehrani, M. Pimková Polidarová, A. Brázdová, R. Liboska, I. Štěpánek, Z. Vavřina, T. Jandušík, R. Nencka, L. Rulíšek, E. Bouřa, J. Brynda, O. Páv, G. Birkuš, *J. Med. Chem.* **2019**, *62*, 10676–10690.

[28] D. Lu, G. Shang, J. Li, Y. Lu, X.-C. Bai, X. Zhang, *Nature* **2022**, *604*, 557–562.

[29] K. E. Sivick, A. L. Desbien, L. H. Glickman, G. L. Reiner, L. Corrales, N. H. Surh, T. E. Hudson, U. T. Vu, B. J. Francica, T. Banda, G. E. Katibah, D. B. Kanne, J. J. Leong, K. Metchette, J. R. Bruml, C. O. Ndubaku, J. M. McKenna, Y. Feng, L. Zheng, S. L. Bender, C. Y. Cho, M. L. Leong, A. van Elsas, T. W. Dubensky, S. M. McWhirter, *Cell Rep.* **2018**, *25*, 3074–3085.

[30] M. F. Gulen, U. Koch, S. M. Haag, F. Schuler, L. Apetoh, A. Villunger, F. Radtke, A. Ablasser, *Nat. Commun.* **2017**, *8*, 427.

[31] W. Saenger, *Principles of Nucleic Acid Structure*, Springer, New York, **1984**.

3.1.2 Towards the synthesis of a 2'3'-deoxy-cGAMP SATE prodrug

3.1.2.a Designing cGAMP analogue prodrugs

As already described in the introduction, the negative charge on the phosphate can be a limiting factor for unobstructed cell penetration and significant oral bioavailability.[43] In Chapter 3.1.1, 2'3'-deoxy-cGAMP (**1**) and 2'3'-deoxy-cAAMP (**2**) were identified as potent STING agonists and promising cancer immunotherapy candidates, however the problem of high polarity still persists. In the context of designing functionalized CDNs that activate STING, our next goal was to implement a prodrug strategy in order to mask the negative charge of our compounds.

The first attempt to conceal polarity was accomplished in our group *by Dr. Clemens Dialer* who synthesized a neutrally charged cGAMP analogue (**17**) by replacing the phosphate groups with a 3'-triazole and an 2'-amide linkage (Figure 23).[137] Follow-up in vitro testing of this compound's efficiency in macrophages demonstrated that this analogue does not have an affinity for STING and type-I interferons are not produced. Furthermore, NMR spectroscopy studies showed that this molecule displays a structural conformation that is way different than cGAMP. From these data it is apparent that the presence of the phosphates, the linkage type and a cGAMP-like conformation are necessary factors for efficient binding on STING.

In continuation to these efforts, as part of his PhD thesis, *Dr. Samuele Stazzoni* utilized 2'3'-deoxy-cAAMP (**2**) since it demonstrates biological STING-related activity and also allows for benchmarked synthetic accessibility (data shown in previous chapter[138]). For the purpose of his prodrug project, 2'3'-deoxy-cAAMP was a fundamental starting point, which can very efficiently serve as a promising candidate and basic building block for prodrug synthesis. In order to ensure complete negative charge elimination, both the phosphate groups were masked by an S-acylthioethyl (SATE) ester (Figure 23). This prodrug moiety was carefully chosen so as to allow selective cleavage after cell penetration mediated by carboxylesterases, which are widely distributed in cells and tissues[139]. Moreover, the prodrug contains a terminal alkyne that can be exploited for late-stage functionalizations via click chemistry. That way, suitable signaling molecules could be conjugated to the CDN and enable targeted cell delivery and enhanced uptake. To that end, bis-SATE prodrug **18** was successfully synthesized.
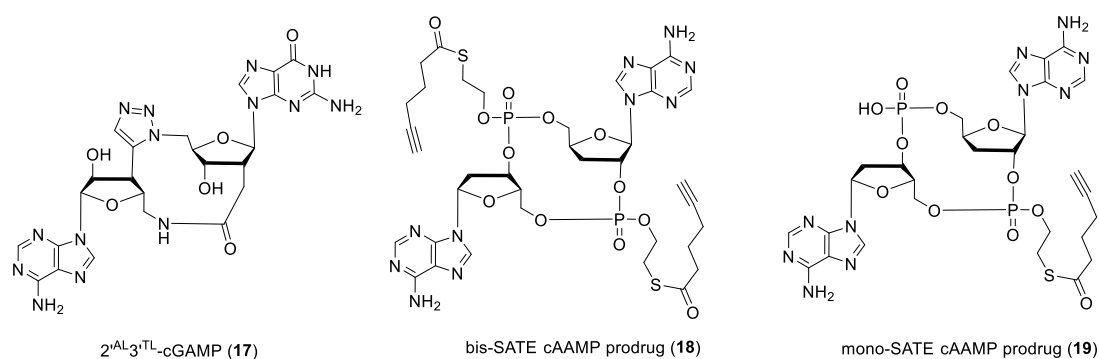

2'AL3'TL-cGAMP (**17**)   bis-SATE cAAMP prodrug (**18**)   mono-SATE cAAMP prodrug (**19**)

Figure 23. Chemical structures of compounds 2'AL3'TL-cGAMP (**17**) (synthesized by *Dr. Clemens Dialer*), bis-SATE cAAMP (**18**) (synthesized by *Dr. Samuele Stazzoni*) and mono-SATE cAAMP (**19**) (synthesized by *Dr. Simon Veth*).

Results and discussion

At the same time, as part of his PhD thesis *Dr. Simon Veth* synthesized a mono-substituted SATE-deoxy-cAAMP prodrug (**19**) (Figure 26) for antibody conjugation that served as a direct comparison for the prodrug masking strategy. Both compounds, the free phosphate analogue 2'3'-deoxy-cAAMP (**2**) (synthesized by *Dr. S. Stazzoni*) and the parent compound 2'3'-cAAMP (synthesized by *Dr. S. Veth*) were tested for their immunity-related luminescence response on THP-1 Dual monocytes and their half-maximum effective concentrations were calculated (in collaboration with *Dr. Dilara Özdemir*). From the resulting data it became clear that the incorporation of a SATE prodrug on the CDN greatly improves cell permeability but the best overall results were achieved with the bis-SATE prodrug. As Figure 24 shows, there is a significant difference at the EC_{50} values between the two prodrugs suggesting that the high polarity of a single, free phosphate group drastically reduces cell uptake compared to the fully masked prodrug.
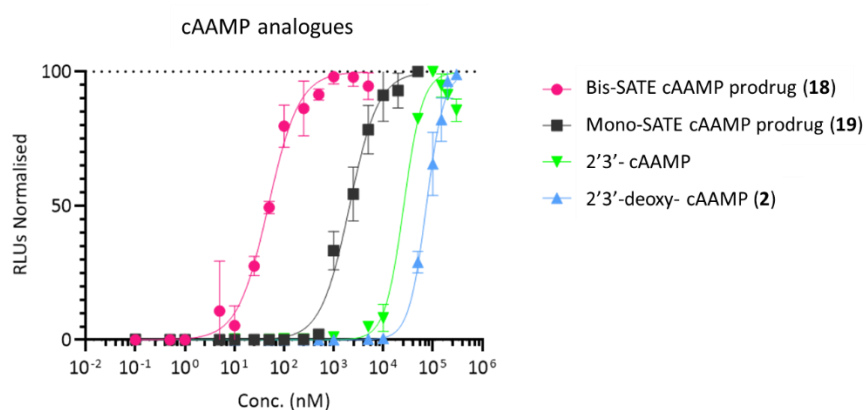

Figure 24. EC_{50} values of SATE prodrugs **18** and **19** and cAAMP analogues. Data resulting from THP-1 Dual cells Luminescence assay. The bis-SATE prodrug **18** has an EC_{50} of 48,9 ± 7.7 nM (pink). The Mono-SATE produrg **19** has an EC50 of 2.1 ± 0.26 μM (black). Reference compounds 2'3'-cAAMP and 2'3'-deoxy-cAAMP (**2**) have an EC_{50} of 26.6 ± 4.9 μM (green) and 74.4 ± 4.6 μM (blue) respectively. Figure adapted from the PhD thesis of *Dr. Dilara Özdemir*.

3.1.2.b Synthetic approaches towards a 2'3'-deoxy-cGAMP prodrug

Based on the previous results, we decided to synthesize a CDN prodrug that consists of a guanine and an adenine nucleobase as a way to closely resemble the natural cGAMP (Figure 25). It is already demonstrated that 2'3'-deoxy-cGAMP **1** has a good affinity for STING ($K_{D(1)}$ = ~0.45μM) and its efficiency is also superior compared to the natural cGAMP ($EC_{50(1)}$ = ~7.4μM versus $EC_{50(cGAMP)}$ = ~10μM).[18, 138] Certainly, the synthesis of 2'3'-deoxy-cGAMP prodrug (**20**, Figure 25) will provide great insight into improved cellular uptake and hence could potentially afford better agonistic behavior than the free phosphate analogue. As for the basic scaffold of the compound, we decided to continue using the adenosine 2'- and guanosine 3'-deoxygenated moiety as a way to bypass the tedious TBS protection strategy of the OH groups that often is followed by 2'-3' migration of the -TBS group. This can occur even at later stages of the synthesis especially under mildly basic conditions. Moreover, the complete elimination of the OH groups is advantageous because it can render the CDN less susceptible to hydrolysis and "opening" of the macrocycle. Finally, the non-canonical 2'-5' phosphodiester linkage of natural cGAMP was also preserved in order to maintain the same structural integrity.
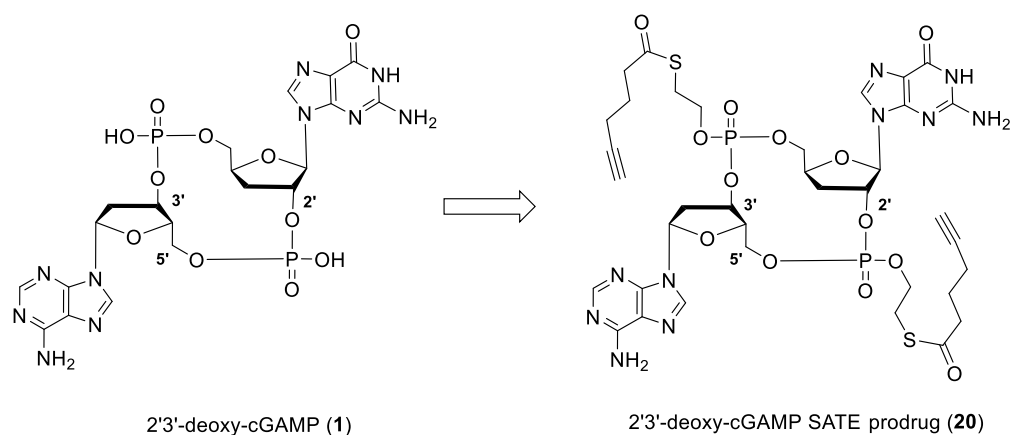
Results and discussion

Figure 25. Chemical structures of parent compound 2'3'-deoxy-cGAMP **1** and proposed prodrug analogue **20**.
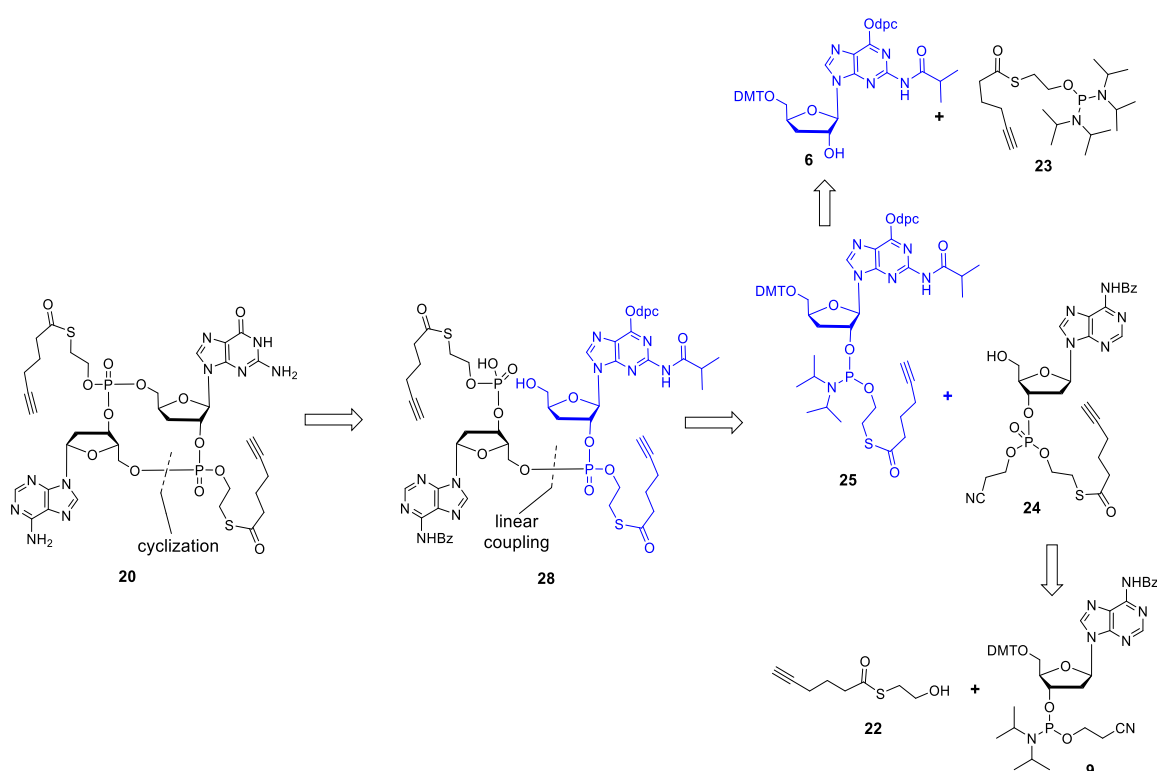

Figure 26. Retrosynthetic analysis for the synthesis of 2'3'-deoxy-cGAMP prodrug **20**. The starting precursors are proposed to be 3'-deoxy guanosine **25** and adenosine phosphoramidite **24** that are coupled and cyclized to afford **20**. **24** can be synthesized from commercially available phosphoramidite **9** while **25** can be accessed from 3'-deoxy-guanosine **6**.

As for the synthesis of the proposed prodrug, the retrosynthetic route is elucidated in Figure 26. We thought that the prodrug can be synthesized by relying on the well-established synthetic route that was initially demonstrated and optimized by *Dr. Samuele Stazzoni* and utilizes phosphoramidite and P(V) chemistry. This route starts from a 3'-deoxy-2'-guanosine phosphoramidite **25** and a 2'-deoxy-3'-adenosine phosphotriester **24** which both bear a SATE prodrug moiety and are coupled via oligonucleotide chemistry methods in order to form the linear intermediate **28**. Then the linear precursor can potentially be cyclized using condensing activators and, finally, we thought that the desired prodrug **20** can be obtained after complete protecting group removal. It is important to note that other literature known methods of CDN synthesis, like enzymatic synthesis or the H-phosphonate approach,[107, 108, 140]

were also taken into consideration but ultimately were not pursued since they usually do not allow big scale reactions or result in lower yields and difficult purifications.

In order to reach adenosine precursor **24**, we started from commercially available phosphoramidite **9** and substituted the diisopropylamino-group with the SATE moiety (Figure 26). For the SATE phosphoramidite **25** we decided to start by using the 3'-deoxy-5'-O-DMT guanosine nucleoside **6** whose synthesis was already shown in Chapter 3.1.1.[138] Following the same steps, we decided to keep the O6-diphenylcarbamoyl and the N2-isobutyryl protection on the base. Briefly, the guanosine precursor **21** was afforded starting from 1,2-O-isopropyliden-α-D-xylofuranose **4** that was first O-benzoyl protected on the 5-position and then deoxygenated in the 3-position via a modified Barton-McCombie reaction (Figure 27). The 3-OH group was reacted with thiocarbonyldiimidazole to afford the thioimidazole intermediate, which was then deoxygenated using tris-trimethylsilane and AIBN to initiate the radical reaction and converted to 1,2-di-O-acetyl-5-O-benzoyl-3-deoxyribofuranose (**S1**) via acidic deprotection with acetic anhydride and acetic acid. Under *Vorbrüggen* conditions, **S1** was glycosylated with O6-dpc-N2-iBu-guanine. Following 5'- and 2'-O-deprotection of **21**, precursor **6** was formed after 5'-O-DMT protection and was ready for further utilization.
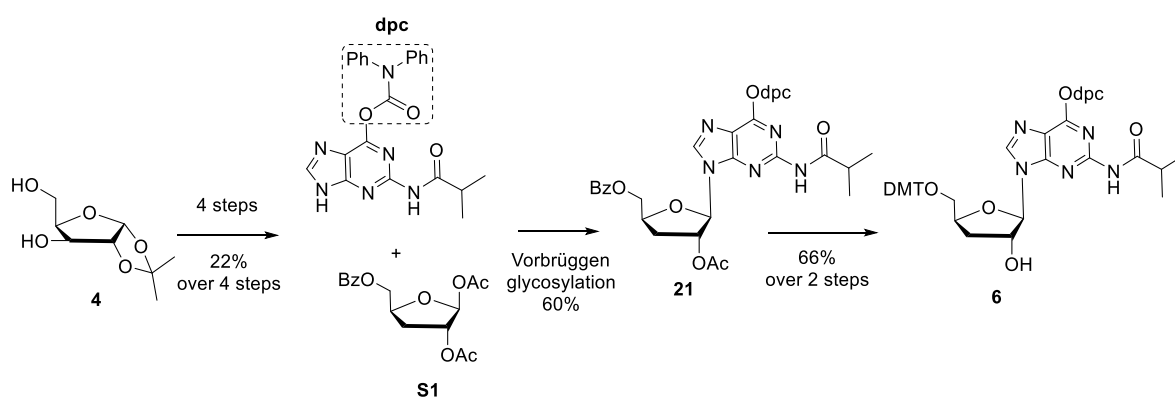

Figure 27. Synthesis of 3'-deoxy guanosine precursor **6** starting from 1,2-O-isopropyliden-α-D-xylofuranose **4**. The 5-O-position was first Bz-protected and the 3-OH was deoxygenated through a Barton McCombie reaction. Then the isopropylidene group was deprotected using Ac$_2$O and AcOH (**S1**) followed by a *Vorbrüggen* glycosylation with dpc-iBu-guanine to afford **21**. Compound 6 was yielded after 2'-O-deprotection and 5'-O-DMT protection. For the detailed synthesis refer to Chapter 3.1.1[138].

Following the construction of the nucleobase precursor, the SATE linker needed to be incorporated in the form of a phosphorodiamidite. First, the SATE alcohol **22** was synthesized by an esterification reaction between 5-hexynoic acid and β-mercaptoethanol (Figure 28). Then the alcohol was phosphitylated using bis(diisopropylamino)chlorophosphine to yield SATE phosphorodiamidite **23**.
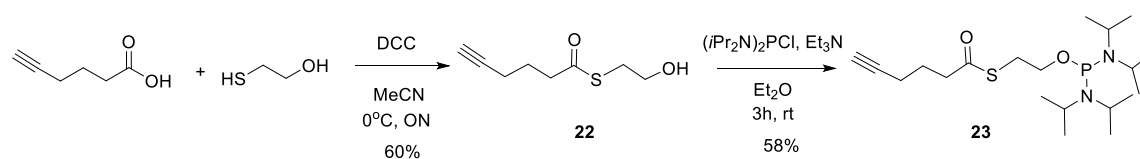

Figure 28. Synthesis of SATE alcohol **22** and SATE phosphorodiamidite **23**.

Results and discussion

Subsequently, the adenosine precursor **24** was synthesized through our straightforward one-pot methodology (Figure 29). Starting from phosphoramidite **9**, the diisopropylamino-group was activated using an excess of BTT activator and then nucleophilically displaced by SATE alcohol **22**. After 1 hour of reaction, *tert*-butyl hydroperoxide was added to oxidize the phosphite (III) to the phosphate (V) and, finally, the DMT protection group was removed with 3% dichloroacetic acid in DCM (Figure 29). The adenosine-SATE phosphotriester **24** was isolated after flash column chromatography at a 84% yield (Figure 29).

The linear dinucleotide **26** could now be constructed. Initially, the guanosine precursor was activated using pyridinium trifluoroacetate and phosphitylated with SATE phosphorodiamidite for the *in-situ* formation of phosphoramidite **25** (Figure 29). Without isolation or purification of **25**, the phosphotriester **24** was added in the mixture alongside BTT to protonate the diisopropylamino-group and promote the 5'-O-coupling. After 1 hour, the guanosine phosphite (III) was oxidized with tert-butyl hydroperoxide. The desired linear intermediate **26** was isolated after the 5'-O-DMT group was removed with 3% DCA in DCM in 59% yield.
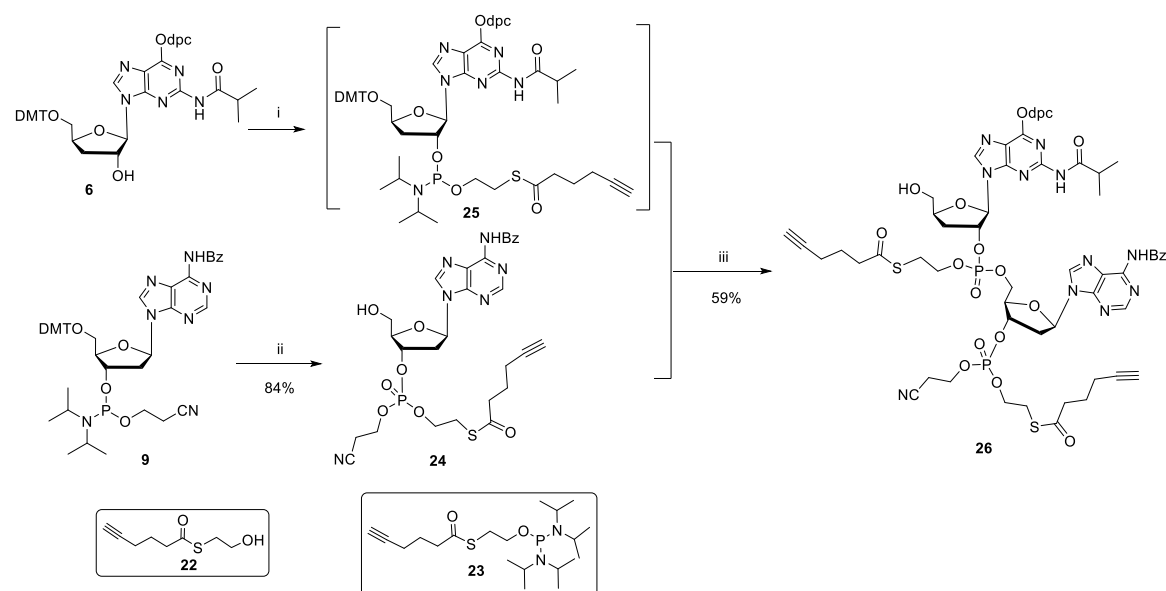

Figure 29. Synthesis of the linear dinucleotide **26**. Conditions: **i.** SATE-phosphorodiamidite **23**, pyr-TFA, DCM, rt, overnight; **ii.** a) SATE-OH, BTT, 1h, rt; b) *t*-BuOOH, 40 min, rt; c) 3% DCA in DCM, 15 min, rt, 84% over 3 steps; **iii.** a) BTT, 1 h, rt; b) *t*-BuOOH, 40 min, rt; c) 3% DCA in DCM, 15 min, rt, 59% over 3 steps.

Next, the O-cyanoethyl protecting group of the adenosine phosphate OH group was cleaved off using *tert*-butyl amine in dry acetonitrile (Figure 30). The obtained linear dinucleotide **27** was then cyclized via macrocyclization with the condensing activator 2,4,6-triisopropylbenzene sulfonyl chloride (TPSCl), along with N-methyl imidazole as the nucleophilic catalyst. The reaction was complete after 24 hours with minimal side products and the protected cyclic dinucleotide **28** was obtained as a P-diastereomeric mixture.

The final step to obtain the desired prodrug **20** was now be the complete deprotection of the nucleobases. Unlike the final deprotection during the synthesis of 2'3'-deoxy-cGAMP, in this case the

use of strongly basic 33% aqueous methylamine or aqueous ammonia - or any other similar reagent, is highly discouraged as it quickly leads to SATE cleavage (data not shown). For this purpose, we needed to utilize proper conditions that not only allow efficient removal of the protecting groups but are also mild enough to be tolerated by the SATE moieties. Hence, the cyclized molecule was dissolved in a mixture of chloroform/methanol (4/1) and zinc bromide was added while the reaction was closely monitored via LCMS. Unfortunately, although N6-benzoyl and O6-diphenylcarbamoyl deprotection were quickly noticed by mass spectrometry, the N2-isobutyryl group remained intact even after 7 days of reaction and the addition of a large excess of zinc bromide.
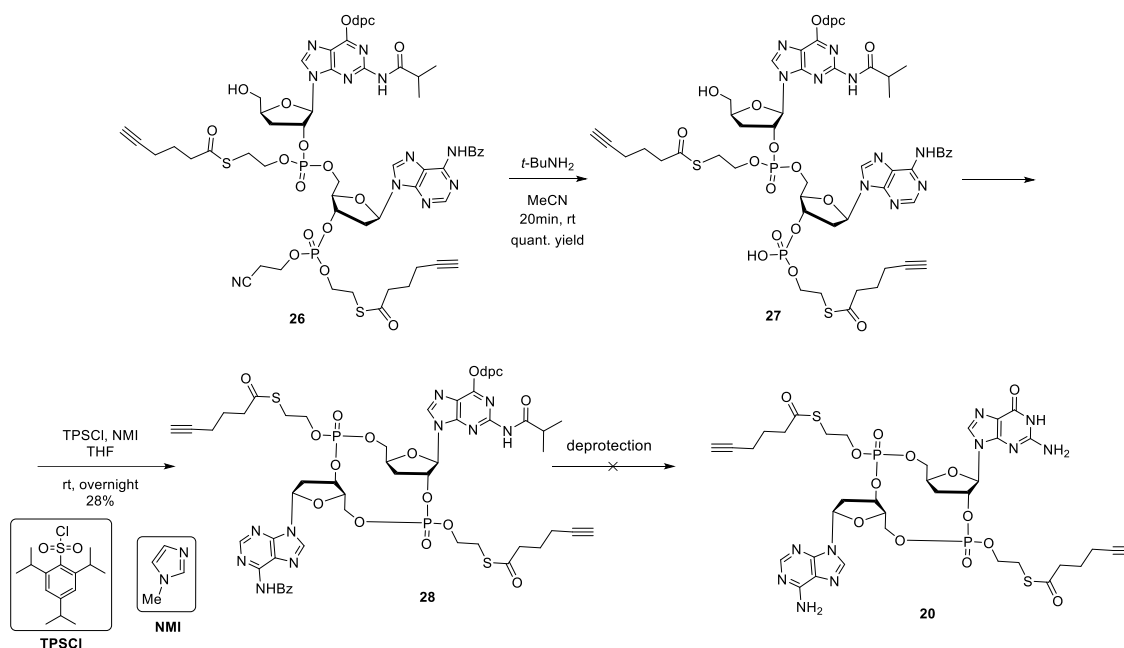

Figure 30. Synthetic route towards 2'3'-deoxy-cGAMP prodrug **20** from linear dinucleotide **26**. Deprotection conditions: 1M ZnBr$_2$ in CHCl$_3$/MeOH (4/1), 7 days. Only the guanosine N2-iBu protected product was obtained.

The above findings indicate that an alternative protecting group strategy needs to be followed. In general, some of the most common protecting groups for the exocyclic amino group are the dimethyformamide (dmf), phenoxyacetyl (PAC), acetyl (Ac) etc., however protection of guanosine nucleosides can be rather challenging. Since the benzoyl group (-Bz) could be effectively cleaved off by the deprotection conditions that we utilized above, we decided to implement it as well on the guanosine 2-amino group.

Thus, the 3'-deoxy precursor **34** needed to be constructed first. The synthesis started from the unprotected guanosine **29** in a one-pot reaction (Figure 31) by first adding trimethylsilyl chloride to protect the ribose OH groups, then the N2 was benzoylated (**30**) and finally the ribose was desilylated by addition of ammonium hydroxide. Then, the 2'-OH was regiospecifically protected using the Markiewicz method. The "clamp" silyl protecting group was inserted at the same time as the 2'-O-TBS protection (**31**) and subsequently removed using hydrofluoric acid in pyridine. After the 5'-DMT protection, the 3'-OH of **32** was removed using a modified Barton McCombie reaction as already shown before for the synthesis of compound **6**. The desirable benzoyl protected 3'-deoxy guanosine **34** was received after 2'-O-TBS deprotection of **33** using TBAF at a 45% overall yield.
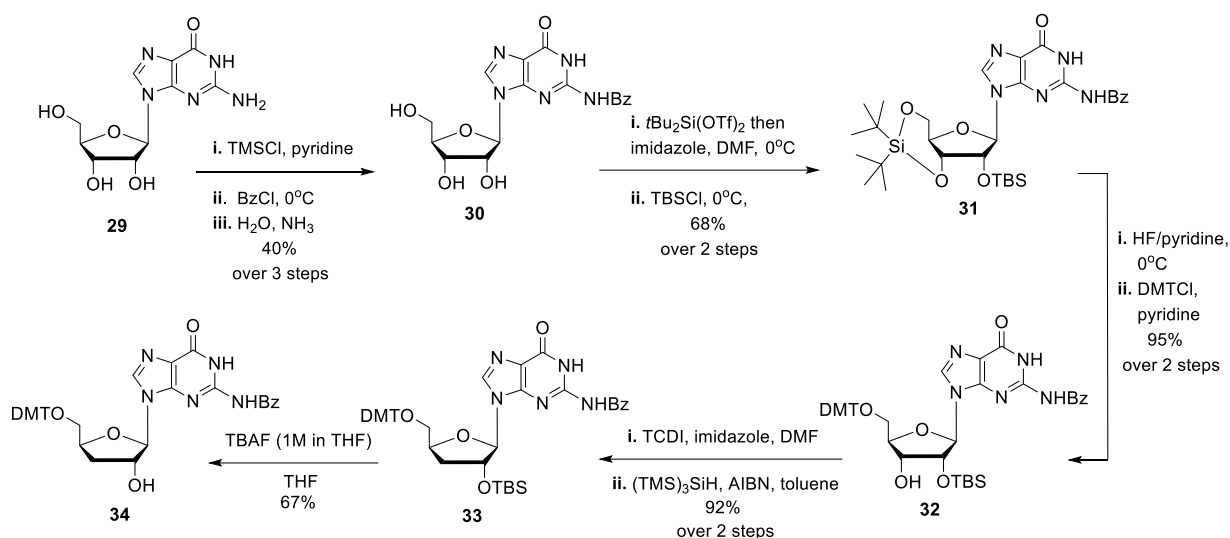
33

Results and discussion

Figure 31. Synthesis of 3'-deoxy-guanosine building block **34** from commercially available guanosine **29**.

Next, following the same procedure as for **6**, the linear compound **36** was formed (Figure 32). Unfortunately, the macrocyclization step could not be successfully carried out, leading to a mixture of undesired isomers. detailed LCMS analysis showed only minimal traces of the expected product.
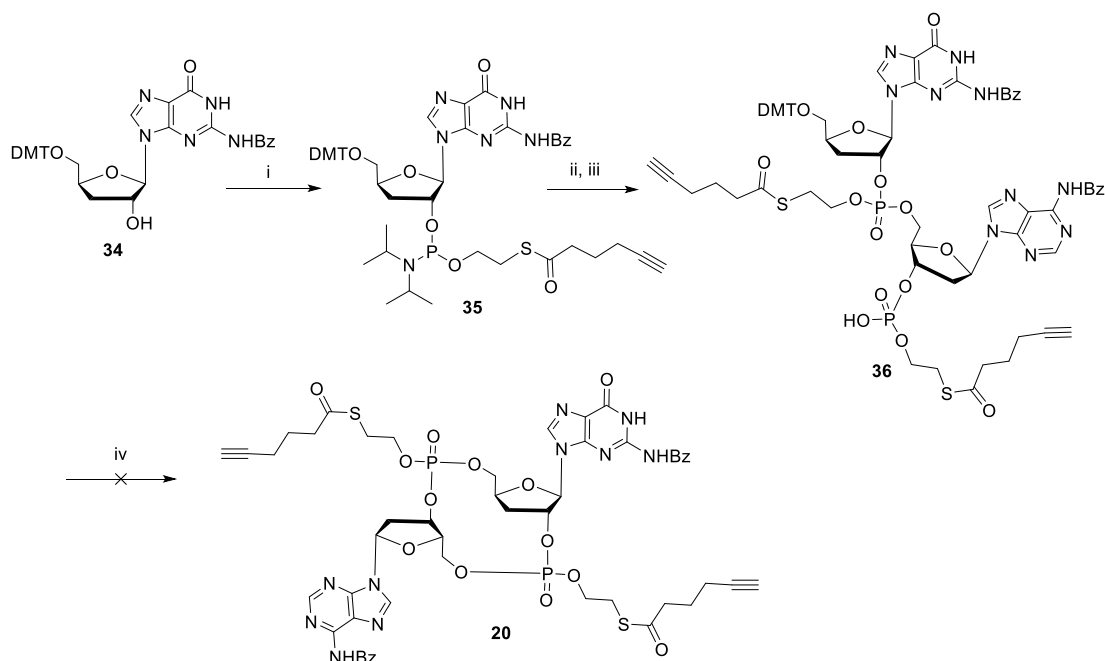

Figure 32. Synthetic route towards 2'3'-deoxy-cGAMP prodrug **20**. Conditions: **i.** SATE-phosphorodiamidite **23**, pyr-TFA, DCM, rt, overnight; **ii.** a) SATE adenosine phosphotriester **24**, BTT, 1 h, rt; b) t-BuOOH, 40 min, rt; c) 3% DCA in DCM, 15 min, rt, 87% over 3 steps; **iii.** t-BuNH$_2$, 20 min, rt; **iv.** TPSCl, NMI, pyridine, rt, overnight.

In order to bypass the problematic final deprotection, we decided to explore the possibility of replacing guanosine with inosine, a different nucleoside that does not contain the exocyclic NH$_2$ group. Along the same lines, *Lioux et al.* previously designed and synthesized novel STING activating CDNs that contained one inosine and one adenosine nucleoside (called cAIMPs) with some of them presenting an

improved type I IFN production in human blood compared to natural cGAMP.[141] With regard to the structure of cGAMP inside STING's binding site, it is clear that guanine's amino group forms strong direct or water mediated hydrogen bonds with residue T263 and with Y163, E260 and Y261 respectively.[19] Considering Lioux's results, it seems that, although those residue interactions of inosine within the binding site are diminished, cAIMP's potency to activate STING is not aggravated in comparison to cGAMP and in some cases their potency is even improved.[141] Along these lines, we hypothesized that an inosine containing CDN (**44**) would be of interest to explore our prodrug theory.

The synthesis started by generating 3'-deoxy-inosine **41** from commercially available inosine **37** (Figure 33). The steps followed were the same as for **34** although along the synthesis we encountered smaller reaction yields and conversion rates due to the noticeably worse solubility of inosine in comparison to guanosine. In spite of that, **41** was synthesized in a 10% overall yield.
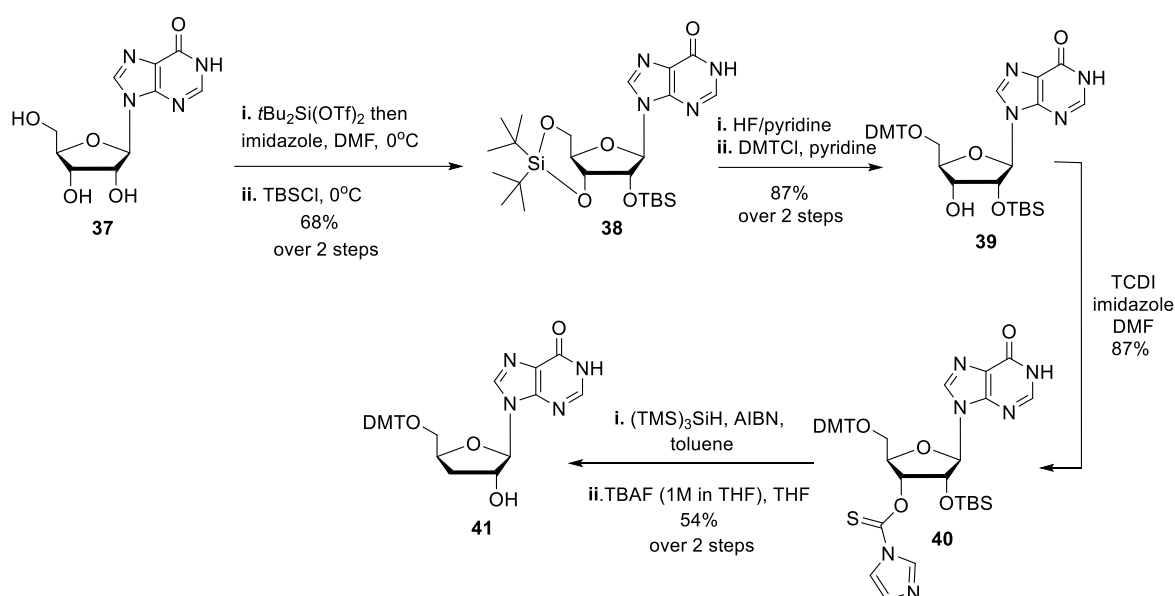

Figure 33. Synthesis of 3'-deoxy-inosine building block **41** from commercially available inosine **37**.

Following the same conditions as for **26**, we managed to in situ generate the inosine SATE-phosphoramidite **42** and then added the adenosine SATE-phosphotriester **24** as a one-pot reaction (Figure 34). The linear compound **43**, although detectable through LCMS, was only formed in a very poor yield alongside many undesirable side products. Additionally, the key linear compound **43** could not undergo the cyclization process using our previous TPSCl methodology. Using the well-known activator 1-(mesitylene-2-sulfonyl)-3-nitro-1,2,4-triazole (MSNT) turned out to be troublesome as well. The poor reactivity towards macrocyclization could be explained by the presence of the inosine acidic lactam type proton on N1 that renders the carbonyl O6 reactive towards our electrophilic activating reagents.
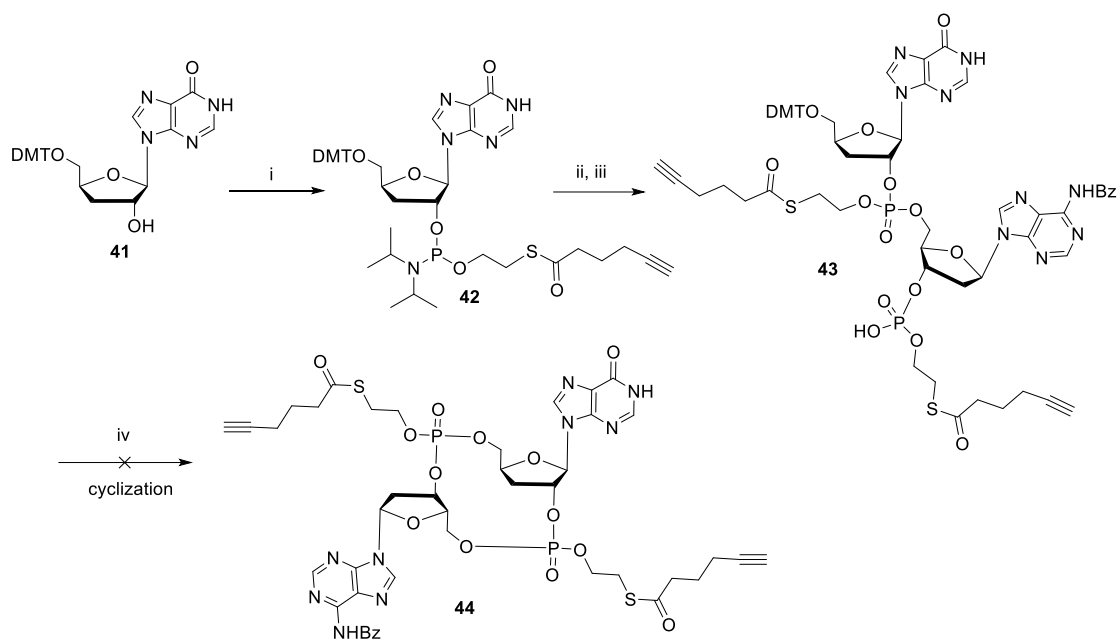
Results and discussion

Figure 34. Synthetic route towards **44**. Conditions: **i.** SATE-phosphorodiamidite **23**, pyr-TFA, DCM, rt, 2h; **ii.** a) SATE adenosine phosphotriester **24**, BTT, 1 h, rt; b) t-BuOOH, 30 min, rt; c) 3% DCA in DCM, 15 min, rt; **iii.** t-BuNH$_2$, 20 min, rt, 25% over 3 steps; **iv.** TPSCl, NMI or MSNT, pyridine, rt, 48hrs.

The synthetic approaches towards prodrugs **20** and **44** were unfortunately not successful. Future investigations towards a more suitable protecting group strategy, as well as different deprotection conditions for the final step, are currently ongoing in our lab.

3.1.3 Conclusions and perspectives

In the first part of this chapter, we synthesized a CDN-based STING agonist whose main scaffold is resembling endogenous cGAMP.[138] Using well-established chemical reactions, we managed to eliminate the 2'- and 3'-OH groups of the riboses of the precursors and we constructed the cyclic dinucleotide 2'3'-deoxy-cGAMP (**1**) while employing a phosphoramidite/phosphotriester based strategy. Compound **1** was obtained in a very satisfactory overall yield and this launches the path to invest in the synthesis of even more modified CDNs using the same methodologies. **1** was then evaluated for its cellular activity by measuring its potency (EC_{50} value) in inducing type I IFN production in a THP-1 Dual monocyte cell line. Notably, in our experimental setup, compound **1** shows better potency at activating STING than natural cGAMP. Next, we employed ITC and nano-DSF assays and measured its binding affinity on STING. We found that, although **1** presents structural alterations that could ameliorate its interaction in the LBD, it nonetheless binds favorably on STING's LBD and it also induces lid-closure which ensures tight binding. This means that **1** is a suitable STING ligand.

Furthermore, compound **1** was tested for its stability against immune evading poxins. Due to the absence of the 2'-OH, **1** cannot be recognized by the poxins and it exhibited complete stability against degradation. In order to evaluate its STING-mediated anticancer activity, **1** was intratumorally injected into a hepatocellular carcinoma murine xenograph where it exhibited promising activity in sustaining tumor size progression compared to natural cGAMP. These results conclude that **1** can act as an effective STING agonist that can presumably be considered as an antitumor drug candidate for cancer immunotherapy or as a vaccine adjuvant.

In the second part of the agonists chapter, we focused on leveraging the advantageous characteristics of 2'3'-deoxy-cGAMP (**1**) by designing a corresponding prodrug. This prodrug (**20**) consisted of **1** as the main active species whose negative charge was concealed by a SATE moiety. By using a prodrug, we were aiming not only to improve the compound's cellular permeability but to also enhance its antitumor activity. Using well established phosphoramidite chemistry, we managed to synthesize the protected cyclic dinucleotide **28**. Despite our efforts, the final deprotection step proved to be challenging and, thus, 2'3'-deoxy-cGAMP prodrug **20** could not be obtained.

In order to circumvent the synthetic challenges, we tried utilizing inosine as an alternative base to guanosine. Previous studies have shown that inosine can effectively be used instead of guanosine as a way to activate STING regardless of the potentially lower binding affinity due to its structural difference. We observed that inosine's O6 is very susceptible to react with the cyclization conditions that we used leading us to the conclusion that the inosine lactam moiety needs to be deactivated against electrophilic reagents. In addition, inosine's disadvantage over guanosine became obvious due to its lower solubility that resulted in worse reaction yields. All in all, inosine prodrug **44** unfortunately could not be synthesized. Future experiments are nowadays taking place in our group towards a cGAMP prodrug and will hopefully address the most suitable protecting group strategy that ensures orthogonality in CDN synthesis.

3.2 STING inhibitors

3.2.1 2'3'-deoxy-cGAMP-PALM: a potential STING palmitoylation inhibitor

3.2.1.a Design of 2'3'-deoxy-cGAMP-PALM

As already discussed in the Introduction, palmitoylation of STING on cysteines 88 and 91 is an essential modification for its downstream signaling. In this part of this dissertation the main focus is the synthesis of a functionalized CDN that can potentially initiate the depalmitoylation of STING as a way to inhibit the production of interferons and other inflammation related signaling messengers. There are 4 thioesterases that are identified as the mammalian depalmitoylation enzymes: acyl-protein thioesterase 1 (APT-1), acyl-protein thioesterase 2 (APT-2), palmitoyl-protein thioesterase 1 (PPT-1) and palmitoyl-protein thioesterase 2 (PPT-2).[142] The two latter ones are lysosomal enzymes, while the formers are primarily cytoplasmic although they can also localize on cellular membranes like the endoplasmatic reticulum and the nuclear membrane.[142] They all belong to the larger lyso-phospholipase family meaning that they hydrolyze ester bonds within lipids, with APT-1 being the most well characterized member. Notably, it is demonstrated to depalmitoylate a number of proteins in cells including G- and Ras proteins.[143] LYPLAL1 (lyso-phospholipase-like 1) is a member of the lyso-phospholypase family and has ~30% identity with APT-1. Although its structure and activity are not fully characterized it is implied that LYPLAL1 can also act as a depalmitoylating enzyme due to its close relation to APT-1 and their conserved catalytic triad. Both enzymes possess a catalytic triad that is comprised of a serine, a histidine and an aspartic acid[144]. Owing to this active triad, they are considered to be serine hydrolases and their mechanism of action is summarized in Figure 35.[142] Briefly, the activated serine residue can nucleophilically attack the carbonyl group of the palmitate. Hydrolysis of the resulting acyl-enzyme intermediate releases the serine to its active state. Although its physiological role is yet unknown, LYPLAL1 has been identified as an acyl-thioesterase that controls BK channel depalmitoylation.[142, 145]
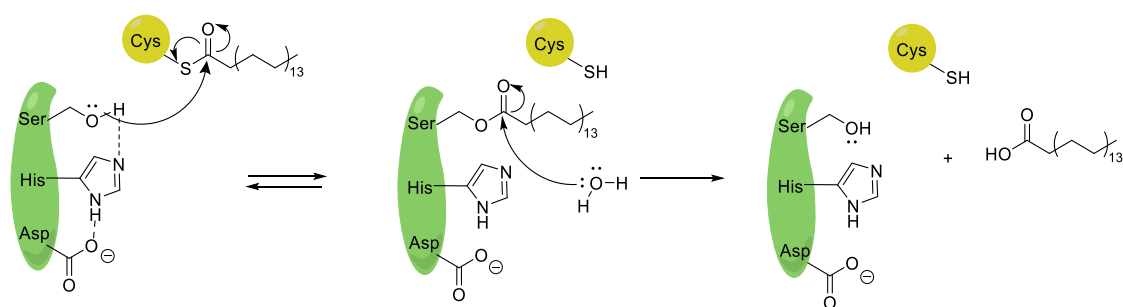

Figure 35. Depiction of the catalytic active site of thioesterases consisting of a serine, a histidine and an aspartic acid and their mechanism of depalmitoylation[142].

Taking everything into consideration, we sought to explore the potential of deploying depalmitoylating enzymes that can selectively act on STING and remove the palmitate tag from cysteines 88 and 91. By doing so, we may be able to target and inhibit aberrant STING activation that leads to autoimmune diseases and chronic inflammation. We designed a CDN-based hybrid molecule (**46**) that consists of 2'3'-deoxy-cGAMP (**1**) which is bonded to a depalmitoylating enzyme activator (recruiter, **45**) via a linker

Results and discussion

(Figure 36). This recruiter was first discovered by *Bernard B. Kok et al.*[146] and was the result of a chemo-proteomic strategy called ABPP (activity-based protein profiling) in order to identify a series of small molecule activators for LYPLAL1[147] aiming to help unveil LYPLAL1's biochemical function as a serine hydrolase. They then applied ABPP-guided medicinal chemistry to optimize a lead into the selective LYPLAL1 activator compound 45, suitable for use in vivo.

Despite their demonstrated inhibitory activity, currently known covalent inhibitors of STING palmitoylation (Chapter 2.6.2), present significant disadvantages. Firstly, some of them are either inactive (C-176, C-178) towards human STING or show lower biological activity (nitro fatty acids).[135, 136] Secondly, cysteine-targeting drugs are non-specific and able to bind to any cysteine residue they can come into contact, leading to many off-target events.[148] Lastly, irreversible binding may reduce the potency of the drug by negating the catalytic cycle and therefore needing higher drug concentrations. Our conjugate is designed in such a way so that it can potentially bypass all of the aforementioned limitations.
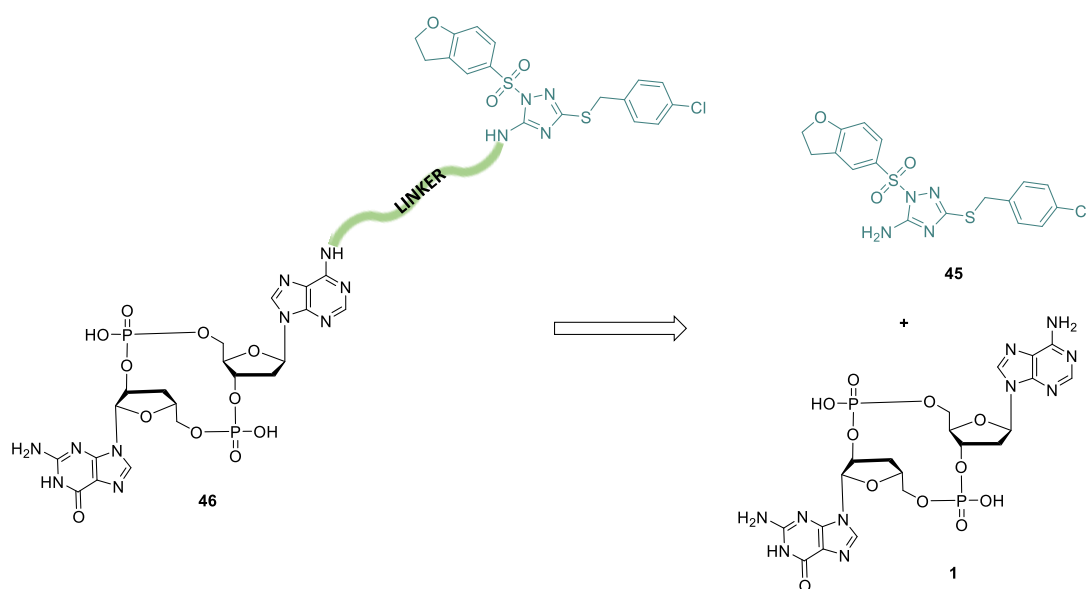

Figure 36. Conceptualization of hybrid compound **46** as a STING inhibitor that promotes STING de-palmitoylation. The molecule consists of 2'3'-deoxy-cGAMP **1** as the CDN that targets and binds on STING and compound **45** (blue) as the activator and recruiter of thio-esterase LYPLAL1.

Our hypothesis is based on the dual action of a small molecule conjugate: Firstly, 2'3'-deoxy-cGAMP (**1**) is a cyclic dinucleotide whose structure closely resembles STING's natural ligand, thus, as demonstrated in Chapter 2.1, shows high STING specificity and considerable binding affinity ($k_D = \pm0.45\mu M$; 2'3'-cGAMP $k_D = 4nM$[138]). That means that **1** will only interact with the STING protein, excluding any possible off-target reactions. Furthermore, the total volume of the ligand binding site area of the apo-STING was calculated to be 952 Å.[149] For this extensive binding area to be fully occupied there is a need for a suitably large ligand. Unlike small molecule inhibitors that may require dimer or trimer formation to occupy the binding cavity of STING, CDNs can efficiently occupy the cavity on their own. Hence, a CDN ligand like **1** can act as a reliable payload of the conjugate. As for the second mode of action, a potent depalmitoylation recruiter is at the same time employed (compound **45**). It is closely bonded to the STING ligand via a flexible linker that allows it to be "swimming" in the cytosol. LYPLAL1, also

residing in the cytosol, can then detect the recruiter and get harnessed by covalently binding **45**. Eventually, active LYPLAL1 can that way come into close contact with Cys91 and 88 and hydrolyze the thioester bond via its catalytic serine residue (Figure 37). S-palmitoylation is a reversible modification[150], which means that even after STING is depalmitoylated it could potentially get palmitoylated again and resume activity. Using our conjugate, the hydrolyzing enzyme is constantly anchored on STING, thus it is able to continuously catalyze cysteine depalmitoylation. That way STING inhibition should be ensured all the way until its lysosomal degradation.
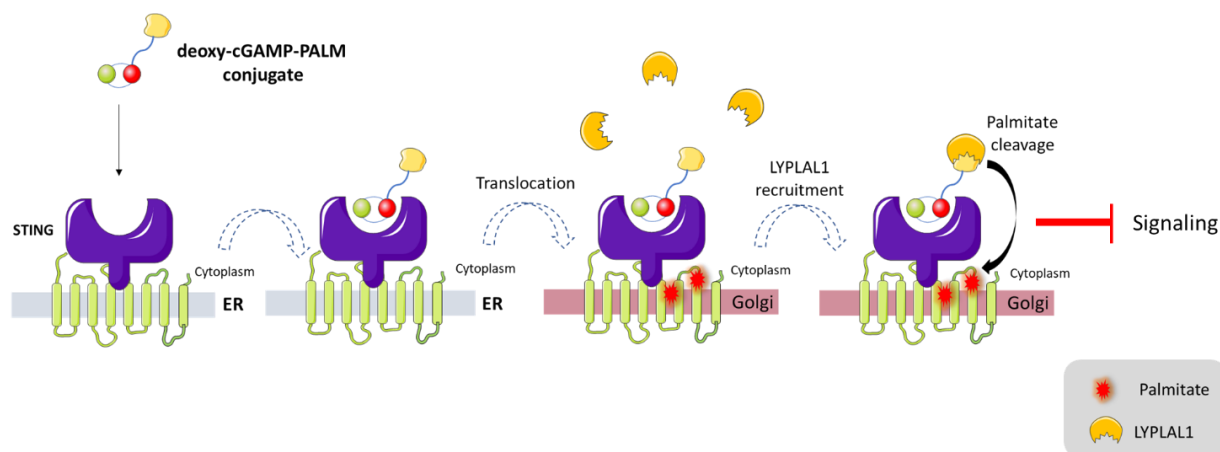

Figure 37. STING signaling inhibition through depalmitoylation, driven by our proposed 2'3'-deoxy-cGAMP-PALM (**46**) conjugate. The conjugate is designed so that its CDN part binds on STING (purple) while the recruiter **45** (yellow) freely accumulates in the cytosol. When the conjugate binds on STING it promotes STING's translocation from the ER to the Golgi compartment where STING undergoes palmitoylation on Cys88 and 91. Then, thio-esterase LYPLAL1 (orange) can detect the recruiter and bind on it. That way, LYPLAL1 can come into close contact with Cys88 and 91, initiate depalmitoylation and inhibit the production of immune signaling.

3.2.1.b Synthesis of 2'3'-deoxy-cGAMP-PALM

Having envisioned the main structure of the conjugate, one challenging task was the design of a suitable linker. Linkers play a very crucial role in the design of bioactive molecules[151]. Their design should be focused on enabling flexibility but also optimizing the ligand's interactions within the active site. For this project, a six membered alkyl chain was used as the linker, bonded with the adenine N6 of **1** to form **47** while the recruiter **45** could be attached to a succinyl acyl chain via its exocyclic amino group (**48**). Eventually, the two precursors could be conjoined via a stable amide bond to form the final linked conjugate **49** (Figure 38). Evidently, these two linkers were designed so that they allow practical advantages in term of availability and easy synthetic accessibility.

In practice, precursor **47** could be synthetically accessed using the 3'-deoxy-O6-dpc-N2-isobutyryl protected guanosine phosphoramidite **50** (synthesis shown in Chapter 3.1.1) that is coupled with the N6-tert-butyl-hexyl-carbamate adenosine phosphotriester **51**. Meanwhile, precursor **48** could be synthesized by reacting **45** with succinic anhydride.
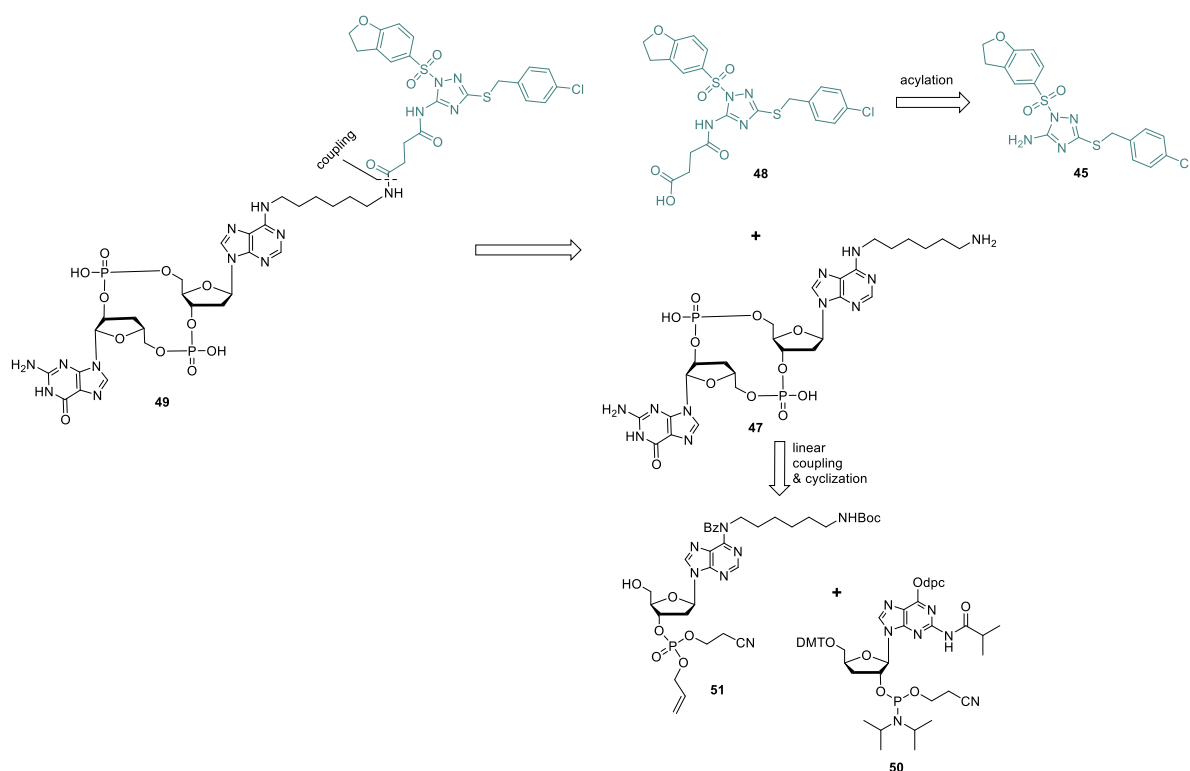
Results and discussion

Figure 38. Retrosynthetic analysis of compound **49**.

Therefore, **45** was firstly synthesized by reacting 3-amino-5-mercapto-1,2,4-triazole **52** with 4-chloro benzylbromide **53** in the presence of triethylamine (Figure 39). Then, compound **54** was sulfonylated using dihydrobenzofuran-5-sulfonyl chloride **55** and triethylamine to afford **45**. To verify that the exocyclic amino group was sulfonylated and not any other nitrogens of the triazole ring we analyzed the spectroscopic data of **45**. Indeed, the presence of a broad single peak that integrates for two hydrogens (for -NH$_2$) versus two distinguishable single peaks (for two -NHs each integrating for one hydrogen) led us to ensure the correct structure. Thus, **45** was afforded in 93% yield.
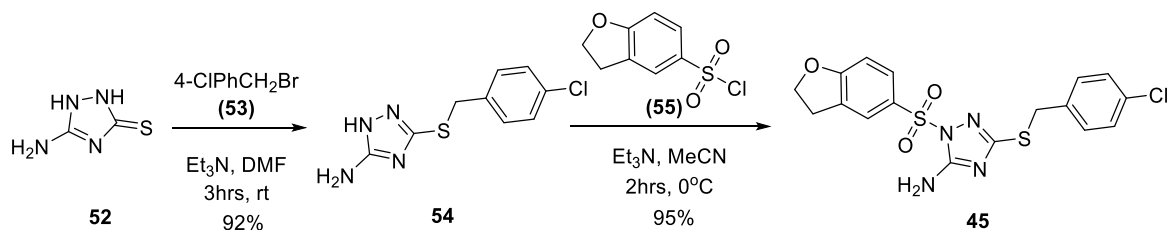

Figure 39. Synthesis of compound **45**.

For the next step, we tried to couple **45** with succinic anhydride (Figure 40). Unfortunately, all the attempts were unsuccessful even with the use of a wide variety of coupling reagents and conditions widely used in amide couplings (Table 1). Specifically, when EDC·HCl, DCC or DMTMM were used LCMS

Results and discussion

monitoring of the reaction showed no conversion, even under reflux and prolonged reaction times. Meanwhile, using HATU catalyzed by HOBt only led to the corresponding guanidinium side product. Attempts to use pyridine as solvent and bulkier or high excess of other non-nucleophilic bases like DBU, TEA, DIPEA were also not successful.
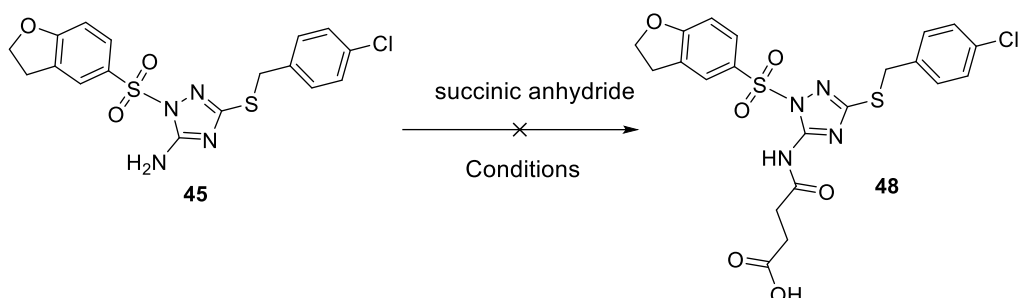

Figure 40. Succinic anhydride coupling with precurson **45** was unsuccessful.

	Reagents	Solvent	Time/ °C	Product (48)
1.	-	pyridine	on/115°C	n.d
2.	DIPEA (10.0eq), succinic anh. (8.0eq)	THF	24hrs/66°C	n.d
3.	EDC·HCl (1.1eq), HOBt (1.2eq)	DMF	48hrs/0°C to rt	n.d
4.	HATU (3.5eq), TEA (7.0eq), HOBt (1.7eq)	DMF	on/rt	n.d [a]
5.	DCC (1.0eq), DMAP (1.0eq), HOBt (0.1eq)	DCM	on/rt	n.d
6.	pyBOP (1.5eq), DIPEA (2.0eq)	DMF	on/rt	n.d
7.	DMTMM (1.5eq), DIPEA (5.0eq)	NMP	on/80°C	n.d

Table 1. Reaction condition screening for the succinic anhydride coupling. 1.5 equivalents of succinic anhydride were used for each reaction unless otherwise stated; on: overnight reaction; n.d: not detected; DMAP: 4-dimethyl-aminopyridine; DIPEA: diisopropylethylamine; EDC.HCl: 1-ethyl 3-(3-dimethylaminopropyl) carbodiimide; HOBt: hydroxybenzotriazole; HATU: Hexafluorophosphate azabenzotriazole tetramethyl uranium; TEA: triethylamine; DCC: N,N'-dicyclohexylcarbodiimide; pyBOP: benzotriazol-1-yloxytripyrrolidinophosphonium hexafluorophosphate; NMP: N-methyl-2-pyrrolidone; DMTMM: 4-(4,6-dimethoxy-1,3,5-triazine-2-yl)-4-methyl-morpholiniumchloride.

[a] only the guanidinium side product was detected

To overcome these synthetic obstacles the acylation reaction was tried out using several different electrophiles that would not compromise our design vision (Figure 41). Various carboxylic acids, like malonic acid **56**, 3-chloropropanoic acid **57** and 4-pentynoic acid **58** and also active acyl chlorides, like methyl malonyl chloride **59** and NHS-esters like NHS-Boc-glycine **60** did not lead to the desired products. This is likely attributed to the highly electron deficient triazole ring which makes the exocyclic amino group less nucleophilic. Nonetheless, chloroacetyl chloride **61** turned out to be a very good solution in combination with diisopropylethylamine, managing to afford acetamide **62** in a good yield after reacting overnight.
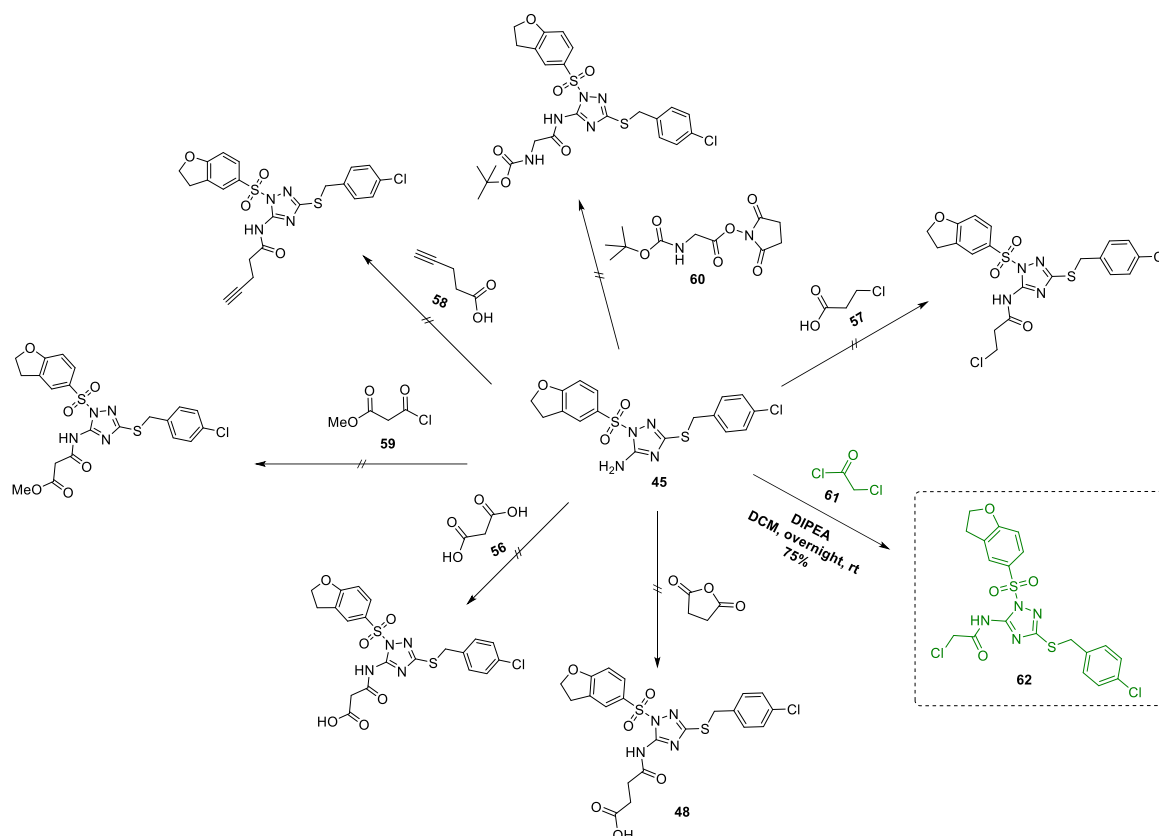
Figure 41. Synthetic challenges for the acylation of compound **45**. Chloroacetyl chloride **61** resulted in successful acylation using DIPEA in DCM.

Next, we tried to construct the dinucleotidic anchor **47** of the conjugate. As mentioned above, first we needed to synthesize the linker-modified adenosine **51**. Compound **51** was easily accessible starting from commercially available N6-benzoyl-5'-O-DMT-2'-deoxy adenosine **63**. We initially protected the 3'-OH group using tert-butyldimethylsilyl chloride (**64**) (Figure 42). Then the alkyl linker was attached on the nucleophilic N6-nitrogen via a *Mitsunobu* reaction using *t*-butyl(6-hydroxyhexyl)carbamate in a solution with triphenylphosphine and diethyl azodicarboxylate (DEAD) (**65**). After flash column chromatography to separate the triphenylphosphine oxide side product, compound **65** was isolated. Finally, treatment with TBAF for 1 hour removed the silyl protecting group yielding **66** in an excellent yield.
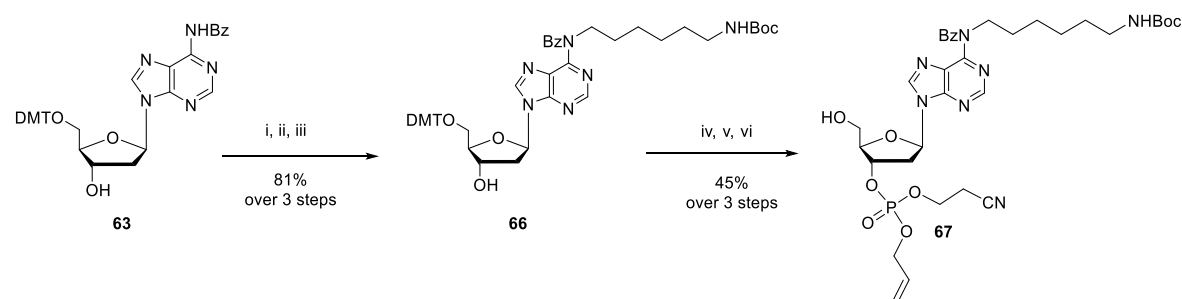

Figure 42: Synthesis of phosphotriester **67. i.** TBSCl, imidazole, pyridine, rt, overnight, 87%; **ii.** 6-(Boc-amino)-1-hexanol, DEAD, PPh₃, THF, rt, 76%; **iii.** TBAF, THF, 1h, 80%; **iv.** 2-cyanoethyl *N,N,N',N'*-tetraisopropyl phosphorodiamidite, pyr-TFA, DCM, 1h, rt; **v.** BTT activator, allyl alcohol, 40min, rt; **vi.** *t*-BuOOH, 30 min, rt; vi. 3% DCA in DCM, 15min, rt.

Results and discussion

Then, **66** needed to be converted to the corresponding phosphotriester **67**. This synthetic procedure was done following our group's well established one-pot methodology. Briefly, **66** was first treated with pyridinium trifluoroacetate and 2-cyanoethyl *N,N,N',N'*-tetraisopropylphosphorodiamidite for 1 hour to form the intermediate phosphoramidite (Figure 42). Then, BTT activator was added to protonate the diisopropylamino group of the phosphoramidite and then allyl alcohol was added to protect the phosphite species. After 40 minutes of stirring, P(III) was oxidized to P(V) using *tert*-butyl hydroperoxide for 30 minutes. Finally, the DMT group was removed with a solution of 3% DCA in DCM. The final phosphotriester **67** was isolated in 45% yield over 4 steps.

For the generation of the linear compound **69** we utilized the already synthesized 3'-deoxy guanosine phosphoramidite **68** (Chapter 3.1.1, Figure 43). After careful drying, **67** and **68** were diluted in dry acetonitrile where the phosphoramidite diisopropylamine group was activated using BTT, following coupling with the 5'-OH of the phosphotriester to occur after 1 hour. Then, after oxidation of the phosphite with tert-butyl hydroperoxide, the 5'-O-DMT group was removed with 3% DCA in DCM and the linear compound **69** was isolated after flash column chromatography in a 62% yield over 3 steps.
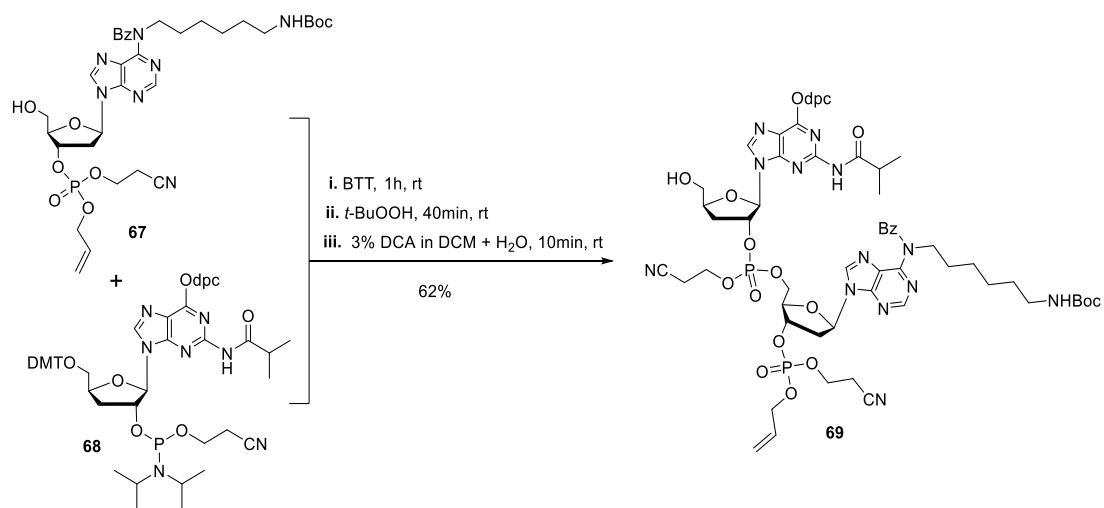

Figure 43. Synthesis of linear precursor **69** from N2-functionalized phosphotriester **67** and 3'-deoxy-guanosine phosphoramidite **68**.

The next reaction was the removal of the allyl protecting group with NaI in refluxing acetone (Figure 44). This step was proven to be a bigger challenge than expected as these conditions are also suitable for N-Boc deprotection. Thus, while closely monitoring the reaction via LCMS, we noticed that there was at least 30% of N-Boc deprotection of the final product taking place, even after only 1 hour of reaction. Finally, after complete conversion of the starting material, we ended up receiving a mixture of NH-Boc protected and free -NH₂ isomers (**70, 71**). Unfortunately, the mixture was unable to be separated via HPLC. Additionally, trying to use the mixture as is to proceed to the macrocyclization led to more difficulties as the strongly electrophilic sulfur atoms of the cyclization reagents (1-(2-Mesitylensulfonyl)-3-nitro-1*H*-1,2,4-triazole (MSNT) and TPSCl straight off started sulfonylating the free -NH₂ of the **71** N6 linker even at very high dilutions. The formation of the end product **49** could not be clearly shown nor could it be detected via high-resolution mass spectrometry.
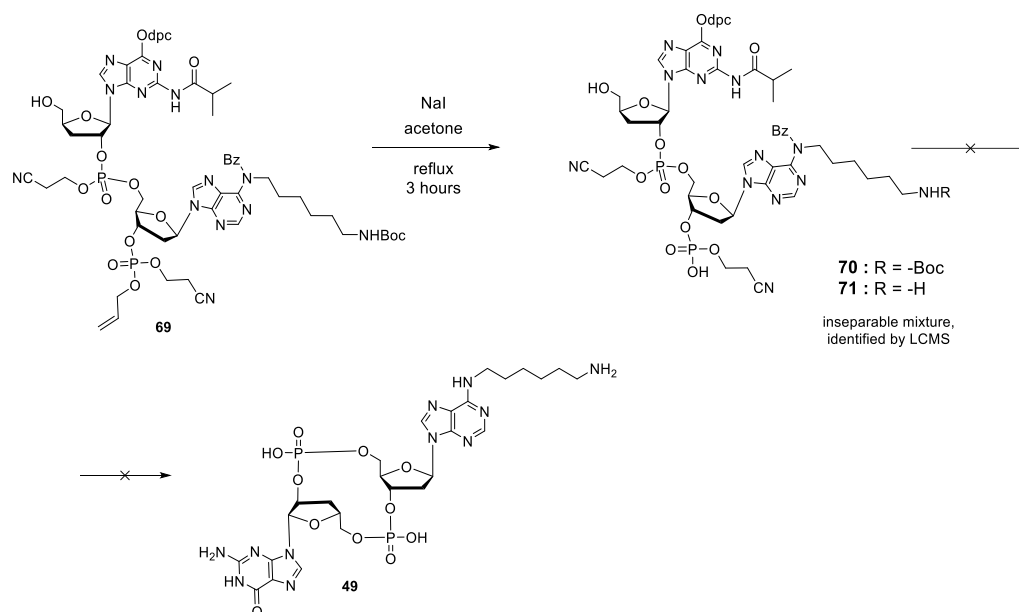
Results and discussion

Figure 44: O-cyanoethyl deprotection of **69** led to an inseparable mixture of allyl deprotected precursors **70** and **71**.

The synthetic approaches for **49** were not successful. Possible solutions for the aforementioned obstacles could be the use of a different protecting group strategy for the NH_2 group of **66** or utilizing a phosphonate adenosine intermediate instead of a phosphotriester so that no deprotection step is needed. But a simpler and less time-consuming solution was the complete redesign of the linker moiety. Therefore, we decided to switch to a PEG3 linker that bears a free terminal alkyne. The linker can conjugate on the CDN anchor **73** which in turn can ligate with the recruiter **72** through a selective Cu(I)-catalyzed click reaction (CuAAC), as seen in Figure 45, in order to form the final compound **75**.
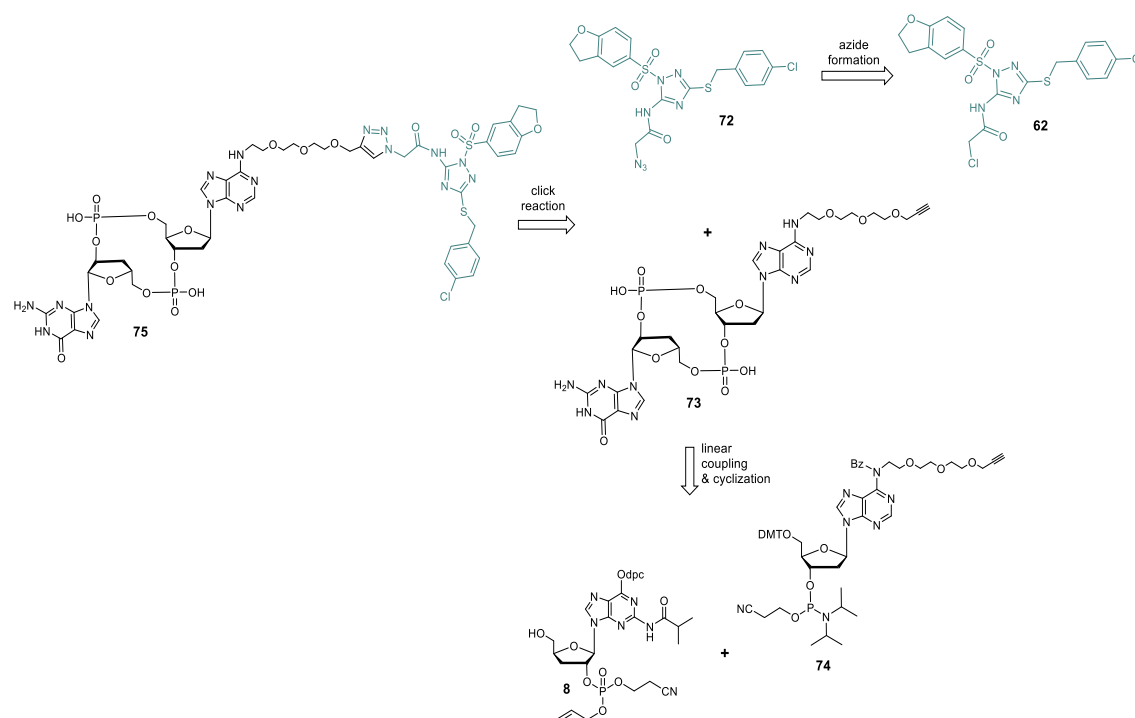

Figure 45. Retrosynthetic analysis of compound **75**.

PEG linkers are extensively used in small molecule chemistry, especially for the synthesis of bioactive Proteolysis Targeting Chimeras (PROTACs), due to their exceptional metabolic stability and biological compatibility.[151] Moreover, they offer easy synthetic access and their lengths can be easily modified to fine-tune the physical properties of the molecule, including solubility, lipophilicity and cell permeability. By introducing clickable groups, we ensured that the coupling of our precursors (compound **45** with 2'3'-deoxy-cGAMP) will be efficient and 100% chemo-selective.[152] In addition to that, the resulting triazole can offer biological stability to the whole structure.[153]

Compound **75** can be synthesized starting from the PEG3-phosphoramidite **74**. The PEG3 linker **77** needed to be synthesized first, starting from triethyl glycol **76** which was converted to an alkoxide using sodium hydride and then nucleophilically attacked by propargyl bromide (Figure 46). Then, utilizing commercially available adenosine phosphoramidite **9**, the PEG3 linker was attached on N6 via a *Mitsunobu* reaction (Figure 47).
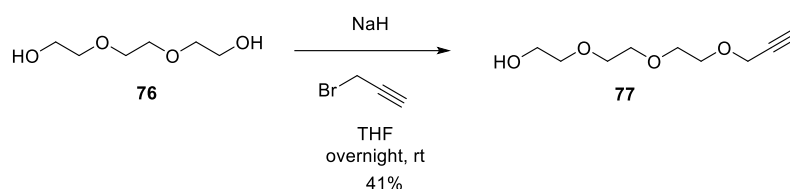

Figure 46. Synthesis of PEG linker **77** functionalized with a terminal alkyne.
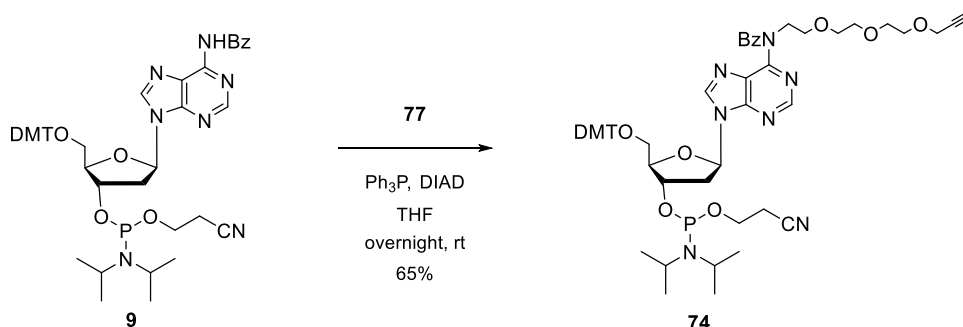

Figure 47. Synthesis of PEG3-functionalized phosphoramidite **74** using a *Mitsunobu* reaction starting from commercially available adenosine phosphoramidite **9**.

Next, guanosine phosphotriester **8** (for synthesis refer to Chapter 3.1.1) was coupled with phosphoramidite **74** as previously described using BTT activator over the course of 1 hour and then tert-butyl hydroperoxide was then added to oxidize the phosphite. After 40 minutes, the DMT group was removed with 3% DCA in DCM and the resulting linear compound was purified via flash column chromatography to afford **78** in 62% yield. To remove the allyl group from the phosphotriester, **78** was dried by co-evaporation with pyridine and subsequently dissolved in dry acetone where sodium iodide was added. The mixture was refluxed at 55°C for 3 hours when LCMS control showed complete conversion to **79**. After evaporation of the solvents, the allyl deprotected **79** was washed with cold acetone to remove any remaining sodium iodide and precipitated from a mixture of ethyl acetate/iso-hexane to afford a yellow solid as a mixture of 4 P-diastereomers. The compound was characterized by high-resolution mass spectrometry.
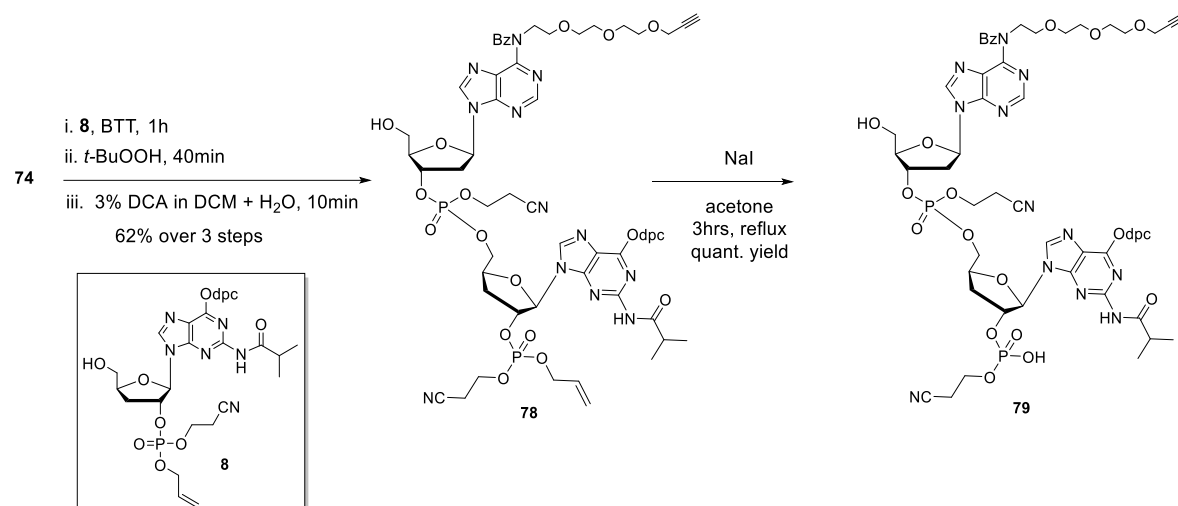
Figure 48. Synthesis of the allyl deprotected linear precursor **79**.

The final macrocyclization was performed in the presence of the nucleophilic activator MSNT in a large excess, diluted in dry pyridine, over the course of 24 hours (Figure 48). LCMS monitoring showed complete conversion of **79**, with no side product formation and, again, the product **80** was received as a mixture of P-diastereomers which was used without further purification for the next step. To obtain the final product **73** all protecting groups were removed using 33% methylamine in absolute ethanol. After 3 hours of stirring **73** was precipitated from cold acetone, dried and purified by reversed-phase HPLC. Overall, this essential building block was synthesized in a 8% overall yield over 7 steps and its structure was characterized by NMR spectroscopy and high-resolution mass spectrometry (Figure 50).
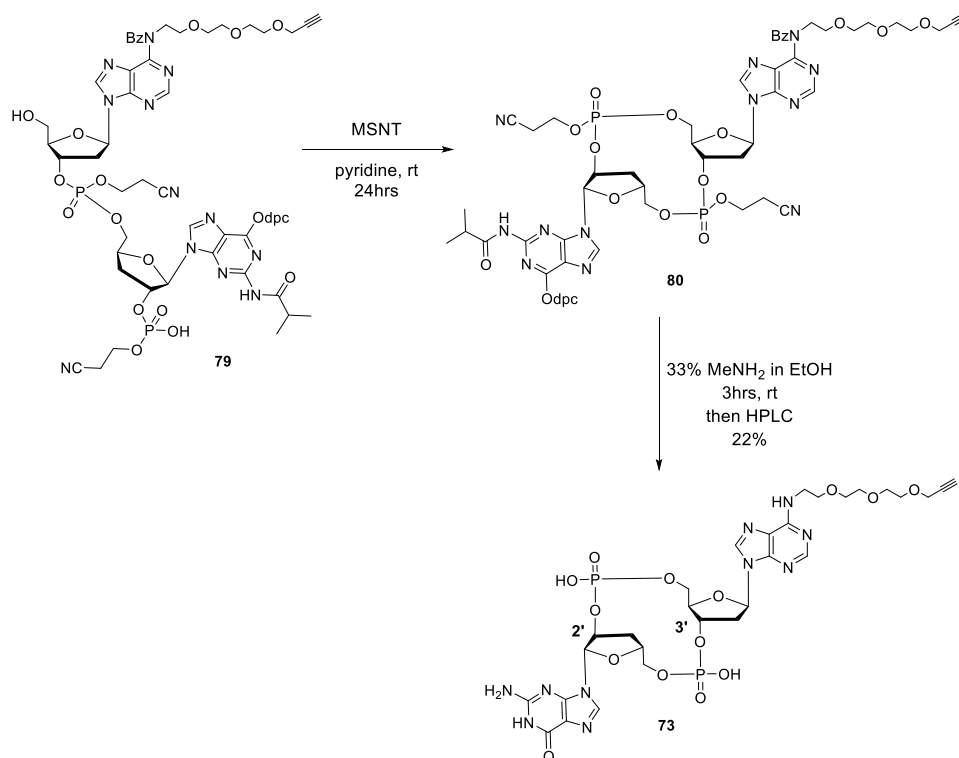
Figure 49. Synthesis of final CDN building block **2'3'-deoxy-cGAMP-PEG3 (73)** from the linear dinucleotide **79**.

Results and discussion
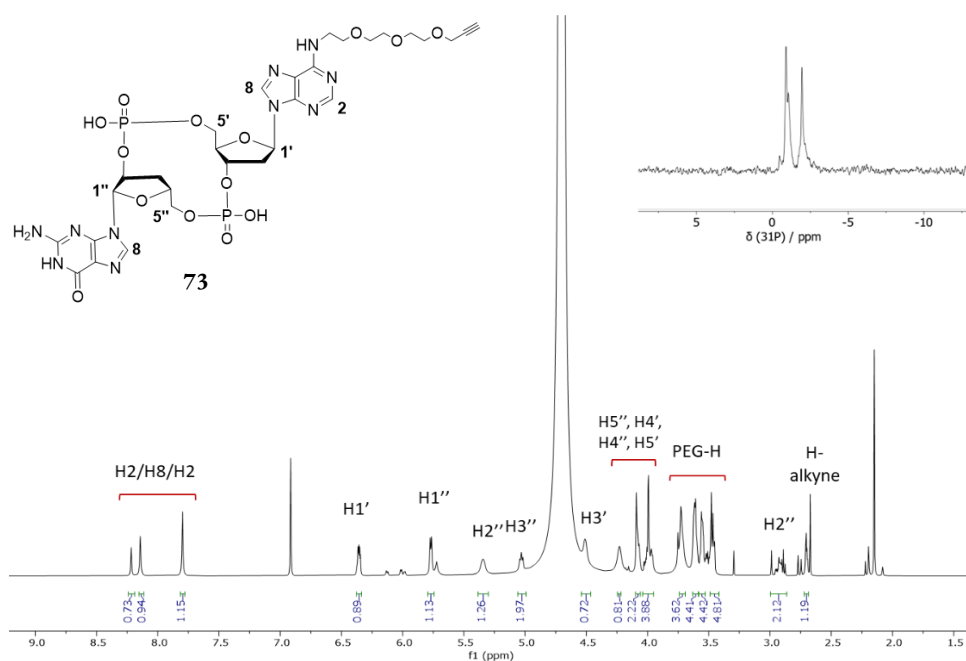
Figure 50. ^{1}H- and ^{31}P-NMR of compound **73**.

As previously shown, precursor **62** can be synthesized by acylating LYPLAL1 recruiter **45** using chloroacetyl chloride with diisopropylethylamine in DCM. Thus, **72** can be constructed by nucleophilic substitution of the chloride with azide using an excess of sodium azide (NaN$_3$) in DMF (Figure 51). This reaction was successful, although due to the good leaving group nature of the sulfonyl dihydroxybenzofurane group we also received the substitution side product **81** in a 30% conversion ratio. Fortunately, we were able to separate the two compounds via preparative reversed-phase HPLC and, thus, isolate the desired product **72** in 20% yield.
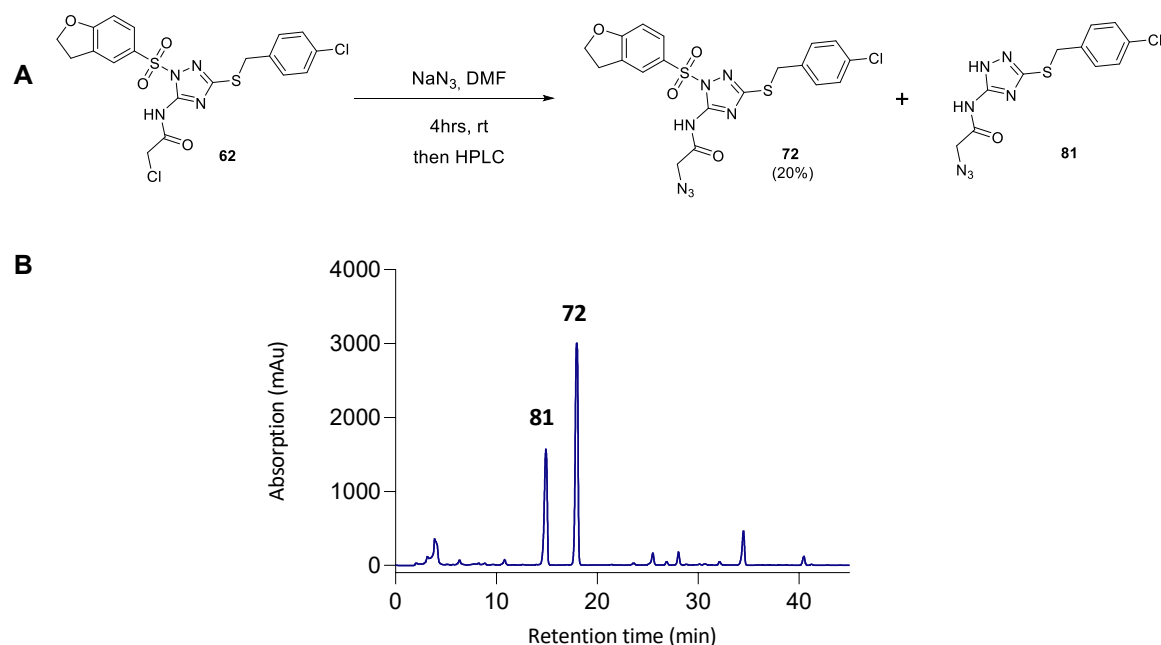
Figure 51. A) Synthesis of compound **72**. B) Separation of **72** and **81** via reversed-phase HPLC (30% → 70% Buffer B over 45 minutes, t$_R$ = 15min, Buffer A = 0.1% TFA in H$_2$O, Buffer B = 0.1% TFA in MeCN).

Results and discussion

The click reaction to ligate the recruiter **72** with the CDN **73** was performed in a mixture of H_2O/DMF due to the low solubility of the recruiter in water (Figure 52). Under inert atmosphere and anaerobic conditions, $CuSO_4$ was used as the copper source and sodium ascorbate was added to function as the Cu(II) reductant. Meanwhile, addition of Cu(I)-binding ligand THPTA was crucial for the acceleration of the reaction and to protect the Cu(I) from oxidation. After 5 hours of reaction at room temperature, LCMS monitoring showed complete conversion of **73**. The crude mixture was immediately purified via reversed-phase HPLC to finally afford 2'3'-deoxy-cGAMP-PALM **75** in 41% yield. As it became obvious during the reaction, side product **82** was also formed alongside **75**. Evidently, this is due to the instability of the recruiter that has a big tendency of eliminating the sulfonyl dihydroxybenzofurane group in these conditions. Luckily, side product **82** could be separated during HPLC (Figure 53) and compound **75**'s structure could be verified by NMR spectroscopy, HRMS and MALDI-TOF.

Figure 52. Click reaction to synthesize final compound 2'3'-deoxy-cGAMP-PALM (**75**).

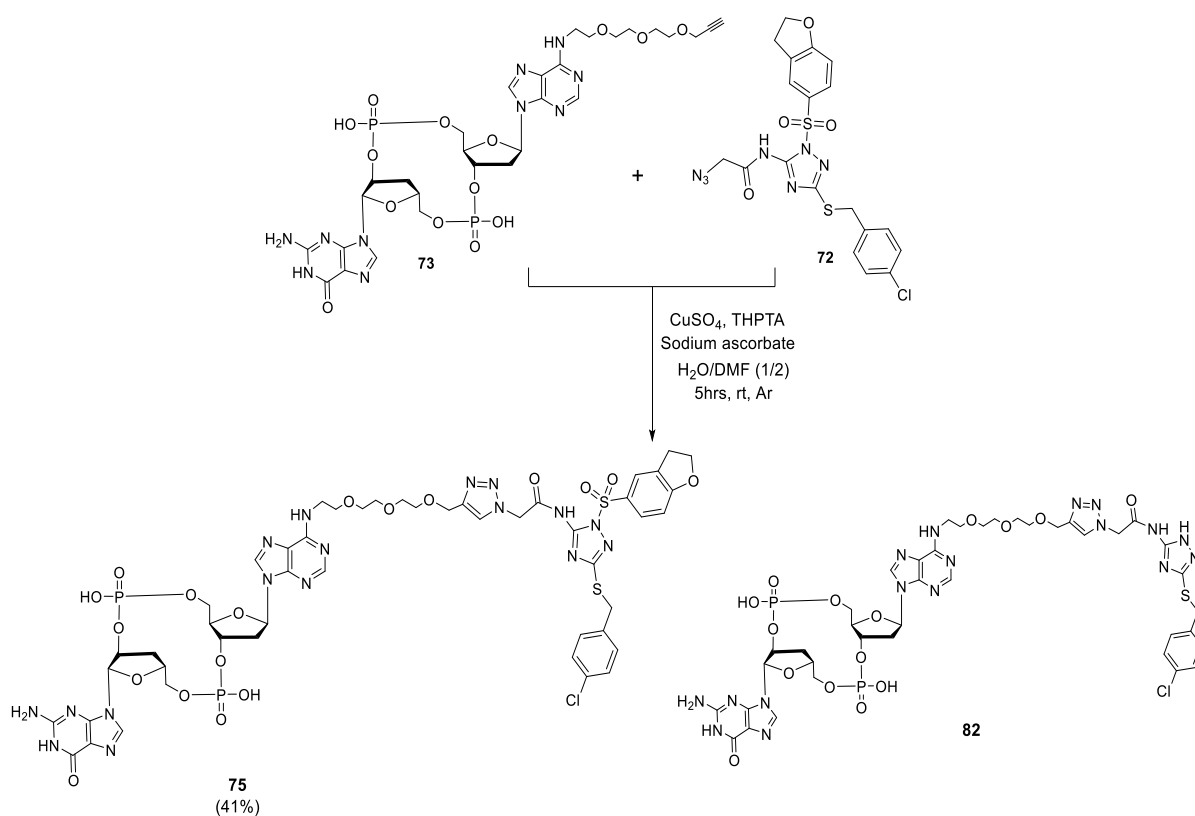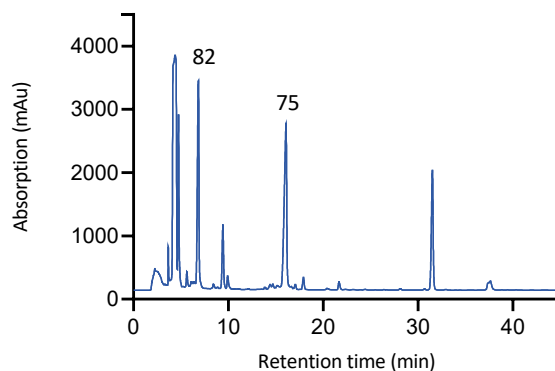**Figure 53.** Reversed-phase HPLC purification of mixture of **75** and **82** (30% → 70% Buffer B over 45 minutes, t_R = 15min, Buffer A = 0.1% TFA in H$_2$O, Buffer B = 0.1% TFA in MeCN). Side product **82** was simultaneously received in an almost 1/1 ratio to **75**.
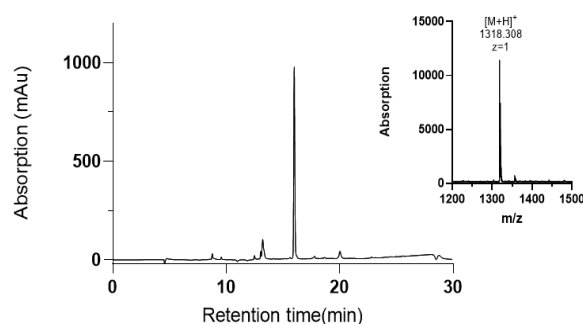
Figure 54. Analytical HPLC chromatogram of **75** ((0-40% TEAA buffer B; buffer B = 0.1M NEt$_3$/HOAc in 80% MeCN; absorption at 260nm) and MALDI-TOF analysis of compound **75**.

3.2.1.c Stability studies

In order to be able to fully assess whether compound **75** can act in vitro as a bioactive compound we primarily needed to test its overall stability. Therefore, we incubated 1 nmol of compound **75** in RPMI cell medium at 37°C over the course of 24 hours. Aliquots were then collected for 5 time points (t0, 2, 4, 8 and 24 hours), freeze-dried and resuspended in a suitable buffer. In collaboration with *Dr. Matthias Heiß*, the samples were measured via QExactive mass spectrometry where their exact mass was identified and their relative abundance was quantified through comparison of the signal integrals between the samples. Compound **1** was used as a positive control since we have already established that it is stable under similar conditions (Chapter 3.1.1).

These results show that although it is less stable compared to **1**, compound **75** can retain its structural integrity for at least the first 8 hours of incubation (Figure 55). With the aid of mass spectrometry, we could also pinpoint that **82** is simultaneously accumulating after 24 hours of incubation.

Results and discussion

The ultimate intention of this project is to incubate STING reporter THP-1 cells with **75** in order to examine whether STING-mediated immunity activation is impaired. A direct way to detect this is through the quantification of IFNs or other pro-inflammatory cytokines produced by the cells, for example IL-6, CXCL-10 etc. For that purpose, the cells need to first be pre-treated with the compound for 4 to 6 hours and then stimulated with cGAMP or other activator agent for 8 to 12 hours to trigger an immunological response.[131, 135, 154] The cellular supernatant can then be analyzed for its cytokine content using an ELISA assay or RT-qPCR. If the amount of IFNs and/or cytokines is overall decreased, it signifies that **75** could potentially act as an off switch for immune signals. Overall, our stability studies indicate that compound **75** is adequately stable for cells to be treated with and to still produce a reliable immune response under physiological conditions in our experimental setting.

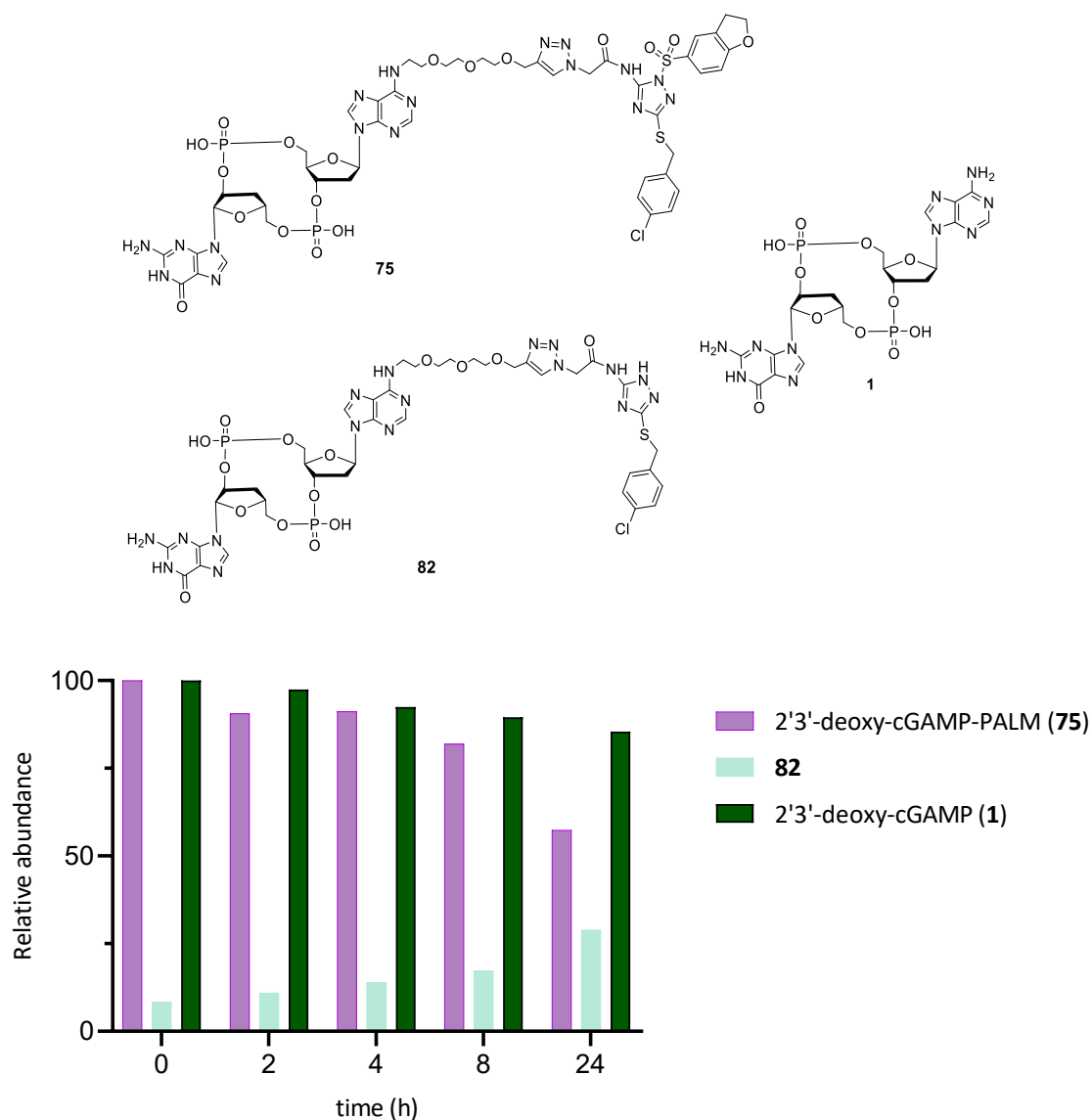**Figure 55.** Stability study of compound **75**. Incubation with $100\mu M$ of **75** and $100\mu M$ of **1** in RPMI cell medium; mass spectrometry: $10\mu M$ aliquots in $5mM$ NH_4OAc buffer, pH 4.9. Data acquired in collaboration with *Dr. Matthias Heiß*.

3.2.2 CDN-folate conjugates: two novel cell permeable analogues

3.2.2.a Design of CDN-folate analogues 83 and 84

Aiming to enhance efficiency, potency and bioavailability, efforts to design and synthesize improved CDNs as potential drug candidates mainly focused on structural modifications.[26, 155] As already discussed, cyclic dinucleotides are polar molecules whose anionic nature can lead to restricted bioavailability in the cytosol. Clearly, due to their polarity, passive diffusion of CDNs in the cells is inadequate. Apart from the prodrug strategy that was discussed on Chapter 3.1.1, most synthetic CDNs rely on augmented molecular concentrations and/or the use of permeabilization reagents like digitonin in order to be able to cross the cell membrane and reach the cytosol.[103, 122] Undoubtedly, the mediation of a transporter or a channel might be the missing link that can presumably lead to improved transmembrane transportation and biological action. In the current part of this dissertation, our CDN design strategy is not to mask the negative charge of the molecules but to target their selective and targeted cell import through the SLC19A1 transporter (Figure 56).
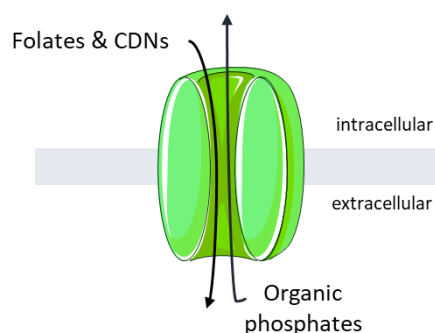
Figure 56: Depiction of the folate transporter SLC19A1. Folates and certain CDNs enter the cell via this transporter while organic phosphates are concurrently being exported.

SLC19A1, also known as reduced folate carrier 1 (RFC1), is a transporter of folates, reduced folates like folinic acid and 5-methyltetrahydrofolate (5-MTHF) and structurally similar antifolates, like methotrexate.[156, 157] Importing of folate is linked to the export of organic phosphate anions (Figure 57), while folates are dietary sourced and essential for the organism to ensure normal metabolism, function and tissue repair.[156] Recently, CRISPR-based genome-wide screens led to the identification of SLC19A1 as a major CDN transporter in human monocytic cell lines.[42, 43] Notably, different cell types like epithelial cells were shown to not rely on SLC19A1 import, suggesting that there are different mechanisms of CDN uptake in every cell type. SLC19A1 was shown to directly import cGAMP but also bacterial (3'3'-cGAMP) and synthetic CDNs (2'3'-cAAMP, 2'3'-cG^{S}A^{S}MP, 3'3'-cAAMP, 2'3'-cA^{S}A^{S}MP), therefore it plays a key role in immunity activation, inflammation and cancer immunotherapy.[1, 42] Furthermore, SLC19A1 is the target transporter in cancer treatment in the clinic as it transports the anti-tumor drugs methotrexate and pemetrexed.[156, 158]
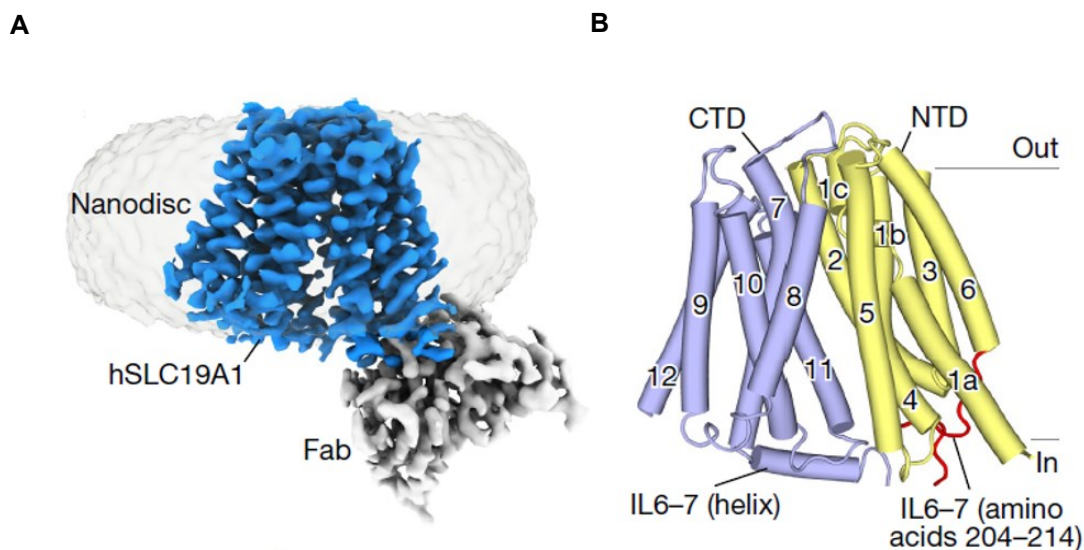
Figure 57. Cryo-EM structures of human SLC19A1 in the apo-state. (A) the cryo-EM structure of apo-state SLC19A1 adopts an inward open conformation (PDB:7XPZ). (B) The apo conformation of SLC19A1. TM1-TM6 are shown in blue, TM7-TM12 are shown in yellow. Figures adapted from Zhang *et al.*[1]

The transmembrane region of SLC19A1 consists of 12 transmembrane segments and structurally it shows an inward-open conformation which allows for the formation of a deep binding cavity (Figure 58). [1] This cavity surpasses from the intracellular side to almost the extracellular side and that way there are two distinct pockets being formed. Recent cryo-EM studies managed to solve the structure of SLC19A1 in complex with cGAMP, but also the thiophosphate analogue (2'3'-cG^{S}A^{S}MP) and 3'3'-cAAMP.[1] These structures show that folates are bound in the upper and more narrow section of the SLC19A1 transporter region while CDNs bind to the additional pocket that is positioned lower and closer to the cytosol[1] (Figure 58).
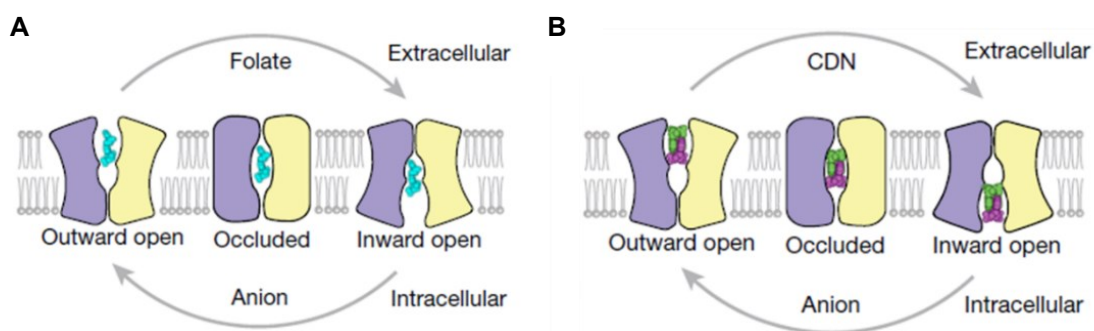
Figure 58. Schematic of the distinct cavities of SLC19A1. Folates occupy the upper narrower cavity (A) while CDNs occupy the lower closer to the cytosol cavity (B). Figures adapted from Zhang *et al.*[1]

A model of structural superimposition between folates and CDNs shows that they occupy different binding cavities that are stacked on top of each other (Figure 59). The folate lies in an almost upright orientation with the pterin moiety facing the extracellular space and the glutamate positioned towards

the intracellular region, close to the cavity where CDNs bind. CDNs are bound to the lower cavity as a dual molecule.[1] When folates or antifolates were used alongside CDNs, the CDN uptake and type I IFN production was significantly inhibited, meaning that folates and CDNs naturally compete with each other for cellular penetration.[43]
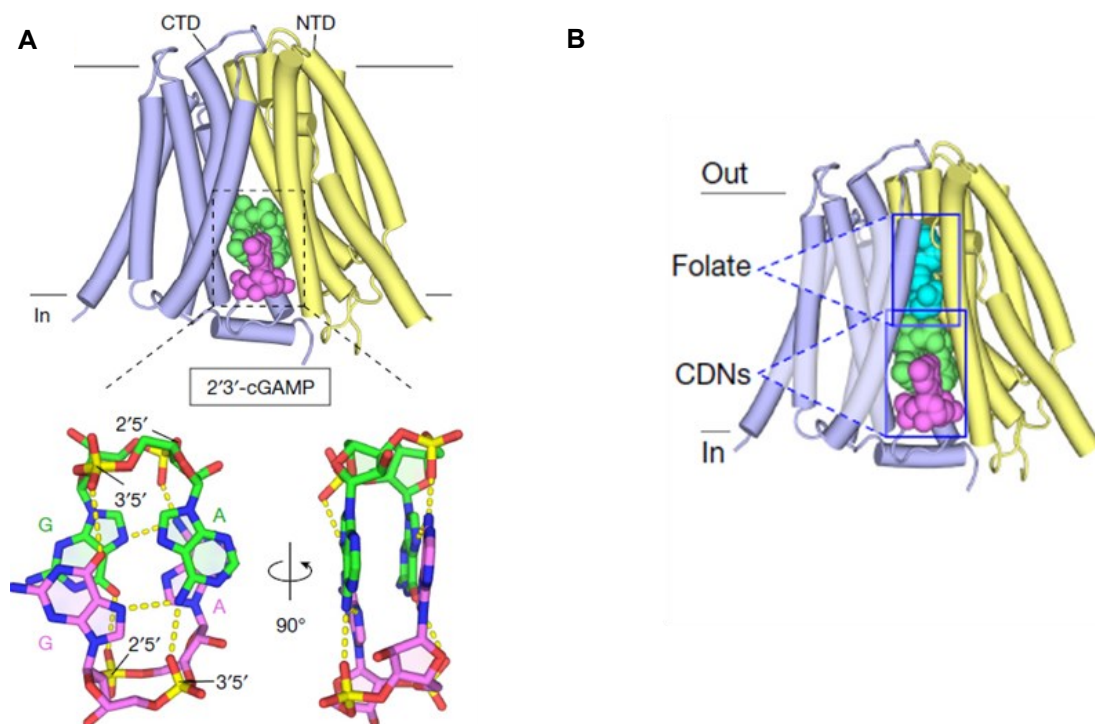
Figure 59. (A) Structure of SLC19A1 bound to 2'3'-cGAMP in an inward open conformation. Two bound cGAMP molecules are occupying the cavity. The CDNs are shown a sticks and hydrogen bonds are shown as yellow dashes. (B) Structural superimposition of 2'3'-cGAMP and folates on the bound state. Figures adapted from *Zhang et al.*[1]

These exciting structural results gave us a head start to design two novel CDN-based conjugates, 2'3'-deoxy-cGAMP-FOL (**83**) and 2'3'-deoxy-cAAMP-FOL (**84**) (Figure 60) that consist of a modified CDN which is covalently bonded with a folate moiety via a versatile linker. By ligating a CDN with a folate moiety we can in this way leverage their favorable cellular uptake through SLC19A1. Owing to the CDN's selectivity towards STING, we opt that when the conjugates enter the cell they will compete with endogenous cGAMP, bind on STING and possibly keep it in an "open-lid" state that impedes and ameliorates its activation.
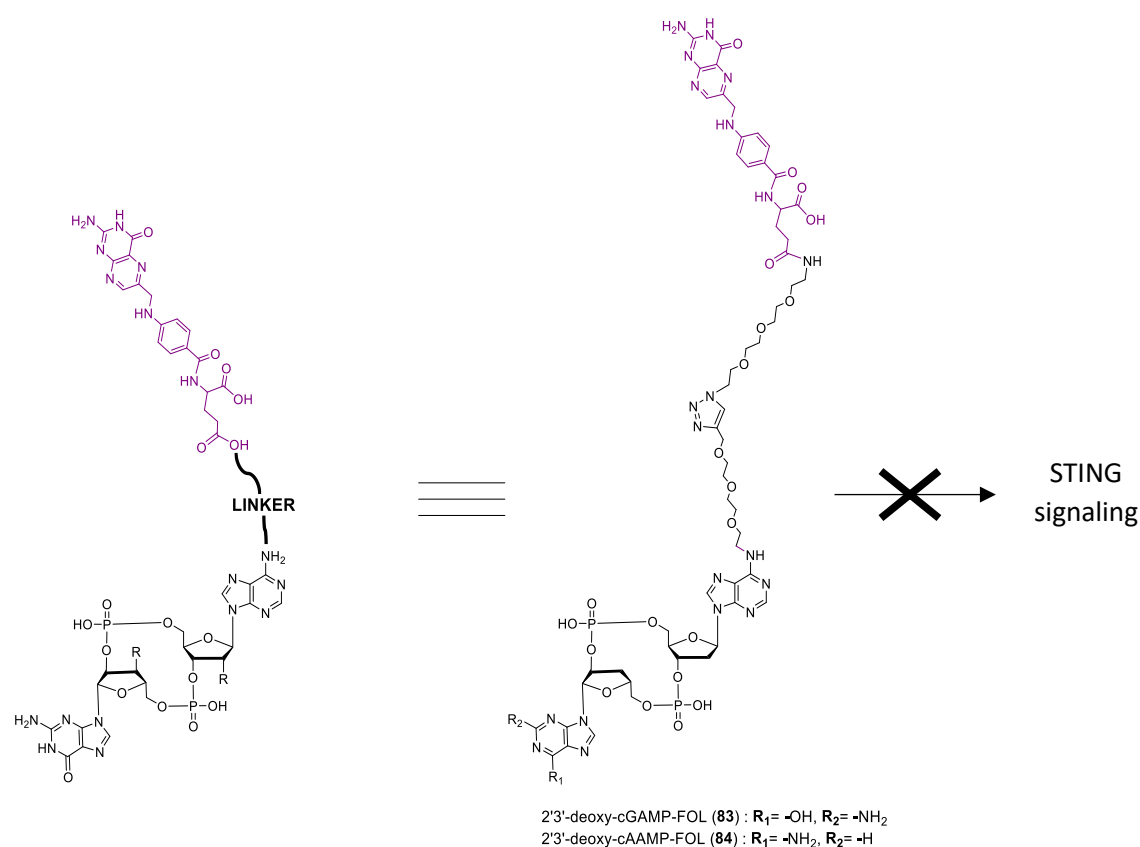
Figure 60. Conceptualization of inhibitors **83** and **84**. Both conjugates consist of a CDN that is linked to a folate moiety (purple). Folates are antiporter SLC19A1's natural substrates and CDNs are known to be imported inside the cell through SLC19A1 as well. We opt that the folate conjugated CDNs present better cellular permeability and, when bound on STING, due to the bulkiness of the folate they will prevent STING's lid closure and therefore block STING signaling downstream.

As already demonstrated, SLC19A1 is known to be selective towards the CDNs that it lets pass and it shows a preference towards linkage types and nucleobases. For this reason, we decided to employ two similar but diverse CDN scaffolds, on the one hand one guanine and one adenine containing 2'3'-deoxy-cGAMP (**1**) and on the other hand two adenine containing 2'3'-deoxy-cAAMP (**2**), in order to evaluate any differences in cell permeation caused by the nucleobases (Figure 61). The folate precursor **87** can be constructed in a straightforward way from pteroic acid (**85**) and a glutamic acid analogue (**86**). We chose to link the CDNs to the folate moiety via a flexible, metabolically stable linker that combines two PEG3 parts conjoined via a triazole. We chose this specific linker first of all to provide the molecule with a high degree of movement freedom so that both the CDNs and the folate moieties can entirely fill up their distinct binding cavities with no obstruction[151] and secondly in order to have an initial estimation of length to activity relationship. Lastly, the linker structures can be easily chemically modified for possible future functionalizations of the conjugates.
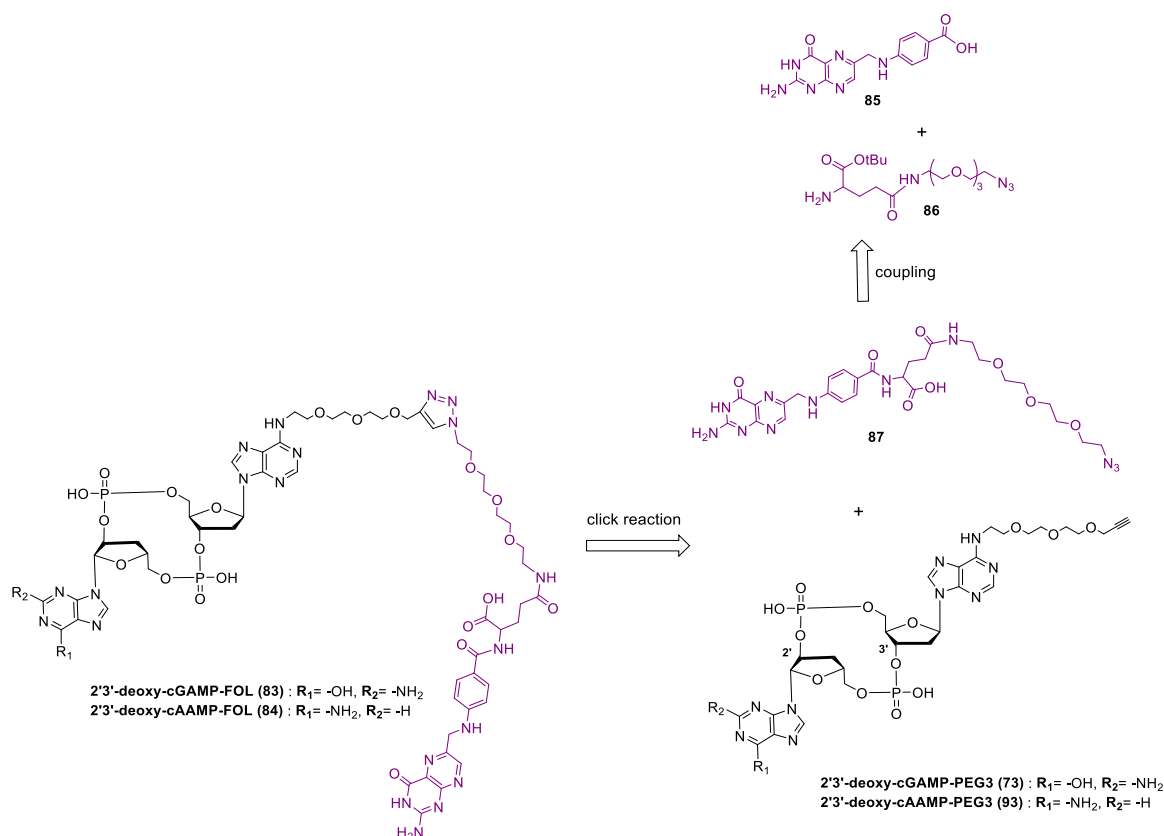
Figure 61. Retrosynthetic analysis of conjugates **83** and **84**. The conjugates consist of a CDN, either 2'3'-deoxy-cGAMP or 2'3'-deoxy-cAAMP which bear a PEG3 linker with a terminal alkyne (compounds **73** and **93**). The folate moiety can be constructed by coupling pteroic acid (**85**) with a PEG3-azide modified glutamic acid (**86**). The CDNs can that way be conjugated to the folate moiety via click-chemistry.

3.2.2.b Synthesis of 2'3'-deoxy-cGAMP-FOL

The synthesis started with constructing the folate precursor **87** based on a modified synthetic procedure that was introduced by our group[159]. Fmoc-O-tert-butyl protected glutamic acid **88** was coupled with 11-azido-3,6,9-trioxaundecan-1-amine **89** using DIPEA and HBTU as a coupling reagent (**90**) (Figure 62).
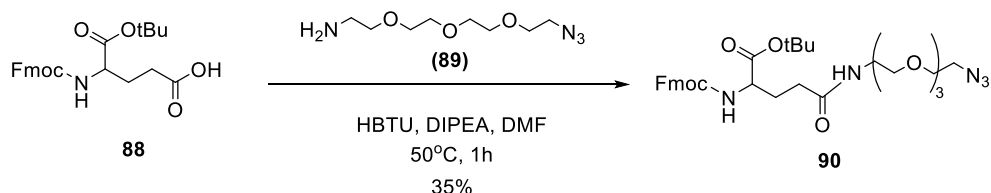
Figure 62. Synthesis of building block **90** starting from commercially available Fmoc-protected glutamic acid **88** and 11-azido-3,6,9-trioxaundecan-1-amine **89**.

Then, the Fmoc protecting group was removed by treatment with dimethylamine in THF to afford the first precursor **91** (Figure 63). Next, **91** was coupled with pteroic acid (**85**) using HBTU and, after the tert-butyl deprotection of **92** in a trifluoroacetic acid/DCM mixture, **87** was furnished in 12% overall yield over 4 steps.
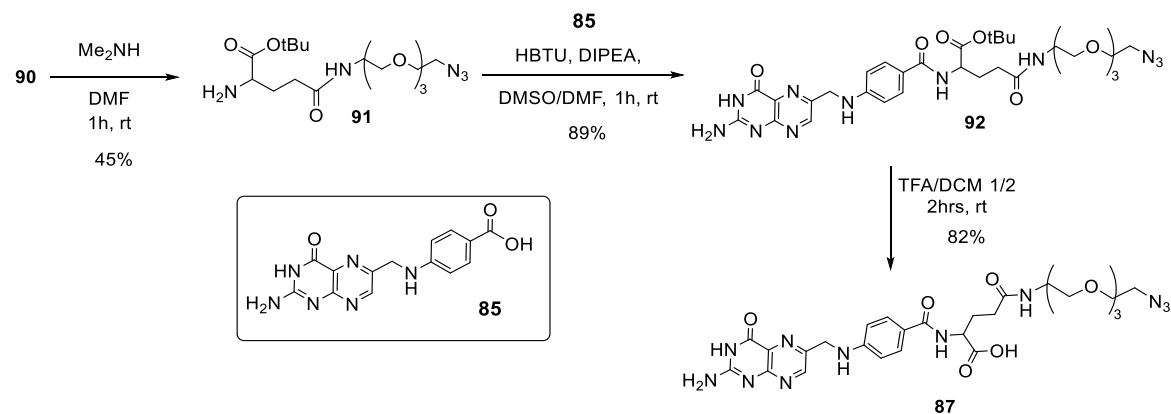
Figure 63. Synthesis of folate precursor **87**.

The folate-azide moiety **87** was subsequently clicked to the terminal alkyne of the N6-PEG linker of compound **73** (synthesis shown on Chapter 3.2.1) (Figure 64). As previously described, Cu(II) was provided from CuSO₄ and was reduced to Cu(I) using sodium ascorbate. An excess of THPTA ligand was once more used to catalyze the reaction and protect the Cu from oxidation. The click reaction was conducted in an aqueous solution under inert anaerobic conditions and was closely monitored by LCMS. Even though **87** was only partially soluble in water forming an emulsion, after 1 hour of reaction it was evident that the emulsion was almost completely clear and the reaction was progressing efficiently (Figure 65). The reaction was stopped after 5 hours and the crude mixture was immediately purified by reversed-phase preparative HPLC. Our first CDN-folate **83** was this way afforded and its structure could be identified by NMR spectroscopy, MALDI-TOF and high-resolution mass spectrometry.
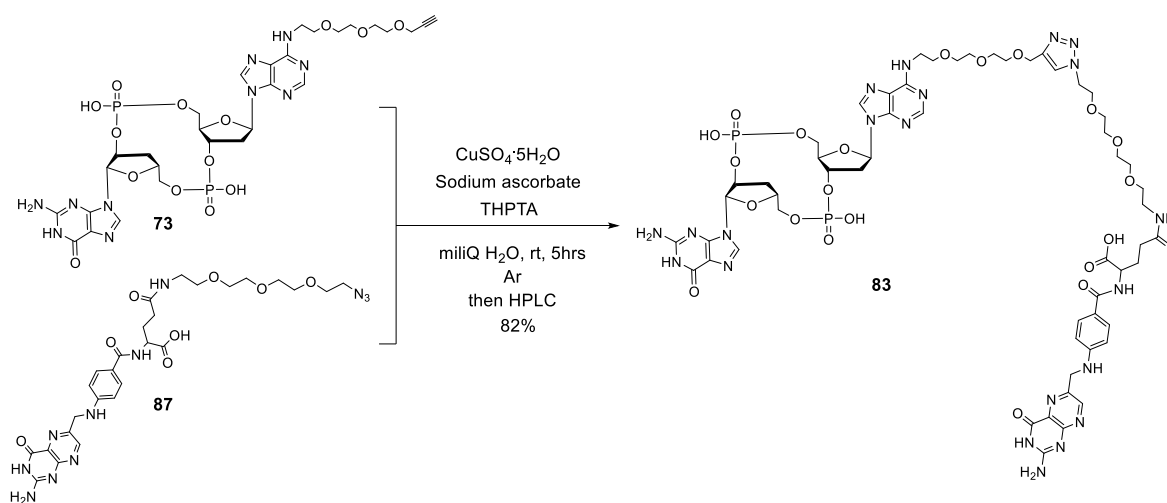
Figure 64. Final conjugate **2'3'-deoxy-cGAMP-FOL** (**83**) synthesis via click reaction.

Figure 65. A) Analytical HPLC chromatogram (0-40% TEAA buffer B; buffer B = 0.1M NEt₃/HOAc in 80% MeCN; absorption at 260 nm) and MALDI-TOF analysis of compound **83**. B) LCMS chromatograms of the progression of the click reaction (method: 5-80 % buffer B in 7 minutes, then 95 % B for 1 minute; Buffer A = 0.01 % formic acid in H_2O, buffer B = 0.01 % formic acid in MeCN). Starting material CDN **73** was completely converted after 4 hours of reaction.

3.2.2.c Synthesis of 2'3'-deoxy-cAAMP-FOL (84)

The cAAMP-folate conjugate **84** synthesis started by initially assembling the CDN structure. 2'3'-deoxy-cAAMP-PEG3 **93** can be synthesized by coupling the already available N6-PEG3-terminal alkyne adenosine phosphoramidite **74** with the 3'-deoxy adenosine phosphotriester **7** (Figure 66).

Figure 66. Retrosynthetic analysis of compound 2'3'-deoxy-cAAMP-PEG3 **93**.

Results and discussion

Compound **7** can be obtained starting from the commercially available DNA nucleoside N6-benzoyl-5'-O-DMT-2'-O-TBS adenosine **94** (Figure 67). Compound **94** was first deoxygenated via a modified Barton-McCombie reaction. In this case, we used the same conditions for the nucleoside as for the sugar **S1** as well. The 3'-deoxy-adenosine precursor **96** was then treated with TBAF to cleave the TBS protecting group to afford **97**. Finally, **97** was converted to the corresponding phosphotriester **7** following the same methodology as described in Chapter 3.1.1. The 3'-deoxy precursor **7** was purified and isolated in a 47% yield over 3 steps.
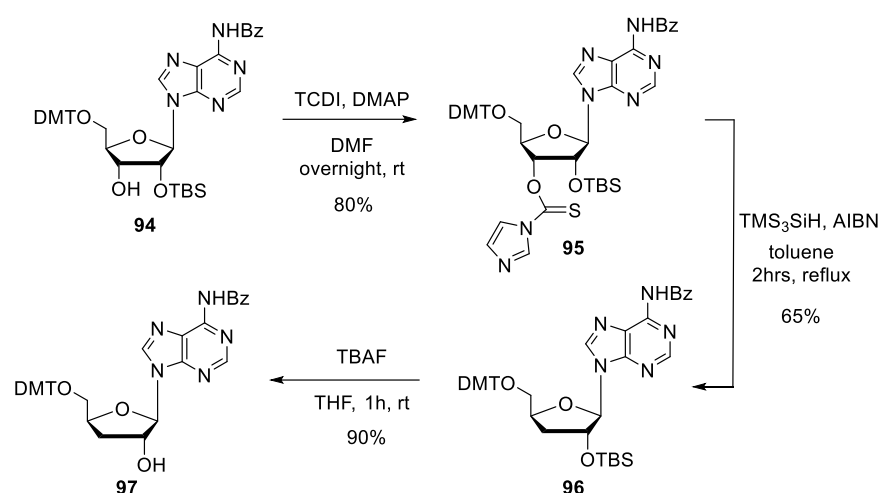
Figure 67. Synthesis of 3'-deoxygenated adenosine building block **97**.
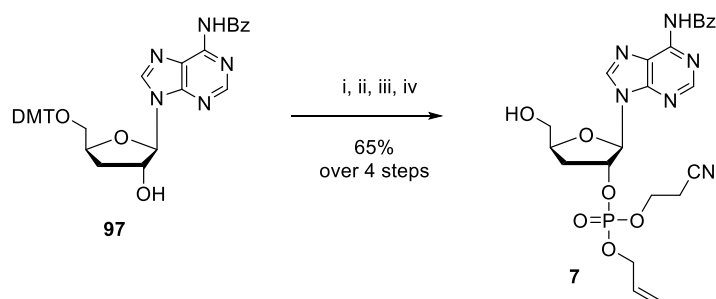
Figure 68. One-pot synthesis of the 3'-deoxy-adenosine phosphotriester **7**; **i.** 2-cyanoethyl *N,N,N',N'*-tetraisopropyl phosphorodiamidite, pyr-TFA, DCM, 1h, rt; **ii.** BTT activator, allyl alcohol, 40min, rt; **iii.** *t*-BuOOH, 30 min, rt; **iv.** 3% DCA in DCM, 15min, rt.

For the production of the linear compound **98**, we employed the already synthesized adenosine phosphoramidite **74** (Chapter 3.2.1). The coupling proceeded using, as already described, excess of BTT activator, then after oxidation of the resulting phosphite the DMT protecting group was cleaved off and the linear precursor was isolated with a yield of 89%.

Results and discussion
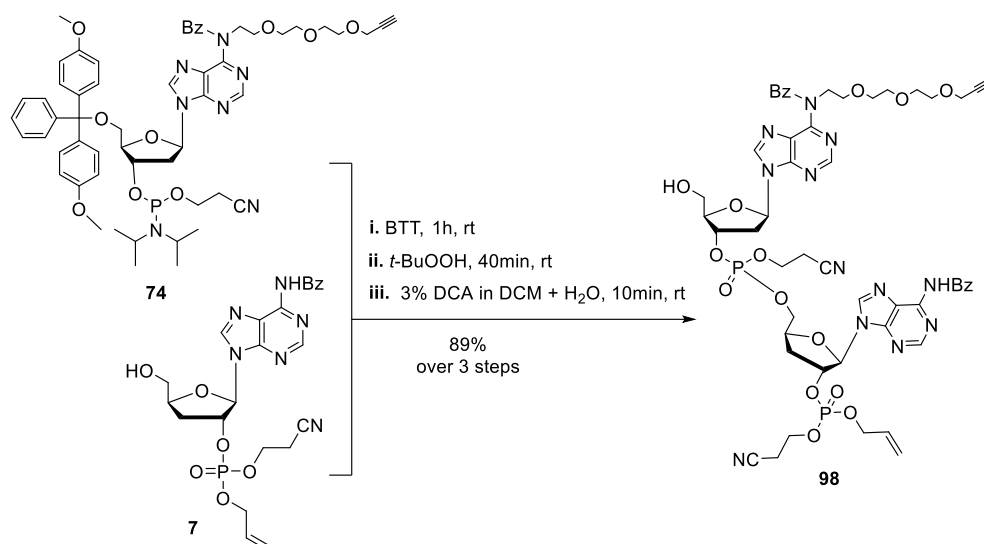
Figure 69. One-pot synthesis of the linear compound **98**; **i.** BTT activator, MeCN, 1h, rt; **ii.** *t*-BuOOH, 40 min, rt; **iii.** 3% DCA in DCM + H₂O, 10min, rt.

The phosphate allyl protecting group of **98** was removed using sodium iodide in refluxing acetone yielding **99** and this way the macrocyclization was possible using MSNT in pyridine (Figure 70). The desirable **93** could then be isolated after complete deprotection of compound **100** with a 33% methylamine solution and subsequent purification by reversed-phase HPLC.
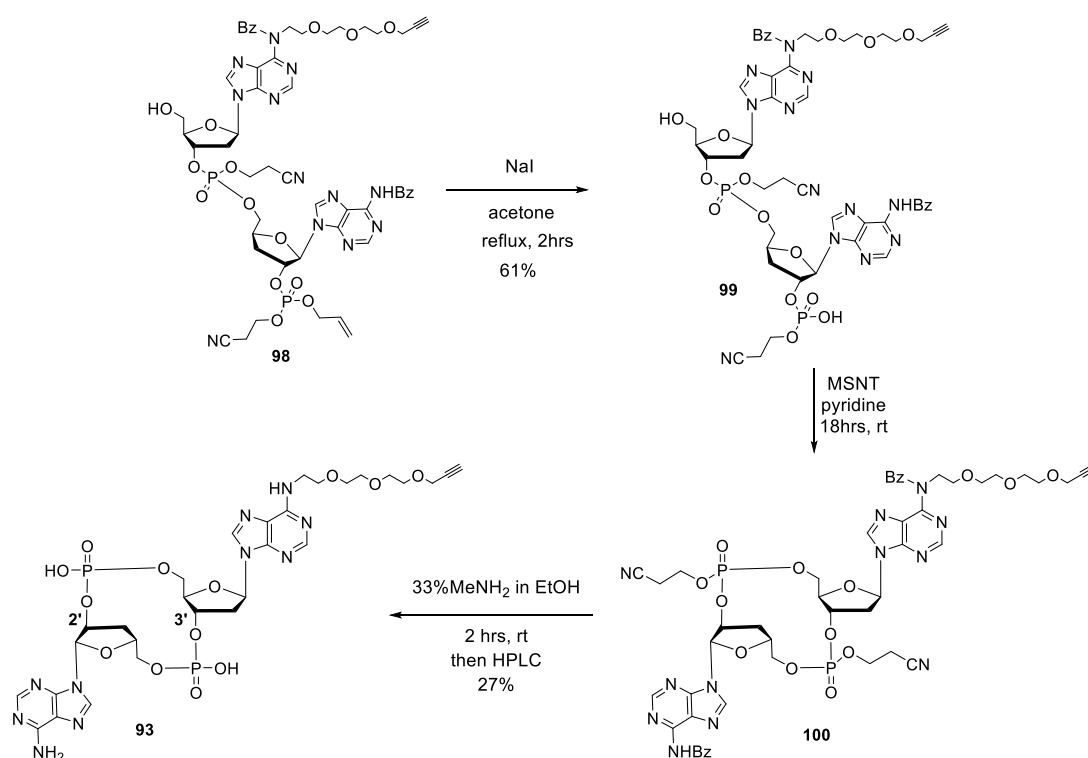
Figure 70. Synthesis of 2'3'-deoxy-cAAMP-PEG3 analogue **93** starting from the linear dinucleotide **98**.

Results and discussion
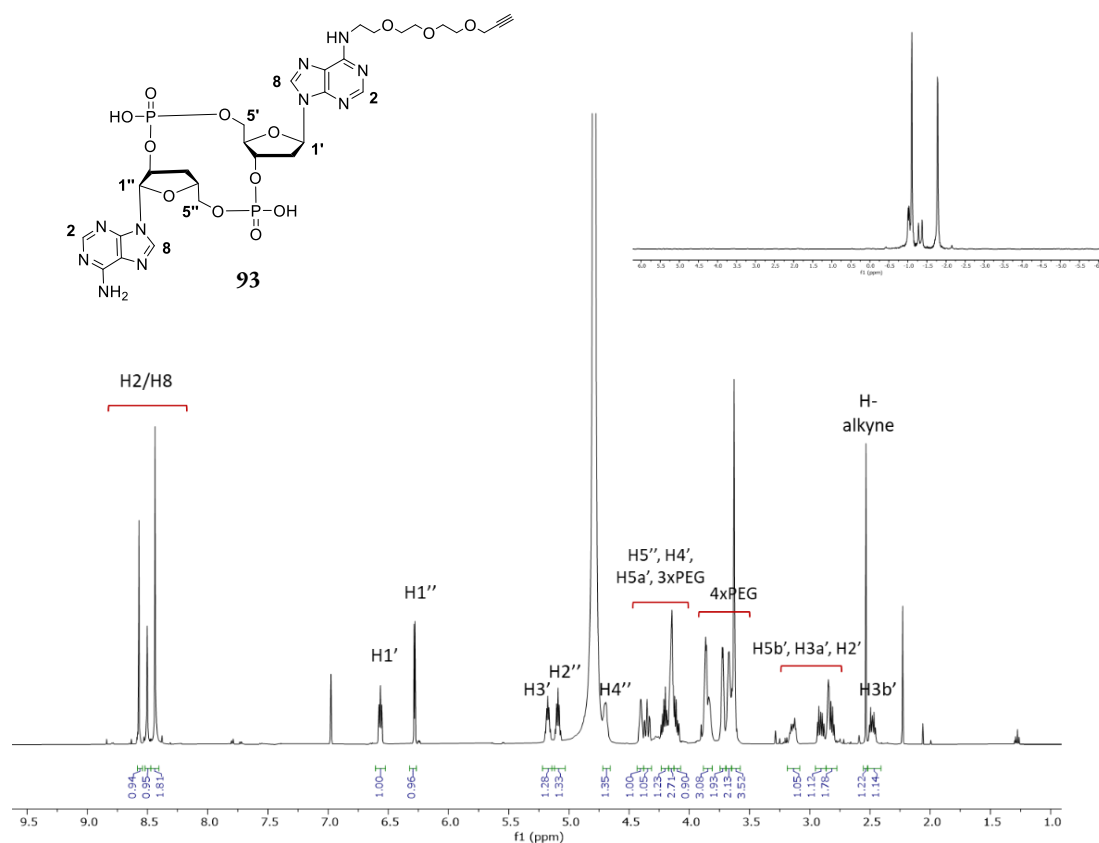
Figure 71. ^{1}H- and ^{31}P-NMR spectra of compound 2'3'-deoxy-cAAMP-PEG3 (**93**).

The functionalized deoxy-cAAMP **93** was then conjugated to the folate moiety **87** via a click reaction. The conditions used were the same as for the cGAMP conjugate **73** and after 5 hours of reaction the crude mixture was immediately purified via reversed-phase HPLC. Compound **93** was characterized by NMR spectroscopy, MALDI-TOF and high-resolution mass spectrometry.
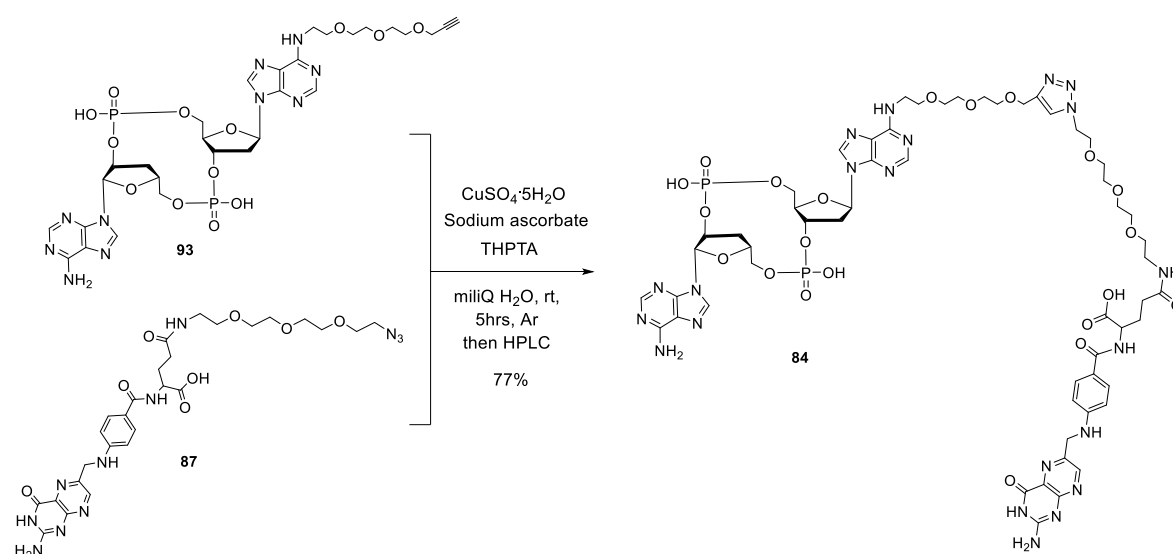
Figure 72. Click reaction for the synthesis of final conjugate **84**.

A

B
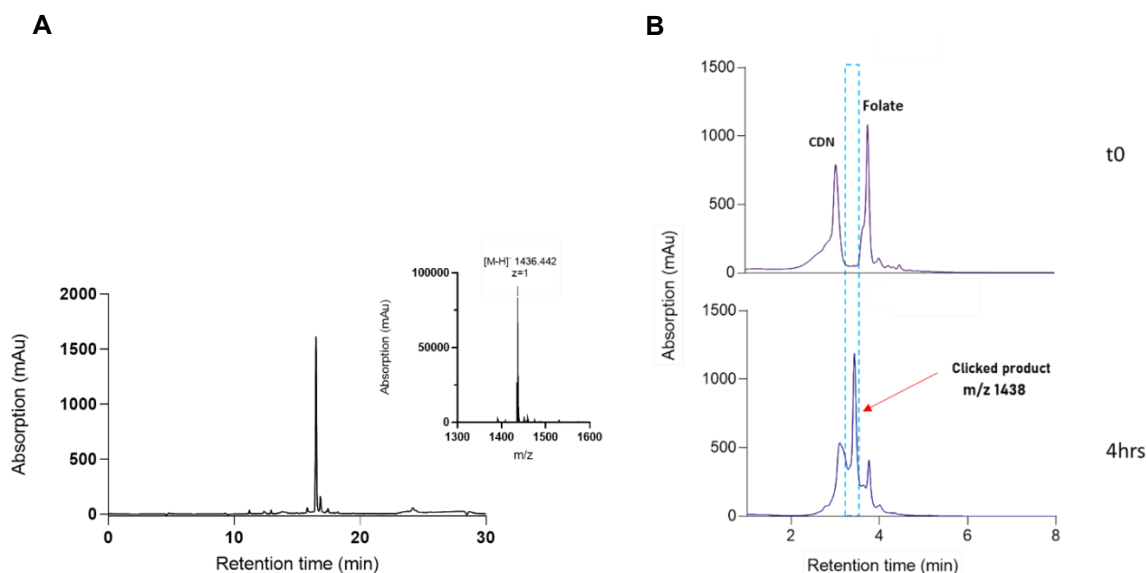
Figure 73. A) Analytical HPLC chromatogram (0-40% TEAA buffer B; buffer B = 0.1M NEt₃/HOAc in 80% MeCN; absorption at 260nm) and MALDI-TOF analysis of compound **93**. B) LCMS chromatograms of the progression of the click reaction (method: 5-80 % buffer B in 7 minutes, then 95 % B for 1 minute; Buffer A = 0.01 % formic acid in H_2O, buffer B = 0.01 % formic acid in MeCN). Starting material CDN **93** was completely converted after 4 hours of reaction.

3.2.2.d Biological evaluation

To be able to test whether our compounds are able to inhibit STING we first decided to exclude the possibility of them being STING agonists. In collaboration with *Yasmin Gärtner,* compounds **83** and **84** were therefore fed to immune cells in order to evaluate if they can induce STING-dependent interferons. For our purpose, THP-1 Dual monocytic cells (Invivogen) were chosen as they are shown to be a very suitable testing model for our concept. Firstly, THP-1 monocytes are highly expressing STING but also SLC19A1.[43] Secondly, THP-1 Dual cells carry a Lucia Luciferase gene under the control of a promoter with 5 IFN-stimulated response elements and, thus, allows for the simultaneous study of the interferon production via the IRF pathway and of the activation of the NF-κB pathway. Through the resulting luminescence this cell line allows quantification of the immunostimulatory effect caused by STING ligands.

Furthermore, it is already been demonstrated that 2'3'-deoxy-cGAMP's **1** and 2'3'-deoxy-cAAMP's **2** immunity related activities are STING dependent (Figure 74) and that they can efficiently act as STING agonists.[138] Thus, by measuring the luminescence of the cells we can have a first proof of concept of whether they can act as agonists or antagonists. In order to do this, THP-1 cells were incubated with our compounds for 24 hours and the resulting luminescence was then measured using a luminometer as Relative Light Units (RLUs). Our compounds were incubated in a concentration range of 5μM to 500μM in order to calculate the EC_{50} value. This value highlights the concentration of the potential agonist needed to generate a half-maximal response and it is essential in order to evaluate the efficiency of the compound as an agonist. **1** and **2** were used as positive controls and to prompt a comparison since their EC_{50} values have already been determined before.[138]

Results and discussion
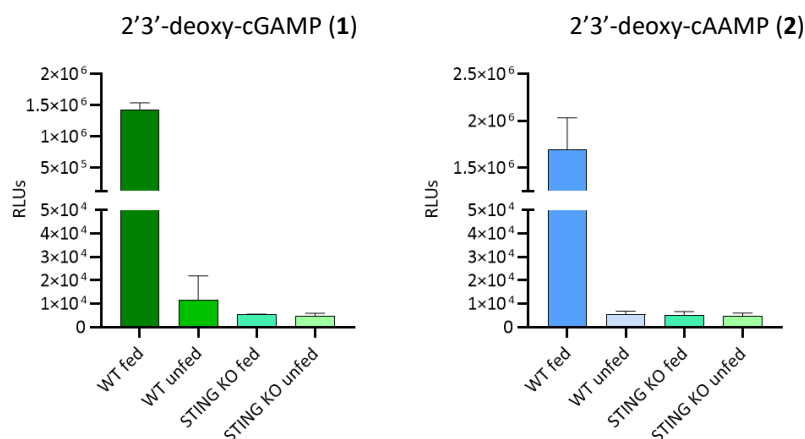
Figure 74. 2'3'-deoxy-cGAMP (**1**) and 2'3'-deoxy-cAAMP 's (**2**) immune activities are STING dependent. Treatment of **1** and **2** in THP-1 cells resulted in luminescence activation while unfed and STING-KO cells did not produce any response. Figure adapted from *Dr. Dilara Özdemir's* PhD thesis.

As observed in Figure 75, when compounds **83** and **84** were fed to the cells no significant luminescence was observed, compared to the activators **1** (orange) and **2** (black). Even while testing at concentrations as high as 500μM, no sigmoidal activation curve could be formed and, therefore, there was no STING activation. Furthermore, when we also tested the CDN precursor of the conjugate, 2'3'-deoxy-cGAMP-PEG3 **73**, we again observed no luminescence response, in a similar way to **83** and **84** (Figure 75).
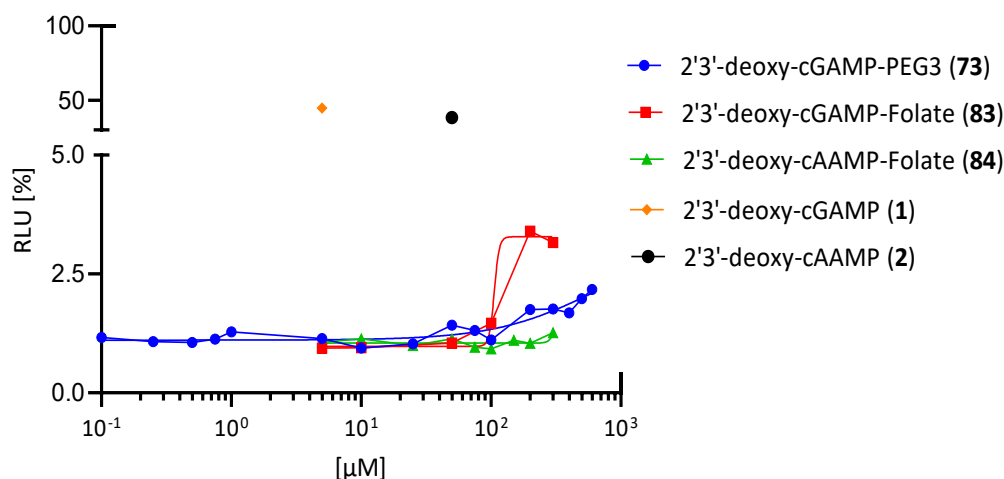
Figure 75. Luminescence in vitro assay to determine immune responsiveness. The cells were incubated with compounds **73**, **83** and **84** in a range of concentrations from 0.1μM to 1000μM for 24 hours. Compounds **1** and **2** were used in their respective active concentrations that were previously reported (**1** : 7μM, **2** : 75μM). Luminescence was measured in a TECAN Genius Pro plate reader. Compounds **83** and **84** do not induce luminescence. Compounds **1** and **2** are STING agonists and trigger Luciferase response. Data acquired in collaboration with *Yasmin Gärtner. RLU: Relative Luminescence Units.*

The collected data conclusively show that there is no direct STING activation mediated by our folate conjugates. In order to undoubtedly confirm our theory, further biological and STING binding assays need to be performed.

More precisely, as a way to prove that our compounds can efficiently penetrate the cell membrane, we can conduct the same Luciferase assay after first permeabilizing the cell using proper agents, like digitonin. As a consequence, the uptake of the CDNs into the cells will not be the limiting step in STING activation. Apart from the luminescence response, a next proof of immunity deactivation would be the quantification of immune-related genes. Thus, future studies are nowadays directed towards incubating our compounds to cells and, after cGAMP or viral stimulation, measure the mRNA levels of IFN-β, cytokines and chemokines, like IP-10, IL-6. That way, we can establish whether and to what extend STING signaling is downstream affected when cells are incubated with our compounds.

Moreover, further studies must be conducted in order to demonstrate whether **83** and **84** exhibit improved SLC19A1-mediated cell permeability. Hence, a straightforward assay could be to incubate a SLC19A1 expressing cell line with our compounds and subsequently either isolate the cells and detect their exact mass via mass spectrometry or employ [^{32}P]-labeled analogues of **83** and **84** and measure their cellular uptake via a radiograph.[43]

3.2.3 Conclusions and perspectives

In this part of this dissertation we managed to synthesize three novel CDN analogues that can act as STING inhibitors in order to battle chronic inflammation. Initially, we designed and synthesized compound 2'3'-deoxy-cGAMP-PALM (**75**), to promote STING's de-palmitoylation on cysteines 88 and 91. **75** comprises on one side of 2'3'-deoxy-cGAMP (**1**) as the main molecular scaffold which ensures STING selectivity. We ligated **1** with the small molecule **72** via a flexible PEG3 linker as a way to recruit lysophospholipase LYPLAL1. This enzyme was recently shown to display thioesterase activity and can cleave the thioacyl bond of the palmitate tag, as a result it is promising to catalyze STING's depalmitoylation. At the synthetic part, we presented a robust and reliable PEG3 functionalization of the adenosine phosphoramidite building block **74** that is chemically stable and tolerable throughout the next synthetic steps and can successfully lead to the functionalized cyclic dinucleotide **73**. Moreover, we resolved the challenging acylation of LYPLAL1 recruiter (**45**), ligated it on **73** via click-chemistry and tested the final conjugate's stability in cell medium. Future studies in our lab are focusing on measuring 2'3'-deoxy-cGAMP-PALM **75** metabolic stability against nucleases, sulfatases and phosphodiesterases.

Overall, by recruiting LYPLAL1 on deoxy-cGAMP we made a novel "proximity inducing" hybrid molecule that presents immense potential for STING signaling deactivation. This hybrid molecule follows the same mindset as other chimeric molecules like PROTACs[154, 160, 161], LYTACs[162], AUTACs[163] but with the main difference that it does not aspire to elicit protein degradation down the road, but rather opts for protein inhibition. Our compound ensures specificity over STING and no off-target reactions as, unlike the known STING palmitoylation inhibitors, it does not irreversibly bind on cysteines 88 and 91. This also means that the drug's catalytic cycle is continuously progressing and no excess drug concentration is needed to compensate. While this dissertation was being written, two new papers involving STING palmitoylation where published[164,165]. In fact, one of them names LYPLAL1 as the thioesterase that deplamitoylates cGAS to negatively regulate it. These papers corroborate that

Results and discussion

palmitoylation is a key target for cGAS-STING signaling inhibition, links it to the action of LYPLAL1 and opens up the path for many new research directions. Future experiments will address our compound's binding affinity on STING and whether **75** exhibits depalmitoylation-mediated inhibitory activity.

In the second part of the inhibitors chapter, we synthesized two novel conjugates that are designed to leverage improved cellular permeability through the folate transporter SLC19A1, but simultaneously act as STING antagonists. Very recently, it was demonstrated that SLC19A1 is an importer for cGAMP and other CDNs and that it forms a distinct cavity with high affinity for CDNs and an additional one for folates that is positioned directly below the CDN cavity. This structural characteristic led us to construct conjugates 2'3'-deoxy-cGAMP-FOL (**83**) and 2'3'-deoxy-cAAMP-FOL (**84**) that beared a CDN bonded to a folate via a long flexible linker and can potentially display favorable cell permeability. At the same time, we opted for the conjugates to act as inhibitors of STING signaling due to the bulkiness of the folate moiety that blocks the closure of STING's "lid" when the conjugates are bound on it.

Apart from the deoxy-cGAMP linked to the terminal alkyne PEG3 linker (**73**), we decided to also use a di-AMP analogue (**93**) in order to facilitate a comparison in activity that would be the result of the difference in nucleobases. The folate moiety was constructed from pteroic acid, conveniently conjugated to a PEG3 linker and ligated to the CDN through a chemoselective and high-yielding click chemistry reaction. Thus, we managed to obtain two CDN-folate analogues using straightforward functionalizations that are compatible with the synthetic conditions that followed. We managed to perform some initial biological assays and we found that they did not trigger an interferon production compared to the parent compounds **1** and **2**. Thus, we showed an initial proof of concept that **83** and **84** do not trigger the activation of STING-related interferon genes. Future experiments in our laboratory are oriented towards measuring the compounds binding affinity on STING and establishing if they can indeed induce STING-mediated signaling inhibition. Of interest would be also to perform thermodynamic studies to establish if they keep STING in an inactive "open-lid" conformation. Finally, part of our plans is the creation of a library of similar compounds that contain different length and rigidity linkers to achieve direct activity comparisons and perform structure-activity-relationship studies.

4 Materials and methods

General methods

All reactions were magnetically stirred under a nitrogen or argon atmosphere and the reaction flasks were dried beforehand via heating under vacuum (heatgun, 450°C). Reactions at low temperatures were carried out using ice baths or ice/NaCl or acetone/dry ice mixtures. Dry solvents and reagents were purchased from commercial suppliers like Sigma-Aldrich, TCI, Biosynth, VWR, Carbolution etc. and, unless otherwise stated, they were used without further purification or processing. Ultrapure water was obtained from a Milli-Q Plus water from Merck Millipore. Chromatographic purifications were carried out via flash column chromatography on Merck Geduren Si 60 (40 – 63 μm) silica gel using pre-distilled solvents as eluents (EA, MeOH, DCM, isohexane). The received fractions and the reaction progress were monitored through Thin Layer Chromatography (TLC) using silica gel aluminum plates (60-F254, Merck). The plates were visualized using a UV light lamp (254 nm or 366 nm) and stained using either cerium ammonium molybdate (10.0 g ammonium molybdate tetrahydrate, 2 g $Ce(SO_4)2\cdot4H_2O$, 180 mL ddH_2O, 20 mL conc. H_2SO_4) or p-anisaldehyde (3.7 mL *p*-anisaldehyde, 135 mL EtOH, 5 mL conc. H_2SO_4, 1.5 mL conc. AcOH) or potassium permanganate stain (3 g $KMnO_4$, 20 g K_2CO_3, 5 mL 5% aqueous NaOH, 300 mL H_2O).

Reactions were additionally monitored using a RP-LC-MS (Reversed-Phase Liquid Chromatography Mass Spectrometry) system from Thermo-Fisher consisted of a DIONEX UltiMate 3000 HPLC System (pump, autosampler, column and diode array detector) and an ESI-MS MSQ Plus single-quadrupole mass spectrometer. The sample analysis was conducted either via a direct injection to the mass spectrometer or via the LC-MS system RP column chromatography methods using a Hypersil Gold C18 column.

RP-HPLC (Reversed-phase High Performance Liquid Chromatography) analysis and purifications were conducted on the following instruments:

Analytical HPLC: Agilent Technologies 1260 Infinity II containing a 1260 Flexible pump, 1260 sampler and 1260 MWD using a EC 250/4 NUCLEODUR 100-3 C18 column from Macherey-Nagel and a 0.5 or 1.0 mL/min flow rate.

Preparative HPLC: Agilent Technologies 1260 Infinity II containing a 1260 Quat pump VL, 1260 manual injection and 1260 MWD using a VP 250/10 NUCLEODUR 100-5 C18 column from Macherey-Nagel and a 5.0 mL/min flow rate.

IR spectra were determined on an IRSpirit Fourier transform spectrometer attached to a QATR-S single reflection accessory from Shimazu. Band frequencies in the region between 4400 and 1400 cm-1 are reported to the nearest cm-1. Signal intensities are reported as very strong (vs), strong (s), medium (m), weak (w), broad (br).

MALDI-TOF mass measurements were performed on an autoflex® maX machine from Bruker. The samples were diluted in MilliQ water, desalted on a MF-Millipore VSWP02500 membrane form Merck Millipore and co-crystalized in a 3-HPA matrix (3-hydroxypicolinic acid, Sigma-Aldrich) to measure.

Materials and methods

The isolated products were characterized by ^{1}H, ^{13}C and, were possible, ^{31}P NMR spectroscopy. The spectra were recorded on Varian VXR400S, Varian INOVA 400, Bruker Avance III 400, Bruker AMX 600, Bruker ARX 600 and Bruker Avance III HD 800 spectrometers and the chemical shift (δ) is given in parts per million (ppm) with tetramethylsilane (TMS) as an internal standard. The multiplicity of the signals was given as s (singlet), d (doublet), t (triplet), q (quartet), p (pentet), m (multiplet) and br (broad) and coupling constants (J) refer to 1H-1H couplings and are given in Hertz (Hz). Suitable deuterated solvents (CDCl$_3$, CD$_2$Cl$_2$, (CD$_3$)$_2$SO, CD$_3$OD, D$_2$O) were used to dissolve the samples, purchased from Eurisotop. For the complete structure characterizations 2D NMR spectra were also attained like homonuclear correlation spectroscopy (COSY), heteronuclear single quantum coherence (HSQC) and heteronuclear multiple bond coherence (HMBC). All spectra were analysed using MestReNOVA 14.2.0 software from Mestrelab Research.

High-resolution mass spectra (HRMS) were recorded by the Analytics Department of the Ludwig-Maximilians-Universität Munich, Department of Chemistry on a Thermo Finnigan MAT 95 machine for Electron Ionization (EI) measurements or a Thermo Finnigan LTQ-FT for Electrospray Ionization (ESI) measurements. Stability studies were performed on a QExactive HF Orbitrap machine from Thermo Fisher.

Organic synthesis procedures

Dideoxy-cGAMP and cAIMP prodrugs

SATE-alkyne-alcohol (22)
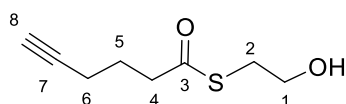
5-hexynoic acid (2.94 mL, 26.64 mmol, 1.0 eq) was dissolved in 250 mL of dry MeCN and β-mercaptoethanol (2.82 mL, 39.96 mmol, 1.5 eq) was added under a nitrogen atmosphere. The mixture was cooled to 0°C and DCC (5.52 g, 26.64 mmol, 1.0 eq) was added. The reaction was left to stir overnight slowly reaching room temperature and the next day any remaining DCC was filtered out. Solvents were then evaporated under vacuum and the crude mixture was diluted in 50mL of cold Et$_2$O, cooled down to force precipitation, filtered and evaporated. The product was purified via flash column chromatography (silica gel, DCM/EA: 100/2 to 100/5) and was received as a colorless oil (2.7 g, 15.6 mmol, 60%).

R$_f$ (DCM/EA : 5/1) = 0.60

^{1}H NMR (400 MHz, CDCl$_3$) δ 3.77 (t, J = 6.0 Hz, 2H, H-1), 3.09 (t, J = 6.0 Hz, 2H, H-2), 2.74 (t, J = 7.4 Hz, 2H, H-4), 2.26 (tt, J = 6.9, 2.6 Hz, 2H, H-6), 1.99 – 1.97 (dt, J = 4.9, 2.6 Hz, 2H, H-8), 1.84 – 1.87 (m, 2H, H-5).

Materials and methods

^{13}**C-NMR** (101 MHz, CDCl$_3$) δ 201.22 (C-3), 84.10 (C-7), 71.55 (C-8), 61.94 (C-1), 44.12 (C-4), 31.87 (C-2), 24.86 (C-5), 18.54 (C-6).

SATE-alkyne bis-phosphoramidite (23)
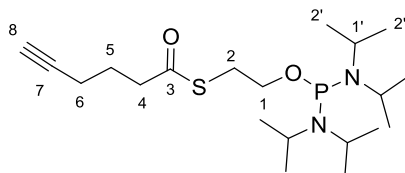
SATE-OH **22** (1.35 g, 7.8 mmol) was dissolved in 25mL of Et$_2$O, then triethylamine (1.85 mL, 13.3 mmol, 1.7 eq) was added dropwise. The mixture was cooled to 0°C and diisopropylamino chlorophosphine (1.7 g, 6.5 mmol, 0.8 eq) was added. The reaction was left to stir at rt for 2hrs. then a 40mL mixture of Et2O/Et3N (9/1) was added to the mixture, solvents were evaporated under pressure and to the remaining crude mixture 30mL of distilled cyclohexane were added. The mixture was evaporated to half the volume and loaded to a silica gel filled column to purify using cyclohexane + 6% Et$_3$N. The pure product was afforded as a viscous colorless oil (1.85 g, 4.60 mmol, 58%).

R$_f$ (cHex/DCM/TEA) = 6/3/1

IR (ATR): ṽ (cm^{-1}) 3298 (s), 3050 (br), 2897 (s), 2055 (br), 1723 (s), 1564 (br), 1423 (s), 1377 (s), 1300 (s), 1067 (s), 1011 (s), 991 (s), 788 (s), 709 (s).

^{1}**H NMR** (400 MHz, CDCl$_3$) δ 3.66 (dt, J = 7.6, 6.3 Hz, 2H, H-1), 3.50 (dp, J = 10.8, 6.8 Hz, 4H, H-1'), 3.13 (t, J = 6.3 Hz, 2H, H-2), 2.70 (t, J = 7.4 Hz, 2H, H-4), 2.25 (td, J = 6.9, 2.7 Hz, 2H, H-6), 1.98 (t, J = 2.6 Hz, 1H, H-8), 1.94 – 1.82 (m, 2H, H-5), 1.15 (dd, J = 6.8, 4.9 Hz, 24H, H-2').

^{13}**C-NMR** (101 MHz, CD2Cl2) δ 200.11 (C-3), 82.77 (C-8), 69.21 (C-8), 63.73 (C-1), 44.90 (C-1'), 41.87 (C-4), 31.90 (d, C-2), 27.45 (d, J = 8.0 Hz, C-2'), 25.31 (C-5), 24.69 (C-2'), 18.11 (C-6).

^{31}**P NMR** (162 MHz, CDCl$_3$) δ 124.32.

3'-O-(Cyanoethyl,SATE-phosphate)-*N*6-Bz-2'-deoxyadenosine (24)
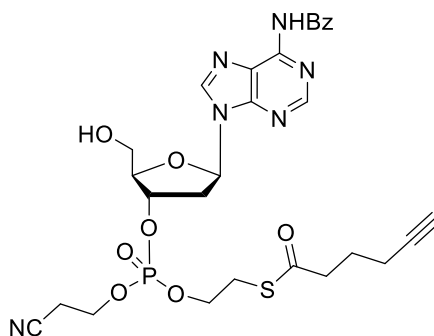
Adenosine 5'-DMT-2'-deoxy-N6-Bz-phosphoramidite (2 g, 2.38 mmol) was co-evaporated with toluene (x3) and then diluted in 20mL dry MeCN under Ar. Then SATE-OH (822 mg, 4.76 mmol, 2.0 eq) and BTT (0.3M in MeCN, 15.7 mL, 4.76 mmol, 2.0eq) were added and the mixture was left to stir under Ar at rt for 1h. Then tert-butyl hydroperoxide (5.0-6.0M in decane, 1.37 mL, 8.3 mmol, 3.0 eq) was added and the mixture continued stirring for 40 minutes. The hydroperoxide was quenched at 0°C using aq. $NaHSO_3$ solution (3 mL, 0.5g/mL). The mixture was stirred for 10min at 0°C and then for 5min at rt. Solvents were evaporated under reduced pressure and the mixture was subsequently dissolved in a 93 mL mixture of 3% DCA in DCM containing 10.0 eq H_2O. The mixture was left to stir for 15min and then was quenched with 100 mL aqueous solution of $NaHCO_3$. The aqueous phase was extracted three times with ethyl acetate and the combined organic layers were dried over $MgSO_4$ and evaporated under reduced pressure. The product was purified via flash column chromatography using DCM/acetone/MeOH (80/17/3) as eluents to afford **24** as a white foam (1.3 g, 2.02 mmol, 84%).

R_f (DCM/MeOH : 10/1) = 0.45

HRMS (ESI): for $C_{28}H_{32}O_8N_6PS^+$ [M+H]$^+$, calc. 643.1662; found 643.1663

IR (ATR): ṽ (cm^{-1}) 3286 (br), 2936 (w), 1677 (s), 1603 (m), 1587 (m), 1440 (m), 1190 (s), 1089 (s), 899 (s).

^{1}H NMR (400 MHz, CDCl$_3$) δ 8.79 (s, 1H), 8.14 (d, J = 7.1 Hz, 1H), 8.11 – 7.99 (m, 2H, H-ar), 7.67 – 7.58 (m, 1H, H-ar), 7.58 – 7.50 (m, 2H, H-ar), 6.45 (dd, J = 9.7, 5.3 Hz, 1H, H-1'), 5.35 (t, J = 4.6 Hz, 1H, H-3'), 4.50 (s, 1H, H-4'), 4.39 – 4.29 (m, 2H), 4.21 (dt, J = 8.2, 6.7 Hz, 2H, SATE-CH$_2$), 4.01 (dd, J = 13.0, 1.7 Hz, 1H, H-5'), 3.89 (d, J = 13.1 Hz, 1H, H-5'), 3.22 (q, J = 7.1 Hz, 3H, SATE-CH$_2$), 2.81 (d, J = 1.1 Hz, 2H, H-2'), 2.78 – 2.65 (m, 3H, SATE-CH$_2$), 2.29 – 2.24 (m, 2H, SATE-CH$_2$), 2.00 (td, J = 2.6, 0.8 Hz, 1H, H-alkyne), 1.95 – 1.80 (m, 2H, SATE-CH$_2$).

2''- SATE- phosphate- *O6*- dpc- N2- iBu- 3''- O - deoxyguanosine- 3'-((cyanoethyl, SATE) phosphate) - *N6*- Bz - 2'- O-deoxyadenosine (26)
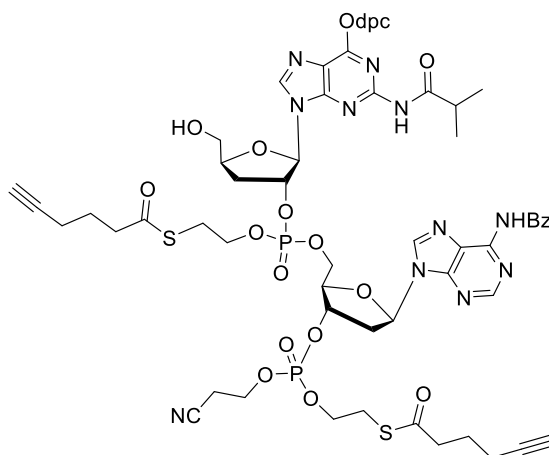
Materials and methods

Compound **6** (560mg, 0.67mmol) was co-evaporated with toluene (x3) and MeCN (x2), then was dissolved in dry DCM (6mL) under an Ar atmosphere. **23** (324mg, 0.805mmol, 1.2eq) and pyr-TFA (155mg, 0.805mmol, 1.2eq) were added and the reaction was let to stir at rt overnight. The next day, adenosine SATE phosphotriester (646mg, 1mmol, 1.5eq) and BTT (0.3M in MeCN, 5mL, 1.34mmol, 2.0eq) were added and the mixture was left to stir for 1h. Then tBuOOH (5.0M in decane, 0.23mL, 2.03mmoL, 3.0eq) was added and the mixture was left to stir for 40min. The solution was cooled to 0°C and an aqueous solution of $NaHSO_3$ (1.5mL, 0.5g/mL) was added. The mixture was stirred for 10min at 0°C and then for 5min at rt. Solvents were evaporated and the resulting mixture was dissolved in a 30mL mixture of 3% DCA in DCM containing 10.0 eq H_2O. The mixture was left to stir for 15min and then was quenched with an aqueous solution of $NaHCO_3$ (80mL). The aqueous phase was extracted three times with ethyl acetate and the combined organic layers were dried over $MgSO_4$ and then evaporated under reduced pressure. The product was purified via flash column chromatography (silica gel, DCM/acetone/MeOH: 80/17/3) and was received as a colorless foam (500mg, 0.395mmol, 59%).

$\mathbf{R_f}$ (DCM/acetone/MeOH : 80/15/5) = 0.15

HRMS (ESI): for $C_{84}H_{87}O_{19}N_{12}P_2S_2^+$ [M+H]$^+$, calc. 1391.5049; found 1391.3701

IR (ATR): $\tilde{v}$ (cm^{-1}) 3385 (br), 2579 (br), 2358 (w), 1701 (s), 1565 (s), 1488 (s), 1253 (m), 1238 (m).

2"- SATE- phosphate- *O6*- **dpc- N2- iBu- 3"- O - deoxyguanosine- 3'- SATE- phosphate -** *N6*- **Bz - 2'- O-deoxyadenosine (27)**
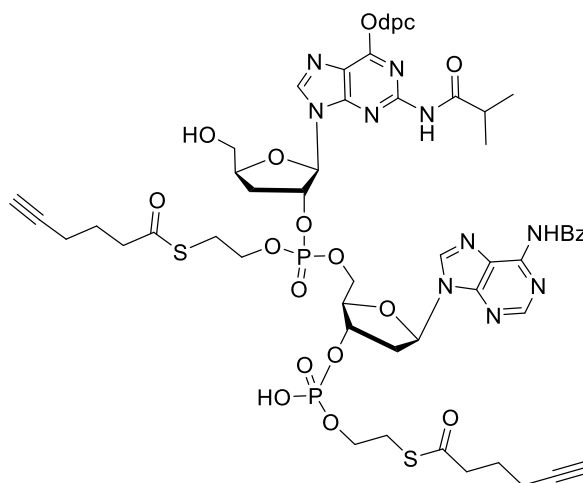
26 (500mg, 0.395mmol) was co-evaporated twice with pyridine and MeCN. Then it was dissolved in 17mL of dry MeCN and 6mL of tBuNH$_2$ were added. The reaction was let to stir at rt for 20 minutes. Subsequently, solvents were removed in vacuo and the product was co-evaporated with pyridine, then with toluene and was left to dry under high vacuum yielding an orange foam. The product was analyzed with mass spectrometry and was used without further purification to the next step.

HRMS (ESI): for $C_{81}H_{84}O_{19}N_{11}P_2S_2^+$ [M+H]$^+$, calc. 1339.4783; found 1339.3289

2',3'- c-Dideoxy- 2"-SATE -phosphate - *O6*- dpc- N2- iBu- 3"- O - deoxyguanosine- 3'- SATE- phosphate- *N6*- Bz - 2'- O-deoxyadenosine (28)
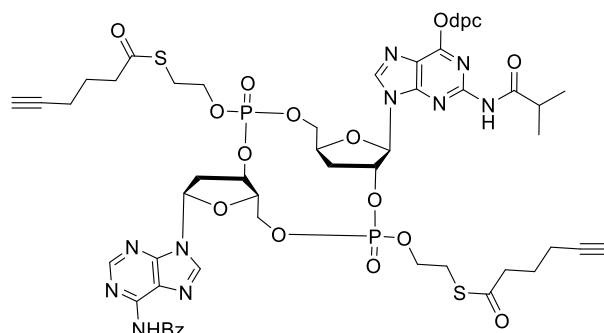
27 (490mg, 0.395mmol) was co-evaporated with pyridine (x3) and dissolved in 100mL dry THF containing 4Å molecular sieves, under Ar. TPSCl (5.9g, 19.78mmol, 50.0eq) and NMI (1.56mL, 19.78mmol, 50.0eq) were then added and the reaction was left to stir overnight at rt. Next day, the reaction was quenched with 50mL water and, after stirring for further 50 minutes, it was extracted with ethyl acetate (x3). The organic phase was evaporated under reduced pressure and the crude mixture was purified via flash column chromatography (silica gel, DCM/MeOH : 100/5). The product was received as a white solid (150mg, 0.11mmol, 28%).

R$_f$ (DCM/MeOH : 10/1) = 0.45

HRMS (ESI): for $C_{60}H_{64}O_{16}N_{11}P_2S_2^+$ [M+H]$^+$, calc. 1320.3371; found 1320.3389

IR (ATR): $\bar{v}$ (cm^{-1}) 3299 (br), 2713 (w), 1734 (s), 1499 (br), 1369 (m), 1213 (m), 1022 (m), 713 (s).

^{31}P NMR (162 MHz, DMSO) δ -1.88, -2.38, -2.53, -2.95.

N2-Benzoyl guanosine (30)
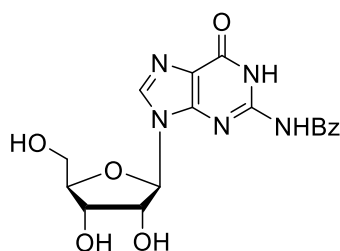
Guanosine (2g, 7.06mmol) was dried via co-evaporation with pyridine (x3) and then high-vacuum. It was then dissolved in pyridine (28mL) under nitrogen and TMSCl (3.2mL, 25.4mmol, 3.6eq) was added. The reaction was left to stir for 1h at rt. Then it was cooled down to 0oC and BzCl (1mL, 8.5mmol, 1.2eq) was dropwise added. The reaction was left to stir overnight while slowly reaching room temperature. Next, water (7mL) was added, stirred for 5min, then NH$_3$ (14mL, 29% aq. solution) was added and stirred for 15 more minutes. Solvents were evaporated under vacuum, the residual solid was suspended in cold water, stirred and filtered, then washed with cold water (x2) and ether (x2). The yellowish solid was left to dry overnight on air (1g, 2.6mmol, 40%).

Materials and methods

¹H NMR (400 MHz, DMSO) δ 8.22 (s, 1H, H-8), 8.01 – 7.92 (m, 2H, H-Bz), 7.62 – 7.53 (m, 1H, H-Bz), 7.46 (dd, J = 8.4, 7.1 Hz, 2H, H-Bz), 5.82 (d, J = 6.1 Hz, 1H, H-1'), 4.38 (dd, J = 6.1, 4.9 Hz, 1H, H-2'), 4.05 (dd, J = 4.9, 3.4 Hz, 1H, H-4'), 3.82 (q, J = 3.9 Hz, 1H, H-3'), 3.55 (dd, J = 11.9, 4.2 Hz, 1H, Ha-5'), 3.46 (dd, J = 11.9, 4.1 Hz, 1H, Hb-5').

For ¹³C spectroscopy and IR data refer to the literature [166]

5',3'-O-DTBS - 2'-O-TBS - N2-benzoyl - guanosine (31)
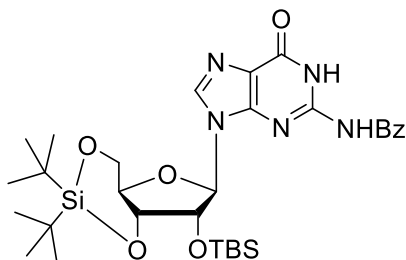
Compound **30** (1 g, 2.6mmol) was dissolved in DMF (10 ml) under N_2 atmosphere. The mixture was cooled to 0 °C and DTBS-bis(F_3MeSO_3) (0.9ml, 2.8 mmol, 1.1eq.) was added dropwise, left to stir for 45 min at 0 °C, and another 10 min at RT. Imidazole (0.88g, 13mmol, 5.0eq.) was added and the mixture was left to stir at 0 °C for 10 min and an additional 25 min at RT. The mixture was cooled to 0 °C, TBSCl (0.78g, 5.2mmol, 2.0eq.) was added, and left to stir overnight. The mixture was concentrated under reduced pressure, washed with a saturated aqueous $NaHCO_3$ solution (20mL), and extracted with ethyl acetate (3x50mL). The organic phase was concentrated under reduced pressure, and, after ¹H NMR spectroscopy analysis, the product was pure enough to be used to the next step. Product **31** was received as a white foam (2.64g, 5.05mmol, 68%).

R$_f$ (DCM/MeOH : 10/1) = 0.60

¹H NMR (400 MHz, CDCl₃) δ 8.67 (s, 1H, H8), 7.86 – 7.79 (m, 1H, H-Bz), 7.63 – 7.55 (m, 1H, H-Bz), 7.48 (t, J = 7.7 Hz, 1H, H-Bz), 5.74 (br, 1H, H-1'), 4.39 (q, J = 4.8 Hz, 2H, H-2' and H-3'), 4.19 (dd, J = 9.6, 4.6 Hz, 1H, Ha-5'), 4.10 (td, J = 9.9, 5.0 Hz, 1H, Hb-5'), 3.93 (t, J = 9.8 Hz, 1H, H-4'), 0.98 (s, 9H, 3xMe-tBu), 0.94 (s, 8H, 3xMe-tBu), 0.85 (s, 9H, 3xMe-tBu), 0.07 (d, J = 8.1 Hz, 6H, 2xMe-TBS).

For ¹³C spectroscopy and IR data refer to the literature [166]

5'-O-DMT - 2'-O-TBS - N2-benzoyl - guanosine (32)
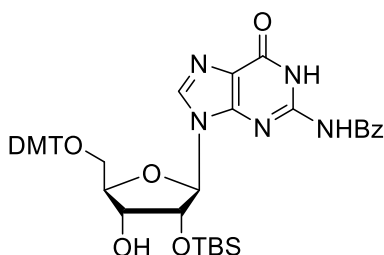
Materials and methods

Compound **31** (1.6 g, 2.50 mmol) was dissolved in DCM (14 mL) in a plastic falcon and cooled down to 0 °C. First pyridine (2.2mL, 15.0eq) and then carefully HF·pyridine (0.38 mL, 70% HF, 30% pyridine, 5.0 eq.) was added dropwise. The mixture was stirred at 0 °C for 2hrs and at room and then was quenched with TMSOMe (6.0 mL). The solution was washed with aqueous solution of NaHCO$_3$ (30mL) and brine, extracted three times with DCM, dried over Na$_2$SO$_4$ and the organic phase was removed *in vacuo*. The product was used to the next step without further purification. First, it was co-evaporated with pyridine (x3) and dissolved in dry pyridine (17mL). DMTCl (0.69mg, 2.04mmol, 1.2eq) was then added and the mixture was stirred under nitrogen overnight to slowly reach room temperature. The next day methanol (15 mL) was added and the solution was dissolved with DCM, washed with NaHCO$_3$ and brine and the aqueous phase was extracted three times with DCM. The organic phase was evaporated *in vacuo* and the crude mixture was loaded in a silica-filled column to purify, using DCM/methanol as eluents (DCM/MeOH = 100/1 to 100/10 +0.1% Et$_3$N). The product was isolated as a colorless foam (1.3g, 1.61mmol, 95%).

R$_f$ (DCM/MeOH : 10/1) = 0.50

IR (ATR): ṽ (cm^{-1}) = 2927 (w), 2001 (w), 1676 (s), 1603 (m), 1558 (m), 1402 (m), 1252 (m), 1148 (m), 1025 (s), 948 (s), 834 (s), 780 (s), 668 (m), 622 (s).

¹H NMR (500 MHz, CDCl$_3$) δ 12.27 (s, 1H, NH), 8.58 (d, J = 4.1 Hz, 2H, H8 and NH), 7.79 (s, 1H, H-Ar), 7.66 (dtd, J = 7.6, 4.1, 2.4 Hz, 2H, H-Ar), 7.54 – 7.43 (m, 3H, H-Ar), 7.35 (tt, J = 7.5, 1.2 Hz, 1H, H-Ar), 7.29 – 7.21 (m, 2H, H-Ar), 7.22 – 7.17 (m, 2H, H-Ar), 7.09 – 6.98 (m, 2H, H-Ar), 6.79 – 6.65 (m, 5H, H-Ar), 5.74 (d, J = 7.6 Hz, 1H, H-1'), 5.19 (dd, J = 7.6, 5.2 Hz, 1H, H-4'), 4.30 (dd, J = 5.2, 1.5 Hz, 1H, H-2'), 4.24 (dt, J = 3.0, 1.7 Hz, 1H, OH), 3.68 – 3.64 (m, 1H, H-4'), 3.63 (d, J = 1.0 Hz, 6H, 2xOMe), 3.03 (dd, J = 10.8, 2.7 Hz, 1H, Ha-5'), 2.91 (s, 1H, Hb-5'), 0.80 (s, 9H, 3xMe-tBu), -0.02 (s, 3H, Me-TBS), -0.21 (s, 3H, Me-TBS).

¹³C NMR (126 MHz, CDCl$_3$) δ 167.87 (C=O), 158.82 (C=O), 155.60, 149.80 (C-N), 148.28 (C-N), 147.41, 145.68, 139.60 (C-Ar),, 136.72 (C-Ar),, 136.11 (C-Ar),, 135.95 (C-Ar),, 132.83 (C-Ar),, 130.99 (C-Ar),, 129.93 (C-Ar),, 128.79 (C-Ar),, 128.32 (C-Ar),, 127.85 (C-Ar),, 127.28 (C-Ar),, 126.96 (C-Ar),, 123.82 (C-Ar),, 123.20, 113.53 (C-Ar),, 88.39 (C1'), 86.38 (C4'), 84.56 (C2'), 74.19, 71.11 (C3'), 63.69 (C5'), 55.28, 55.26, 25.57, 17.89, -5.06 (C- SiC(Me)$_3$), -5.09 (C- Si(Me)$_2$).

5'-O-DMT - 2'-O-TBS – 3'-O-deoxy- N2-benzoyl guanosine (32)
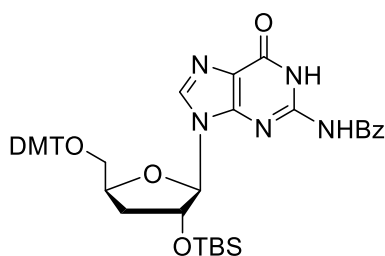
Compound **32** (1.3 g, 1.62 mmol) was diluted in 11mL of dry DMF. Then thiocarbonyldiimidazole (326 mg, 1.94 mmol, 1.2 eq) and imidazole (22 mg, 0.325 mmol, 0.2 eq) were added and the mixture was

left to stir overnight at room temperature. The next day, the solvent was evaporated under reduced pressure, the crude mixture was diluted in ethyl acetate and washed twice with $NaHCO_3$. The aqueous phase was re-extracted three times with ethyl acetate and the combined organic phases were washed with brine and then dried over $MgSO_4$. After filtration and evaporation of the solvent the crude product was purified via flash column chromatography on silica gel using ethyl acetate/i-hexane (2/1 to 5/1 to 100% EA) as eluting solvents and immediately dissolved in 9 mL of dry toluene. N_2 gas was bubbled in the mixture for 45 minutes and then $(TMS)_3SiH$ (0.44 mL, 1.44 mmol, 1.2 eq) and AIBN (40 mg, 0.24 mmol, 0.2 eq) were added. The reaction was stirred at 90°C for 2 hours and after TLC monitoring and SM conversion the mixture was left to reach room temperature and immediately added to a silica gel filled column to purify via flash column chromatography. Elution solvents were DCM/MeOH = 100/3 + 0.1% Et_3N. The product was isolated as a yellow foam (870 mg, 1.1 mmol, 92%).

$\mathbf{R_f}$ (DCM/MeOH : 10/1) = 0.27.

HRMS (ESI) : calc. for $C_{44}H_{49}N_5O_7Si^+$ $[M+H]^+$: 787.3114, found: 787.3144.

IR (ATR): $\tilde{v}$ (cm^{-1}) = 2928 (w), 2857 (w), 1694 (s), 1591 (w), 1418 (w), 1252 (m), 1213 (m), 1085 (s), 865 (m), 835 (s), 785 (s).

^{1}H NMR (400 MHz, DMSO, ppm): δ = 12.42 (s, 1H, N2-H), 8.37 (s, 1H, H8), 5.90 (d, J = 5.7 Hz, 1H, H1'), 5.17 (s, 1H, OH), 4.57 (t, J = 5.3 Hz, 1H, H2'), 3.98 (q, J = 3.6 Hz, 1H, H4'), 3.70 (m, 1H, H5'), 3.58 (m, 1H, H5'), 0.73 (s, 9H, 3xMe-tBu), - 0.07 (s, 3H, Me-TBS), -0.17 (s, 3H, Me-TBS).

^{13}C NMR (101 MHz, DMSO, ppm): δ = 156.6 (C6), 148.1 (C4), 146.0 (C2), 138.7 (C8), 124.5 (C5), 87.6 (C1'), 86.0 (C4'), 76.2 (C2'), 70.3 (C3'), 61.2 (C5'), 26.0 (C11), 17.8 (C12), -4.9 (C-TBS), -5.4 (C-TBS).

5'-O-DMT - 3'-O-deoxy - N2-benzoyl guanosine (34)
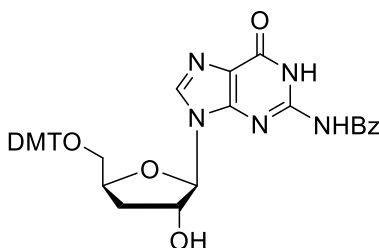
Compound **33** (0.87g, 1.1mmol) was dissolved in 8mL of dry THF. Then TBAF (1M solution in THF, 1.21mL, 1.21mmol, 1.1eq) was added dropwise and the reaction mixture was left to stir for 5hrs at rt. The reaction was quenched using 0.25mL methoxytrimethylsilane and was let to stir for 15min more. Solvents were evaporated under reduced pressure and the crude product was purified via flash column chromatography using DCM/MeOH (100/2 +0.1% Et_3N) as eluents. **34** was isolated as a yellowish foam (471mg, 0.74mmol, 67%).

$\mathbf{R_f}$ (DCM/MeOH : 10/1) = 0.40

Materials and methods

IR (ATR): ṽ (cm⁻¹) = 2930 (w), 2360 (w), 1698 (w), 1608 (m), 1581 (m), 1508 (m), 1454 (m), 1298 (m), 1246 (s), 1175 (s), 1029 (s), 900 (m), 827 (s), 792 (m), 755 (m), 704 (s).

¹H NMR (400 MHz, CDCl₃) δ 7.75 (s, 1H, H8), 7.42 (d, *J* = 7.6 Hz, 3H, H-Ar), 7.34 – 7.19 (m, 4H, H-Ar), 7.14 – 7.03 (m, 3H, H-Ar), 7.03 – 6.90 (m, 2H, H-Ar), 6.82 – 6.74 (m, 2H, H-Ar), 6.70 (dd, *J* = 17.0, 8.6 Hz, 4H, H-Ar), 5.74 (s, 1H, H-1'), 4.95 (s, 1H, H-4'), 4.49 (s, 1H, H-2'), 3.65 (d, *J* = 4.9 Hz, 6H, 2xOMe), 3.58 (s, 1H, Ha-3'), 3.34 (d, *J* = 10.5 Hz, 1H, Hb-3'), 2.25 (dq, *J* = 14.4, 6.7 Hz, 1H, Ha-5'), 2.06 – 1.96 (m, 1H, Hb-5').

¹³C NMR (126 MHz, CDCl₃) δ 167.46 (C=O), 158.76 (C=O), 155.64 (C-N), 147.74 (C-N), 147.19, 145.33 (C-Ar), 138.36 (C-Ar), 136.45 (C-Ar), 136.13 (C-Ar), 133.39 (C-Ar), 131.32 (C-Ar), 130.09 (C-Ar), 129.15 (C-Ar), 128.21 (C-Ar), 127.16 (C-Ar), 122.87 (C-Ar), 113.45 (C-Ar), 91.86, 86.30 (C2'), 78.45 (C4'), 75.17 (C-1'), 64.93 (C5'), 55.35 (C-OMe), 34.77 (C-3').

5''-O -DMT- 2''- SATE- phosphate- N2- Bz- 3''- O - deoxyguanosine- 3'- SATE- phosphate - *N*6-Bz - 2'- O-deoxyadenosine (36)
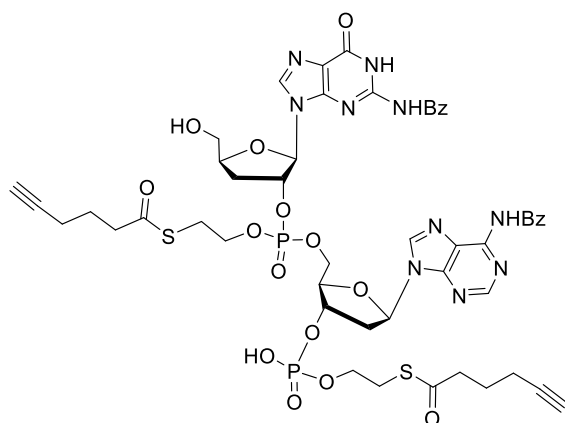
Compound **34** (200 mg, 2.79 mmol) was dissolved in 2 mL of dry DCM under Ar and **23** (180 mg, 0.44 mmol, 1.5eq) was added followed by pyridine trifluoroacetate (70 mg, 0.35 mmol, 1.2 eq). The mixture was stirred at room temperature overnight until LCMS monitoring showed completion. The next day, **24** (197 mg, 0.31 mmol, 1.5 eq) diluted in 1 mL of dry MeCN was added followed by BTT (0.3M solution in MeCN, 1.37 mL, 0.41 mmol, 2.0 eq) and the reaction was let to stir for 1 hour. Then tBuOOH (5M solution in decane, 0.18 mL, 1.0 mmol 3.0 eq) was added, the reaction was stirred for 40 min more and quenched with aq. NaHSO₃ solution (0.5 g/mL, 2 mL). The aqueous phase was extracted three times with EA and evaporated under reduced pressure. It was immediately dissolved in a 3% DCA in DCM solution (10 mL) containing 10.0 eq H₂O, stirred for 15 min and quenched with an aqueous NaHCO₃ solution. The aqueous phase was extracted three times with ethyl acetate and the combined organic layers were dried over MgSO₄ and then evaporated under reduced pressure. The crude product was dissolved in 2 mL of dry MeCN and 0.35 mL of tBuNH₂ were added. After 20 min of stirring, the solvents were removed under reduced pressure and the product was co-evaporated twice with MeCN to

Materials and methods

afford **36** as a yellow foam (210 mg, 0,177 mmol, 87%). The product was used to the next step without further purification.

LC-MS (Buffer A = 0.01 % formic acid in H$_2$O, buffer B = 0.01 % formic acid in MeCN, method: 5-80 % buffer B in 7 minutes, then 95 % B for 1 minute): t_R: 4.6 min, m/z = 1177.1 [M+H]$^+$.

5',3'-O-DTBS - 2'-O-TBS - inosine (38)
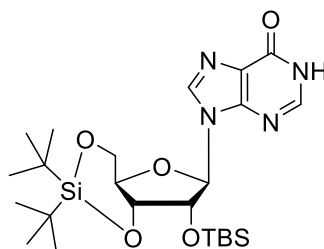
Inosine (2 g, 7.46mmol) was dissolved in DMF (30 ml) under N$_2$ atmosphere. The mixture was cooled to 0 °C and DTBS-bis(F$_3$MeSO$_3$) (2.67ml, 8.2 mmol, 1.1eq.) was added dropwise, left to stir for 45 min at 0 °C, and another 10 min at RT. Imidazole (2.5g, 37mmol, 5.0eq.) was added and the mixture was left to stir at 0 °C for 10 min and an additional 25 min at RT. The mixture was cooled to 0 °C, TBSCl (2.2g, 14.9mmol, 2.0eq.) was added, and left to stir overnight. The mixture was concentrated under reduced pressure, washed with a saturated aqueous NaHCO$_3$ solution (50mL), and extracted with ethyl acetate (3x100mL). The organic phase was concentrated under reduced pressure, and the crude product was purified via silica gel chromatography (DCM:MeOH = 100:2). Product **38** was received as a white foam (2.64g, 5.05mmol, 68%).

¹H NMR (400 MHz, CDCl$_3$) δ 11.95 (s, 1H NH), 7.86 (s, 2H, H2 and H8), 5.71 (d, J = 6.3 Hz, 1H, H-1'), 4.88 (d, J = 5.6 Hz, 1H, H-2'), 4.47 (dd, J = 5.8, 3.3 Hz, 1H, H-5a'), 3.54 (dd, J = 10.9, 2.2 Hz, 1H, H-3'), 3.21 (d, J = 7.0 Hz, 1H, H-4'), 3.06 (dd, J = 10.8, 3.4 Hz, 1H, H-5b'), 0.99 – 0.90 (m, 3H, Me-tBu), 0.88 – 0.78 (m, 21H, Me-tBu), 0.73 (d, J = 6.9 Hz, 3H, Me-tBu), 0.03 (s, 3H, Me-TBS), -0.07 (s, 3H, Me-TBS).

For ¹³C and mass spectrometry analytics refer to the literature[167].

5'-O-DMT-2'-O-TBS - inosine (39)
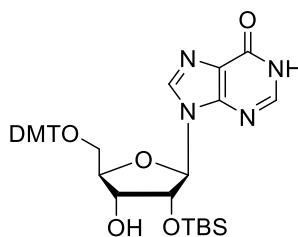
Compound **38** (3.540 g, 6.50 mmol, 1.0 eq.) was dissolved in DCM (28 mL) in a plastic falcon and cooled down to 0 °C. First pyridine (5.6 mL) and then carefully HF·pyridine (0.98 mL, 70%, 32.50 mmol, 5.0 eq.) was added dropwise. The mixture was stirred at 0 °C for 1 h and at room temperature for another 1.5 h before quenching it with TMSOMe (12.0 mL). The solution was washed with sodium hydrogen carbonate and brine, extracted three times with DCM, dried over sodium sulfate and the organic phase was removed *in vacuo*. The product was used for the next step without further purification. DMTCl (1.26 g, 3.72 mmol, 1.2 eq.) was left in hv for 1 h to remove excess moisture while the starting compound (1.19 g, 3.11 mmol, 1.0 eq) was co-evaporated twice with pyridine and left in hv for 30 min. It was then dissolved in pyridine (31 mL) and cooled down to 0 °C. The DMTCl was added and the mixture was stirred under nitrogen overnight to slowly come to room temperature. The next day methanol (15 mL) was added and the solution was dissolved with DCM, washed with sodium hydrogen carbonate and brine and the aqueous phase was extracted three times with DCM. The organic phase was evaporated *in vacuo* and the crude mixture was loaded in a silica-filled column to purify, using DCM/methanol as eluents (DCM/MeOH = 100/2 to 100/20). The product was isolated as a yellow foam (1.86 g, 2.71 mmol, 87%).

R$_f$ = 0.51 (DCM/MeOH : 10/1).

HRMS (ESI$^+$): calc. for $C_{37}H_{45}N_4O_7Si^+$ [M+H]$^+$: 685.8613, found: 685.3045.

IR (ATR): $\tilde{v}$ (cm^{-1}) = 3074 (w), 2929 (m), 2857 (w), 1706 (s), 1692 (s), 1608 (w), 1510 (m), 1252 (m), 1177 (m), 1129 (m), 1084 (s), 1032 (m), 985 (w), 888 (m), 830 (s).

¹H NMR (400 MHz, CDCl3, ppm): δ = 8.04 (s, 1H, H8), 8.01 (s, 1H, H2), 7.47 - 7.18 (m, 9H, H15,19-21,23), 6.86 – 6.77 (m, 4H, H16,24), 6.01 (d, *J* = 5.6 Hz, 1H, H-1'), 4.89 (t, *J* = 5.3 Hz, 1H, H-2'), 4.33 (br s, 1H, H-3'), 4.27 (m, 1H, H-4'), 3.78 (s, 6H, H26,27), 3.50 (dd, *J* = 10.7, 3.1 Hz, 1H, H-5'), 3.40 (dd, *J* = 10.7, 3.9 Hz, 1H, H-5'), 2.72 (br s, 1H, OH), 0.85 (s, 9H, Me-TBS), 0.01 (s, 3H, Me-TBS), -0.13 (s, 3H, Me-TBS).

¹³C NMR (101 MHz, CDCl3, ppm): δ = 159.7 (C=O), 159.1 (C-Ar), 149.4, 145.2 (C2), 145.0 (C-Ar), 139.4 (C8), 136.0 (C-Ar), 130.5 (C-Ar), 128.6 (C-Ar), 128.4 (C-Ar), 127.5 (C-Ar), 125.6 (C-Ar), 113.7 (C-Ar), 88.6 (C-Ar), 87.2 (C1'), 84.8 (C4'), 76.6 (C2'), 72.1 (C3'), 63.9 (C5'), 55.7 (C-Ar), 26.0 (3C, C-TBS), 18.4 (C-TBS), -4.5 (C- Si(Me)$_2$), -4.7 (C- Si(Me)$_2$)

5'-O-DMT-3'-thionylcarbamate-2'-O-TBS - inosine (40)
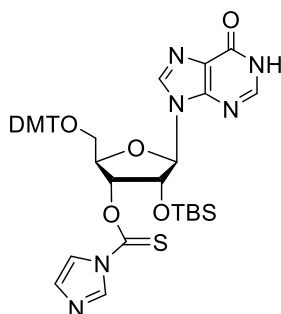
Materials and methods

Compound **39** (1 g, 10.65 mmol) was diluted in 10mL of dry DMF. Then thiocarbonyldiimidazole (578 mg, 3.25 mmol, 5.0 eq) and imidazole (22 mg, 0.325 mmol, 0.5eq) were added and the mixture was left to stir overnight at room temperature. The next day, the solvent was evaporated under reduced pressure, the crude mixture was diluted in ethyl acetate and washed twice with $NaHCO_3$. The aqueous phase was re-extracted three times with ethyl acetate and the combined organic phases were washed with brine and then dried over $MgSO_4$. After filtration and evaporation of the solvent the crude product was purified via flash column chromatography on silica gel using ethyl acetate/i-hexane (2/1 to 5/1 to 100% EA) as eluting solvents. **40** was afforded as a white foam (500 mg, 0.56 mmol, 87%).

R_f = 0.75 (EA/iHex : 2/1)

HRMS (ESI): for $C_{41}H_{46}O_7N_6SSi^+$ $[M+H]^+$, calc. 795.2918; found 795.345

IR (ATR): $\tilde{v}$ (cm^{-1}) = 2988 (w), 1719 (m), 1601 (w), 1466 (w), 1390 (m), 1329 (m), 1270 (s), 1209 (s), 1162 (m), 1089 (s), 1069 (s), 1015 (s), 979 (s), 890 (m), 837 (m), 708 (s), 653 (m).

^{1}H NMR (400 MHz, $CDCl_3$) δ 11.89 (s, 1H, NH), 7.81 (s, 1H, H2), 7.74 (s, 1H, H8), 7.49 (dd, J = 8.5, 1.5 Hz, 2H, H-aromatic), 7.36 (dd, J = 8.9, 1.7 Hz, 4H, H-aromatic), 7.22 (m, 4H, 2xH-imidazole and 2xH-aromatic), 6.83 – 6.68 (m, 6H, H-imidazole and 5xH-aromatic), 5.65 (d, J = 6.4 Hz, 1H, H-1'), 4.84 (m, 1H, H-2'), 4.43 (dd, J = 5.8, 3.2 Hz, 1H, H-4'), 3.74 (d, J = 4.2 Hz, 6H, 2xOMe), 3.51 (dd, J = 10.9, 2.2 Hz, 1H, Ha-5'), 3.02 (dd, J = 10.9, 3.3 Hz, 1H, Hb-5'), 2.92 (d, J = 8.4 Hz, 1H, H-3'), 0.84 (s, 9H, SiC(Me)$_3$), 0.00 (s, 3H, Si(Me)$_2$), -0.10 (s, 3H, Si(Me)$_2$).

^{13}C NMR (126 MHz, $CDCl_3$) δ 183.08 (C=S), 162.73 (C=O), 159.25 (C=O), 158.82, 149.27, 144.44, 138.77 (C-imidazole), 135.44, 131.31 (C-imidazole), 130.16, 128.16, 127.24 (C-imidazole), 125.30, 117.96, 113.46, 88.31 (C-4'), 87.28, 82.16 (C-1'), 81.09, 74.53 (C-5'), 62.98 (C-3'), 55.36 (C-2'), 36.61, 31.56, 25.37, 17.74, -5.06 (C- SiC(Me)$_3$),, -5.23 (C- SiC(Me)$_3$).

5'-O-DMT-3'-O-deoxy - inosine (41)
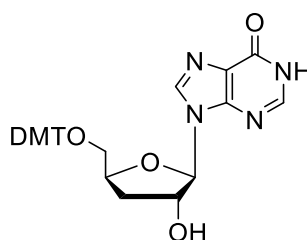
Compound **40** (2.5 g, 3.14 mmol) was dissolved in 24mL of dry toluene. N_2 gas was then bubbled in the solution for 30min. Next, AIBN (107 mg, 0.74 mmol, 0.2 eq) and tris-trimethylsilylsilane (1.2 mL, 3.92 mmol, 1.2eq) were added and the reaction mixture was heated to reflux (95°C) for 5hrs until all starting material was consumed. The reaction flask was let to cool down to room temperature and then immediately added in a silica gel filled column to partially purify using ethyl acetate/i-hexane (1/1 to 2/1) as eluents. Then the compound was diluted in 7 mL of dry THF under N_2 and cooled to 0°C. TBAF

Materials and methods

(1M solution in THF, 1 mL, 1 mmol, 1.1eq) was added dropwise and the reaction mixture was left to stir for 5 hrs while slowly reaching room temperature. The reaction was quenched using 2 mL methoxytrimethylsilane and was let to stir for 15min more. Solvents were evaporated under reduced pressure and the crude product was purified via flash column chromatography using DCM/MeOH (100/3) as eluents. **41** was isolated as a yellow foam (941 mg, 1.69 mmol, 54%).

R_f = 0.50 (DCM/MeOH :10/1)

HRMS (ESI): for $C_{13}H_{31}O_6N_4^+$ [M+H]$^+$, calc. 555.2165; found 555.0315

IR (ATR): $\tilde{v}$ (cm^{-1}) 3414.4 (w), 3004.7 (m), 2362.0 (s), 1710.1 (m), 1609.5 (s), 1555.9 (m), 1510.1 (s), 1419.6 (w), 1358.6 (s), 1220.0 (s), 1091.9 (w), 1034.0 (s), 902.5 (s), 835.1 (w).

^{1}H NMR (400 MHz, DMSO) δ 12.41 (s, 1H, NH), 8.15 (s, 1H, H2), 8.06 (s, 1H, H8), 7.36 – 7.15 (m, 9H, Ar-H), 6.81 (m, 4H, Ar-H), 5.92 (d, J = 1.5 Hz, 1H, H-1'), 4.67 (d, J = 5.3 Hz, 1H, H-2'), 4.50 (tt, J = 9.6, 4.4 Hz, 1H, H-4'), 3.72 (d, J = 1.5 Hz, 6H, 2xOMe), 3.22 – 3.09 (m, 2H, Ha-3' and Ha-5'), 2.37 – 2.25 (m, 1H, Hb-3'), 1.94 (ddd, J = 13.1, 6.0, 2.0 Hz, 1H, Hb-5').

^{13}C NMR (101 MHz, CDCl$_3$) δ 159.49 (C=O), 158.67 (C-Ar), 148.47 (C-Ar), 144.68 (C-2), 138.57 (C-8), 135.77 (C-Ar), 130.23 (C-Ar), 128.06 (C-Ar), 127.07 (C-Ar), 125.38 (C-Ar), 113.32 (C-Ar), 92.43 (C-1'), 86.55 (C-4'), 80.33 (C-2'), 64.98 (C-3'), 55.36 (C-5'), 53.57, 35.35.

5''-O -DMT- 2''- SATE- phosphate- N2- Bz- 3''- O - deoxyguanosine- 3'- SATE- phosphate - *N6*-Bz - 2'- O-deoxyadenosine (43)
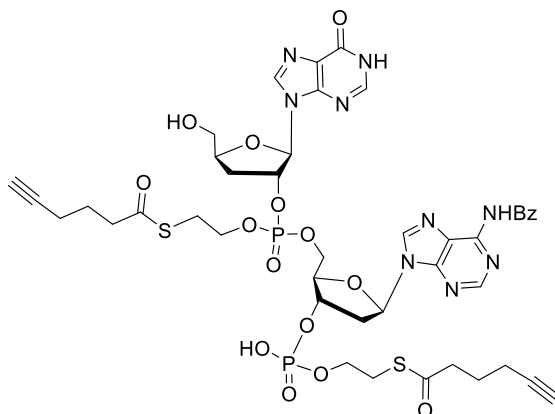
Compound **40** (300 mg, 0.54 mmol) was dissolved in 3 mL of dry DCM under Ar and **23** (326 mg, 0.81 mmol, 1.5eq) was added followed by pyridine trifluoroacetate (124 mg, 0.65 mmol, 1.2 eq). The mixture was stirred at room temperature overnight until LCMS monitoring showed completion. The next day, **24** (340 mg, 0.52 mmol, 1.5 eq) diluted in 1.5 mL of dry MeCN was added followed by BTT (0.3M solution in MeCN, 2.34 mL, 0.70 mmol, 2.0 eq) and the reaction was let to stir for 1 hour. Then tBuOOH (5M solution in decane, 0.21 mL, 1.05 mmol 3.0 eq) was added, the reaction was stirred for 40 min more and quenched with aq. NaHSO$_3$ solution (0.5 g/mL, 2 mL). The aqueous phase was extracted three times with EA and evaporated under reduced pressure. It was immediately dissolved in a

Materials and methods

3% DCA in DCM solution (13 mL) containing 10.0 eq H_2O, stirred for 15 min and quenched with an aqueous $NaHCO_3$ solution. The aqueous phase was extracted three times with ethyl acetate and the combined organic layers were dried over $MgSO_4$ and then evaporated under reduced pressure. The crude product was dissolved in 4 mL of dry MeCN and 0.7 mL of $tBuNH_2$ were added. After 20 min of stirring, the solvents were removed under reduced pressure and the product was co-evaporated twice with MeCN to afford **43** as a yellow foam (100 mg, 0.094 mmol, 25%). The product was used to the next step without further purification.

LC-MS (Buffer A = 0.01 % formic acid in H_2O, buffer B = 0.01 % formic acid in MeCN, method: 5-80 % buffer B in 7 minutes, then 95 % B for 1 minute): t_R: 3.7 min, m/z = 1057.2 $[M+H]^+$.

Dideoxy-cGAMP-palmitate conjugate

5-Amino-3-(4-chlorobenzyl)thio-1,2,4-triazole (54)[146]
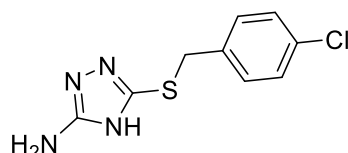
5-amino-3-mercapto-1,2,4-triazole (**52**) (1 g, 8.61 mmol) was dissolved in DMF (13 mL) under N_2, then triethylamine (1.32 mL, 9.51 mmol, 1.1 eq) was added dropwise. The mixture was left to stir for 15 min at RT. 4-chlorobenzylbromide (**53**) (1.92 g, 9.5 mmol, 1.1 eq) was subsequently added and the mixture was left to stir for 3hrs. TLC and LCMS monitoring showed completion at 1h. Solvent was evaporated and the residue was dissolved in EA and washed with H_2O and brine and dried over $MgSO_4$. The crude product was purified via flach column chromatography on silica gel using DCM/MeOH 100/5 as eluents. The pure product was isolated as a colorless solid (1.9 g, 7.9 mmol, 92%).

R_f = 0.45 (DCM/MeOH = 10/1)

HRMS (ESI): for $C_9H_{10}ClN_4S^+$ $[M+H]^+$, calc. 241.0314; found 241.0335

¹H NMR (500 MHz, DMSO) δ 11.96 (s, 1H, N-H), 7.36 (q, J = 8.6 Hz, 4H, aromatic-H), 6.09 (s, 2H, -NH_2), 4.20 (s, 2H, -S-CH2-).

For ¹³C and IR spectra refer to the literature[146].

3-((4-Chlorobenzyl)thio)-1-((12,13-dihydrobenzofuran-11-yl)sulfonyl)-5-amino-1,2,4-triazole (45) [146]
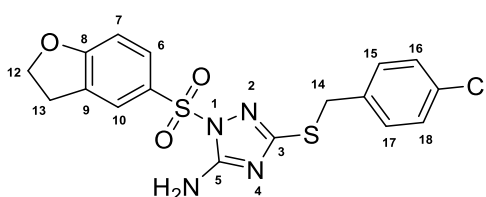
Materials and methods

Compound **54** (1 g, 4.1 mmol) was dissolved in 40mL MeCN under N_2. Triethylamine (0.7 mL, 5 mmol, 1.2 eq) was then added dropwise at 0°C followed by the 2,3-dihydrobenzofuran-5-sulfonyl chloride (**55**) (1.08 g, 5 mmol, 1.2 eq). The mixture was left to stir for 2h while slowly reaching room temperature. The solvent was evaporated and the crude product was directly added into a silica-gel filled column to purify using DCM/MeOH (100/2) as eluents. The pure product was isolated as a colorless solid (1.7 g, 4 mmol, 95%).

Rf = 0.80 (DCM/MeOH = 10/1)

HRMS (ESI): for $C_{17}H_{16}ClO_3N_4S_2^+$ [M+H]$^+$, calc. 423.0347; found 423.0315

IR (ATR): ṽ (cm^{-1}) 3446 (m), 2924(w), 1646(s), 1481(s), 1365(s), 1267(s), 1241(s), 1189(s), 1164(s), 606(s), 590(s).

¹H NMR (500 MHz, CDCl$_3$) δ 7.65 (dd, J = 8.6, 2.1 Hz, 1H, H-7), 7.62 – 7.44 (m, 1H, H-6), 7.15 (d, J = 10.5 Hz, 2H, benzyl-H), 7.09 (d, J = 8.5 Hz, 2H, benzyl-H), 6.77 (d, J = 8.6 Hz, 1H, H-10), 5.68 (s, 2H, -NH2), 4.63 (t, J = 8.8 Hz, 2H, H-13), 4.07 (s, 2H, H-14), 3.16 (t, J = 8.8 Hz, 2H, H-12).

¹³C NMR (126 MHz, CDCl$_3$) δ 166.08, 161.76, 156.24, 136.01, 133.17, 130.52 (C-7 and C-benzyl), 129.24, 128.59 (C-benzyl), 127.61, 125.49 (C-6), 110.10 (C-10), 72.92 (C-13), 34.61(C-14), 28.96 (C-12).

3-((4-Chlorobenzyl)thio)-1-((12,13-dihydrobenzofuran-11-yl)sulfonyl)-1,2,4-triazol-5-yl-chloroacetamide (62)
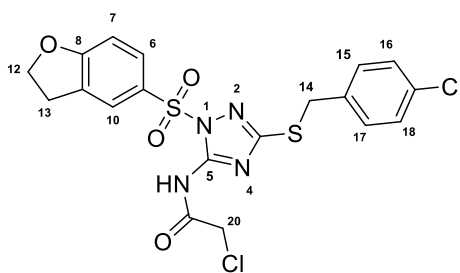
Compound **45** (677 mg, 1.6 mmol) was dissolved in 25 mL dry DCM under N_2 followed by dropwise addition of acetyl chloride (**61**) (191µL, 2.4mmol, 1.5eq). After 10min of stirring, triethylamine (463 µL, 2.4 mmol, 1.5 eq) was added dropwise and the reaction mixture turned black. The mixture was left to stir overnight at room temperature and subsequently was evaporated under reduced pressure. The crude product was immediately passed through a flash column chromatography using DCM/EA : 5/1 as eluents to afford **62** as a yellowish solid (598 mg, 1.2 mmol, 75%).

R$_f$ = 0.60 (DCM/MeOH = 10/1)

HRMS (ESI): for $C_{19}H_{16}Cl_2O_4N_4S_2^+$ [M+H]$^+$, calc. 498.9990; found 499.0011

Materials and methods

IR (ATR): ṽ (cm⁻¹) 3356 (w), 2786(w), 1733(s), 1602(s), 1241(s), 1148(s), 1060(s), 892(s), 699(s).

¹H NMR (500 MHz, CDCl₃) δ 10.21 (s, 1H, N5-H), 7.78 (dd, J = 8.6, 2.2 Hz, 1H, H-7), 7.71 (d, J = 1.9 Hz, 1H, H-6), 7.31 – 7.24 (m, 2H, benzyl-H), 7.23 – 7.16 (m, 2H, benzyl-H), 6.90 (d, J = 8.6 Hz, 1H, benzyl-H), 4.76 (t, J = 8.9 Hz, 2H, H-13), 4.36 (s, 2H, H-20), 4.22 (s, 2H, H-14), 3.27 (t, J = 8.8 Hz, 2H, H-12).

¹³C NMR (126 MHz, CDCl₃) δ 166.81 (C-19), 148.20, 135.65, 133.27, 131.13 (C-7), 130.57 (aromatic-C), 129.72 (aromatic-C), 128.60 (aromatic-C), 126.37 (aromatic-C), 125.81 (C-6), 110.44, 73.15 (C-13), 60.56, 43.21 (C-20), 34.85 (C-14), 29.84, 28.87 (C-12), 21.22, 14.34.

3-((4-Chlorobenzyl)thio)-1-((12,13-dihydrobenzofuran-11-yl)sulfonyl)-1,2,4-triazol-5-yl-azidoacetamide (72)
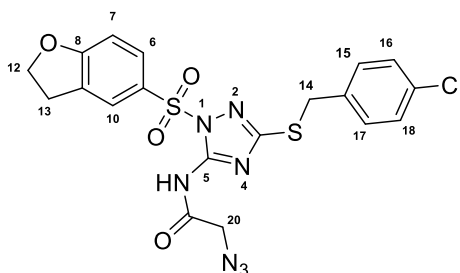
Compound **62** (100 mg, 0.2 mmol) was dissolved in 5 mL of dry DMF and sodium azide (52 mg, 0.8 mmol, 4.0 eq) was added. The mixture was stirred at room temperature overnight. The next day, water was added in the flask and the mixture was stirred for 10 minutes followed by extractions using ethyl acetate (x4). The organic phases were lastly washed with brine and dried over MgSO4. The product was purified via reverse phase HPLC using a 30-70% Buffer B method for 45 minutes (flow 1ml/min, t_R = 31 min) (Buffer A = 0.1% TFA in H₂O, Buffer B = 0.1% TFA in MeCN) and **72** was obtained as a brown solid (17 mg, 33.6 umol, 20%).

HRMS (ESI): for C₁₉H₁₆ClO₄N₇S₂⁺ [M+H]⁺ , calc. 506.0394; found 506.0454

IR (ATR): ṽ (cm⁻¹) 3321 (br), 2924 (s), 2359 (s), 2109 (s), 1707 (s), 1534 (s), 1487 (s), 1470 (s), 1438 (s), 1244 (s), 1061 (s).

¹H NMR (500 MHz, CDCl₃) δ 9.85 (s, 1H, N5-H), 7.72 (dd, J = 8.6, 2.2 Hz, 1H, H-7), 7.65 (dd, J = 2.3, 1.2 Hz, 1H, H-6), 7.22 – 7.16 (m, 2H, benzyl-H), 7.19 – 7.09 (m, 2H, benzyl-H), 6.83 (d, J = 8.6 Hz, 1H, benzyl-H), 4.69 (t, J = 8.9 Hz, 2H, H-13), 4.26 (s, 2H, H-20), 4.14 (s, 2H, H-114), 3.21 (t, J = 8.8 Hz, 2H, H-12).

¹³C NMR (126 MHz, DMSO) δ 167.93 (C=O), 165.99, 160.57, 136.61, 131.86 (aromatic-C), 130.99 (aromatic-C), 130.78 (aromatic-C), 130.71 (aromatic-C), 130.54 (aromatic-C), 130.01 (aromatic-C),

128.33 (aromatic-C), 128.19 (aromatic-C), 126.18 (aromatic-C), 125.94 (C-6), 109.84, 73.10 (C-13), 51.26 (C-20), 33.54 (C-14), 28.17 (C-12).

5'-O-DMT-2'-deoxy-3'-O-TBS N2-benzoyl adenosine (64)
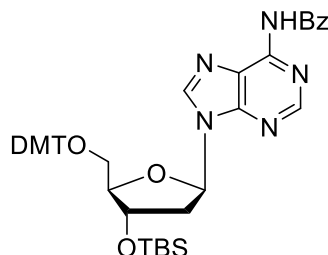
N6-benzoyl-5'-O-DMT-2'-deoxy-3'-O-TBS adenosine (1.00 g, 1.5 mmol, 1.0 equiv.) was dissolved in pyridine (6 mL), *t*-butyldimethylsilyl chloride (0.35 g, 2.3 mmol, 1.5 equiv.) and imidazole (0.21 mg, 3.1 mmol, 2.0 equiv.) were added and the solution was stirred overnight under nitrogen atmosphere. The reaction was quenched with a NaHCO₃ aqueous solution (saturated, 30 mL) and then was extracted with ethyl acetate (3×100mL), the organic phase was washed with brine (100mL) and dried over MgSO₄. After evaporation of the solvents *in vacuo* and purification by column chromatography (silica gel, DCM/MeOH: 100/2), **64** (1.03 g, 1.3 mmol, 87%) was obtained as a white foam.

R$_f$ = 0.62 (DCM/MeOH = 10/1).

IR (ATR): ṽ (cm^{-1}) = 2855 (w), 1701 (b), 1608 (m), 1579 (m), 1507 (m), 1297 (m), 1247 (s), 1175 (m), 1093 (m), 1067 (m), 1030 (m), 949 (b), 872 (b), 830 (s).

HRMS (ESI): calculated for $C_{44}H_{49}N_5NaO_6Si^+$ [M+Na]$^+$: 794.3344, found: 794.3335.

¹H NMR (500 MHz, CDCl3): δ (ppm) = 9.00 (s, 1H, NH), 8.76 (s, 1H, H-8), 8.22 (s, 1H, H-2), 8.02 (d, J = 7.0 Hz, 2H, Ar-H), 7.55 – 7.17 (m, 12H, Ar-H), 6.80 (d, J = 8.8 Hz, 4H, Ar-H), 6.49 (t, J = 6.5 Hz, 1H, H-1'), 4.61 (dt, J = 6.1, 3.4 Hz, 1H, H-3'), 4.13 (q, J = 4.3 Hz, 1H, H-4'), 3.77 (s, 6H, 2xO-CH3), 3.40 (dd, J = 10.4, 4.5 Hz, 1H, H-5$_a$'), 3.29 (dd, J = 10.4, 4.3 Hz, 1H, H-5$_b$'), 2.80 (dt, J = 12.9, 6.0 Hz, 1H, H-2$_a$'), 2.49 – 2.43 (m, 1H, H-2$_b$'), 0.87 (s, 9H, Si-C(CH₃)₃), 0.06 (s, 3H, Si-CH₃), 0.02 (s, 3H, Si-CH₃).

¹³C NMR (126 MHz, CDCl₃): δ (ppm) = 158.65 (C=O), 152.72 (C8), 141.71 (C2), 133.8 (ArC) 132.91 (ArC), 130.13 (ArC), 129.02 (ArC), 128.24 (ArC), 128.00 (ArC), 127.96 (ArC), 127.06 (ArC), 113.27 (ArC), 87.18 (C4'), 86.62 (C-Ar3), 85.02 (C1'), 72.67 (C3'), 63.30 (C5'), 55.36 (O-CH₃), 40.84 (C2'), 25.88 (Si-C), 25.79 (Si-(CH₃)₃), -4.55 (Si-CH₃), -4.67 (Si-CH₃).

5'-O-DMT-2'-deoxy-3'-O-TBS N2-(*tert*-butyl-hexylcarbamate, benzoyl) adenosine (65)
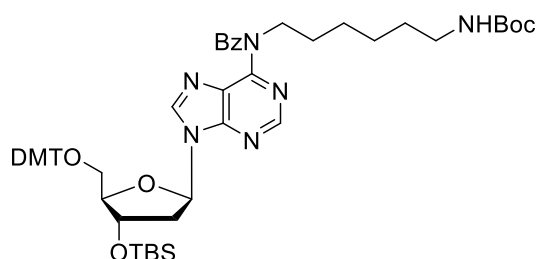
Compound **64** (1.02 g, 1.3 mmol, 1.0 equiv.) was dried twice with toluene by co-evaporation and then dissolved in THF (15 mL) under argon atmosphere. After the addition of DEAD (0.80 mL, 2.0 mmol, 1.5 equiv.), triphenylphosphine (0.52 g, 2.0 mmol, 1.5 equiv.) and *t*-butyl(6-hydroxyhexyl)carbamate (0.44 g, 2.0 mmol, 1.5 equiv.), the solution was stirred overnight at room temperature and the crude product was purified via column chromatography (silica gel, isohexane/ethyl acetate 1/1) yielding **65** (0.94 g, 1.0 mmol, 76%) as a yellow-white foam.

R_f = 0.67 (*i*Hex:EA = 1:2).

IR (ATR): $\tilde{v}$ (cm^{-1}) = 2930 (w), 2858 (w), 2359 (w), 1708 (s), 1572 (m), 1508 (m), 1418 (w), 1363 (m), 1299 (w), 1248 (s), 1220 (s), 1175 (s), 1097 (m), 1063 (m), 1031 (m), 832 (m).

HRMS (ESI): calculated for $C_{55}H_{70}N_6NaO_8Si^+$ [M+Na]$^+$: 993.4922, found: 993.4916.

^{1}H NMR (500 MHz, CD2Cl2): δ (ppm) = 8.47 (s, 1H, H-8), 8.04 (s, 1H, H-2), 7.40 – 6.72 (m, 18H, Ar-H), 6.37 (t, J = 6.5 Hz, 1H, H-1'), 4.66 – 4.60 (m, 1H, H-3'), 4.57 (s, 1H, NH), 4.31 – 4.25 (m, 2H, -CH$_2$-), 4.18 – 4.10 (m, 2H, -CH$_2$-), 4.05 (q, J = 4.4 Hz, 1H, H-4'), 3.77 (s, 6H, 2xO-CH3), 3.32 (dd, J = 10.5, 4.5 Hz, 1H, H$_a$-5'), 3.21 (dd, J = 10.5, 4.6 Hz, 1H, H$_b$-5'), 3.03 – 2.95 (m, 2H, -CH$_2$-), 2.77 – 2.70 (m, 1H, H$_a$-2'), 2.41 – 2.33 (m, 1H, H$_b$-2'), 1.64 (p, J = 7.6 Hz, 2H, -CH$_2$-), 1.39 (s, 9H, O-C(CH$_3$)$_3$), 1.37 – 1.33 (m, 2H, CH$_2$), 1.32 – 1.30 (m, 2H, -CH$_2$-), 1.27 – 1.28 (m, 2H, -CH$_2$-), 0.87 (s, 9H, Si-C(CH$_3$)$_3$), 0.06 (s, 3H, Si-CH$_3$), 0.03 (s, 3H, Si-CH$_3$).

^{13}C NMR (126 MHz, CDCl3): δ (ppm) = 172.10 (C=O), 158.67 (C8), 154.60 (ArC), 152.39 (ArC), 152.04 (ArC), 142.06 (C2), 135.81 (ArC), 130.61 (ArC), 130.11 (ArC), 128.71 (ArC), 128.18 (ArC), 127.99 (ArC), 127.92 (ArC), 127.19 (ArC), 127.01 (ArC), 113.27 (ArC), 86.97 (C4'), 86.54 (C-Ar3), 84.55 (C1'), 72.47 (C3'), 63.11 (C5'), 55.37 (O-CH$_3$), 48.58 (CH$_2$), 40.36 (CH$_2$, C2'), 28.57 (CH$_2$, CH2, (CH$_3$)$_3$), 26.58 (CH$_2$), 26.51 (CH$_2$), 25.87 (Si-C(CH$_3$)$_3$), 18.11 (Si-C), -4.57 (Si-CH$_3$), -4.65 (Si-CH$_3$).

Materials and methods

5'-O-DMT-3'-deoxy-N2-(*tert*-butyl-hexylcarbamate, benzoyl) adenosine (66)
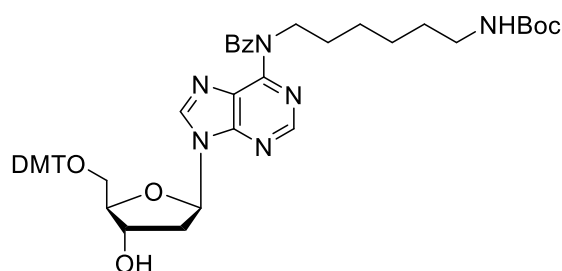
Compound **65** (0.94 g, 1.0 mmol, 1.0 equiv.) was dissolved in THF (6 mL) under nitrogen atmosphere and cooled to 0 °C. After the dropwise addition of TBAF (1.1 mL, 1M in THF, 1.1 mmol, 1.1 equiv.) the solution was stirred for 30 min at 0 °C and overnight at room temperature. The excess TBAF was quenched with a solution of methoxytrimethylsilane (2 mL, 15 min) and the solvent was removed *in vacuo*. Following the purification by column chromatography (SiO$_2$, MeOH (1%→10%) in DCM), **66** (0.66 g, 0.8 mmol, 80%) was obtained as a white foam.

R_f = 0.67 (DCM:MeOH = 10:1).

IR (ATR): $\tilde{v}$ (cm^{-1}) = 3855 (w), 3736 (w), 3650 (w), 3630 (w), 3568 (w), 2933 (w), 2359 (m), 2343 (m), 1608 (w), 1570 (m), 1507 (s), 1448 (m), 1388 (w), 1365 (m), 1297 (m), 1248 (s), 1218 (m), 1174 (s), 1064 (m), 1033 (m), 827 (m).

HRMS (ESI): calculated for C$_{49}$H$_{56}$KN$_6$O$_8^+$ [M+K]$^+$: 895.3797, found: 895.3796.

¹H NMR (500 MHz, CD$_2$Cl$_2$): δ (ppm) = 8.45 (s, 1H, H-8), 8.02 (s, 1H, H-2), 7.41 – 6.77 (m, 18H, Ar-H), 6.40 (t, J = 6.5 Hz, 1H, H-1'), 4.67 – 4.63 (m, 1H, H-3'), 4.60 (s, 1H, NH), 4.32 – 4.27 (m, 2H, -CH$_2$-), 4.11 – 4.08 (m, 1H, H-4'), 3.78 (s, 6H, O-CH$_3$), 3.36 – 3.31 (m, 2H, H-5'), 3.02 – 2.97 (m, 2H, -CH$_2$-), 2.79 – 2.73 (m, 1H, H$_a$-2'), 2.50 – 2.44 (m, 1H, H$_b$-2'), 1.70 – 1.59 (m, 2H, -CH$_2$-), 1.39 (s, 9H, O-C(CH$_3$)$_3$), 1.34 – 1.30 (m, 2H, -CH$_2$-), 1.29 – 1.24 (m, 2H, -CH$_2$-).

¹³C NMR (126 MHz, CDCl$_3$): δ (ppm) = 172.33 (C=O), 162.79 (C=O), 159.23 (ArC), 154.89 (ArC), 152.78 (ArC), 152.28 (C8), 145.84 (ArC), 142.54 (C2), 137.26 (ArC), 136.23 (ArC), 136.16 (ArC), 130.93 (ArC), 130.55 (ArC), 130.52 (ArC), 129.08 (ArC), 128.53 (ArC), 128.42 (ArC), 128.26 (ArC), 127.55 (ArC), 127.40 (ArC), 113.66 (ArC), 87.01 (C-Ar3), 86.59 (C4'), 84.82 (C1'), 79.07 (C-(CH$_3$)$_3$), 72.68 (C3'), 64.20 (C5'), 55.76 (O-CH$_3$), 48.81 (CH$_2$), 40.92 (CH$_2$), 40.50 (C2'), 30.39 (CH$_2$), 29.00 (CH$_2$), 28.67 ((CH$_3$)$_3$), 26.94 (CH$_2$), 26.87 (CH$_2$).

Materials and methods

2'-Deoxy- 3'-O-(allyl, cyanoethyl) phosphate N2-*tert*-butyl-hexylcarbamate, benzoyl adenosine (67)
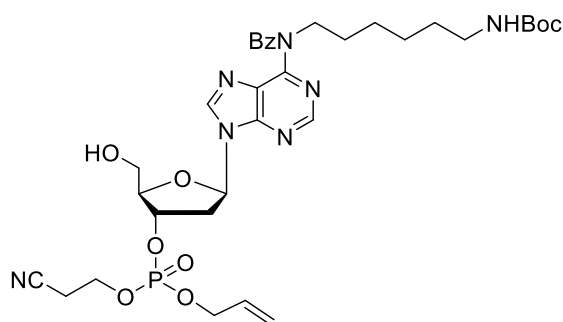
Compound **66** (65 mg, 0.075 mmol) was co-evaporated using toluene (x2) and then diluted in 3mL dry DCM under Ar. Then 2-cyanoethyl-N,N,N',N'-tetraisopropylphosphorodiamidite (28 uL, 0.091 mmol, 1.2 eq) and pyr-TFA (17 mg, 0.091 mmol, 1.2 eq) were added and the mixture was left to stir under Ar at rt overnight. Then BTT (0.3M in MeCN, 0.5 mL, 0.151 mmol, 2.0 eq) and allyl alcohol (26uL, 0.379mmol, 5.0eq) were added to the mixture and stirring continued for another hour. Subsequently, tert-butyl hydroperoxide (5.0-6.0M in decane, 45 uL, 0.227mmol, 3.0eq) was added and the mixture continued stirring for 40 minutes. The hydroperoxide was quenched at 0°C using aq. NaHSO₃ solution (1.5mL, 0.5g/mL). The mixture was stirred for 10min at 0°C and then for 5min at rt. Solvents were evaporated under reduced pressure until a foam was formed which was subsequently dissolved in a 10mL mixture of 3% DCA in DCM (3.2 mL DCM, 0.094 mL DCA) containing 10.0 eq H₂O. The mixture was left to stir for 10min and then was quenched with an aqueous solution of NaHCO₃. The aqueous phase was extracted three times with ethyl acetate and the combined organic layers were dried over MgSO₄ and evaporated under reduced pressure. The product was purified via flash column chromatography using DCM/acetone/MeOH (80/15/5) as eluents to afford **67** as a mixture of 2 P-diastereomers in the form of a colorless foam (25 mg, 0.034 mmol, 45%).

R$_f$ = 0.55 (DCM/MeOH)

LC-MS (Buffer A = 0.01 % formic acid in H₂O, buffer B = 0.01 % formic acid in MeCN, method: 5-80 % buffer B in 7 minutes, then 95 % B for 1 minute): t_R: 5.5 min, m/z = 728.5 [M+H]⁺.

2'-Deoxy- 3'-O-(allyl, cyanoethyl) phosphate N2-(*tert*-butyl-hexylcarbamate, benzoyl) adenosine 3"-deoxy-2"-cyanoethyl-phosphate O6-dpc-N2-iBu guanosine (69)
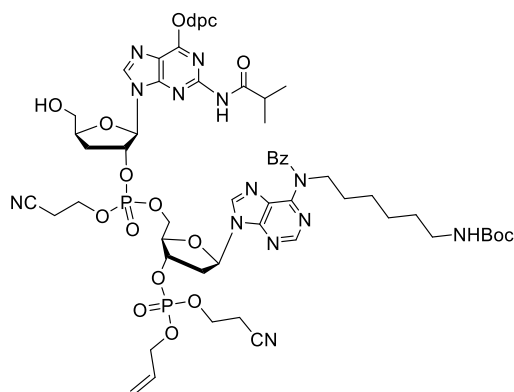
67 (25 mg, 0.034 mmol) and **68** (38 mg, 0.051 mmol, 1.2 eq) were co-evaporated with MeCN (x3), then they were dissolved in dry MeCN (0.5mL) under an Ar atmosphere. BTT (0.3M in MeCN, 230 uL, 0.068 mmol, 2.0 eq) was added and the mixture was left to stir for 1h. Then tBuOOH (5.0M in decane, 20 uL, 0.103 mmoL, 3.0 eq) was added and the mixture was left to stir for 40min. The solution was cooled to 0°C and an aqueous solution of $NaHSO_3$ (50 uL, 0.5g/mL) was added. The mixture was stirred for 10min at 0°C and then for 5min at rt. Solvents were evaporated until a foam was formed which was subsequently dissolved in a 1.44mL mixture of 3% DCA in DCM. The mixture was left to stir for 15 min and then was quenched with an aqueous solution of $NaHCO_3$ (10 mL). The aqueous phase was extracted three times with DCM and ethyl acetate and the combined organic layers were dried over $MgSO_4$ and evaporated under reduced pressure. The product was purified via flash column chromatography (silica gel, DCM/acetone/MeOH: 80/15/5) and was isolated as a colorless foam (25 mg, 18 umol, 53%). The product was obtained as an inseparable mixture of 4 P-diastereomers and was not further characterized.

LC-MS (Buffer A = 0.01 % formic acid in H_2O, buffer B = 0.01 % formic acid in MeCN, method: 5- 80 % buffer B in 7 minutes, then 95 % B for 1 minute): t_R: 6.7 min, m/z = 1375.5 $[M+H]^+$, 1373.3 $[M-H]^-$

PEG3-alkyne (77)
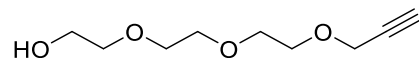
Triethylene glycol (**76**) (5.05 g, 33.62 mmol, 5.0 eq) was dissolved in 40mL dry THF under N_2 atmosphere and sodium hydride (60% in mineral oil, 268 mg, 6.72 mmol, 1.0 eq) was carefully added. After 10 minutes of stirring propargyl bromide (636 uL, 6.72 mmol, 1.0eq) was finally added. The reaction mixture turned light brown from colorless. Stirring continued overnight at rt. The next day the reaction was quenched with water and then extracted using ethyl acetate. The organic phases were pooled and washed with brine and then dried over $MgSO_4$. After filtration and solvent evaporation, the crude product was purified via flash column chromatography using DCM/MeOH (100/4) as eluents. The pure product was isolated as a slight yellow oil (520 mg, 2.76 mmol, 41%).

¹H NMR (500 MHz, $CDCl_3$) δ 4.19 (d, J = 2.4 Hz, 2H, $-CH_2C\equiv CH$), 3.76 – 3.55 (m, 12H, $-(O-CH_2-CH_2)_6$), 2.56 (t, J = 6.2 Hz, 1H, -OH), 2.43 (t, J = 2.4 Hz, 1H, $-C\equiv CH$).

¹³C NMR (126 MHz, $CDCl_3$) δ 79.61 ($-\mathbf{C}\equiv CH$), 74.73 ($-C\equiv \mathbf{C}H$), 72.60 (PEG-C), 70.66 (PEG-C), 70.39 (PEG-C), 70.35 (PEG-C), 69.11 (PEG-C), 61.74 (PEG-C), 58.44 ($-\mathbf{C}H_2C\equiv CH$).

HRMS (ESI): for $C_9H_{16}O_4Na$ $[M+Na]^+$, calc. 211.0946; found 211.0947.

For IR spectra refer to the literature [168].

Materials and methods

5'-O-DMT 2'-deoxy 3'-O-cyanoethyl N2- (PEG3-alkyne, benzoyl) adenosine phosphoramidite (74)
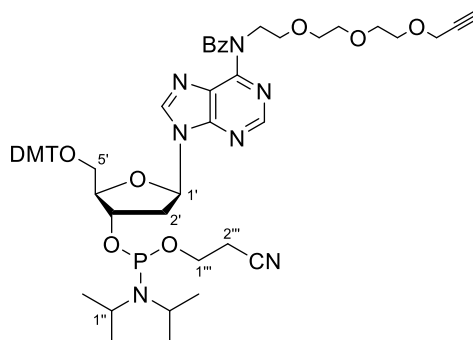
N6-Benzoyl-2'-deoxy-5'-DMT-3'-OCE-adenosine phosphoramidite (**9**) (500 mg, 0.582 mmol) was co-evaporated using toluene (x2) and then dissolved in 5mL dry THF under Ar atmosphere. **77** (164 mg, 0.874 mmol, 1.5 eq) was also co-evaporated with MeCN (x2) and toluene (x2) and then added to the phosphoramidite mixture followed by PPh₃ (229 mg, 0.874 mmol, 1.5 eq). After 5 minutes of stirring DIAD (40% in THF, 0.34 mL, 0.874 mmol, 1.5 eq) was added dropwise. The mixture was stirred for 16 hours at rt, until TLC check showed no more starting material. The solvents were evaporated under reduced pressure and the crude product was purified via flash column chromatography using DCM/acetone/MeOH 90/7/3 as eluents. The product was isolated as a colorless foam (380 mg, 0.369 mmol, 65%).

R$_f$ = 0.9 (DCM/MeOH = 10/1)

HRMS (ESI): for $C_{56}H_{66}N_7O_{10}PNa^+$ [M+Na]$^+$, calc. 1050.4506; found 1050.4528

IR (ATR): $\tilde{v}$ (cm^{-1}) 3268 (br), 3058 (m), 2928 (m), 2256 (w), 1697 (m), 1582 (m), 1453 (m).

^{1}H NMR (500 MHz, CD$_2$Cl$_2$) δ 8.43 (d, J = 3.7 Hz, 1H, H-8), 8.04 (d, J = 6.6 Hz, 1H, H-2), 7.44 – 7.35 (m, 5H, aromatic-H), 7.32 – 7.23 (m, 7H, aromatic-H), 7.22 (m, 2H, aromatic-H), 7.11 (td, J = 7.8, 2.3 Hz, 2H, aromatic-H), 6.83 – 6.74 (m, 4H, aromatic-H), 6.40 (t, J = 6.6 Hz, 1H, H-1'), 4.74 (ddq, J = 15.1, 9.3, 3.3 Hz, 1H, H-4'), 4.49 (t, J = 6.1 Hz, 2H, PEG-H), 4.25 (dd, J = 15.2, 4.1 Hz, 1H, H-5'), 4.18 - 4.14 (m, 1H, H-5'), 4.12 (dd, J = 2.4, 1.5 Hz, 2H, PEG-H), 3.84 – 3.79 (m, 2H, PEG-H), 3.78 (s, 6H, 2xDMT-OCH3), 3.65 – 3.55 (m, 3H, PEG-H and H-1''), 3.55 – 3.48 (m, 2H, PEG-H), 3.47 – 3.39 (m, 3H, PEG-H and H-1''), 3.37 (dd, J = 10.4 Hz, 4.1 Hz, 1H, alkyne-H), 3.35 – 3.25 (m, 4H, PEG-H and H-1'''), 2.88 – 2.78 (m, 1H, H-2'), 2.61 (t, J = 6.2 Hz, 1H, H-2'), 2.55 (ddd, J = 13.5, 6.3, 3.5 Hz, 1H, H-3'), 2.52 – 2.40 (m, 2H, H-2'''), 1.23 – 1.03 (m, 10H, iPr-Me), 1.11 (d, J = 6.7 Hz, 2H, iPr-Me).

^{13}C NMR (126 MHz, CD$_2$Cl$_2$) δ 172.34, 159.02, 154.92, 152.55, 151.99 (C-8), 145.13, 142.35 (C-2), 136.70, 136.06, 134.11, 133.95, 130.93, 130.40, 129.02, 128.88, 128.43, 128.37, 128.21, 128.12, 127.21, 126.99, 118.03, 113.45, 86.72, 86.14 (C-5'), 84.81 (C-1'), 80.21 (C-PEG), 80.20, 74.50 (C-4'), 70.63 (C-alkyne), 69.68 (C-PEG), 69.47 (C-PEG), 58.52 (C-PEG), 55.59 (C-PEG), 55.56 (C-PEG), 48.10 (C-PEG), 43.54, 39.45 (C-2'), 39.41 (C-3'), 24.68 (C-iPr).

^{31}P NMR (202 MHz, CD$_2$Cl$_2$) δ 148.71, 148.66, 148.62, 148.57.

2'-Deoxy- 3'-O-cyanoethyl- phosphate N2-(*PEG3-alkyne*, benzoyl) adenosine 3''-deoxy-2''-(allyl, cyanoethyl) phosphate O6-dpc-N2-iBu guanosine (78)
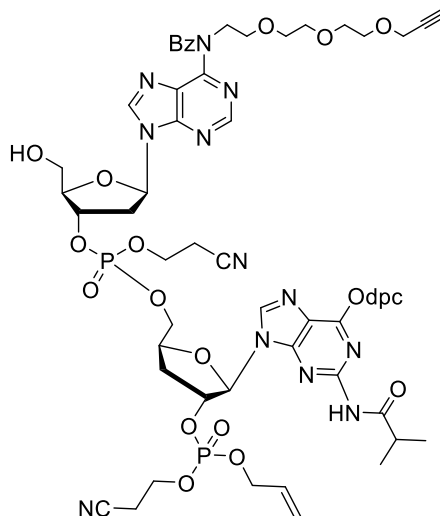
8 (530 mg, 0.751 mmol) and **74** (926 mg, 0.901 mmol, 1.2 eq) were co-evaporated with toluene (x3) and MeCN (x2), then they were dissolved in dry MeCN (25mL) under an Ar atmosphere. BTT (0.3M in MeCN, 5 mL, 1.5 mmol, 2.0 eq) was added and the mixture was left to stir for 1h. Then tBuOOH (5.0M in decane, 0.45 mL, 2.25 mmoL, 3.0 eq) was added and the mixture was left to stir for 40min. The solution was cooled to 0°C and an aqueous solution of $NaHSO_3$ (1.5mL, 0.5g/mL) was added. The mixture was stirred for 10min at 0°C and then for 5min at rt. Solvents were evaporated until a foam was formed which was subsequently dissolved in a 30mL mixture of 3% DCA in DCM containing 10.0 eq H_2O. The mixture was left to stir for 10min and then was quenched with an aqueous solution of $NaHCO_3$ (80mL). The aqueous phase was extracted three times with ethyl acetate and the combined organic layers were dried over $MgSO_4$ and evaporated under reduced pressure. The product was purified via flash column chromatography (silica gel, DCM/MeOH: 100/2 to 100/10) and was isolated as a colorless foam (630 mg, 0.467 mmol, 62%). The product was an inseparable mixture of 4 P-diastereomers.

R_f (DCM/MeOH : 10/1) = 0.55

HRMS (ESI): for $C_{62}H_{69}N_{13}O_{18}P_2^+$ [M+Na]$^+$, calc. 1368.4256; found 1368.4262.

IR (ATR): v̄ (cm^{-1}) 3012(w), 2362(w), 1750(m), 1576(s), 1493(s), 1450(s), 1271(s), 1220(s), 1184(s), 1000(br), 698(s).

^{31}P NMR (202 MHz, CD_2Cl_2) δ -2.75(m).

2'-Deoxy- 3'-O-cyanoethyl- phosphate N2-(*PEG3-alkyne*, benzoyl) adenosine 3''-deoxy-2''-cyanoethyl phosphate O6-dpc-N2-iBu guanosine (79)

Materials and methods
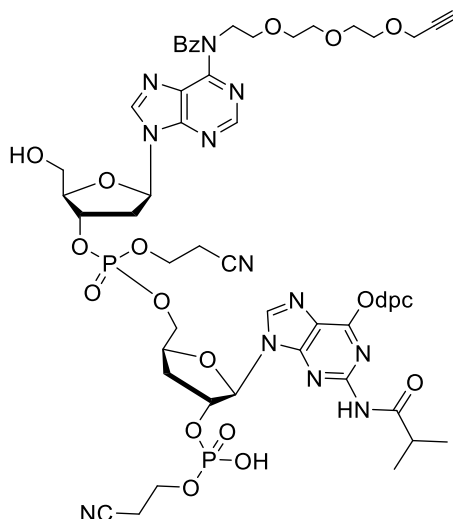
Compound **78** (300 mg, 0.222 mmol) was co-evaporated with toluene(x2). Then it was diluted in dry acetone (13 mL) and NaI (334 mg, 2.22 mmol, 10.0 eq) was added. The mixture was stirred at 55°C for 3hrs until LCMS monitoring showed no more SM. The flask was let to come to rt and then the solvent was evaporated under reduced pressure. The product was precipitated from a 1:1 mixture of cold ethyl acetate : isohexane, washed with cold ethyl acetate and dried under high vacuum to give a yellowish solid (291 mg, 0.222 mmol, quantitative yield). The product was consisted of a mixture of 4 P-diastereomers and was used for the next step without further purification.

HRMS (ESI): for $C_{62}H_{69}N_{13}O_{18}P_2^-$ [M-H]$^-$, calc. 1304.4046; found 1304.3969.

IR (ATR): ṽ (cm^{-1}) 3493(br), 2362(s), 1559(w), 1491(w), 1339(w), 1218(s), 1050(s), 668(s).

2'3'-Cyclic-2'-deoxy- 3'-O-cyanoethyl phosphate N2-(*PEG3-alkyne*, benzoyl) adenosine 3"-deoxy-2"-cyanoethyl phosphate O6-dpc-N2-iBu guanosine (80)
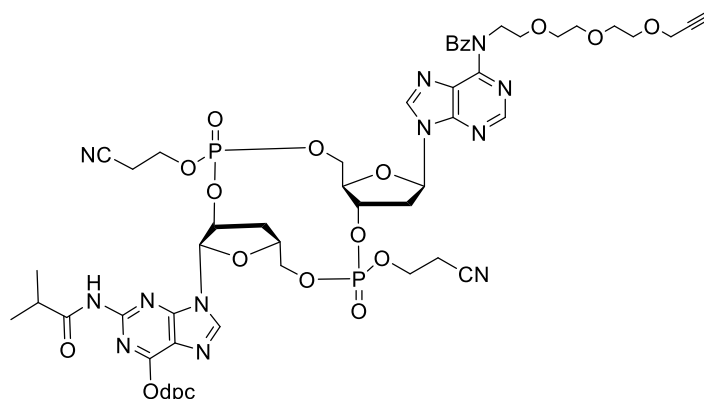
Compound **79** (291 mg, 0.222mmol) was co-evaporated using toluene (x2) and dissolved in 45mL of dry pyridine under Ar atmosphere. 1-(2-Mesitylensulfonyl)-3-nitro-1*H*-1,2,4-triazole (MSNT, 680mg, 2.30mmol, 10.0eq) was then added, the flask was covered with aluminum foil and the deep red mixture was left to stir for 18 hours at rt when LCMS monitoring showed complete conversion of the starting

Materials and methods

material. Pyridine was evaporated under reduced pressure and the resulted dark orange solid was dried under vacuum. The product was isolated as a mixture of 4 P-diastereomers and was used for the next step as it is without further purification.

HRMS (ESI): for $C_{59}H_{64}N_{13}O_{17}P_2^+$ [M+H]$^+$, calc. 1288.3940; found 1288.3933.

IR (ATR): $\tilde{v}$ (cm^{-1}) 3500(br), 3010(w), 2361(w), 1684(s), 1477(s), 1362(s), 1204(s), 1086(s), 1014(s), 834(s), 681(s).

2'3'-Deoxy-cGAMP-PEG3-alkyne (73)
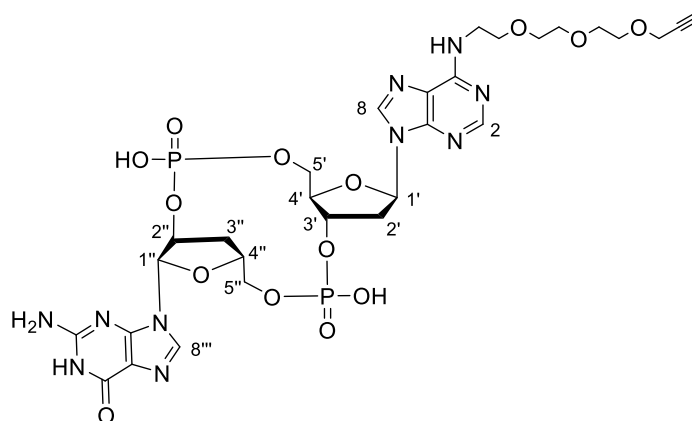
Compound **80** (200 mg, 155 umol) was dissolved in 40mL of 33% MeNH$_2$ in ethanol and the mixture was stirred at rt. After 3 hours LCMS monitoring showed no more starting material. Solvents where then evaporated under reduced pressure and the crude product was dissolved in a minimum amount of methanol (2mL) and subsequently precipitated from cold acetone. The resulting solid was collected after centrifuge and purified via reversed-phase HPLC using a 0-20% Buffer B method over 45 minutes (t$_R$ = 27 min) (Buffer A = 0.1% TFA in H$_2$O, Buffer B = 0.1% TFA in MeCN). All the fractions containing the product were collected and lyophilized to afford **73** as a white powder (23 mg, 28.30 umol, 22%).

HRMS (ESI): for $C_{29}H_{37}N_{10}O_{14}P_2^-$ [M-H]$^-$, calc. 811.1966; found 811.1979.

IR (ATR): $\tilde{v}$ (cm^{-1}) 3390 (br w), 1590 (m), 1231 (s), 1108 (m), 905 (s), 827 (s), 642 (s).

^{31}P NMR (202 MHz, D$_2$O) δ -0.90, -1.95.

^{1}H NMR (500 MHz, D$_2$O) δ 8.22 (s, 1H, H-2), 8.14 (s, 1H, H-8), 7.80 (s, 1H, H-8'''), 6.36 (dt, J = 6.8, 3.6 Hz, 1H, H-1'), 5.77 (d, J = 5.6 Hz, 1H, H-1''), 5.34 (s, 1H, H-2''), 5.03 (t, J = 6.6 Hz, 1H, H-3''), 4.51 (s, 1H, H-3'), 4.23 (s, 2H, H-4'), 4.12 – 4.04 (m, 2H, H-5''), 4.04 – 3.90 (m, 3H, H-4'' and H-5'), 3.76 – 3.34 (m, 14H, PEG-H), 3.04 – 2.85 (m, 2H, H-2''), 2.70 (m,1H, H-alkyne).

^{13}C NMR (126 MHz, D$_2$O) δ 164.52, 152.37, 149.68, 138.56, 136.61, 131.14, 130.13, 128.86, 116.94, 88.48, 86.44, 83.85, 83.01, 79.39, 76.61, 71.64, 68.98, 65.51, 62.86, 61.41, 60.31, 57.83, 38.23, 33.55, 27.08.

Materials and methods

2'3'-Deoxy-cGAMP-PALM (75)
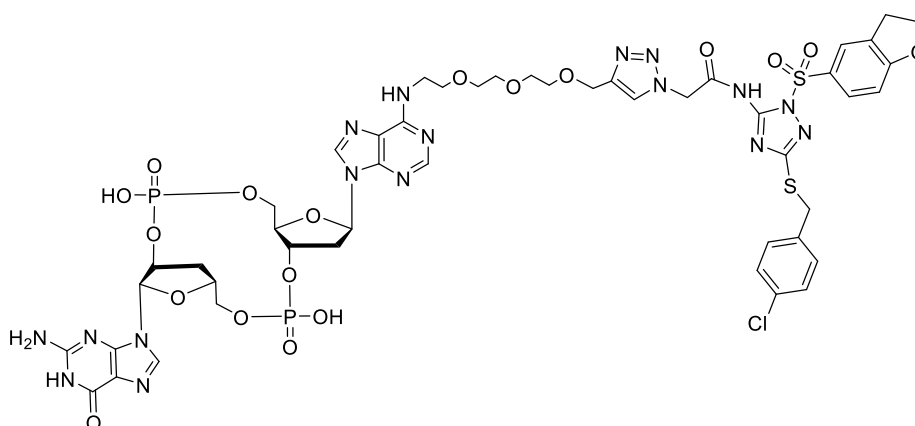
All the solutions and solvents for this reaction were first thoroughly degassed with an argon stream for 30 minutes. **73** (3 mg, 3.69 umol) was dissolved in miliQ water (150 uL, final concentration 10mM) and THPTA (8mg, 18.4umol, 5.0eq) followed by an aqueous solution of CuSO₄ (25mg/mL, 100 mM, 62 uL, 6.28 umol, 1.0 eq) were added. The azide **72** (4mg, 7.38umol, 2.0eq) was dissolved in a 300uL mixture of DMF/H2O (2/1) and then added to the mixture. Finally, an aqueous solution of sodium ascorbate (200 mg/mL, 1.0M, 29 uL, 29.53 umol, 8.0 eq) was added and the reaction mixture was stirred for 5 hours at rt while monitoring its progression via LC-MS. After completion the mixture was directly purified by reversed phase HPLC (30% → 70% Buffer B over 45 minutes, t_R = 15min, Buffer A = 0.1% TFA in H₂O, Buffer B = 0.1% TFA in MeCN) and **75** was obtained as a white powder (2 mg, 1.51 umol, 41%).

The amount of the obtained compound was not sufficient in order to measure ^{1}H and ^{13}C NMR, but was enough to ensure its molecular weight via high-resolution mass spectrometry and evaluate its purity via analytical HPLC.

HRMS (ESI): for $C_{48}H_{53}N_{17}O_{18}ClP_2S_2^+$ [M-H]⁻, calc. 1318.2438, found 1318.3079.

MALDI-TOF (negative mode): for $C_{48}H_{54}ClN_{17}O_{18}P_2S_2^-$ [M+H]⁻ calc. 1318.244 found 1318.308.

IR (ATR): ṽ (cm⁻¹) 2931 (m), 2844 (m), 2120 (m), 1608 (s), 1508 (s), 1247 (s), 1175 (s), 1030 (s), 830 (s), 704 (s).

LC-MS (Buffer A = 0.01 % formic acid in H₂O, buffer B = 0.01 % formic acid in MeCN, method: 5-80 % buffer B in 7 minutes, then 95 % B for 1 minute): t_R: 6.8-7.5 min, m/z = 1320.8 [M+H]⁺, 1318.7 [M-H]⁻.

Extinction coefficient compound 75

slope = 36.900 $M^{-1}cm^{-1}$
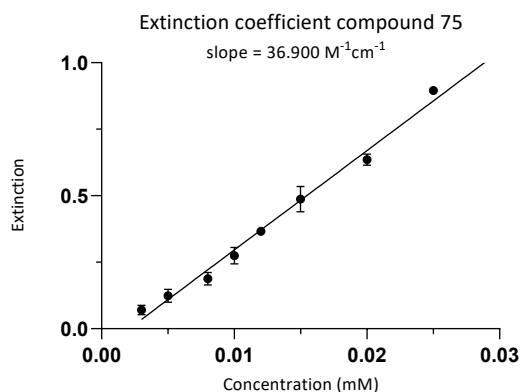
Dideoxy-cGAMP-folate conjugates

Nγ-(((Azidoethoxy)ethoxy)ethoxy)ethyl-α-(tertbutyl)-Nα-Fmoc-L-glutamic acid(90)
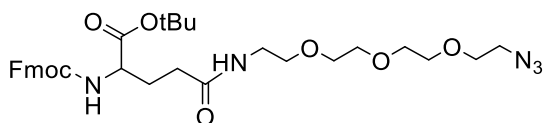
Compound **88** (70 mg, 0.16 mmol) was dissolved in DMF (6.5 mL) under N_2 and then DIPEA (39 μL, 0.23 mmol, 1.4 eq) and HBTU (69 mg, 0.23 mmol, 1.4 eq) were added. After 10 minutes **89** (45 μL, 0.23 mmol, 1.4 eq) was added and the mixture was stirred at 50°C for 1hr. Then DMF was evaporated and the crude mixture was dissolved in ethyl acetate and washed with water(x3). The aqueous phase was extracted using ethyl acetate(x3) and DCM(x2). After drying of the organic phase over $MgSO_4$ it was evaporated under reduced pressure and then purified via flash column chromatography (DCM/MeOH 100/2 →100/10) to afford **90** as a yellow oil (35 mg, 0.055 mmol, 35%).

R$_f$ = 0.5 (DCM/MeOH = 10/1)

HRMS (ESI): for $C_{32}H_{44}N_5O_8^+$ [M+H]$^+$: calc. 626.3112, found 626.3123.

¹H NMR (500 MHz, CD_2Cl_2) δ 7.75 (dd, J = 7.5, 1.0 Hz, 2H, aromatic-2xH), 7.63 – 7.56 (m, 2H, aromatic-2xH), 7.42 – 7.35 (m, 2H, aromatic-2xH), 7.29 (tt, J = 7.5, 1.3 Hz, 2H, aromatic-2xH), 6.23 (s, 1H, NH), 5.85 (d, J = 8.0 Hz, 1H, NH), 4.34 (qd, J = 10.6, 7.1 Hz, 2H, Fmoc-CH$_2$), 4.20 (t, J = 7.2 Hz, 1H, Fmoc-CH$_2$), 4.13 (td, J = 8.4, 4.4 Hz, 1H, α-CH), 3.63 – 3.53 (m, 10H, ethyleneglycol 5xCH$_2$), 3.52 – 3.42 (m, 2H, ethyleneglycol CH$_2$), 3.41 – 3.16 (m, 4H, ethyleneglycol 2xCH$_2$), 2.22 (dt, J = 14.5, 6.7 Hz, 2H, γ-CH$_2$), 2.15 – 2.05 (m, 1H, β-CH$_2$), 1.95 – 1.83 (m, 1H, β-CH$_2$), 1.43 (s, 9H, 3xCH$_3$).

¹³C NMR (126 MHz, CDCl$_3$) δ 171.31(C=O), 162.66(C=O), 156.39, 143.87, 141.44, 127.85, 127.22, 125.29, 120.11, 82.52(t-butyl-CH), 70.85, 70.78, 70.73, 70.65, 70.39, 70.18, 70.14, 69.89, 67.07(Fmoc-

CH$_2$), 54.22(α-CH$_2$), 50.82, 50.77, 47.32(Fmoc-CH$_2$), 39.44, 36.63, 32.64(γ-CH$_2$), 28.87(β-CH$_2$), 28.13(3xCH$_3$).

For IR data refer to the literature[159].

Nγ-(((Azidoethoxy)ethoxy)ethoxy)ethyl-α-(tertbutyl)-L-glutamic acid (91)
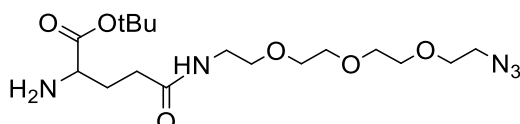
Compound **90** (35 mg, 55.9 μmol) was dissolved in DMF (0.4 mL) and then dimethylamine (2M in THF, 139 μL, 5.0 eq) was added. The reaction mixture was left to stir for 1h at rt until LCMS control showed full conversion. Then DMF was evaporated, the crude was dissolved in ethyl acetate and washed with water (x3). The aqueous phase was extracted with ethyl acetate (x3) and DCM (x2) and the combined organic phases were dried over MgSO$_4$. After evaporation under reduced pressure the product was purified via flash column chromatography (silica gel, DCM/MeOH = 100/3 → 100/10) to afford the azide modified amino acid **91** as a colorless oil (10 mg, 24.7 μmol, 45%).

R$_f$ = 0.3 (DCM/MeOH = 10/1)

HRMS (ESI): for C$_{17}$H$_{34}$N$_5$O$_6^+$ [M+H]$^+$: calc. 404.2431, found 404.2491.

^{1}H NMR (400 MHz, CDCl$_3$) δ 6.53 (s, 1H, NH), 3.70 – 3.57 (m, 10H, ethyleneglycol 5xCH$_2$), 3.58 – 3.51 (m, 2H, ethyleneglycol 1xCH$_2$), 3.49 – 3.35 (m, 4H, ethylenglycol 2xCH$_2$), 2.33 (m, 2H, γ-CH$_2$), 2.16 – 2.00 (m, 3H, NH$_2$ and β-CH$_2$), 1.76 (hex, J = 14.8, 7.6 Hz, 1H, β-CH$_2$), 1.45 (s, 9H, 3xCH$_3$).

^{13}C NMR (126 MHz, CDCl$_3$) δ 174.83(C=O), 172.59(C=O), 162.60(C=O), 81.43(t-butyl-CH), 70.73, 70.69, 70.60, 70.28, 70.08, 69.88(Fmoc-CH$_2$), 54.30(α-CH$_2$), 50.72(Fmoc-CH$_2$), 39.23, 32.90(γ-CH$_2$), 30.23(β-CH$_2$), 28.09(3xCH$_3$).

For IR data refer to the literature[159].

Nγ-(((Azidoethoxy)ethoxy)ethoxy)ethyl-α-(tertbutyl)-pteroyl-L-glutamic acid (92)
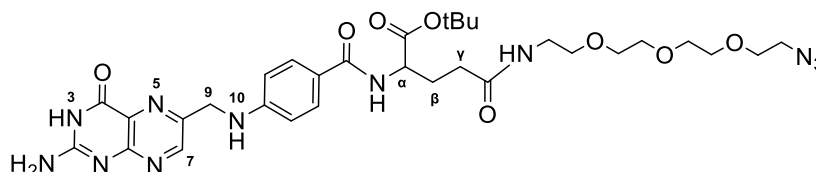
Pteroic acid (**85**) (7 mg, 22.4 μmol) was suspended in a 1/1 mixture of DMF/DMSO (0.8 mL total) and HBTU (11 mg, 19.1 μmol, 1.3 eq) and DIPEA (5 μL, 29.4 μmol, 1.4 eq) were subsequently added. After 30min of stirring at rt a solution of **91** (10.85 mg, 26.9 μmol, 1.2 eq) in a 1/1 mixture of DMF/DMSO (0.8 mL total) was added to the reaction mixture and stirring continued for 1h. The product was precipitated from cold Et_2O, spinned down and was obtained as a yellow solid (14 mg, 19.9 μmol, 89%) which was used without further purification for the next reaction.

R_f = 0.35 (DCM/MeOH = 10/1)

HRMS (ESI): for $C_{31}H_{44}N_{11}O_8^+$ [M+H]$^+$: calc. 698.3296, found 698.7521.

Nγ-(((Azidoethoxy)ethoxy)ethoxy)ethyl-pteroyl-L-glutamic acid (87)
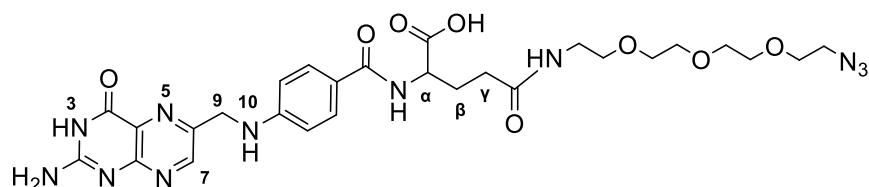
Compound **92** (40 mg, 57.33 mmol) was dissolved in DCM (2 mL). TFA (1 mL) was then added and the mixture was left to stir at rt for 1.5h. Then solvents were evaporated, the crude was dissolved in the minimum amount of methanol and precipitated from cold Et_2O. After washing of the precipitation with cold Et_2O, **87** was purified by HPLC (0-40% B for 45 min, Buffer A: H_2O + 0.1% TFA, Buffer B: MeCN + 0.1% TFA, t_R = 26 min) to afford **87** as a yellow solid (30 mg, 46.75 μmol, 82%).

HRMS (ESI): $C_{27}H_{36}N_{11}O_8^+$ [M+H]$^+$: calc. 642.6460, found 642.6500.

IR (ATR): ṽ (cm^{-1}) 2154(w), 1606(s), 1557(s), 1506(s), 1129(s), 988(s), 879(s), 767(s).

^{1}H NMR (500 MHz, DMSO) δ 8.64 (s, 1H, H-7), 7.94 (s, 1H, N3-H), 7.67 (d, J = 8.7 Hz, 1H, aryl-H), 7.59 (d, J = 8.4 Hz, 1H, aryl-H), 6.93 (m, 1H, N10-H), 6.64 (m, 2H, aryl-H), 4.48 (d, J = 6.0 Hz, 2H, 2xH-9), 4.08 (m, 1H, α-CH), 3.63 – 3.14 (m, 16H, ethyleneglycol 16xCH2), 2.12 (q, J = 8.1 Hz, 2H, γ-CH2), 2.05 – 1.98 (m, 1H, β-CH2), 1.92 – 1.85 (m, 1H, β-CH2).

^{13}C NMR (126 MHz, DMSO, ppm) δ = 172.61 (*C*=O), 171.65 (*C*=O), 163.22 (*C*=O), 160.12(*C*ar.), 159.76 (*C*ar.), 152.62 (*C*ar.), 150.79 (*C*ar.), 147.92 (*C*-7), 147.25 (*C*ar.), 131.1, 128.9, 127.9 (*C*ar.), 121.33 (Car.), 111.34, 111.1, 69.7, 69.7, 69.6, 69.5, 69.2, 69.0, 52.2 (α-CH2), 50.0, 45.9 (*C*-9H2), 38.5, 31.9 (γ-*C*H2), 26.5 (β-*C*H2).

5'-O-DMT-3'-thionylcarbamate-2'-O-TBS N2-benzoyl adenosine (95)
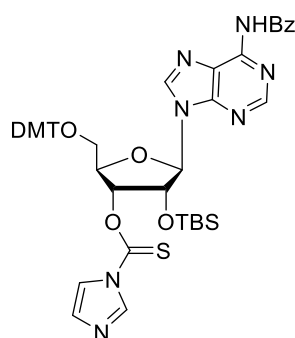
N6-benzoyl-5'-DMT-2'-O-TBDMS adenosine (**94**) (9 g, 11.4 mmol) was diluted in 70 mL of dry DMF. Then thiocarbonyldiimidazole (2.44 g, 13.68 mmol, 1.2 eq) and DMAP (0.283 g, 2.32 mmol, 0.2 eq) were added and the mixture was left to stir overnight at room temperature. The next day, the solvent was evaporated under reduced pressure, the crude mixture was diluted in ethyl acetate and washed twice with NaHCO$_3$. The aqueous phase was re-extracted three times with ethyl acetate and the combined organic phases were washed with brine and then dried over MgSO$_4$. After filtration and evaporation of the solvent the crude product was purified via flash column chromatography on silica gel using ethyl acetate/i-hexane (3/1 to 5/1) as eluting solvents. **95** was afforded as a white foam (8.18 g, 9.12 mmol, 80%).

R$_f$ = 0.30 (ethyl acetate/i-hexane = 3/1)

HRMS (ESI): for C$_{48}$H$_{52}$O$_7$N$_7$SSi$^+$ [M+H]$^+$, calc. 898.3340; found 898.5010.

^{1}H NMR (400 MHz, CDCl$_3$) δ 9.05 (s, 1H, NH), 8.85 (s, 1H, H-8), 8.27 (s, 1H, H-2), 8.14 – 7.98 (m, 2H, imidazole-H), 7.83 (t, J = 1.6 Hz, 1H, imidazole-H), 7.68 – 7.59 (m, 1H), 7.62 – 7.50 (m, 2H), 7.40 – 7.20 (m, 6H), 7.23 – 7.11 (m, 4H), 6.91 – 6.69 (m, 5H), 6.15 (d, J = 7.8 Hz, 1H, H-1'), 6.13 (d, J = 5.1 Hz, 1H, H-2'), 5.40 (dd, J = 7.8, 5.0 Hz, 1H, H-4'), 4.62 (s, 1H, H-3'), 4.08 – 3.93 (m, 2H, H-5'), 3.79 (s, 6H, 2xOMe), 0.67 (s, 9H, SiC(Me)$_3$), -0.15 (s, 3H, Si(Me)$_2$), -0.46 (s, 3H, Si(Me)$_2$).

^{13}C NMR (126 MHz, CDCl$_3$) δ 183.02 (C=S), 158.81 (C=O), 144.44, 141.63, 139.64 (C-imidazole), 135.52, 135.37, 132.97 (C-imidazole), 130.15, 129.26, 129.01, 128.16, 128.02, 127.22 (C-imidazole), 113.45, 88.55 (C-4'), 87.26, 82.17 (C-1'), 81.15 , 73.96 (C-5'), 62.90 (C-3'), 55.37 (C-2'), 31.04, 25.38, 17.73, -5.04 (C- SiC(Me)$_3$), -5.20 (C- Si(Me)$_2$).

5'-O-DMT-3'-deoxy-2'-O-TBS N2-benzoyl adenosine (96)
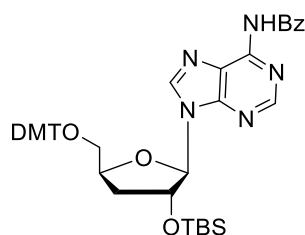
Materials and methods

95 (7.8 g, 8.68 mmol) was dissolved in 40mL of dry toluene. N_2 gas was then bubbled in the solution for 30min. Next, AIBN (285 mg, 1.74 mmol, 0.2 eq) and tris-trimethylsilylsilane (3.22 mL, 10.42 mmol, 1.2 eq) were added and the reaction mixture was heated to reflux (95°C) for 2hrs until all starting material was consumed. The reaction flask was let to cool down to room temperature and then immediately added in a silica gel filled column to purify using ethyl acetate/i-hexane (1/1 to 2/1) as eluents. **96** was isolated as a yellowish foam (4.3 g, 5.65 mmol, 65%).

Rf = 0.80 (ethyl acetate/i-hexane = 3/1)

HRMS (ESI): for $C_{44}H_{50}O_6N_5Si^+$ [M+H]$^+$, calc. 772.3452; found 772.3577.

^{1}H NMR (500 MHz, CDCl$_3$) δ 8.99 (s, 1H, -NH), 8.79 (s, 1H, H-2), 8.28 (s, 1H, H-8), 7.65 – 7.58 (m, 1H), 7.58 – 7.50 (m, 2H), 7.48 – 7.42 (m, 2H), 7.37 – 7.25 (m, 8H), 7.25 – 7.15 (m, 1H), 6.83 (d, J = 8.8 Hz, 4H), 6.06 (d, J = 1.4 Hz, 1H, H-1'), 4.84 (d, J = 4.8 Hz, 1H, H-2'), 4.77 – 4.63 (m, 1H, H-4'), 3.78 (d, J = 1.0 Hz, 7H), 3.47 (dd, J = 10.6, 3.0 Hz, 1H, H-5'), 3.37 (dd, J = 10.6, 4.9 Hz, 1H, H-5'), 2.22 (ddd, J = 13.1, 10.0, 4.9 Hz, 1H, H-3'), 1.95 (ddd, J = 13.1, 5.6, 2.1 Hz, 1H, H-3'), 0.91 (s, 9H, -OSi(Me)$_3$), 0.18 – 0.09 (m, 6H, -OSi(Me)$_2$).

^{13}C NMR (126 MHz, CDCl$_3$) δ 158.68, 152.71, 151.26, 144.65, 141.47, 135.80, 132.89, 130.17, 129.27, 129.02, 128.30, 128.07, 127.97, 127.09, 123.61, 113.33, 92.67, 86.56, 80.56, 64.73, 60.56, 55.37, 35.15, 25.83, 18.08, 1.16, -4.54 (C- SiC(Me)$_3$), -4.83 (C- Si(Me)$_2$).

5'-O-DMT-3'-deoxy N2-benzoyl adenosine (97)
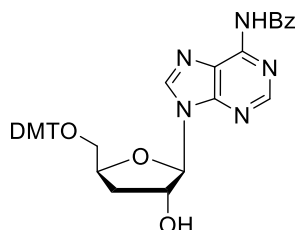
Compound **96** (3.9 g, 5 mmol) was diluted in 15 mL of dry THF under N_2 and cooled to 0°C. Then TBAF (1M solution in THF, 5.5 mL, 5.5 mmol, 1.1 eq) was added dropwise and the reaction mixture was left to stir for 2hrs while slowly reaching room temperature. The reaction was quenched using 5 mL methoxytrimethylsilane and was let to stir for 15 min more. Solvents were evaporated under reduced pressure and the crude product was purified via flash column chromatography using DCM/MeOH (100/1 to 100/5) as eluents. **97** was isolated as a white foam (2.95 g, 4.41 mmol, 90%).

Rf = 0.5 (DCM/MeOH : 10/1)

HRMS (ESI): for $C_{38}H_{36}O_6N_5^+$ [M+H]$^+$, calc. 658.2587; found 658.4028.

IR (ATR): ṽ (cm^{-1}) 3269 (br), 2931 (w), 1722 (br), 1611 (s), 1598 (m), 1503 (s), 1423 (s), 1388 (w), 1296 (m), 1289 (s), 1222 (m), 1190 (s), 1028 (s), 909 (m), 811 (s), 801 (m), 745 (s).

Materials and methods

¹H NMR (500 MHz, CDCl₃) δ 9.07 (s, 1H, -NH), 8.79 (s, 1H, H-2), 8.29 (s, 1H, H-8), 7.65 – 7.58 (m, 1H), 7.56 – 7.50 (m, 2H), 7.37 – 7.31 (m, 2H), 7.29 – 7.16 (m, 9H), 6.77 (dd, J = 8.9, 1.8 Hz, 4H), 5.98 (d, J = 3.2 Hz, 1H, H-1'), 4.92 (s, 1H, H-4'), 4.69 (d, J = 3.3 Hz, 1H, H-2'), 3.77 (s, 6H, -OMe), 3.41 (dd, J = 10.5, 3.3 Hz, 1H, H-5a'), 3.26 (dd, J = 10.5, 4.3 Hz, 1H, H-5b'), 2.34 (dt, J = 13.2, 6.7 Hz, 1H, H-3a'), 2.23 (ddd, J = 12.9, 7.2, 5.3 Hz, 1H, H-3b').

¹³C NMR (126 MHz, CDCl₃) δ 164.64, 162.68, 158.63 (C=O), 152.43 (C-2), 149.76, 144.59, 141.27 (C-8), 135.77, 133.01 (C-aromatic), 130.08 (C-aromatic), 129.05 (C-aromatic), 127.99 (C-aromatic), 127.04 (C-aromatic), 113.27 (C-aromatic), 93.45 (C-1'), 86.58, 80.62 (C-2'), 76.46 (C-4'), 65.17 (C-5'), 55.36 (C-OMe), 36.64, 34.38 (C-3'), 31.58.

3'-Deoxy-2'-O-(allyl, cyanoethyl) phosphate N2-benzoyl adenosine (7)
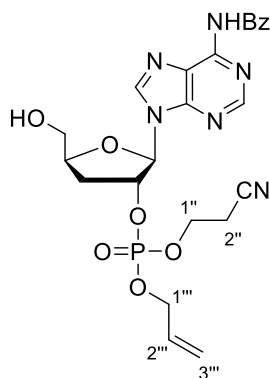
Compound **97** (200 mg, 0.304 mmol) was co-evaporated using toluene (x2) and then diluted in 5 mL dry DCM under Ar. Then 2-cyanoethyl-N,N,N',N'-tetraisopropylphosphorodiamidite (115 uL, 0.364 mmol, 1.2 eq) and pyr-TFA (70 mg, 0.364 mmol, 1.2 eq) were added and the mixture was left to stir under Ar at rt for 2.5 hours, until TLC monitoring showed no more starting material. Then BTT (0.3M in MeCN, 2 mL, 0.608 mmol, 2.0 eq) and allyl alcohol (0.103 mL, 1.52 mmol, 5.0 eq) were added to the mixture and stirring continued for another hour. Subsequently, tert-butyl hydroperoxide (5.0-6.0M in decane, 0.182 mL, 0.912 mmol, 3.0 eq) was added and the mixture continued stirring for 40 minutes. The hydroperoxide was quenched at 0°C using aq. NaHSO₃ solution (1.5 mL, 0.5g/mL). The mixture was stirred for 10min at 0°C and then for 5 min at rt. Solvents were evaporated under reduced pressure until a foam was formed which was subsequently dissolved in a 10 mL mixture of 3% DCA in DCM (0.3 mL of DCA) containing 10.0 eq H₂O. The mixture was left to stir for 10min and then was quenched with an aqueous solution of NaHCO₃ (80 mL). The aqueous phase was extracted three times with ethyl acetate and the combined organic layers were dried over MgSO₄ and evaporated under reduced pressure. The product was purified via flash column chromatography using DCM/MeOH (100/2 to 100/5) as eluents to afford **7** as a colorless foam (100 mg, 0.189 mmol, 65%).

R$_f$ = 0.65 (DCM/MeOH=10/1)

HRMS (ESI): for $C_{23}H_{26}O_7N_6P^+$ [M+H]⁺ , calc. 529.1595; found 529.

IR (ATR): ṽ (cm^{-1}) 3393 (br), 2920 (w), 2359 (s), 1700 (s), 1610 (s), 1582 (s), 1454 (s), 1250 (s), 1001 (s).

^{1}H NMR (500 MHz, CD$_2$Cl$_2$) δ 9.48 (s, 1H, -NH), 8.58 (s, 1H, H-2), 8.32 (d, J = 5.1 Hz, 1H, H-8), 7.91 (d, J = 7.6 Hz, 2H, aromatic H), 7.51 (t, J = 7.4 Hz, 1H, aromatic H), 7.42 (t, J = 7.6 Hz, 2H, aromatic H), 6.11 (d, J = 3.0 Hz, 1H, H-1'), 5.79 (dtt, J = 16.9, 11.3, 5.7 Hz, 1H, H-4'), 5.35 (d, J = 3.8 Hz, 1H, H-1'''), 5.27 – 5.19 (m, 1H, H-2'''), 5.15 (dd, J = 10.6, 3.9 Hz, 1H, H-2'), 4.51 – 4.39 (m, 3H, H-1'' and H-1'''), 4.12 (ddt, J = 11.4, 8.0, 6.1 Hz, 2H, H-3'''), 3.92 (dd, J = 12.6, 2.0 Hz, 1H, H-5'), 3.54 (dd, J = 12.6, 2.5 Hz, 1H, H-5'), 2.65 (dt, J = 12.5, 6.0 Hz, 2H, H-2''), 2.61 – 2.53 (m, 1H, H-3'), 2.25 (dtd, J = 13.4, 6.5, 4.4 Hz, 1H, H-3').

^{13}C NMR (126 MHz, CD$_2$Cl$_2$) δ 150.49 (C-8), 149.07, 145.16, 142.71 (C-2), 137.63, 131.42 (C-2'''), 98.62 (CN), 98.15 (C-1'''), 88.59 (C-1'), 79.81 (C-4'), 78.81 (C-3'''), 78.63, 76.46, 70.30 (C-3'), 70.14, 70.00 (C-5'), 69.18 (C-1''), 58.42, 40.83 (C-2'), 34.76 (C-3'), 22.55 (C-2''), 20.44 (C-2'').

2'-Deoxy-3'-O-cyanoethyl phosphate N2-(PEG3-alkyne, benzoyl) adenosine 3''-deoxy- 2''-O-(allyl, cyanoethyl) phosphate N2-benzoyl adenosine (98)

Compounds **7** (440 mg, 0.832 mmol) and **74** (1.03 g, 0.999 mmol, 1.2 eq) were co-evaporated with toluene (x3) and MeCN (x2), then they were dissolved in dry MeCN (20 mL) under an Ar atmosphere. BTT (0.3M in MeCN, 5.5 mL, 1.67 mmol, 2.0 eq) was added and the mixture was left to stir for 1h. Then tBuOOH (5.0M in decane, 0.5 mL, 2.5 mmoL, 3.0 eq) was added and the mixture was left to stir for 40 min. The solution was cooled to 0°C and an aqueous solution of NaHSO$_3$ (1.5 mL, 0.5g/mL) was added. The mixture was stirred for 10 min at 0°C and then for 5 min at rt. Solvents were evaporated until a foam was formed which was subsequently dissolved in a 30 mL mixture of 3% DCA in DCM containing 170 uL H$_2$O. The mixture was left to stir for 10 min and then was quenched with an aqueous solution of NaHCO$_3$ (80 mL). The aqueous phase was extracted three times with DCM and ethyl acetate and the combined organic layers were dried over MgSO$_4$ and evaporated under reduced pressure. The product was purified via flash column chromatography (silica gel, DCM/MeOH: 100/2 to 100/10) and

was isolated as a colorless foam (870 mg, 0.744 mmol, 89%). The product was obtained as an inseparable mixture of 4 P-diastereomers.

Rf (DCM/MeOH : 10/1) = 0.55

HRMS (ESI): for $C_{52}H_{59}N_{12}O_{16}P_2Na^+$ [M+Na]$^+$, calc. 1191.3464; found 1191.3461

IR (ATR): ṽ (cm^{-1}) 2361 (s), 1684 (s), 1636 (s), 1540 (s), 1507 (s), 1217 (s), 1000 (s).

^{31}P NMR (202 MHz, CD$_2$Cl$_2$) δ -2.81 (m).

2'-Deoxy-3'-O-cyanoethyl phosphate N2-(PEG3-alkyne, benzoyl) adenosine 3"-deoxy- 2"-O-cyanoethyl phosphate N2-benzoyl adenosine (99)

Compound **98** (220 mg, 0.188 mmol) was co-evaporated with toluene(x2). Then it was diluted in dry acetone (12 mL) and NaI (282 mg, 1.88 mmol, 10.0 eq) was added. The mixture was stirred at 55°C for 3hrs until LCMS monitoring showed no more SM. The flask was let to come to rt and then was placed over ice. The formed precipitation was received via vacuum filtration and washed with cold ethyl acetate. The supernatant was evaporated under reduced pressure and subsequently dissolved in a minimum amount of methanol and added to a 1/1 mixture of ethyl acetate/i-hexane for precipitation to be formed. The product was dried under high vacuum to afford a yellowish solid (130 mg, 0.115 mmol, 61%). The product consisted of a mixture of 4 P-diastereomers and was used for the next step without further purification.

HRMS (ESI): for $C_{49}H_{53}N_{12}O_{16}P_2^-$ [M-H]$^-$, calc. 1127.3178; found 1127.3200

IR (ATR): ṽ (cm^{-1}) 3420 (s), 1605 (s), 1508 (s), 1253 (s), 1179 (s), 1084 (s), 827 (s).

**2'3'-Cyclic-2'-deoxy- 3'-cyanoethyl phosphate N2-(PEG3-alkyne, benzoyl) adenosine 3"-deoxy-2"-O-cyanoethyl phosphate N2-benzoyl adenosine (100)**

Compound **99** (90 mg, 0.07 mmol) was co-evaporated using toluene (x2) and dissolved in 15mL of dry pyridine under an Ar atmosphere. 1-(2-Mesitylensulfonyl)-3-nitro-1*H*-1,2,4-triazole (MSNT, 236 mg, 0.797 mmol, 10.0 eq) was then added, the flask was covered with aluminum foil and the deep red mixture was left to stir for 18 hours at rt when LCMS monitoring showed complete conversion of the starting material. Pyridine was evaporated under reduced pressure and the resulted dark orange solid was dried under vacuum. The product was isolated as a mixture of 4 P-diastereomers and was used for the next step as it is without further purification.

LC-MS (Buffer A = 0.01 % formic acid in H_2O, buffer B = 0.01 % formic acid in MeCN, method: 5-80 % buffer B in 7 minutes, then 95 % B for 1 minute): t_R: 5.6 min, m/z = 1111.7 $[M+H]^+$, 1109.7 $[M-H]^-$

2'3'-cAAMP-PEG3-alkyne (93)
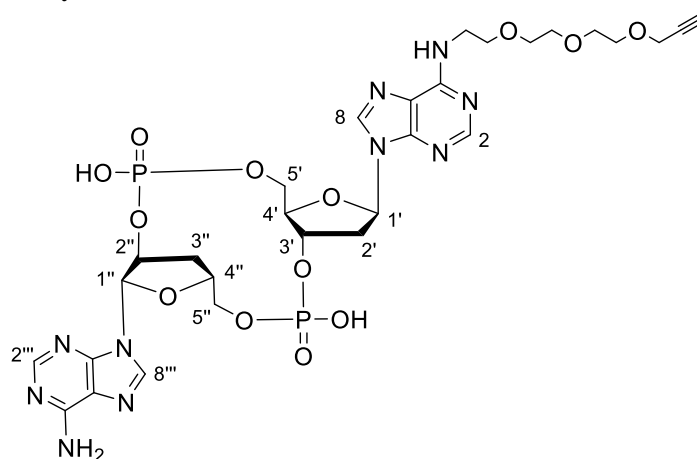
Compound **100** (90 mg, 81 umol) was dissolved in 15 mL of 33% $MeNH_2$ in ethanol and the mixture was stirred at rt. After 3 hours LCMS monitoring showed no more starting material. Solvents where then evaporated under reduced pressure and the crude product was dissolved in a minimum amount of methanol (1 mL) and subsequently precipitated from cold acetone. The resulting solid was collected after

centrifuge and purified via reversed-phase HPLC using a 0-20% Buffer B method over 45 minutes (t_R = 28 min) (Buffer A = 0.1% TFA in H_2O, Buffer B = 0.1% TFA in MeCN). All the fractions containing the product were collected and lyophilized to afford **93** as a white powder (18 mg, 27 umol, 27%).

HRMS (ESI): for $C_{29}H_{37}N_{10}O_{13}P_2^-$ [M-H]$^-$, calc. 795.2017; found 795.2027.

IR (ATR): $\bar{v}$ (cm^{-1}) 3400 (br), 1610 (s), 1418 (s), 1337 (s), 1171 (s), 988 (s), 797 (s).

¹H NMR (500 MHz, D_2O) δ 8.57 (s, 1H, H-2), 8.50 (s, 1H, H-8), 8.44 (s, 2H, H-2''' and H-8'''), 6.57 (t, J = 6.0 Hz, 1H, H-1'), 6.28 (d, J = 4.2 Hz, 1H, H-1''), 5.18 (p, J = 5.6 Hz, 1H, H-3'), 5.09 (p, J = 5.7 Hz, 1H, H-2''), 4.69 (dt, J = 9.1, 4.7 Hz, 1H, H-4''), 4.45 – 4.37 (m, 1H, Ha-5'), 4.35 (ddd, J = 12.2, 9.8, 2.9 Hz, 1H, H-4'), 4.30 – 4.07 (m, 5H, 3xPEG-H and H-5''), 3.86 (q, J = 8.1 Hz, 3H, PEG-H), 3.72 (dd, J = 6.2, 2.7 Hz, 2H, PEG-H), 3.67 (d, J = 4.8 Hz, 2H, PEG-H), 3.63 (s, 4H, PEG-H), 3.14 (dt, J = 14.1, 5.9 Hz, 1H, Hb-5'), 2.91 (dt, J = 14.1, 6.4 Hz, 1H, Ha-2'), 2.87 – 2.77 (m, 2H, Ha-3'' and Hb-2'), 2.53 (s, 1H, H-alkyne), 2.48 (dt, J = 13.4, 5.9 Hz, 1H, Hb-3'').

¹³C NMR (126 MHz, D_2O) δ 162.44, 149.82, 148.30, 147.45, 140.06, 130.91, 130.36, 128.97, 126.29, 125.49, 121.25, 117.05, 113.87, 88.36, 78.72, 77.71, 74.79, 74.54, 74.28, 70.50, 66.76, 60.54, 59.76, 29.72.

³¹P NMR (162 MHz, D_2O) δ -1.10, -1.78.

2'3'-Deoxy-cGAMP-FOL (83)
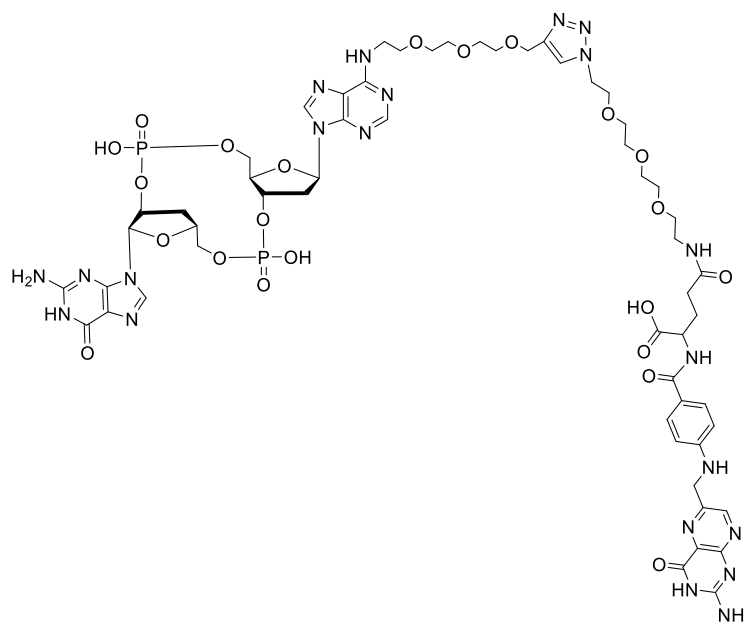
All the solutions and solvents for this reaction were first thoroughly degassed with an argon stream for 30 minutes. **73** (4 mg, 5 umol) was dissolved in miliQ water (300 uL, final concentration 10mM) and THPTA (10 mg, 24.6 umol, 5.0 eq) was added followed by an aqueous solution of $CuSO_4$ (25mg/mL,

100mM, 49 uL, 4.92 umol, 1.0 eq) and **87** (6.32 mg, 9.84 umol, 2.0 eq). Finally, an aqueous solution of sodium ascorbate (200mg/mL, 1.0M, 39 uL, 39.38 umol, 8.0 eq) was added and the reaction mixture was stirred for 4 hours at rt while monitoring its progression via LC-MS. After completion the mixture was directly purified by reversed phase HPLC (0% → 30% Buffer B over 45 minutes, t_R = 31min, Buffer A = 0.1% TFA in H_2O, Buffer B = 0.1% TFA in MeCN) and **83** was obtained as a yellowish powder (6 mg, 4.13 umol, 82%).

MALDI-TOF (negative mode): for $C_{56}H_{71}N_{21}O_{22}P_2^{2-}$ [M-2H]$^-$ calc. 1452.463, found 1452.471.

LC-MS (Buffer A = 0.01 % formic acid in H_2O, buffer B = 0.01 % formic acid in MeCN, method: 5-80 % buffer B in 7 minutes, then 95 % B for 1 minute): t_R: 3.0 min, m/z = 1455.3 [M+H]$^+$.

IR (ATR): $\tilde{v}$ (cm^{-1}) 2928 (br), 2120 (m), 1608 (s), 1579 (s), 1405 (m), 1362 (s), 1175 (s), 1090 (s), 1031 (s), 951 (s), 833 (s).

^{1}H NMR (500 MHz, DMSO) δ 10.75 (s, 1H, guanine N-H), 8.68 (s, 1H, H-7), 8.40 (s, 1H, adenine H-2), 8.26 (s, 1H, adenine H-8), 8.20 (d, J = 7.5 Hz, 1H, guanine H-8), 8.03 (s, 1H, H-triazole), 7.98 (s, 1H, N3-H), 7.89 (t, J = 5.6 Hz, 1H, N10-H), 7.65 (d, J = 8.8 Hz, 2H, aryl-H), 6.64 (d, J = 8.9 Hz, 2H, aryl-H), 6.42 (t, J = 7.0 Hz, 1H, H-1'), 5.87 (d, J = 5.0 Hz, 1H, H-1''), 5.25 – 5.19 (m, 1H, H-3'), 5.16 (m, 1H, H-2''), 4.51 (d, J = 11.1 Hz, 2H, 2xH-9), 4.35 – 4.23 (m, 2H, H-2'), 4.18 (t, J = 10.5 Hz, 3H, 2xH-5'' and H-4'), 3.97 (d, J = 7.1 Hz, 2H, H-4'' and α-CH), 3.72 – 3.26 (m, 30H, PEG7-H and PEG8-H), 3.17 (q, J = 5.8 Hz, 2H, 2xH-5'), 2.73 (d, J = 12.7 Hz, 2H, 2xH-3''), 2.25 – 2.15 (m, 2H, γ-CH2), 2.10 – 1.96 (m, 1H, β-CH2), 1.96 – 1.85 (m, 1H, β-CH2).

The amount of the obtained compound was not sufficient to measure a ^{13}C NMR spectrum, however the structure was verified through proton NMR and mass spectrometry and the compound's purity was validated via analytical HPLC.

2'3'-Deoxy-cAAMP-FOL (84)
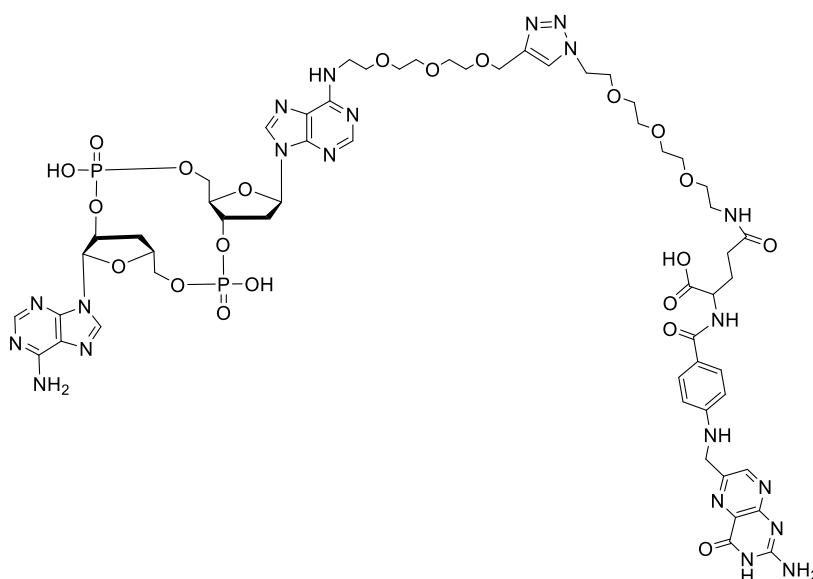
Materials and methods

All the solutions and solvents for this reaction were first thoroughly degassed with an argon stream for 30 minutes. **93** (5 mg, 6.28 umol) was dissolved in miliQ water (300 uL, final concentration 10mM) and THPTA (13 mg, 31.4 umol, 5.0 eq) was added followed by an aqueous solution of $CuSO_4$ (25 mg/mL, 100mM, 62 uL, 6.28 umol, 1.0 eq) and **87** (8 mg, 12.55 umol, 2.0 eq). Finally, an aqueous solution of sodium ascorbate (20 0mg/mL, 1.0M, 50 uL, 50.21 umol, 8.0 eq) was added and the reaction mixture was stirred for 4 hours at rt while monitoring its progression via LC-MS. After completion the mixture was directly purified by reversed phase HPLC (0% → 30% Buffer B over 45 minutes, t_R = 31min, Buffer A = 0.1% TFA in H_2O, Buffer B = 0.1% TFA in MeCN) and **84** was obtained as a yellowish powder (7 mg, 4.8 umol, 77%).

MALDI-TOF (negative mode): for $C_{56}H_{72}N_{21}O_{21}P_2^-$ [M-H]$^-$ calc. 1436.469 found 1436.442.

LC-MS (Buffer A = 0.01 % formic acid in H_2O, buffer B = 0.01 % formic acid in MeCN, method: 5-80 % buffer B in 7 minutes, then 95 % B for 1 minute): t_R: 3.4 min, m/z = 1439.3 [M+H]$^+$, 1453.6 [M-H]$^-$.

IR (ATR): $\tilde{v}$ (cm^{-1}) 2856 (br), 2280 (w), 1608 (s), 1508 (s), 1457 (s), 1247 (s), 1175 (m), 1031 (s), 833 (s), 778 (s).

^{1}H NMR (500 MHz, DMSO) δ 8.67 (s, 1H, H-7), 8.48 (s, 1H, adenosine H-2), 8.40 (s, 1H, adenosine H-8), 8.31 (s, 1H, adenosine H-2'''), 8.20 (d, J = 7.5 Hz, 1H, adenosine H-8'''), 8.03 (s, 1H, H-triazole), 7.93 (s, 1H, N3-H), 7.89 (t, J = 5.6 Hz, 1H, N10-H), 7.65 (d, J = 8.8 Hz, 2H, aryl-H), 6.64 (d, J = 8.8 Hz, 2H, aryl-H), 6.41 (t, J = 7.0 Hz, 1H, H-1'), 6.14 (d, J = 4.6 Hz, 1H, H-1''), 5.27 – 5.20 (m, 1H, H-3'), 5.17 (m, 1H, H-2''), 4.50 (s, 2H, 2xH-9), 4.37 – 4.21 (m, 4H, H-2' and H-5''), 4.07 (m, 2H, H-5'), 3.98 (m, 2H, α-CH and H-4'), 2.76 – 2.69 (m, 2H, H-3''), 2.23 – 2.16 (m, 2H, γ-CH2), 2.10 – 1.97 (m, 1H, β-CH2), 1.91 (m, 1H, β-CH2).

The amount of the obtained compound was not sufficient to measure a ^{13}C NMR spectrum, however the structure was verified through proton NMR and mass spectrometry and the compound's purity was validated via analytical HPLC.

Extinction coefficient compound 84

$\varepsilon(268nm) = 49.270\ M^{-1}cm^{-1}$
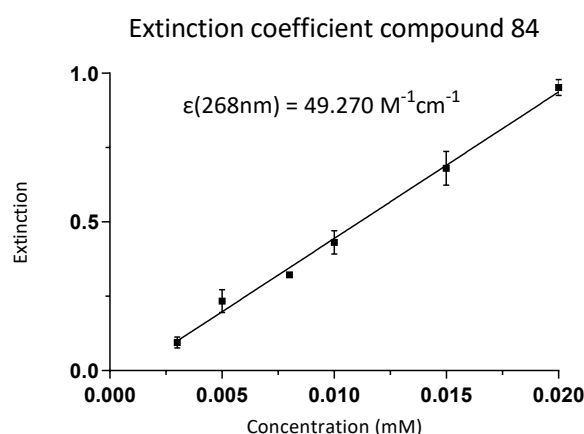
Supporting Information

Novel Poxin Stable cGAMP-Derivatives Are Remarkable STING Agonists

S. Stazzoni, D. F. R. Böhmer, F. Hernichel, D. Özdemir, A. Pappa, D. Drexler, S. Bauernfried, G. Witte, M. Wagner, S. Veth, K.-P. Hopfner, V. Hornung*, L. M. König*, T. Carell*

Supporting Information

Table of Contents

Supplementary Figures
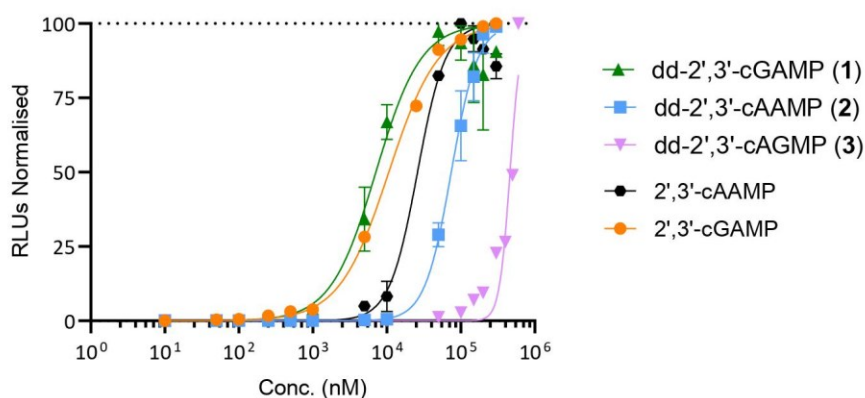
Figure SI-1: EC_{50} curves of values presented in Table 1. dd-2',3'-cGAMP (**1**): in green n=3, dd-2',3'-cAAMP (**2**): in blue n=3, dd-2'3'-cAGMP (**3**): in pink n=1, 2',3'-cAAMP: in black n=2, 2',3'-cGAMP: in orange n=1. The integrated luciferase reporter for interferon production in THP-1 Dual WT cells was used as a read-out for induced STING activity. Concentrations ranging from 0-300 µM of each compound was added on the THP-1 Dual WT cells and incubated for 24 hours. The luciferase signal was measured in Relative Light Units (RLUs) by a plate reader. The medium only background control was subtracted from all RLU values. These values were normalised on a scale from 0-100% in which the highest value was taken 100%. The EC_{50} curves and values were plotted and calculated on GraphPad Prism software utilising the Hill slope in agonist vs normalised response function with variable slope.
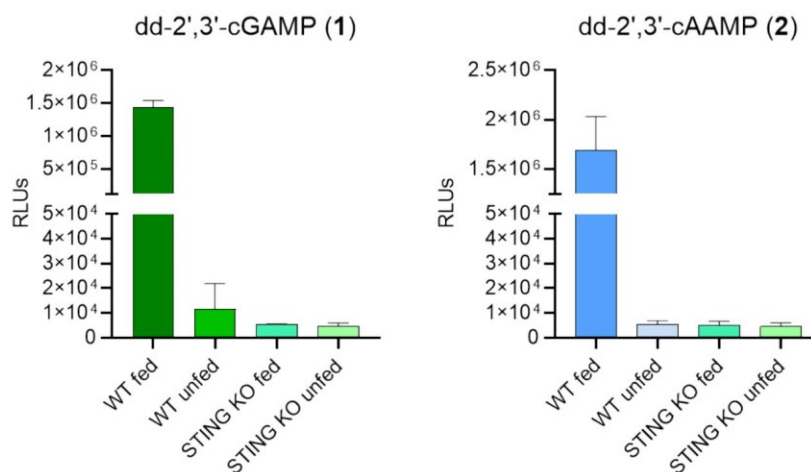
Figure SI-2: Activity of 200 µM dd-2',3'-cGAMP (**1**) and 300 µM dd-2',3'-cAAMP (**2**) on THP-1 Dual WT and STING-KO cells. Activity is measured by the luciferase reporter for interferon production.
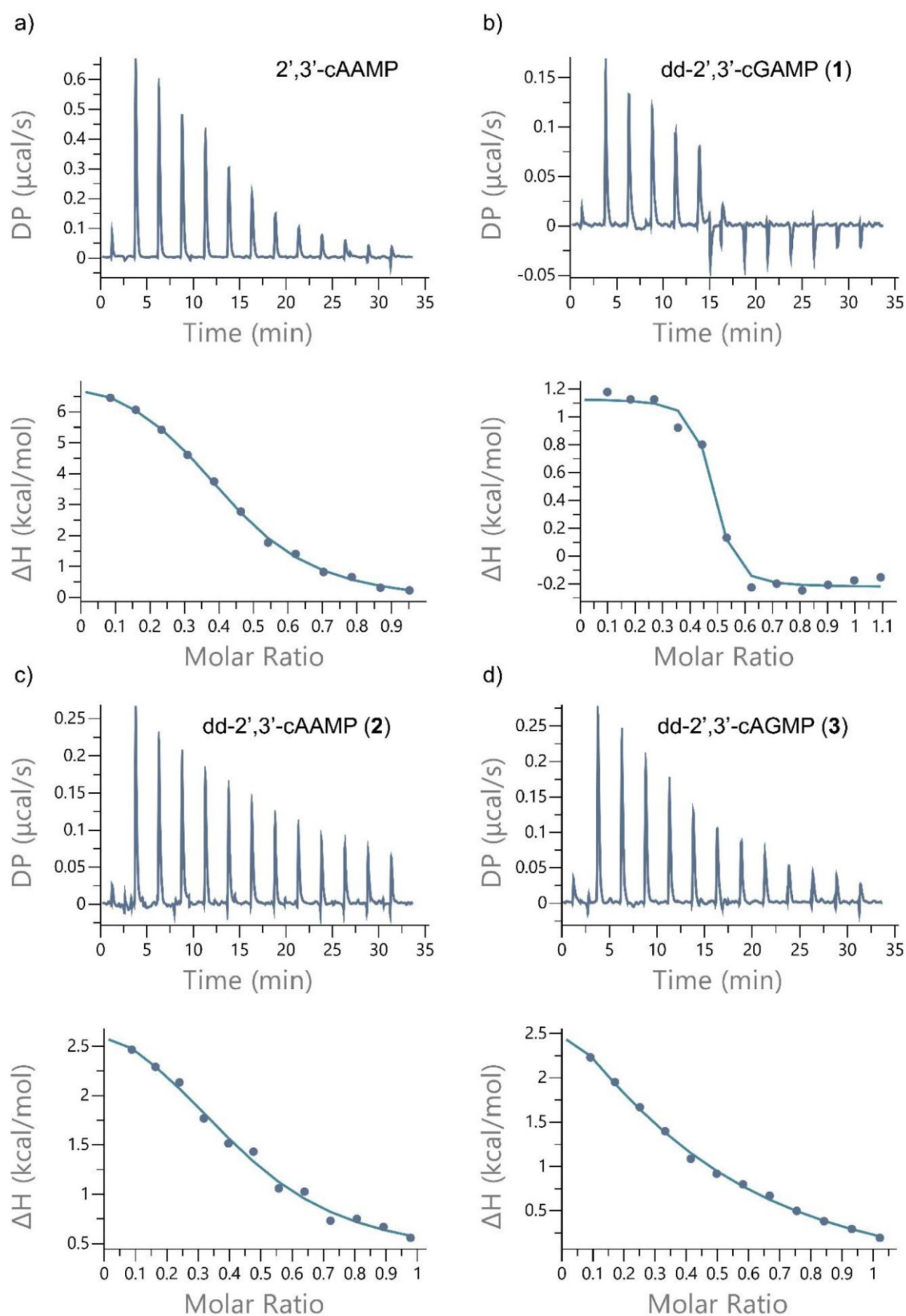
Figure SI-3: ITC experiments with human STING CTD. a) ITC measurement of 83 µM human STING AA139-379 (R220H) with 406 µM 2',3'-cAAMP at 25°C (upper panel) and the respective binding curve fit (lower panel); b) ITC measurement of 97 µM human STING AA139-379 (R220H) with 545 µM dd-2',3'-cGAMP (**1**) at 25°C (upper panel) and the respective binding curve fit (lower panel); c) ITC measurement of 81 µM human STING AA139-379 (R220H) with 407 µM dd-2',3'-cAAMP (**2**) at 25°C (upper panel) and the respective binding curve fit (lower panel); d) ITC measurement of 100 µM human STING AA139-379 (R220H) with 525 µM dd-2',3'-cAGMP (**3**) at 25°C (upper panel) and the respective binding curve fit (lower panel).

Table SI-1: Dissociation Constants (K_D) and thermodynamic parameters (ΔG, ΔH and $-T\Delta S$) from ITC measurements of human STING AA139-379 (R220H).

Compound	K_D [µM]	ΔG [kcal/mol]	ΔH [kcal/mol]	$-T\Delta S$ [kcal/mol]
dd-2',3'-cGAMP (**1**)	0.45 ± 0.23	-9.02	1.35	-10.4
dd-2',3'-cAGMP (**3**)	42.9 ± 35.1	-5.91	6.37	-12.3
dd-2',3'-cAAMP (**2**)	15.1 ± 14.5	-6.86	2.87	-9.73
2',3'-cAAMP	4.98 ± 0.82	-7.29	7.83	-15.1
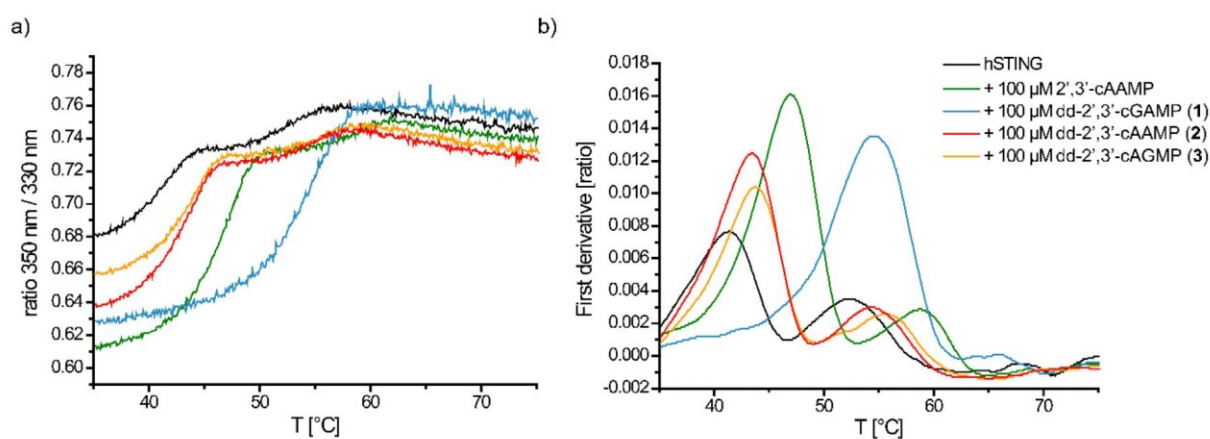
Figure SI-4: nanoDSF thermal shift experiments with human STING CTD. Thermal shift assay of 5 µM human STING AA139-379 (R220H) with 100 µM of dd-CDNs **1**–**3** and reference compound 2',3'-cAAMP. a) ratio 350 nm/330 nm; b) first derivative (ratio).

Figure SI-5: Comparison of tumour volumes at day 12. Adjusted p values: solvent control vs. 2',3'-cGAMP = 0.0026, solvent control vs. dd-2',3'-cAAMP = 0.0001, solvent control vs. dd-2',3'-cGAMP = 0.0005.

Materials and Methods

General Chemistry Methods

Chemicals were purchased from Sigma-Aldrich, TCI, Fluka, ABCR, Carbosynth or Acros Organics and used without further purification. Solvents of reagent grade were purified by distillation. Reactions and column chromato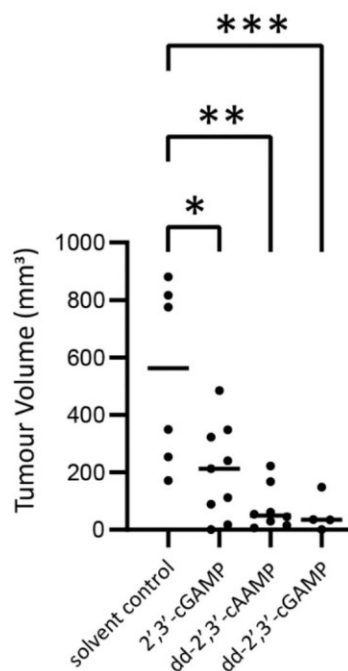graphy fractions were monitored by thin-layer chromatography (TLC) on silica gel F254TLC plates from Merck KGaA. Flash column chromatography was performed on Geduran® Si60 (40-63 μm) silica gel from Merck KGaA applying nitrogen pressure. Chemical transformations were conducted under nitrogen or argon atmosphere in oven-dried glassware unless otherwise specified. NMR spectra were recorded on Bruker AVIIIHD 400 (400 MHz) or Varian NMR-System600 (600 MHz) spectrometers. ^{1}H-NMR shifts were calibrated to the residual solvent resonances: CD_2Cl_2 (5.32 ppm), CD_3OD (3.31 ppm) and D_2O (4.79 ppm). ^{13}C-NMR shifts were calibrated to the residual solvent resonances: CD_2Cl_2 (53.84 ppm) and CD_3OD (49.00 ppm). All NMR spectra were analysed using the program MestReNova 10.0.1 from Mestrelab Research S.L. High resolution mass spectra (HRMS) were measured by the analytical section of the Department of Chemistry of the Ludwigs-Maximilians-Universität München on a MAT 90 (ESI) from Thermo Finnigan GmbH. IR spectra were recorded on a PerkinElmer Spectrum BX II FT-IR system. Substances were applied as a film or directly as solids on the ATR unit. Analytical RP-HPLC was performed on an Agilent 1260 Infinity II Analytical LC System equipped with the column Nucleodur 100-3 C18ec from Macherey-Nagel applying eluent flow of 0.5 mL/min. Preparative RP-HPLC was performed on an Agilent 1260 Infinity II Manual Preparative LC System equipped with the column Nucleodur 100-5 C18ec from Macherey-Nagel. A flowrate of 5 mL/min was applied.

Synthetic Procedures

The common precursor of compounds **1 − 3**, 1,2-di-*O*-acetyl-5-*O*-benzoyl-3-deoxyribofuranose (**S1**), was obtained in four steps from 1,2-*O*-isopropyliden-α-D-xylofuranose (**4**) according to published literature procedures.[1, 2] **S1** was then glycosylated under Vorbrüggen conditions using either commercially available N^6-benzoyladenine or O^6-(diphenylcarbamoyl)-N^2-isobutyrylguanine, which was synthesized according to published literature procedures.[3, 4] The glycosylated precursors **S2** and **S3** where then selectively deprotected on the 5'-OH and the 3'-OH and selectively tritylated on the 5'-OH to give precursors **5** and **6** according to published literature procedures.[2, 5] All structures were determined and characterized via ^{1}H-NMR spectroscopy and were found to be corresponding to the literature. From this point on, the analogous syntheses of dd-CDNs **1 − 3** are presented in the example of the synthesis of dd-2',3'-cAAMP (**2**).

_N_⁶-(Bz)-2'-_O_-(allyl)(CE)phosphotriester-3'-deoxyadenosine (**7**)
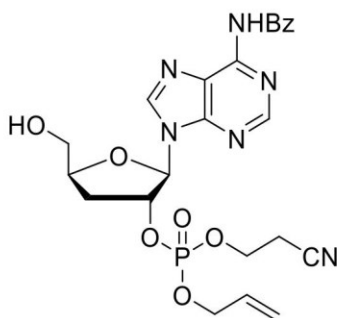
Compound **5** (300 mg, 456 μmol, 1.00 eq.) was dissolved in 5 mL (c=0.09M) of DCM under argon atmosphere. 2-Cyanoethyl-_N,N,N',N'_-tetraisopropylphosphordiamidite (188 μL, 593 μmol, 1.30 eq.) was added, followed by pyridine trifluoroacetate (106 mg, 547 μmol, 1.20 eq.). The mixture was stirred at rt for 3 h until TLC (_iso_-hexane/EtOAc 1:5) showed disappearance of the starting material. Allyl alcohol (155 μL, 2.28 mmol, 5.00 eq.) was added, followed by a 0.3 M solution of BTT in MeCN (3.0 mL, 912 μmol, 2.00 eq.) and the reaction was stirred for 1 h at rt. A 5 M solution of _t_-butyl hydroperoxide in decane (274 μL, 1.37 mmol, 3.00 eq.) was added and the solution stirred for 40 min and then quenched with a solution of NaHSO$_3$ (1 mL, 0.5 g/mL) in water. The mixture was diluted with 50 mL of EtOAc, washed with brine and the organic phase was collected and directly evaporated _in vacuo_. The residue was redissolved in 20 mL of a 3% _v/v_ solution of DCA in DCM. The deep red solution was stirred for 15 min and then carefully quenched with a saturated aqueous NaHCO$_3$ solution (30 mL). The product was extracted with EtOAc and the combined organic layers were washed with brine, dried over Na$_2$SO$_4$ filtered and evaporated _in vacuo_. The crude was purified by column chromatography (5% to 10% MeOH in DCM) to yield **7** as a white foam (147 mg, 278 μmol, 61%).

R$_f$: 0.17 (4% MeOH in DCM)

ESI-HRMS: calculated for C$_{23}$H$_{26}$N$_6$O$_7$P$^+$ [M+H]$^+$: 529.1595; found: 529.1592.

IR (ATR): $\tilde{v}$ (cm^{-1}) = 3268 (br), 3058 (m), 2928 (m), 2256 (w), 1697 (m), 1582 (m), 1453 (m).

^{1}H NMR (400 MHz, CD$_2$Cl$_2$): δ in ppm = 8.64 (s, 1H), 8.21 (2 s, 1H), 7.97 − 7.84 (m, 2H), 7.60 − 7.39 (m, 3H), 6.07 (dd, _J_ = 3.9, 1.8 Hz, 1H), 5.78 (tdt, _J_ = 16.4, 10.4, 5.7 Hz, 1H), 5.48 − 5.32 (m, 1H), 5.28 − 5.11 (m, 2H), 4.51 (td, _J_ = 6.9, 6.5, 1.9 Hz, 1H), 4.42 (dddt, _J_ = 14.2, 7.1, 4.4, 1.4 Hz, 2H), 4.10 (ddt, _J_ = 10.8, 8.1, 6.1 Hz, 2H), 3.94 (m, 1H), 3.63 − 3.49 (m, 1H), 2.75 − 2.56 (m, 3H), 2.39 − 2.22 (m, 1H).

^{13}C NMR (100 MHz, CD$_2$Cl$_2$): δ in ppm = 164.52, 152.14, 150.82, 150.02, 142.64, 142.57, 133.76, 132.77, 131.84, 128.83, 127.84, 124.11, 118.94, 116.60, 116.52, 91.06, 90.99, 81.21, 81.18, 79.94, 79.89, 69.11, 69.03, 63.33, 63.31, 62.39, 32.38, 32.34, 19.68, 19.64.

^{31}P NMR (162 MHz, CD$_2$Cl$_2$): δ in ppm = -2.54.

Protected dideoxy AMP-AMP linear dinucleotide **12**
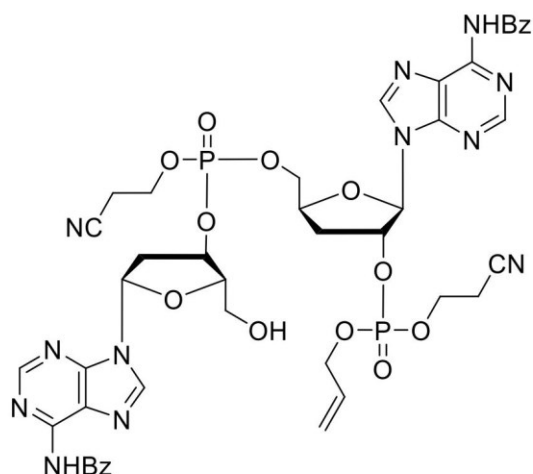
Compound **7** (70 mg, 133 μmol, 1.00 eq.) was dissolved in 3 mL (c=0.04M) of dry MeCN. N^6-(Bz)-5'-*O*-(DMT)-2'-deoxyadenosine-3'-*O*-(CE)-*N*,*N*'-diisopropylphosphoramidite (**9**) (125 mg, 146 μmol, 1.10 eq.) and a 0.3 M solution of BTT in MeCN (880 μL, 265 μmol, 2.00 eq.) were added and the solution stirred at r.t. for 1 h. A 5 M solution of *t*-butyl hydroperoxide in decane (80 μL, 397 μmol, 3.00 eq.) was added and the mixture stirred for 40 min at r.t. and then quenched with a solution of NaHSO₃ (1 mL, 0.5 g/mL) in water. The solution was diluted with 50 mL of EtOAc, washed with brine and the organic phase was directly evaporated *in vacuo*. The residue was dissolved in 6.2 mL of 3% *v/v* DCA in DCM, stirred at r.t. for 15 min and quenched with a saturated aqueous NaHCO₃ solution and the product was extracted with EtOAc. The combined organic layers were washed with brine and dried over Na₂SO₄, filtered, and dried *in vacuo*. The crude was purified by column chromatography (2% to 7.5% MeOH in DCM) to yield **12** as a white solid (80 mg, 80 μmol, 61%). Linear dinucleotide **12** was obtained as a mixture of four diastereomers and therefore not further characterized at this stage.

R_f: 0.38 (8% MeOH in DCM)

ESI-HRMS: calculated for $C_{43}H_{43}O_{13}N_{12}P_2^-$ [M-H]⁻: 997.25533; found: 997.25543.

Dideoxy AMP-AMP linear dinucleotide **15**
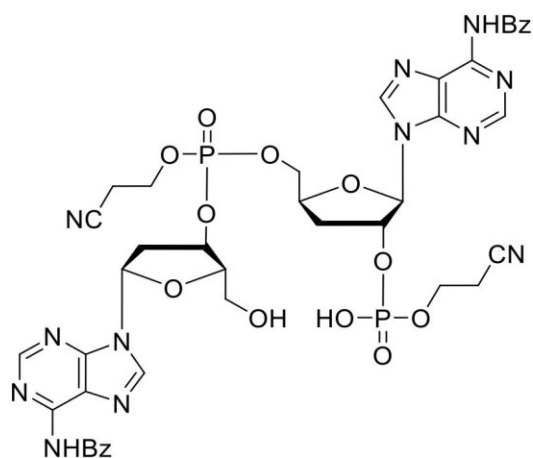
Compound **12** (80.0 mg, 80.1 μmol, 1.00 eq.) was suspended in 10 mL (c=8 mM) acetone, NaI (180 mg, 1.20 mmol, 15.0 eq) was added and the reaction vigorously stirred under reflux for 3 h. The cloudy mixture was cooled down to r.t. and filtered. The solid was collected, coevaporated three times with

pyridine and dried overnight under high vacuum to afford **15** (78.0 mg, 80.1 µmol, quant. yield) as a white foam. The analytical data pictured below are relative to a mixture of two diastereomers.

ESI-HRMS: calculated for $C_{40}H_{39}O_{13}N_{12}P_2^-$ [M-H]$^-$: 957.22403; found: 957.22365.

IR (ATR): $\tilde{v}$ (cm^{-1}) = 3347 (br), 2656 (s), 2923 (vs), 2853 (s), 2360 (w), 1728 (w), 1614 (w), 1455 (m).

^{1}H NMR (800 MHz, CD$_3$OD): δ = 8.72 (s, 1H), 8.68 (2 s, 1H), 8.58 (4 s, 2H), 8.12 − 8.07 (m, 2H), 8.02 (ddd, J = 40.2, 8.3, 1.4 Hz, 2H), 7.68 (dddq, J = 8.9, 5.8, 3.1, 1.5 Hz, 1H), 7.59 (tdd, J = 8.4, 4.5, 2.2 Hz, 2H), 7.56 − 7.48 (m, 2H), 6.55 − 6.32 (m, 2H), 5.49 (dddd, J = 15.2, 13.3, 6.7, 1.4 Hz, 1H), 5.23 (tt, J = 6.1, 1.8 Hz, 1H), 4.81 (s, 1H), 4.53 (ddd, J = 11.5, 6.3, 2.4 Hz, 1H), 4.44 (dddd, J = 25.9, 11.4, 6.4, 5.1 Hz, 1H), 4.35 − 4.23 (m, 4H), 4.09 (p, J = 6.2 Hz, 4H), 3.78 − 3.69 (m, 2H), 2.99 − 2.88 (m, 3H), 2.87 − 2.66 (m, 4H), 2.53 (dddd, J = 13.6, 6.0, 4.5, 1.6 Hz, 1Hs).

^{13}C NMR (100 MHz, CD$_3$OD): δ in ppm = 166.70, 151.99, 151.50, 149.71, 143.31, 133.37, 132.65, 128.38, 128.31, 128.08, 127.93, 123.57, 118.06, 117.23, 91.22, 86.48, 85.33, 85.07, 79.67, 79.27, 78.77, 68.68, 63.08, 61.52, 60.48, 18.97, 18.79.

^{31}P NMR (162 MHz, CD$_3$OD): δ in ppm = -1.30, -1.35, -3.03, -3.08.

dd-2',3'-cAAMP (**2**)
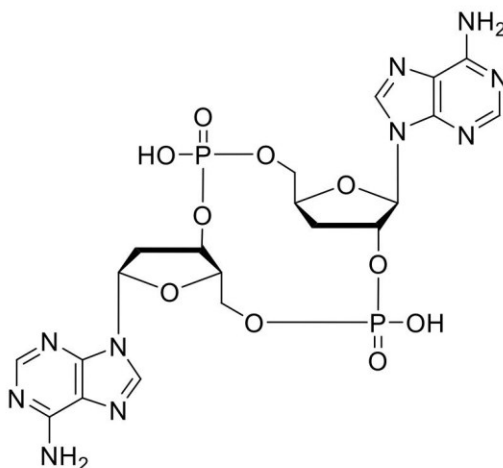
Compound **15** (75.0 mg, 78.2 µmol, 1.00 eq.) was redissolved in 15 mL (c=4.8 mM) of dry pyridine and MSNT (232 mg, 782 µmol, 10.0 eq.) was added. After stirring the mixture overnight at r.t. the solvents were removed *in vacuo*. The crude intermediate was directly used without further purification in the next step. The solid residue was dissolved in 8 mL of 33% *v/v* MeNH$_2$ in absolute EtOH. After stirring 3 h at r.t. LC-MS control showed no more starting material present. The solvent was evaporated, the residue coevaporated twice with pyridine and dried under high vacuum. The dry solid was redissolved in a minimal amount of MeOH, transferred to a falcon tube and precipitated with cold acetone. The precipitate was collected after centrifugation and purified by RP-HPLC (0% to 10% buffer B in 45 min; buffer A = 0.1% *v/v* TFA in H$_2$O, buffer B = 0.1% *v/v* TFA in MeCN). Compound **2** was obtained as a white solid (14.0 mg, 22.4 µmol, 29%).

ESI-HRMS: calculated for $C_{20}H_{25}N_{10}O_{10}P_2^+$ [M+H]$^+$: 627.1225; found: 627.1240.

IR (ATR): $\tilde{v}$ (cm^{-1}) = 3074 (br), 2362 (w), 1692 (s), 1606 (w), 1418 (w).

¹H NMR (400 MHz, D₂O): δ in ppm = 8.43 (s, 1H), 8.37 (s, 1H), 8.30 (s, 1H), 8.29 (s, 2H), 6.43 (dd, *J* = 6.9, 4.7 Hz, 1H), 6.15 (d, *J* = 4.3 Hz, 1H), 5.08 – 5.00 (m, 1H), 4.96 (p, *J* = 5.9 Hz, 1H), 4.56 (d, *J* = 6.3 Hz, 1H), 4.32 – 4.16 (m, 2H), 4.08 (dt, *J* = 11.2, 5.5 Hz, 1H), 4.05 – 3.92 (m, 2H), 3.09 – 2.95 (m, 1H), 2.76 (dt, *J* = 13.8, 6.7 Hz, 1H), 2.69 (dt, *J* = 13.5, 6.8 Hz, 1H), 2.41 – 2.27 (m, 1H).

¹³C NMR (201 MHz, D₂O): δ in ppm = 150.33, 150.30, 148.38, 147.88, 145.05, 144.97, 143.47, 141.79, 118.51, 115.51, 88.43, 84.51, 83.26, 78.28, 77.89, 72.91, 68.33, 62.88, 38.22, 34.26.

³¹P NMR (162 MHz, D₂O): δ in ppm = -1.10, -1.86.

Analytical Data

*N*²-isobutyryl-*O*⁶-diphenylcarbamate-2'-*O*-(allyl)(CE)phosphotriester-3'-deoxyguanosine (**8**)
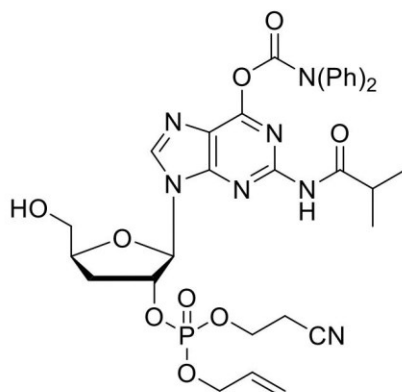
R$_f$: 0.54 (DCM/MeOH = 10:1)

¹H NMR (800 MHz, CD$_2$Cl$_2$): δ in ppm = 8.33 (d, *J* = 16.9 Hz, 1H), 8.26 (d, *J* = 29.8 Hz, 1H), 7.45 (br s, 3H), 7.39 (t, *J* = 7.8 Hz, 5H), 7.29 (br s, 2H), 6.13 (dd, *J* = 16.4, 2.2 Hz, 1H), 5.99 − 5.94 (m, 2H), 5.92 − 5.86 (m, 1H), 5.42 (m, 1H), 5.39 (dd, *J* = 17.2, 1.4 Hz, 1H), 5.28 (dd, *J* = 10.4, 1.1 Hz, 1H), 5.23 (d, *J* = 10.4 Hz, 1H), 4.58 − 4.56 (m, 2H), 4.22 (tdd, *J* = 9.4, 6.1, 3.1 Hz, 2H), 4.20 − 4.18 (m, 1H), 3.94 (ddd, *J* = 11.5, 8.7, 2.5 Hz, 1H), 3.70 − 3.68 (m, 1H), 3.03 − 2.98 (m, 1H), 2.70 (t, *J* = 6.1 Hz, 1H, CH-*i*Bu), 2.35 − 2.32 (m, 1H), 1.23 (t, *J* = 6.7 Hz, 6H, *i*Bu-Me).

¹³C NMR (201 MHz, CD$_2$Cl$_2$): δ in ppm = 180.21, 156.57, 154.62, 152.43, 150.84, 144.19, 143.72, 132.90, 132.48, 129.79, 121.32, 119.39, 118.88, 117.93, 91.35, 81.87, 69.44, 68.95, 63.16, 63.08, 62.89, 62.32, 58.18, 47.21, 36.69, 34.00, 33.03, 21.82, 20.04 19.46, 19.40, 19.23, 19.12.

³¹P NMR (162 MHz, CD$_2$Cl$_2$): δ in ppm = -2.65, -2.66.

ESI-HRMS: calculated for C$_{33}$H$_{37}$O$_9$N$_7$P$^+$ [M+H]$^+$: 706.2346; found: 706.2395

IR(ATR): $\tilde{v}$ (cm^{-1}) = 3395, 2694, 2358, 1699, 1582, 1452, 1253, 1182, 1000, 693.

Protected dideoxy GMP-AMP linear dinucleotide **11**
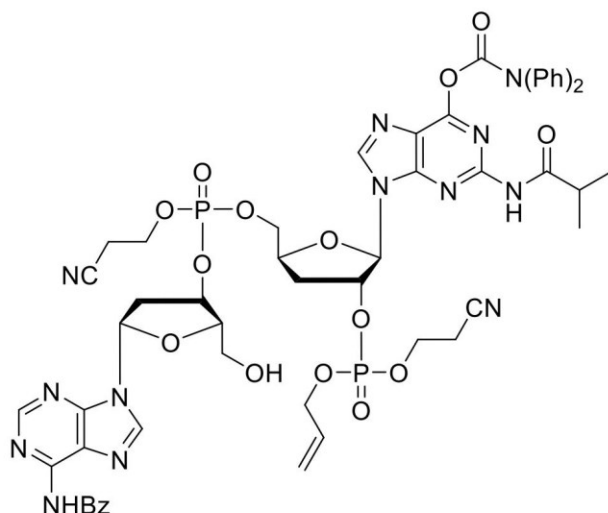
The product was obtained as a mixture of 4 P-diastereomers and therefore not further characterized at this stage.

R$_f$: 0.38 (DCM/Acetone/MeOH = 80:15:5)

ESI-HRMS: calculated for $C_{53}H_{56}O_{15}N_{13}P_2^+$ [M+H]$^+$: 1176.3449; found: 1176.3507

Dideoxy GMP-AMP linear dinucleotide **14**
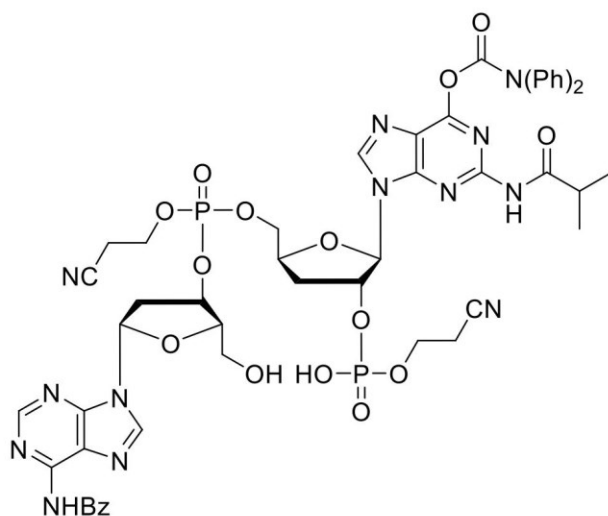
^{1}H NMR (800 MHz, CD$_3$OD): δ in ppm = 8.69 (d, J = 12.9 Hz, 1H), 8.57 (d, J = 22.1 Hz, 1H), 8.49 (d, J = 8.8 Hz, 1H), 8.11 – 8.07 (m, 3H), 7.71 – 7.64 (m, 2H), 7.57 (t, J = 7.8 Hz, 3H), 7.38 – 7.33 (m, 5H), 7.28 – 7.22 (m, 2H), 6.46 (ddd, J = 21.4, 8.2, 6.0 Hz, 1H, H-1''), 6.34 (d, J = 11.6 Hz, 1H, H-1'), 5.46 – 5.41 (m, 1H, H-2'), 5.24 – 5.16 (m, 1H, H-3''), 4.80 – 4.74(m, 1H, H-4'), 4.47 (dt, J = 8.4, 4.3 Hz, 2H, -OCH$_2$CH$_2$CN), 4.22 – 4.15 (m, 2H, H-5'), 4.08 – 4.02 (m, 3H, -OCH$_2$CH$_2$CN and H$_a$-5''), 3.69 (dt, J = 5.3, 3.8 Hz, 1H, H$_b$-5''), 3.03 – 2.88 (m, 2H, H-3'), 2.85 – 2.80 (m, 2H, -OCH$_2$CH$_2$CN), 2.78 – 2.73 (m, 3H, -OCH$_2$CH$_2$CN and H$_a$-2''), 2.66 (dddd, J = 34.1, 14.1, 6.0, 2.0 Hz, 1H, H-4''), 2.46 – 2.40 (m, 1H, H$_b$-2''), 1.22 – 1.19 (m, 6H, NHCOCHMe$_2$).

^{13}C NMR (201 MHz, CD$_3$OD): δ in ppm = 178.05, 168.21(C=O), 156.96, 155.42, 153.82, 152.97, 152.80, 152.17, 151.18, 147.24, 145.83, 144.84, 144.73, 142.27, 134.91, 134.12, 133.98, 130.26, 129.79,

129.47, 126.82, 122.48, 119.33, 118.50, 93.05(C-1'), 87.86(C-4'), 86.57(C-1''), 80.96(C-3''), 80.21(C-2'), 70.20, 64.32(C-5'), 62.88(C-5''), 61.80(C$_a$-5''), 39.59(C-3'), 36.96(C-4''), 34.51, 20.32, 20.05, 19.76.

^{31}P NMR (162 MHz, CD$_3$OD): δ in ppm = -1.18, -1.23, -2.96, -3.00, -3.05.

ESI-HRMS: calculated for C$_{50}$H$_{52}$O$_{15}$N$_{13}$P$_2$$^+$ [M+H]$^+$: 1136.3136; found: 1136.3190

IR(ATR): $\tilde{v}$ (cm^{-1}) = 3397, 2695, 1704, 1491,1361, 1220, 1046, 701.

dd-2',3'-cGAMP (**1**)

^{1}H NMR (400 MHz, D$_2$O): δ in ppm = 8.22 (s, 1H), 8.13 (s, 1H), 7.79 (s, 1H), 6.36 (dd, J = 6.7, 3.1 Hz, 1H, H1''), 5.76 (d, J = 5.7 Hz, 1H, H1'), 5.33 (dt, J = 12.7, 5.9 Hz, 1H, H2'), 5.01 (dq, J = 14.7, 8.0, 7.4 Hz, 1H, H3''), 4.50 (m, 1H, H4'), 4.25 − 4.18 (m, 1H, H$_b$5''), 4.17 − 4.12 (m, 1H, H$_a$5''), 4.10 − 4.04 (m, 2H, H$_a$5' and H4''), 3.99 (ddd, J = 11.8, 8.0, 4.3 Hz, 1H, H$_b$5'), 3.02 − 2.84 (m, 1H, H$_a$2''), 2.77 − 2.67 (m, 1H, H$_b$2''), 2.54 (dt, J = 13.1, 8.1 Hz, 1H, H$_a$3'), 2.39 − 2.31 (m, 1H, H$_b$3').

^{13}C NMR (201 MHz, D$_2$O): δ in ppm = 158.88, 153.37, 151.50, 147.84, 138.82, 137.09, 130.87, 118.64, 116.75, 88.29, 83.86, 82.90, 76.80, 75.46, 71.14, 67.81, 62.52, 44.05, 38.83, 33.44.

^{31}P NMR (162 MHz, D$_2$O): δ in ppm = -0.90, -1.92.

ESI-HRMS: calculated for C$_{20}$H$_{25}$O$_{11}$N$_{10}$P$_2$$^+$ [M+H]$^+$: 643.1135; found: 643.1172
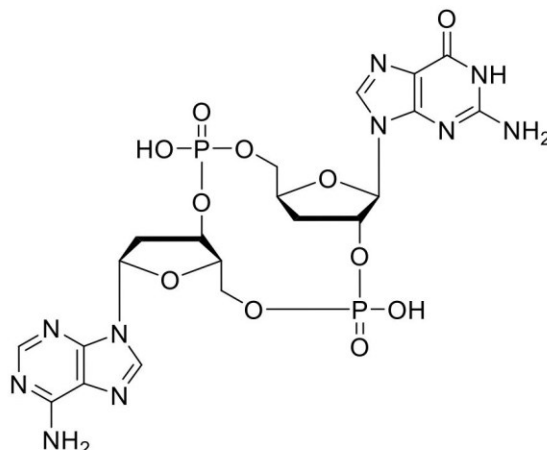
IR(ATR): $\tilde{v}$ (cm^{-1}) = 3110, 2358, 1692, 1608, 1402, 1200, 1057, 1011, 679.

Protected dideoxy AMP-GMP linear dinucleotide **13**
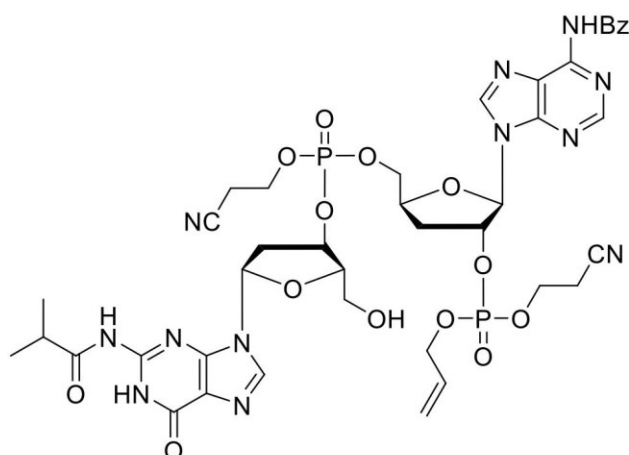
The synthetic procedure of dinucleotide **13** is analogous to the procedure described above for protected AMP-AMP linear dinucleotide **12**, with the only exception that N^2-isobutyryl-5'-O-(DMT)-2'-deoxyguanosine-3'-O-(CE)-N,N'-diisopropylphosphoramidite (**10**) was used. The product was obtained as a mixture of 4 P-diastereomers and therefore not further characterized at this stage.

ESI-HRMS: calculated for $C_{40}H_{47}N_{12}O_{14}P_2^+$ [M+H]$^+$: 981.2804; found: 981.2824.

Dideoxy AMP-GMP linear dinucleotide **16**
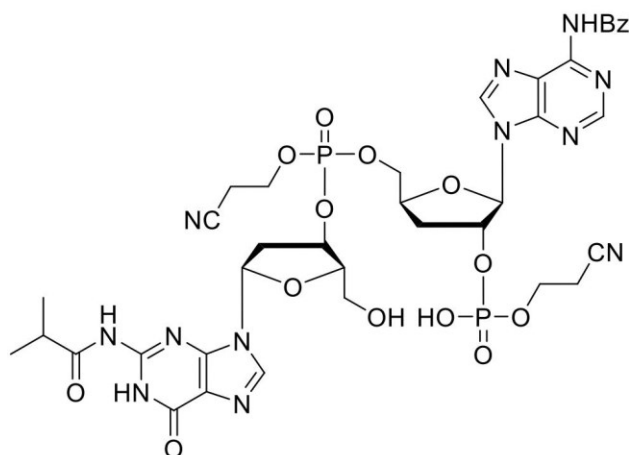
^{1}H NMR (800 MHz, CD$_3$OD): δ in ppm = 8.77 (s, 1H), 8.59 (s, 1H), 8.20 (s, 1H), 8.05 – 8.00 (m, 1H), 8.00 – 7.91 (m, 1H), 7.69 – 7.59 (m, 1H), 7.59 – 7.51 (m, 1H), 6.46 – 6.37 (m, 1H, H-1'), 6.32 – 6.16 (m, 1H, H-1''), 5.51 (dt, J = 28.6, 6.6 Hz, 1H, H-2'), 5.10 (tdt, J = 6.4, 4.5, 1.8 Hz, 1H, H-3''), 4.80 (s, 1H, H-4'), 4.54 – 4.36 (m, 2H, H-5'), 4.33 – 4.20 (m, 2H, -OCH$_2$CH$_2$CN), 4.16 – 3.89 (m, 3H, -OCH$_2$CH$_2$CN and H-4''), 3.73 – 3.56 (m, 2H, H-5''), 2.98 – 2.84 (m, 2H, H$_a$-3' isomer A and -OCH$_2$CH$_2$CN), 2.79 (tdd, J = 10.5, 7.3, 5.0 Hz, 4H, H$_a$-3' isomer B, -NHCOCHMe$_2$, -OCH$_2$CH$_2$CN), 2.65 – 2.56 (m, 1H, H$_b$-2''), 2.53 (dtd, J = 13.7, 5.9, 1.6 Hz, 1H, H$_b$-3') 1.36 – 1.18 (m, 6H, NHCOCHMe$_2$).

^{13}C NMR (201 MHz, D$_2$O): δ in ppm = 180.41, 166.57, 155.86, 152.01, 151.46, 149.70, 148.76, 148.21, 143.30, 138.20, 133.18, 132.59, 128.20, 127.97, 127.83, 123.65, 119.92, 117.98, 117.24, 91.21, 86.07, 83.75, 79.56, 78.75, 68.61, 63.04, 61.08, 60.49, 38.72, 38.17, 35.58, 33.27, 18.99, 18.05.

^{31}P NMR (162 MHz, CD$_3$OD): δ in ppm = -1.31, -1.41, -2.70, -3.01.

ESI-HRMS: calculated for $C_{37}H_{43}N_{12}O_{14}P_2^+$ [M+H]$^+$: 941.2491; found: 941.2502.

IR (ATR): $\tilde{\nu}$ (cm^{-1}) = 3349 (br), 2956 (s), 2923 (vs), 2854 (s), 2358 (w), 1676 (m), 1603 (m), 1456 (m).

dd-2',3'-cAGMP (**3**)
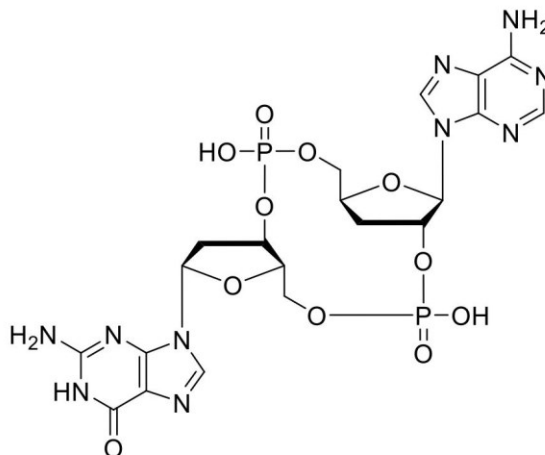
^{1}H NMR (400 MHz, D$_2$O): δ in ppm = 8.68 (s, 1H, H-8-A), 8.39 (s, 1H, H-8-G), 8.29 (s, 1H, H-2-A), 6.26 (dd, J = 6.8, 3.1 Hz, 1H, H-1''), 6.15 (d, J = 4.2 Hz, 1H, H-1'), 5.02 (m, J = 5.8 Hz, 1H, H-2'), 4.85 (p, J = 6.6 Hz, 1H, H-3''), 4.59 – 4.50 (m, 1H, H-4'), 4.31 – 4.25 (m, 1H, H-4''), 4.24 – 4.02 (m, 3H, H-5'' and H$_a$-5'), 3.97 (td, J = 11.3, 5.5 Hz, 1H, H$_b$-5'), 3.11 – 2.97 (m, 1H, H$_a$-2'), 2.69 (m, 2H, H$_b$-2' and H$_a$-3''), 2.33 (dt, J = 12.8, 5.8 Hz, 1H, H$_b$-3'').

^{13}C NMR (201 MHz, D$_2$O): δ in ppm = 155.20, 149.78, 149.12, 148.20, 144.51, 142.04, 137.11, 135.56, 118.55, 109.21, 88.53, 85.82, 83.61, 78.58, 77.90, 71.67, 68.29, 62.74, 38.23, 34.31.

^{31}P NMR (162 MHz, D$_2$O): δ in ppm = -1.10, -2.04.

ESI-HRMS: calculated for $C_{20}H_{23}N_{10}O_{11}P_2^-$ [M-H]$^-$: 641.10285; found: 641.10241.

Cell Culture and Biological Assays

Cell Culture:

THP-1 Dual^{TM} monocytic cells were purchased from Invivogen and cultured according to the guidelines provided by the manufacturer. The cells were kept at 37°C in water saturated, 5% CO$_2$-enriched atmosphere. RPMI 1640 (Sigma-Aldrich) supplemented with 20% (*v/v*) fetal bovine serum (FBS) (Invitrogen), 2 mM L-alanyl-L-glutamine (Sigma-Aldrich), 1% (*v/v*) penicillin-streptomycin (Sigma-Aldrich), 25 mM HEPES (Sigma-Aldrich), 100 μg/mL Normocin^{TM} (Invivogen) was used as initial growth medium. When the cells reached a doubling time of three days, 10% (*v/v*) FBS was used and 10 μg/ml of blasticidin (Invivogen) and 100 μg/ml of Zeocin^{TM} (Invivogen) were added freshly to the growth medium upon each passaging of cells. The cells were kept between 0.4x10^6/mL and 2x10^6/mL in culture, while the maintaining medium was changed every two days.

The BHK-21 cells were cultivated in Glasgow Modified Essential Medium (Thermo Fisher Scientific) supplemented with 10% fetal calf serum (Thermo Fisher Scientific), 1% penicillin-streptomycin (Thermo Fisher Scientific), 4% tryptose-phosphate (Thermo Fisher Scientific), 1% non-essential aminoacids (NEAA from Thermo Fisher Scientific). Cells were routinely split and cultured for appropriate confluency to conduct experiments.

RIL-175 cells (kindly provided by Tim Greten (NCI, Bathesda, USA; described in Kapanadze, T. *et al*. J Hepatol 2013) were cultivated in Dulbecco's modified Eagle's medium supplemented with 10% fetal calf serum, 2 mM l-glutamine, penicillin (100 U/l), streptomycin (0.1 mg/ml). Cells were routinely tested for absence of contamination with mycoplasma by PCR.

Activity (EC$_{50}$) Assay:

The activity of dd-2',3'-CDNs **1** − **3** was measured by the luciferase reporter system provided in the THP-1 Dual^{TM} cells. For this purpose, concentrations ranging from 5 nM to 300 µM of each compound were added on 0.125 x 10^6 cells in 96-well plates with an end volume of 200 µM. Of the compound dd-2',3'-cAGMP concentrations up to 600 µM were added on the cells. A test medium without Blasticidin, Zeocin^{TM} and Normocin^{TM} was used. THP-1 Dual^{TM} STING KO cells were used as a negative control with the highest concentration of each compound added to the THP-1 Dual^{TM} cells. All cells were incubated with the compounds for 24 hours. A 20 µL of the medium was transferred in duplicates of each well to a white opaque 96-well plate. On each well, 50 µL of the QUANTI-Luc^{TM} reagent (Invivogen) containing the luciferase substrate coelenterazine was injected and measured immediately after 5 seconds of shaking by a plate reader (Tecan Genios Pro) for luminescence. The read-out was normalised to the medium-only background signal. The highest read-out was taken 100% and the lowest as 0% in each data set. The normalised values were plotted and analysed on the Graph Pad Prism 8 software using the Hill-equation. All experiments were repeated three times.

Protein overexpression and purification:

Plasmids for human STING AA139-379 (R220H) and mouse STING AA138-378 have been expressed and purified as described previously by Cavlar *et*. *al*. except for using Turbo broth (Molecular Dimensions) instead of LB medium for expression.[6]

Isothermal Titration Calorimetry:

ITC experiments were performed using a Malvern PEAQ-ITC system with human STING AA139-379 (R220H) in ITC buffer (50 mM HEPES pH 7.5, 150 mM NaCl) in the cell. The respective compounds were titrated at different concentrations (see figure legends of Figure SI-1) into the cell by 13 injections of 2 µL, spaced 150 seconds apart, at 25°C. Data analysis was performed with the Malvern software package. All experiments were repeated at least once to confirm the robustness of the assay.

Nano Differential Scanning Fluorimetry:

Thermal Shift experiments were performed using a Tycho NT.6 instrument (NanoTemper Technologies) with 5 µM human STING AA139-379 (R220H) or 5 µM mouse STING AA139-379 and 100 µM of the respective compound. The samples were heated in a glass capillary at a rate of 30K/min and the internal fluorescence at 330 nm and 350 nm was recorded. Data evaluation was performed using the internal analysis tool of the Tycho instrument.

Poxin Degradation Assay:

1x10^6 BHK21 cells were plated in a 10 cm dish and the following day the cells were either infected with Vaccina virus strain Western Reserve (VACV WR) or control-treated the similar way without addition of viral particles. For the infection, the medium of the cells was replaced with 5 mL PBS supplemented with 1 mM CaCl$_2$, 1 mM MgCl$_2$, and 10 x 10^6 PFUs of VACV WR and cells were infected for 1 hour with shaking of the plate every 15 minutes. After one hour, the medium was exchanged to 12 mL DMEM supplemented with 1% Na-pyruvate, 2.5% fetal calf serum, 50 mM HEPES and, penicillin-streptomycin the cells were incubated for 14 hours overnight. The next day, control treated cells or infected cells were lysed in 4 mL lysis buffer consisting of 20 mM HEPES-NaOH pH 7.5, 150 mM NaCl, 1% NP-40, and

1 mM TCEP-KOH for 15 minutes, followed by a 10-minute centrifugation at 1000 g. The supernatant was frozen in liquid nitrogen and the protein concentration was determined by BCA assay.

For the degradation assay, a master mix was prepared for the time points 0 h, 30 minutes, 1 h, 3 h and 24 h for each compound. Each mix consisted of 3 ng/µL cell lysate (control or VACV WR infected) and 5 µM compound in a reaction buffer composed of 50 mM HEPES-KOH (pH 7.5), 35 mM KCl, 1 mM DTT (adapted from Eaglesham et al.[7]) allowing to have 750 pmol compound and 450 ng lysate in 150 µL collected sample per time point. The mix was incubated at 37°C and at each time point 150 µL sample was collected to another tube and the reaction was stopped by the addition of 150 µL Roti-Phenol (phenol/chloroform/isoamyl alcohol; 25/24/1). After vortexing and centrifugation for 1 minute at 14000 rpm, the upper layer was transferred to a new tube and equi-volume chloroform was added. The sample was vortexed at least 10 seconds and centrifuged for 1 minute at 14000 rpm. The upper layer was transferred into a clean tube and this process was repeated two more times. The last centrifugation step was 5 minutes to ensure complete separation of layers. The upper layer was taken and lyophilised. The dry sample was then dissolved in 150 µL room temperature ddH$_2$O, and both the phenol chloroform extraction and the lyophilisation were repeated to ensure optimal purification of the sample before submission to LC-MS analysis (HPLC-ESI-MS, see below).

Liquid chromatography – mass spectrometry (LC-MS)

The lyophilized samples of the poxin degradation assay were dissolved in 100 µL of MQ water and kept on ice during handling. All samples were filtrated before measurement using an AcroPrep Advance 96 filter plate 0.2 µm Supor from Pall Life Sciences. The HPLC-HESI-MS analyses were performed on a Dionex Ultimate 3000 HPLC system coupled to a Thermo Fisher LTQ Orbitrap XL mass spectrometer. Compounds of interest (injection volume: 85 µL) were separated with an Interchim Uptisphere120-3HDO C18 column whose temperature was maintained at 30 °C. Elution buffers were buffer X (2 mM NH$_4$HCOO in H$_2$O; pH 5.5) and buffer Y (2 mM NH$_4$HCOO in H$_2$O/MeCN 20/80 v/v; pH 5.5) with a flow rate of 150 µL/min. The gradient was as follows: 0→5 min, 0 % Y; 5→20 min, 0→15 % Y; 20→40 min, 15→100 % Y; 40→47 min, 100% Y. The chromatogram was recorded at 260 nm with a Dionex Ultimate 3000 Diode Array Detector with a data collection rate of 20 Hz and a response time 0.10 s. The chromatographic eluent was directly injected into the ion source of the mass spectrometer without prior splitting. Ions were scanned in the positive polarity mode over a full-scan range of m/z = 225-2000 with a resolution of 100,000. Parameters of the mass spectrometer were tuned with a freshly mixed solution of inosine (5 µM) in buffer X. Source-dependent parameters were set as follows: Capillary temperature 275 °C; APCI vaporizer temperature 100 °C; sheath gas flow 5.00; auxiliary gas flow 21.0; sweep gas flow 1.00; source voltage 4.80 kV; capillary voltage 0 V; tube lens voltage 45.00 V. Data analysis was performed using the program Xcalibur from Thermo Scientific: Ion chromatograms of the compounds of interest were extracted from the total ion current (TIC) chromatogram with a mass range set to +/- 0.0050 u around the exact mass [M+H]$^+$ of the compound of interest. The corresponding peak area in the UV chromatogram (which is directly proportional to the amount of the compound in the sample) was integrated and normalized with respect to the respective peak area at t = 0.

Animal experiments

Mice:

Female C57Bl/6j mice were purchased from Charles River. Mice were at least 6 weeks of age at the onset of experiments and were kept under pathogen–free conditions. Animal studies were approved by the local authorities (Regierung von Oberbayern, Munich, Germany; file number 55.2-2532.Vet_02-17-12).

Tumour challenge:

Mice were injected subcutaneously with 1×10^6 RIL-175 cells. The tumour size and health status were monitored every other day. Tumour volume was calculated as follows: volume = (width^2 x length)/2. Mice were randomized and therapy was initiated when tumours reached a mean volume of 20 mm^3. Mice were sacrificed when the maximum tumor diameter exceeded 15 mm or at signs of affliction in accordance to predefined endpoint criteria. Mean tumor growth analysis was discontinued when the first animal per group had to be sacrificed due to tumor progression.

Treatment:

For treatment, tumours were injected with 15 nmol cyclic dinucleotides (CDNs) dissolved in 0.9 % NaCl containing 0.4 % (v/v) DMSO in a total volume of 25 µl every 3 days for up to 5 injections.

[1]   F. Hulpia, S. Van Calenbergh, G. Caljon, L. Maes, (Universiteit Gent, Universiteit Antwerpen), WO2019076633, **2019**

[2]   A. Kumar, S. I. Khan, A. Manglani, Z. K. Khan, S. B. Katti, *Nucleosides Nucleotides Nucleic Acids* **1994**, *13*, 1049-1058.

[3]   M. J. Robins, R. Zou, Z. Guo, S. F. Wnuk, *J. Org. Chem.* **1996**, *61*, 9207-9212.

[4]   T. F. Jenny, K. C. Schneider, S. A. Benner, *Nucleosides Nucleotides Nucleic Acids* **1992**, *11*, 1257-1261.

[5]   C. Meier, J. M. Neumann, F. Andre, Y. Henin, T. Huynh Dinh, *J. Org. Chem.* **1992**, *57*, 7300-7308.

[6]   T. Cavlar, T. Deimling, A. Ablasser, K.-P. Hopfner, V. Hornung, *EMBO J.* **2013**, *32*, 1440–1450.

[7]   J. B. Eaglesham, Y. Pan, T. S. Kupper, P. J. Kranzusch, *Nature* **2019**, *566*, 259–263.

5 List of abbreviations

ABZI: Aminobenzimidazole

AIBN: 2,2'-azodisisobutyronitrile

APC: Antigen presenting cell

ATP: Adenosine triphosphate

BSA: bis(trimethylsilyl)acetamide

BTT: 5-(benzylthio)-1H-tetrazole

Bz: Benzoyl

CDN: Cyclic dinucleotide

cGAMP: cyclic guanosine monophosphate-adenosine monophosphate

cGAS: cyclic adenosine monophosphate-adenosine monophosphate synthase

COPA: Coatomer subunit-α

COPI: Coatomer complex I

COVID: Coronavirus

Cryo-EM: Cryo-electron microscopy

CTT: C-terminal tail

DCA: dichloroacetic acid

DCC: *N,N'*-dicyclohexylcarbodiimide

DCM: dichloromethane

DIPEA: Diisopropylethylamine

DMAP: 4-dimethyl-aminopyridine

DMF: dimethylformamide

DMSO: dimethylsulfoxide

DMTMM: 4-(4,6-dimethoxy-1,3,5-triazine-2-yl)-4-methyl-morpholiniumchloride

DMT: 4,4'-dimethoxytrityl

DMXAA: 5,6-Dimethylxanthenone-4-acetic acid

DSF: differential scanning fluorimetry

EC$_{50}$: half maximal effective concentration

EDC·HCl: 1-ethyl 3-(3-dimethylaminopropyl)carbodiimide

List of abbreviations

EI: electron ionization

ENPP1: Ecto-nucleotide pyrophosphatase phosphodiesterase

ER: Endoplasmatic reticulum

ERGIC: Endoplasmatic reticulum-Golgi intermediate compartment

ESI: Electrospray ionization

EtOAc: Ethyl acetate

EtOH: Ethanol

GTP: Guanosine triphosphate

HATU: Hexafluorophosphate azabenzotriazole tetramethyl uranium

HIV: Human Immunodeficiency Virus

HOBt: Hydroxybenzotriazole

HPLC: high pressure liquid chromatography

HSV-1: Herpes simplex virus 1

iBu: iso-butyryl

ICI: Immune checkpoint inhibitor

IFN: Interferon

IL: Interleucine

IRF3: Interferon regulatory factor 3

IRGs: Interferon related genes

ITC: Isothermal Titration Calorimetry

KO: knockout

LBD: Ligand binding domain

LC: Liquid chromatography

MeCN: acetonitrile

MeOH: methanol

MLV: Murine leukemia virus

MS: mass spectrometry

NF-κB: Nuclear factor kappa beta

NHS: N-hydroxysuccinimide

NMI: N-methylimidazole

List of abbreviations

NMR: nuclear magnetic resonance

pyBOP: Benzotriazol-1-yloxytripyrrolidinophosphonium hexafluorophosphate

RPMI: Roswell Park Memorial Institute

SASP: Senescence-associated secretory phenotype

SATE: S-acylthioethyl

SAVI: STING-associated vasculopathy with onset in infancy

SIV: Simian immunodeficiency virus

STING: Stimulator of interferon genes

TBK1: TANK-binding kinase 1

TBS: *tert*-butyldimethylsilyl

tBuOOH: *tert*-butylhydroperoxide

TEA: Triethylamine

TFA: trifluoroacetic acid

TM: Transmembrane

TME: Tumor microenvironment

TMS: trimethylsilyl

TNF: Tumor necrosis factor

TPSCl: 2,4,5-triisopropylbenzenesulfonyl chloride

TREX1: Three prime repair exonuclease 1

VRAC: Volume-regulated anion channel

6 Literature

(1) Zhang, Q.; Zhang, X.; Zhu, Y.; Sun, P.; Zhang, L.; Ma, J.; Zhang, Y.; Zeng, L.; Nie, X.; Gao, Y.; et al. Recognition of cyclic dinucleotides and folates by human SLC19A1. *Nature* **2022**. DOI: 10.1038/s41586-022-05452-z From NLM Publisher.

(2) Ishikawa, H.; Barber, G. N. The STING pathway and regulation of innate immune signaling in response to DNA pathogens. *Cell Mol. Life Sci.* **2011**, *68* (7), 1157-1165. DOI: 10.1007/s00018-010-0605-2 From NLM.

(3) Civril, F.; Deimling, T.; de Oliveira Mann, C. C.; Ablasser, A.; Moldt, M.; Witte, G.; Hornung, V.; Hopfner, K. P. Structural mechanism of cytosolic DNA sensing by cGAS. *Nature* **2013**, *498* (7454), 332-337. DOI: 10.1038/nature12305 From NLM.

(4) Burdette, D. L.; Monroe, K. M.; Sotelo-Troha, K.; Iwig, J. S.; Eckert, B.; Hyodo, M.; Hayakawa, Y.; Vance, R. E. STING is a direct innate immune sensor of cyclic di-GMP. *Nature* **2011**, *478* (7370), 515-518. DOI: 10.1038/nature10429.

(5) Barber, G. N. STING: infection, inflammation and cancer. *Nat. Rev. Immunol.* **2015**, *15* (12), 760-770. DOI: 10.1038/nri3921.

(6) Ishikawa, H.; Barber, G. N. STING is an endoplasmic reticulum adaptor that facilitates innate immune signalling. *Nature* **2008**, *455* (7213), 674-678. DOI: 10.1038/nature07317.

(7) Abe, T.; Barber, G. N. Cytosolic-DNA-mediated, STING-dependent proinflammatory gene induction necessitates canonical NF-κB activation through TBK1. *J Virol* **2014**, *88* (10), 5328-5341. DOI: 10.1128/jvi.00037-14 From NLM.

(8) Wu, J.; Sun, L.; Chen, X.; Du, F.; Shi, H.; Chen, C.; Chen, Z. J. Cyclic GMP-AMP Is an Endogenous Second Messenger in Innate Immune Signaling by Cytosolic DNA. *Science* **2013**, *339* (6121), 826-830. DOI: doi:10.1126/science.1229963.

(9) Decout, A.; Katz, J. D.; Venkatraman, S.; Ablasser, A. The cGAS-STING pathway as a therapeutic target in inflammatory diseases. *Nat. Rev. Immunol.* **2021**, *21* (9), 548-569. DOI: 10.1038/s41577-021-00524-z.

(10) Zhong, B.; Yang, Y.; Li, S.; Wang, Y. Y.; Li, Y.; Diao, F.; Lei, C.; He, X.; Zhang, L.; Tien, P.; et al. The adaptor protein MITA links virus-sensing receptors to IRF3 transcription factor activation. *Immunity* **2008**, *29* (4), 538-550. DOI: 10.1016/j.immuni.2008.09.003 From NLM.

(11) Sun, W.; Li, Y.; Chen, L.; Chen, H.; You, F.; Zhou, X.; Zhou, Y.; Zhai, Z.; Chen, D.; Jiang, Z. ERIS, an endoplasmic reticulum IFN stimulator, activates innate immune signaling through dimerization. *PNAS* **2009**, *106* (21), 8653-8658. DOI: doi:10.1073/pnas.0900850106.

(12) Zhang, C.; Shang, G.; Gui, X.; Zhang, X.; Bai, X.-C.; Chen, Z. J. Structural basis of STING binding with and phosphorylation by TBK1. *Nature* **2019**, *567* (7748), 394-398. DOI: 10.1038/s41586-019-1000-2.

(13) Gui, X.; Yang, H.; Li, T.; Tan, X.; Shi, P.; Li, M.; Du, F.; Chen, Z. J. Autophagy induction via STING trafficking is a primordial function of the cGAS pathway. *Nature* **2019**, *567* (7747), 262-266. DOI: 10.1038/s41586-019-1006-9.

(14) Ishikawa, H.; Ma, Z.; Barber, G. N. STING regulates intracellular DNA-mediated, type I interferon-dependent innate immunity. *Nature* **2009**, *461* (7265), 788-792. DOI: 10.1038/nature08476.

(15) Burdette, D. L.; Vance, R. E. STING and the innate immune response to nucleic acids in the cytosol. *Nat. Immunol.* **2013**, *14* (1), 19-26. DOI: 10.1038/ni.2491 From NLM.

(16) Danilchanka, O.; Mekalanos, John J. Cyclic Dinucleotides and the Innate Immune Response. *Cell* **2013**, *154* (5), 962-970. DOI: 10.1016/j.cell.2013.08.014 (acccessed 2023/10/05).

(17) Gao, P.; Ascano, M.; Wu, Y.; Barchet, W.; Gaffney, Barbara L.; Zillinger, T.; Serganov, Artem A.; Liu, Y.; Jones, Roger A.; Hartmann, G.; et al. Cyclic [G(2',5')pA(3',5')p] Is the Metazoan Second Messenger Produced by DNA-Activated Cyclic GMP-AMP Synthase. *Cell* **2013**, *153* (5), 1094-1107. DOI: 10.1016/j.cell.2013.04.046 (acccessed 2023/10/23).

(18) Zhang, X.; Shi, H.; Wu, J.; Zhang, X.; Sun, L.; Chen, C.; Chen, Z. J. Cyclic GMP-AMP containing mixed phosphodiester linkages is an endogenous high-affinity ligand for STING. *Mol. Cell* **2013**, *51* (2), 226-235. DOI: 10.1016/j.molcel.2013.05.022.

(19) Gao, P.; Ascano, M.; Zillinger, T.; Wang, W.; Dai, P.; Serganov, A. A.; Gaffney, B. L.; Shuman, S.; Jones, R. A.; Deng, L.; et al. Structure-function analysis of STING activation by c[G(2',5')pA(3',5')p] and targeting by antiviral DMXAA. *Cell* **2013**, *154* (4), 748-762. DOI: 10.1016/j.cell.2013.07.023.

(20) Sun, Z.; Hornung, V. cGAS-STING signaling. *Curr. Biol.* **2022**, *32* (13), R730-R734. DOI: 10.1016/j.cub.2022.05.027 From NLM Medline.

(21) Shi, H.; Wu, J.; Chen, Z. J.; Chen, C. Molecular basis for the specific recognition of the metazoan cyclic GMP-AMP by the innate immune adaptor protein STING. *Proc. Natl. Acad. Sci. USA* **2015**, *112* (29), 8947-8952. DOI: 10.1073/pnas.1507317112.

(22) Chen, C. 10th anniversary of discovering cGAMP: synthesis and beyond. *Org. Chem. Front.* **2023**, *10* (4), 1086-1098. DOI: 10.1039/d2qo02033e.

(23) Shang, G.; Zhang, C.; Chen, Z. J.; Bai, X.-C.; Zhang, X. Cryo-EM structures of STING reveal its mechanism of activation by cyclic GMP–AMP. *Nature* **2019**, *567* (7748), 389-393. DOI: 10.1038/s41586-019-0998-5.

(24) Shang, G.; Zhu, D.; Li, N.; Zhang, J.; Zhu, C.; Lu, D.; Liu, C.; Yu, Q.; Zhao, Y.; Xu, S.; et al. Crystal structures of STING protein reveal basis for recognition of cyclic di-GMP. *Nat. Struct. Mol. Biol.* **2012**, *19* (7), 725-727. DOI: 10.1038/nsmb.2332.

(25) Ergun, S. L.; Fernandez, D.; Weiss, T. M.; Li, L. STING Polymer Structure Reveals Mechanisms for Activation, Hyperactivation, and Inhibition. *Cell* **2019**, *178* (2), 290-301 e210. DOI: 10.1016/j.cell.2019.05.036.

(26) Zhang, H.; You, Q. D.; Xu, X. L. Targeting Stimulator of Interferon Genes (STING): A Medicinal Chemistry Perspective. *J. Med. Chem.* **2020**, *63* (8), 3785-3816. DOI: 10.1021/acs.jmedchem.9b01039.

(27) Hopfner, K. P.; Hornung, V. Molecular mechanisms and cellular functions of cGAS-STING signalling. *Nat Rev Mol Cell Biol* **2020**, *21* (9), 501-521. DOI: 10.1038/s41580-020-0244-x.

(28) Balka, K. R.; Louis, C.; Saunders, T. L.; Smith, A. M.; Calleja, D. J.; D'Silva, D. B.; Moghaddas, F.; Tailler, M.; Lawlor, K. E.; Zhan, Y.; et al. TBK1 and IKKε Act Redundantly to Mediate STING-Induced NF-κB Responses in Myeloid Cells. *Cell Rep* **2020**, *31* (1), 107492. DOI: 10.1016/j.celrep.2020.03.056 From NLM.

(29) Mukai, K.; Konno, H.; Akiba, T.; Uemura, T.; Waguri, S.; Kobayashi, T.; Barber, G. N.; Arai, H.; Taguchi, T. Activation of STING requires palmitoylation at the Golgi. *Nat. Commun.* **2016**, *7*, 11932. DOI: 10.1038/ncomms11932.

(30) Taguchi, T.; Mukai, K.; Takaya, E.; Shindo, R. STING Operation at the ER/Golgi Interface. *Front. Immunol.* **2021**, *12*, 646304. DOI: 10.3389/fimmu.2021.646304.

(31) Ablasser, A.; Goldeck, M.; Cavlar, T.; Deimling, T.; Witte, G.; Röhl, I.; Hopfner, K.-P.; Ludwig, J.; Hornung, V. cGAS produces a 2'-5'-linked cyclic dinucleotide second messenger that activates STING. *Nature* **2013**, *498* (7454), 380-384. DOI: 10.1038/nature12306.

(32) Yi, G.; Brendel, V. P.; Shu, C.; Li, P.; Palanathan, S.; Cheng Kao, C. Single nucleotide polymorphisms of human STING can affect innate immune response to cyclic dinucleotides. *PLoS One* **2013**, *8* (10), e77846. DOI: 10.1371/journal.pone.0077846 From NLM.

(33) Yin, Q.; Tian, Y.; Kabaleeswaran, V.; Jiang, X.; Tu, D.; Eck, M. J.; Chen, Z. J.; Wu, H. Cyclic di-GMP sensing via the innate immune signaling protein STING. *Mol Cell* **2012**, *46* (6), 735-745. DOI: 10.1016/j.molcel.2012.05.029 From NLM.

(34) Shu, C.; Yi, G.; Watts, T.; Kao, C. C.; Li, P. Structure of STING bound to cyclic di-GMP reveals the mechanism of cyclic dinucleotide recognition by the immune system. *Nat. Struct. Mol. Biol.* **2012**, *19* (7), 722-724. DOI: 10.1038/nsmb.2331 From NLM.

(35) Huang, Y.-H.; Liu, X.-Y.; Du, X.-X.; Jiang, Z.-F.; Su, X.-D. The structural basis for the sensing and binding of cyclic di-GMP by STING. *Nat. Struct. Mol. Biol.* **2012**, *19* (7), 728-730. DOI: 10.1038/nsmb.2333.

(36) Ouyang, S.; Song, X.; Wang, Y.; Ru, H.; Shaw, N.; Jiang, Y.; Niu, F.; Zhu, Y.; Qiu, W.; Parvatiyar, K.; et al. Structural analysis of the STING adaptor protein reveals a hydrophobic dimer interface and mode of cyclic di-GMP binding. *Immunity* **2012**, *36* (6), 1073-1086. DOI: 10.1016/j.immuni.2012.03.019 From NLM.

(37) Garland, K. M.; Sheehy, T. L.; Wilson, J. T. Chemical and Biomolecular Strategies for STING Pathway Activation in Cancer Immunotherapy. *Chem Rev* **2022**, *122* (6), 5977-6039. DOI: 10.1021/acs.chemrev.1c00750 From NLM Medline.

(38) Matteo Gentili, J. K., Mercedes Tkach, Takeshi Satoh, Xavier Lahaye, Cécile Conrad, Marilyn Boyron, Bérangère Lombard, Sylvère Durand, Guido Kroemer, Damarys Loew, Marc Dalod, Clotilde Théry and Nicolas Manel. Viruses transfer the antiviral second messenger cGAMP between cells. *Science* **2015**, *349* (6253), 1232-1236.

(39) A. Bridgeman, J. M., T. Davenne, T. Partridge, Y. Peng, A. Mayer, T. Dong, V. Kaever, P. Borrow and J. Rehwinkel. Transmission of innate immune signaling by packaging of cGAMP in viral particles. *Science* **2015**, *349,1232-1236*.

(40) Ablasser, A.; Schmid-Burgk, J. L.; Hemmerling, I.; Horvath, G. L.; Schmidt, T.; Latz, E.; Hornung, V. Cell intrinsic immunity spreads to bystander cells via the intercellular transfer of cGAMP. *Nature* **2013**, *503* (7477), 530-534. DOI: 10.1038/nature12640 From NLM.

(41) Cordova, A. F.; Ritchie, C.; Bohnert, V.; Li, L. Human SLC46A2 Is the Dominant cGAMP Importer in Extracellular cGAMP-Sensing Macrophages and Monocytes. *ACS Cent Sci* **2021**, *7* (6), 1073-1088. DOI: 10.1021/acscentsci.1c00440 From NLM PubMed-not-MEDLINE.

(42) Ritchie, C.; Cordova, A. F.; Hess, G. T.; Bassik, M. C.; Li, L. SLC19A1 Is an Importer of the Immunotransmitter cGAMP. *Mol. Cell* **2019**, *75* (2), 372-381 e375. DOI: 10.1016/j.molcel.2019.05.006 From NLM Medline.

(43) Luteijn, R. D.; Zaver, S. A.; Gowen, B. G.; Wyman, S. K.; Garelis, N. E.; Onia, L.; McWhirter, S. M.; Katibah, G. E.; Corn, J. E.; Woodward, J. J.; et al. SLC19A1 transports immunoreactive cyclic dinucleotides. *Nature* **2019**, *573* (7774), 434-438. DOI: 10.1038/s41586-019-1553-0 From NLM Medline.

(44) Lahey, L. J.; Mardjuki, R. E.; Wen, X.; Hess, G. T.; Ritchie, C.; Carozza, J. A.; Böhnert, V.; Maduke, M.; Bassik, M. C.; Li, L. LRRC8A:C/E Heteromeric Channels Are Ubiquitous Transporters of cGAMP. *Mol. Cell* **2020**, *80* (4), 578-591.e575. DOI: 10.1016/j.molcel.2020.10.021 From NLM.

(45) Maltbaek, J.; Snyder, J.; Stetson, D. *ABCC1/MRP1 exports cGAMP and modulates cGAS-dependent immunity*; 2021. DOI: 10.1101/2021.12.03.470980.

(46) Zhou, C.; Chen, X.; Planells-Cases, R.; Chu, J.; Wang, L.; Cao, L.; Li, Z.; López-Cayuqueo, K. I.; Xie, Y.; Ye, S.; et al. Transfer of cGAMP into Bystander Cells via LRRC8 Volume-Regulated Anion Channels Augments STING-Mediated Interferon Responses and Anti-viral Immunity. *Immunity* **2020**, *52* (5), 767-781.e766. DOI: 10.1016/j.immuni.2020.03.016 From NLM.

Literature

(47) Maltbaek, J. H.; Snyder, J. M.; Stetson, D. B. ABCC1 transporter exports the immunostimulatory cyclic dinucleotide cGAMP. *Immunity* **2022**, *Oct 11;55(10):1799-1812*. DOI: 10.1016/j.immuni.2022.08.006.

(48) Li, L.; Yin, Q.; Kuss, P.; Maliga, Z.; Millan, J. L.; Wu, H.; Mitchison, T. J. Hydrolysis of 2′3′-cGAMP by ENPP1 and design of nonhydrolyzable analogs. *Nat. Chem. Biol.* **2014**, *10* (12), 1043-1048. DOI: 10.1038/nchembio.1661.

(49) Kato, K.; Nishimasu, H.; Oikawa, D.; Hirano, S.; Hirano, H.; Kasuya, G.; Ishitani, R.; Tokunaga, F.; Nureki, O. Structural insights into cGAMP degradation by Ecto-nucleotide pyrophosphatase phosphodiesterase 1. *Nat. Commun.* **2018**, *9* (1), 4424. DOI: 10.1038/s41467-018-06922-7.

(50) Gao, J.; Tao, J.; Liang, W.; Zhao, M.; Du, X.; Cui, S.; Duan, H.; Kan, B.; Su, X.; Jiang, Z. Identification and characterization of phosphodiesterases that specifically degrade 3′3′-cyclic GMP-AMP. *Cell Res* **2015**, *25* (5), 539-550. DOI: 10.1038/cr.2015.40 From NLM.

(51) Dennis, M. L.; Newman, J.; Dolezal, O.; Hattarki, M.; Surjadi, R. N.; Nuttall, S. D.; Pham, T.; Nebl, T.; Camerino, M.; Khoo, P. S.; et al. Crystal structures of human ENPP1 in apo and bound forms. *Acta Crystallogr. D. Struct. Biol.* **2020**, *76* (Pt 9), 889-898. DOI: 10.1107/s2059798320010505 From NLM.

(52) Carozza, J. A.; Bohnert, V.; Nguyen, K. C.; Skariah, G.; Shaw, K. E.; Brown, J. A.; Rafat, M.; von Eyben, R.; Graves, E. E.; Glenn, J. S.; et al. Extracellular cGAMP is a cancer cell-produced immunotransmitter involved in radiation-induced anti-cancer immunity. *Nat Cancer* **2020**, *1* (2), 184-196. DOI: 10.1038/s43018-020-0028-4.

(53) Li, J.; Duran, M. A.; Dhanota, N.; Chatila, W. K.; Bettigole, S. E.; Kwon, J.; Sriram, R. K.; Humphries, M. P.; Salto-Tellez, M.; James, J. A.; et al. Metastasis and Immune Evasion from Extracellular cGAMP Hydrolysis. *Cancer Discovery* **2021**, *11* (5), 1212-1227. DOI: 10.1158/2159-8290.Cd-20-0387 (acccessed 12/7/2023).

(54) Lau, W. M.; Doucet, M.; Stadel, R.; Huang, D.; Weber, K. L.; Kominsky, S. L. Enpp1: a potential facilitator of breast cancer bone metastasis. *PLoS One* **2013**, *8* (7), e66752. DOI: 10.1371/journal.pone.0066752 From NLM.

(55) Hamann, L.; Ruiz-Moreno, Juan S.; Szwed, M.; Mossakowska, M.; Lundvall, L.; Schumann, Ralf R.; Opitz, B.; Puzianowska-Kuznicka, M. STING SNP R293Q Is Associated with a Decreased Risk of Aging-Related Diseases. *Gerontology* **2018**, *65* (2), 145-154. DOI: 10.1159/000492972 (acccessed 10/10/2023).

(56) Jin, L.; Xu, L. G.; Yang, I. V.; Davidson, E. J.; Schwartz, D. A.; Wurfel, M. M.; Cambier, J. C. Identification and characterization of a loss-of-function human MPYS variant. *Genes Immun* **2011**, *12* (4), 263-269. DOI: 10.1038/gene.2010.75 From NLM.

(57) Patel, S.; Blaauboer, S. M.; Tucker, H. R.; Mansouri, S.; Ruiz-Moreno, J. S.; Hamann, L.; Schumann, R. R.; Opitz, B.; Jin, L. The Common R71H-G230A-R293Q Human TMEM173 Is a Null Allele. *J Immunol* **2017**, *198* (2), 776-787. DOI: 10.4049/jimmunol.1601585 From NLM.

(58) Rivera Vargas, T.; Benoit-Lizon, I.; Apetoh, L. Rationale for stimulator of interferon genes-targeted cancer immunotherapy. *Eur J Cancer* **2017**, *75*, 86-97. DOI: 10.1016/j.ejca.2016.12.028 From NLM.

(59) Volpi, S.; Picco, P.; Caorsi, R.; Candotti, F.; Gattorno, M. Type I interferonopathies in pediatric rheumatology. *Pediatric Rheumatology* **2016**, *14* (1), 35. DOI: 10.1186/s12969-016-0094-4.

(60) Lin, B.; Berard, R.; Al Rasheed, A.; Aladba, B.; Kranzusch, P. J.; Henderlight, M.; Grom, A.; Kahle, D.; Torreggiani, S.; Aue, A. G.; et al. A novel STING1 variant causes a recessive form of STING-associated vasculopathy with onset in infancy (SAVI). *J Allergy Clin Immunol* **2020**, *146* (5), 1204-1208.e1206. DOI: 10.1016/j.jaci.2020.06.032 From NLM.

(61) Steiner, A.; Hrovat-Schaale, K.; Prigione, I.; Yu, C.-H.; Laohamonthonkul, P.; Harapas, C. R.; Low, R. R. J.; De Nardo, D.; Dagley, L. F.; Mlodzianoski, M. J.; et al. Deficiency in coatomer complex I causes aberrant activation of STING signalling. *Nature Communications* **2022**, *13* (1), 2321. DOI: 10.1038/s41467-022-29946-6.

(62) Crow, Y. J.; Manel, N. Aicardi-Goutières syndrome and the type I interferonopathies. *Nat Rev Immunol* **2015**, *15* (7), 429-440. DOI: 10.1038/nri3850 From NLM.

(63) Lee-Kirsch, M. A.; Gong, M.; Chowdhury, D.; Senenko, L.; Engel, K.; Lee, Y. A.; de Silva, U.; Bailey, S. L.; Witte, T.; Vyse, T. J.; et al. Mutations in the gene encoding the 3′-5′ DNA exonuclease TREX1 are associated with systemic lupus erythematosus. *Nat Genet* **2007**, *39* (9), 1065-1067. DOI: 10.1038/ng2091 From NLM.

(64) Dou, Z.; Ghosh, K.; Vizioli, M. G.; Zhu, J.; Sen, P.; Wangensteen, K. J.; Simithy, J.; Lan, Y.; Lin, Y.; Zhou, Z.; et al. Cytoplasmic chromatin triggers inflammation in senescence and cancer. *Nature* **2017**, *550* (7676), 402-406. DOI: 10.1038/nature24050.

(65) Yang, H.; Wang, H.; Ren, J.; Chen, Q.; Chen, Z. J. cGAS is essential for cellular senescence. *PNAS* **2017**, *114* (23), E4612-E4620. DOI: doi:10.1073/pnas.1705499114.

(66) Paul, B. D.; Snyder, S. H.; Bohr, V. A. Signaling by cGAS-STING in Neurodegeneration, Neuroinflammation, and Aging. *Trends Neurosci* **2021**, *44* (2), 83-96. DOI: 10.1016/j.tins.2020.10.008.

(67) Wu, J.; Chen, Z. J. Innate immune sensing and signaling of cytosolic nucleic acids. *Annu Rev Immunol* **2014**, *32*, 461-488. DOI: 10.1146/annurev-immunol-032713-120156 From NLM.

(68) Cheng, Z.; Dai, T.; He, X.; Zhang, Z.; Xie, F.; Wang, S.; Zhang, L.; Zhou, F. The interactions between cGAS-STING pathway and pathogens. *Sign Transduct Target Ther* **2020**, *5* (1), 91. DOI: 10.1038/s41392-020-0198-7.

(69) Wang, C.; Sharma, N.; Veleeparambil, M.; Kessler, P. M.; Willard, B.; Sen, G. C. STING-Mediated Interferon Induction by Herpes Simplex Virus 1 Requires the Protein Tyrosine Kinase Syk. *mBio* **2021**, *12* (6), e0322821. DOI: 10.1128/mbio.03228-21 From NLM.

(70) Li, X. D.; Wu, J.; Gao, D.; Wang, H.; Sun, L.; Chen, Z. J. Pivotal roles of cGAS-cGAMP signaling in antiviral defense and immune adjuvant effects. *Science* **2013**, *341* (6152), 1390-1394. DOI: 10.1126/science.1244040 From NLM.

(71) Jin, L.; Getahun, A.; Knowles, H. M.; Mogan, J.; Akerlund, L. J.; Packard, T. A.; Perraud, A. L.; Cambier, J. C. STING/MPYS mediates host defense against Listeria monocytogenes infection by regulating Ly6C(hi) monocyte migration. *J Immunol* **2013**, *190* (6), 2835-2843. DOI: 10.4049/jimmunol.1201788 From NLM.

(72) Gao, D.; Wu, J.; Wu, Y.-T.; Du, F.; Aroh, C.; Yan, N.; Sun, L.; Chen, Z. J. Cyclic GMP-AMP Synthase Is an Innate Immune Sensor of HIV and Other Retroviruses. *Science* **2013**, *341* (6148), 903-906. DOI: doi:10.1126/science.1240933.

(73) Yan, N.; Regalado-Magdos, A. D.; Stiggelbout, B.; Lee-Kirsch, M. A.; Lieberman, J. The cytosolic exonuclease TREX1 inhibits the innate immune response to human immunodeficiency virus type 1. *Nat Immunol* **2010**, *11* (11), 1005-1013. DOI: 10.1038/ni.1941 From NLM.

(74) Domizio, J. D.; Gulen, M. F.; Saidoune, F.; Thacker, V. V.; Yatim, A.; Sharma, K.; Nass, T.; Guenova, E.; Schaller, M.; Conrad, C.; et al. The cGAS–STING pathway drives type I IFN immunopathology in COVID-19. *Nature* **2022**, *603* (7899), 145-151. DOI: 10.1038/s41586-022-04421-w.

(75) Neufeldt, C. J.; Cerikan, B.; Cortese, M.; Frankish, J.; Lee, J.-Y.; Plociennikowska, A.; Heigwer, F.; Prasad, V.; Joecks, S.; Burkart, S. S.; et al. SARS-CoV-2 infection induces a pro-inflammatory cytokine response through cGAS-STING and NF-κB. *Communications Biology* **2022**, *5* (1), 45. DOI: 10.1038/s42003-021-02983-5.

(76) Eaglesham, J. B.; Pan, Y.; Kupper, T. S.; Kranzusch, P. J. Viral and metazoan poxins are cGAMP-specific nucleases that restrict cGAS-STING signalling. *Nature* **2019**, *566* (7743), 259-263. DOI: 10.1038/s41586-019-0928-6.

(77) Dodantenna, N.; Ranathunga, L.; Chathuranga, W. A. G.; Weerawardhana, A.; Cha, J. W.; Subasinghe, A.; Gamage, N.; Haluwana, D. K.; Kim, Y.; Jheong, W.; et al. African Swine Fever Virus EP364R and C129R Target Cyclic GMP-AMP To Inhibit the cGAS-STING Signaling Pathway. *J Virol* **2022**, *96* (15), e0102222. DOI: 10.1128/jvi.01022-22 From NLM.

(78) Dubensky, T. W., Jr.; Kanne, D. B.; Leong, M. L. Rationale, progress and development of vaccines utilizing STING-activating cyclic dinucleotide adjuvants. *Ther Adv Vaccines* **2013**, *1* (4), 131-143. DOI: 10.1177/2051013613501988 From NLM.

(79) Chen, Daniel S.; Mellman, I. Oncology Meets Immunology: The Cancer-Immunity Cycle. *Immunity* **2013**, *39* (1), 1-10. DOI: 10.1016/j.immuni.2013.07.012.

(80) Gresser, I.; Bandu, M.-T.; Brouty-Boyé, D. Interferon and Cell Division. IX. Interferon-Resistant L1210 Cells: Characteristics and Origin. *JNCI: Journal of the National Cancer Institute* **1974**, *52* (2), 553-559. DOI: 10.1093/jnci/52.2.553.

(81) Gresser, I.; Bourali, C. Antitumor effects of interferon preparations in mice. *J Natl Cancer Inst* **1970**, *45* (2), 365-376. From NLM.

(82) Woo, S.-R.; Fuertes, Mercedes B.; Corrales, L.; Spranger, S.; Furdyna, Michael J.; Leung, Michael Y. K.; Duggan, R.; Wang, Y.; Barber, Glen N.; Fitzgerald, Katherine A.; et al. STING-Dependent Cytosolic DNA Sensing Mediates Innate Immune Recognition of Immunogenic Tumors. *Immunity* **2014**, *41* (5), 830-842. DOI: 10.1016/j.immuni.2014.10.017.

(83) Demaria, O.; De Gassart, A.; Coso, S.; Gestermann, N.; Di Domizio, J.; Flatz, L.; Gaide, O.; Michielin, O.; Hwu, P.; Petrova, T. V.; et al. STING activation of tumor endothelial cells initiates spontaneous and therapeutic antitumor immunity. *PNAS* **2015**, *112* (50), 15408-15413. DOI: doi:10.1073/pnas.1512832112.

(84) Li, T.; Cheng, H.; Yuan, H.; Xu, Q.; Shu, C.; Zhang, Y.; Xu, P.; Tan, J.; Rui, Y.; Li, P.; et al. Antitumor Activity of cGAMP via Stimulation of cGAS-cGAMP-STING-IRF3 Mediated Innate Immune Response. *Scientific Reports* **2016**, *6* (1), 19049. DOI: 10.1038/srep19049.

(85) Jing, W.; McAllister, D.; Vonderhaar, E. P.; Palen, K.; Riese, M. J.; Gershan, J.; Johnson, B. D.; Dwinell, M. B. STING agonist inflames the pancreatic cancer immune microenvironment and reduces tumor burden in mouse models. *Journal for ImmunoTherapy of Cancer* **2019**, *7* (1), 115. DOI: 10.1186/s40425-019-0573-5.

(86) Zhang, Y.; Zhang, Z. The history and advances in cancer immunotherapy: understanding the characteristics of tumor-infiltrating immune cells and their therapeutic implications. *Cellular & Molecular Immunology* **2020**, *17* (8), 807-821. DOI: 10.1038/s41423-020-0488-6.

(87) Dagher, O. K.; Schwab, R. D.; Brookens, S. K.; Posey, A. D., Jr. Advances in cancer immunotherapies. *Cell* **2023**, *186* (8), 1814-1814.e1811. DOI: 10.1016/j.cell.2023.02.039 From NLM.

(88) Tan, M.; Quintal, L. Pembrolizumab: a novel antiprogrammed death 1 (PD-1) monoclonal antibody for treatment of metastatic melanoma. *J Clin Pharm Ther* **2015**, *40* (5), 504-507. DOI: 10.1111/jcpt.12304 From NLM.

(89) Ferris, R. L.; Blumenschein, G., Jr.; Fayette, J.; Guigay, J.; Colevas, A. D.; Licitra, L.; Harrington, K.; Kasper, S.; Vokes, E. E.; Even, C.; et al. Nivolumab for Recurrent Squamous-Cell Carcinoma of the Head and Neck. *N Engl J Med* **2016**, *375* (19), 1856-1867. DOI: 10.1056/NEJMoa1602252 From NLM.

(90) Larkin, J.; Chiarion-Sileni, V.; Gonzalez, R.; Grob, J. J.; Cowey, C. L.; Lao, C. D.; Schadendorf, D.; Dummer, R.; Smylie, M.; Rutkowski, P.; et al. Combined Nivolumab and Ipilimumab or

Monotherapy in Untreated Melanoma. *N Engl J Med* **2015**, *373* (1), 23-34. DOI: 10.1056/NEJMoa1504030 From NLM.

(91) Tomasini, P.; Khobta, N.; Greillier, L.; Barlesi, F. Ipilimumab: its potential in non-small cell lung cancer. *Ther Adv Med Oncol* **2012**, *4* (2), 43-50. DOI: 10.1177/1758834011431718 From NLM.

(92) Govindan, R.; Szczesna, A.; Ahn, M. J.; Schneider, C. P.; Gonzalez Mella, P. F.; Barlesi, F.; Han, B.; Ganea, D. E.; Von Pawel, J.; Vladimirov, V.; et al. Phase III Trial of Ipilimumab Combined With Paclitaxel and Carboplatin in Advanced Squamous Non-Small-Cell Lung Cancer. *J Clin Oncol* **2017**, *35* (30), 3449-3457. DOI: 10.1200/jco.2016.71.7629 From NLM.

(93) Weinmann, H. Cancer Immunotherapy: Selected Targets and Small-Molecule Modulators. *ChemMedChem* **2016**, *11* (5), 450-466. DOI: 10.1002/cmdc.201500566 From NLM.

(94) Cheng, B.; Yuan, W. E.; Su, J.; Liu, Y.; Chen, J. Recent advances in small molecule based cancer immunotherapy. *Eur J Med Chem* **2018**, *157*, 582-598. DOI: 10.1016/j.ejmech.2018.08.028 From NLM.

(95) Feng, M.; Zhao, Z.; Yang, M.; Ji, J.; Zhu, D. T-cell-based immunotherapy in colorectal cancer. *Cancer Lett* **2021**, *498*, 201-209. DOI: 10.1016/j.canlet.2020.10.040 From NLM.

(96) Córdova-Bahena, L.; Velasco-Velázquez, M. A. Anti-PD-1 And Anti-PD-L1 Antibodies as Immunotherapy Against Cancer: A Structural Perspective. *Rev Invest Clin* **2020**, *73* (1), 008-016. DOI: 10.24875/ric.20000341 From NLM.

(97) Zhang, J.; Huang, D.; Saw, P. E.; Song, E. Turning cold tumors hot: from molecular mechanisms to clinical applications. *Trends Immunol* **2022**, *43* (7), 523-545. DOI: 10.1016/j.it.2022.04.010 From NLM.

(98) Corrales, L.; McWhirter, S. M.; Dubensky, T. W., Jr.; Gajewski, T. F. The host STING pathway at the interface of cancer and immunity. *J Clin Invest* **2016**, *126* (7), 2404-2411. DOI: 10.1172/jci86892 From NLM.

(99) Vavrina, Z.; Perlikova, P.; Milisavljevic, N.; Chevrier, F.; Smola, M.; Smith, J.; Dejmek, M.; Havlicek, V.; Budesinsky, M.; Liboska, R.; et al. Design, Synthesis, and Biochemical and Biological Evaluation of Novel 7-Deazapurine Cyclic Dinucleotide Analogues as STING Receptor Agonists. *J Med Chem* **2022**, *65* (20), 14082-14103. DOI: 10.1021/acs.jmedchem.2c01305 From NLM Medline.

(100) Veth, S.; Fuchs, A.; Ozdemir, D.; Dialer, C.; Drexler, D. J.; Knechtel, F.; Witte, G.; Hopfner, K. P.; Carell, T.; Ploetz, E. Chemical synthesis of the fluorescent, cyclic dinucleotides cthGAMP. *Chembiochem* **2022**. DOI: 10.1002/cbic.202200005.

(101) Fink, B. E. Z., Y.; Chen, L.; Huang, A. Cyclic Dinucleotides as Anticancer Agents, WO2019079261A1. 2019.

(102) Vyskocil, S. C., J.; Cullis, C.; England, D. B.; Gould, A.; E.; Greenspan, P. H., Y.; Langston, S.; Li, G.; Mizutani, H.;; Okaniwa, M. STING Modulator Compounds and Methods of Making and Using, WO2019092660A1. 2019.

(103) Dejmek, M.; Sala, M.; Brazdova, A.; Vanekova, L.; Smola, M.; Klima, M.; Brehova, P.; Budesinsky, M.; Dracinsky, M.; Prochazkova, E.; et al. Discovery of isonucleotidic CDNs as potent STING agonists with immunomodulatory potential. *Structure* **2022**. DOI: 10.1016/j.str.2022.05.012.

(104) Dubensky, T. W., Jr.; Kanne, D. B.; Leong, M. L.; Glickman,; L. H.; Vance, R. E. L., E. E. Compositions and Methods for Activating "Stimulator of Interferon Gene"Dependent Signalling, WO2014189805A1. 2017.

(105) Glick, G. G., S.; Roush, W. R.; Olhava, E. J.; Jones, R. Cyclic Dinucleotide Analogs for Treating Conditions Associated with STING (Stimulator of Interferon Genes) Activity. WO2018045204A1. 2018.

(106) Zhong, B. S., L.; Wei, Q.; Dai, Y.; Chen, C.; Chen, Z. Cyclic Di-Nucleotide Compounds and Methods of Use. WO2017161349A1. 2017.

(107) Novotna, B.; Vanekova, L.; Zavrel, M.; Budesinsky, M.; Dejmek, M.; Smola, M.; Gutten, O.; Tehrani, Z. A.; Pimkova Polidarova, M.; Brazdova, A.; et al. Enzymatic Preparation of 2′-5′,3′-5′-Cyclic Dinucleotides, Their Binding Properties to Stimulator of Interferon Genes Adaptor Protein, and Structure/Activity Correlations. *J Med Chem* **2019**, *62* (23), 10676-10690. DOI: 10.1021/acs.jmedchem.9b01062 From NLM Medline.

(108) Rosenthal, K.; Becker, M.; Rolf, J.; Siedentop, R.; Hillen, M.; Nett, M.; Lütz, S. Catalytic Promiscuity of cGAS: A Facile Enzymatic Synthesis of 2′-3′-Linked Cyclic Dinucleotides. *ChemBioChem* **2020**, *21* (22), 3225-3228. DOI: https://doi.org/10.1002/cbic.202000433.

(109) Corrales, L.; Glickman, L. H.; McWhirter, S. M.; Kanne, D. B.; Sivick, K. E.; Katibah, G. E.; Woo, S. R.; Lemmens, E.; Banda, T.; Leong, J. J.; et al. Direct Activation of STING in the Tumor Microenvironment Leads to Potent and Systemic Tumor Regression and Immunity. *Cell Rep* **2015**, *11* (7), 1018-1030. DOI: 10.1016/j.celrep.2015.04.031.

(110) Khvorova, A.; Watts, J. K. The chemical evolution of oligonucleotide therapies of clinical utility. *Nat Biotechnol* **2017**, *35* (3), 238-248. DOI: 10.1038/nbt.3765 From NLM.

(111) Eckstein, F. Phosphorothioates, essential components of therapeutic oligonucleotides. *Nucleic Acid Ther* **2014**, *24* (6), 374-387. DOI: 10.1089/nat.2014.0506 From NLM.

(112) Meric-Bernstam, F.; Sweis, R. F.; Kasper, S.; Hamid, O.; Bhatia, S.; Dummer, R.; Stradella, A.; Long, G. V.; Spreafico, A.; Shimizu, T.; et al. Combination of the STING Agonist MIW815 (ADU-S100) and PD-1 Inhibitor Spartalizumab in Advanced/Metastatic Solid Tumors or Lymphomas: An Open-Label, Multicenter, Phase Ib Study. *Clin Cancer Res* **2023**, *29* (1), 110-121. DOI: 10.1158/1078-0432.Ccr-22-2235 From NLM.

(113) Piha-Paul, S. A.; Geva, R.; Tan, T. J.; Lim, D. W.; Hierro, C.; Doi, T.; Rahma, O.; Lesokhin, A.; Luke, J. J.; Otero, J.; et al. First-in-human phase I/Ib open-label dose-escalation study of GWN323 (anti-GITR) as a single agent and in combination with spartalizumab (anti-PD-1) in patients with advanced solid tumors and lymphomas. *J Immunother Cancer* **2021**, *9* (8). DOI: 10.1136/jitc-2021-002863 From NLM.

(114) Chang, W.; Altman, M. D.; Lesburg, C. A.; Perera, S. A.; Piesvaux, J. A.; Schroeder, G. K.; Wyss, D. F.; Cemerski, S.; Chen, Y.; Dinunzio, E.; et al. Discovery of MK-1454: A Potent Cyclic Dinucleotide Stimulator of Interferon Genes Agonist for the Treatment of Cancer. *J Med Chem* **2022**. DOI: 10.1021/acs.jmedchem.1c02197.

(115) McIntosh, J. A.; Liu, Z.; Andresen, B. M.; Marzijarani, N. S.; Moore, J. C.; Marshall, N. M.; Borra-Garske, M.; Obligacion, J. V.; Fier, P. S.; Peng, F.; et al. A kinase-cGAS cascade to synthesize a therapeutic STING activator. *Nature* **2022**, *603* (7901), 439-444. DOI: 10.1038/s41586-022-04422-9.

(116) Kuttruff, C. A.; Fleck, M.; Carotta, S.; Arnhof, H.; Bretschneider, T.; Dahmann, G.; Gremel, G.; Grube, A.; Handschuh, S.; Heimann, A.; et al. Discovery of BI 7446: A Potent Cyclic Dinucleotide STING Agonist with Broad-Spectrum Variant Activity for the Treatment of Cancer. *J Med Chem* **2023**, *66* (14), 9376-9400. DOI: 10.1021/acs.jmedchem.3c00510 From NLM Medline.

(117) Kim, D. S.; Endo, A.; Fang, F. G.; Huang, K. C.; Bao, X.; Choi, H. W.; Majumder, U.; Shen, Y. Y.; Mathieu, S.; Zhu, X.; et al. E7766, a Macrocycle-Bridged Stimulator of Interferon Genes (STING) Agonist with Potent Pan-Genotypic Activity. *ChemMedChem* **2021**, *16* (11), 1740-1743. DOI: 10.1002/cmdc.202100068.

(118) Wu, Y.-t.; Fang, Y.; Wei, Q.; Shi, H.; Tan, H.; Deng, Y.; Zeng, Z.; Qiu, J.; Chen, C.; Sun, L.; et al. Tumor-targeted delivery of a STING agonist improves cancer immunotherapy. *PNAS* **2022**, *119* (49), e2214278119. DOI: doi:10.1073/pnas.2214278119.

(119) Dando, T.; Plosker, G. Adefovir dipivoxil: a review of its use in chronic hepatitis B. *Drugs* **2003**, *63* (20), 2215-2234. DOI: 10.2165/00003495-200363200-00007 From NLM.

(120) Sofia, M. J.; Bao, D.; Chang, W.; Du, J.; Nagarathnam, D.; Rachakonda, S.; Reddy, P. G.; Ross, B. S.; Wang, P.; Zhang, H.-R.; et al. Discovery of a β-d-2′-Deoxy-2′-α-fluoro-2′-β-C-methyluridine Nucleotide Prodrug (PSI-7977) for the Treatment of Hepatitis C Virus. *Journal of Medicinal Chemistry* **2010**, *53* (19), 7202-7218. DOI: 10.1021/jm100863x.

(121) Vargas, D. F.; Larghi, E. L.; Kaufman, T. S. Evolution of the Synthesis of Remdesivir. Classical Approaches and Most Recent Advances. *ACS Omega* **2021**, *6* (30), 19356-19363. DOI: 10.1021/acsomega.1c03082.

(122) Pimkova Polidarova, M.; Brehova, P.; Kaiser, M. M.; Smola, M.; Dracinsky, M.; Smith, J.; Marek, A.; Dejmek, M.; Sala, M.; Gutten, O.; et al. Synthesis and Biological Evaluation of Phosphoester and Phosphorothioate Prodrugs of STING Agonist 3′,3′-c-Di(2′F,2′dAMP). *J Med Chem* **2021**, *64* (11), 7596-7616. DOI: 10.1021/acs.jmedchem.1c00301.

(123) Xie, Z.; Lu, L.; Wang, Z.; Luo, Q.; Yang, Y.; Fang, T.; Chen, Z.; Ma, D.; Quan, J.; Xi, Z. S-acylthioalkyl ester (SATE)-based prodrugs of deoxyribose cyclic dinucleotides (dCDNs) as the STING agonist for antitumor immunotherapy. *Eur J Med Chem* **2022**, *243*, 114796. DOI: 10.1016/j.ejmech.2022.114796 From NLM Publisher.

(124) Gao, P.; Zillinger, T.; Wang, W.; Ascano, M.; Dai, P.; Hartmann, G.; Tuschl, T.; Deng, L.; Barchet, W.; Patel, Dinshaw J. Binding-Pocket and Lid-Region Substitutions Render Human STING Sensitive to the Species-Specific Drug DMXAA. *Cell Reports* **2014**, *8* (6), 1668-1676. DOI: 10.1016/j.celrep.2014.08.010 (acccessed 2023/10/23).

(125) Allen, B. K.; Kulkarni, M. M.; Chamberlain, B.; Dwight, T.; Koh, C.; Samant, R.; Jernigan, F.; Rice, J.; Tan, D.; Li, S.; et al. Design of a systemic small molecule clinical STING agonist using physics-based simulations and artificial intelligence. *bioRxiv 2022.05.23.493001* **2022**. DOI: 10.1101/2022.05.23.493001.

(126) Ramanjulu, J. M.; Pesiridis, G. S.; Yang, J.; Concha, N.; Singhaus, R.; Zhang, S. Y.; Tran, J. L.; Moore, P.; Lehmann, S.; Eberl, H. C.; et al. Design of amidobenzimidazole STING receptor agonists with systemic activity. *Nature* **2018**, *564* (7736), 439-443. DOI: 10.1038/s41586-018-0705-y.

(127) Ding, C.; Song, Z.; Shen, A.; Chen, T.; Zhang, A. Small molecules targeting the innate immune cGASSTINGTBK1 signaling pathway. *Acta Pharm Sin B* **2020**, *10* (12), 2272-2298. DOI: 10.1016/j.apsb.2020.03.001.

(128) Zhang, S.; Zheng, R.; Pan, Y.; Sun, H. Potential Therapeutic Value of the STING Inhibitors. *Molecules* **2023**, *28* (7). DOI: 10.3390/molecules28073127 From NLM.

(129) Li, S.; Hong, Z.; Wang, Z.; Li, F.; Mei, J.; Huang, L.; Lou, X.; Zhao, S.; Song, L.; Chen, W.; et al. The Cyclopeptide Astin C Specifically Inhibits the Innate Immune CDN Sensor STING. *Cell Reports* **2018**, *25* (12), 3405-3421.e3407. DOI: 10.1016/j.celrep.2018.11.097 (acccessed 2023/10/21).

(130) Siu, T.; Altman, M. D.; Baltus, G. A.; Childers, M.; Ellis, J. M.; Gunaydin, H.; Hatch, H.; Ho, T.; Jewell, J.; Lacey, B. M.; et al. Discovery of a Novel cGAMP Competitive Ligand of the Inactive Form of STING. *ACS Med Chem Lett* **2019**, *10* (1), 92-97. DOI: 10.1021/acsmedchemlett.8b00466.

(131) Hong, Z.; Mei, J.; Li, C.; Bai, G.; Maimaiti, M.; Hu, H.; Yu, W.; Sun, L.; Zhang, L.; Cheng, D.; et al. STING inhibitors target the cyclic dinucleotide binding pocket. *Proc Natl Acad Sci U S A* **2021**, *118* (24). DOI: 10.1073/pnas.2105465118 From NLM Medline.

(132) Aicart-Ramos, C.; Valero, R. A.; Rodriguez-Crespo, I. Protein palmitoylation and subcellular trafficking. *Biochim Biophys Acta* **2011**, *1808* (12), 2981-2994. DOI: 10.1016/j.bbamem.2011.07.009 From NLM.

(133) Kong, E.; Peng, S.; Chandra, G.; Sarkar, C.; Zhang, Z.; Bagh, M. B.; Mukherjee, A. B. Dynamic palmitoylation links cytosol-membrane shuttling of acyl-protein thioesterase-1 and acyl-protein thioesterase-2 with that of proto-oncogene H-ras product and growth-associated protein-43. *J Biol Chem* **2013**, *288* (13), 9112-9125. DOI: 10.1074/jbc.M112.421073 From NLM.

(134) Linder, M. E.; Deschenes, R. J. Palmitoylation: policing protein stability and traffic. *Nat Rev Mol Cell Biol* **2007**, *8* (1), 74-84. DOI: 10.1038/nrm2084 From NLM.

(135) Haag, S. M.; Gulen, M. F.; Reymond, L.; Gibelin, A.; Abrami, L.; Decout, A.; Heymann, M.; Van Der Goot, F. G.; Turcatti, G.; Behrendt, R.; et al. Targeting STING with covalent small-molecule inhibitors. *Nature* **2018**, *559* (7713), 269-273. DOI: 10.1038/s41586-018-0287-8.

(136) Hansen, A. L.; Buchan, G. J.; Ruhl, M.; Mukai, K.; Salvatore, S. R.; Ogawa, E.; Andersen, S. D.; Iversen, M. B.; Thielke, A. L.; Gunderstofte, C.; et al. Nitro-fatty acids are formed in response to virus infection and are potent inhibitors of STING palmitoylation and signaling. *Proc Natl Acad Sci U S A* **2018**, *115* (33), E7768-E7775. DOI: 10.1073/pnas.1806239115 From NLM Medline.

(137) Dialer, C. R.; Stazzoni, S.; Drexler, D. J.; Muller, F. M.; Veth, S.; Pichler, A.; Okamura, H.; Witte, G.; Hopfner, K. P.; Carell, T. A Click-Chemistry Linked 2'3'-cGAMP Analogue. *Chemistry* **2019**, *25* (8), 2089-2095. DOI: 10.1002/chem.201805409 From NLM PubMed-not-MEDLINE.

(138) Stazzoni, S.; Böhmer, D. F. R.; Hernichel, F.; Özdemir, D.; Pappa, A.; Drexler, D.; Bauernfried, S.; Witte, G.; Wagner, M.; Veth, S.; et al. Novel Poxin Stable cGAMP-Derivatives Are Remarkable STING Agonists. *Angewandte Chemie International Edition* **2022**, *61* (40). DOI: 10.1002/anie.202207175.

(139) M. Jason Hatfield, R. A. U., Janice L. Hyatt, Carol C. Edwards, Monika; Wierdl, L. T., Michael R. Taylor, Philip M. Potter. Carboxylesterases: General detoxifying enzymes. *Chemico-Biological Interactions* **2016**, *259*, 327-331.

(140) Gaffney, B. L.; Veliath, E.; Zhao, J.; Jones, R. A. One-Flask Syntheses of c-di-GMP and the [Rp,Rp] and [Rp,Sp] Thiophosphate Analogues. *Org Lett* **2010**, *12* (14), 3269-3271. DOI: 10.1021/ol101236b.

(141) Lioux, T.; Mauny, M. A.; Lamoureux, A.; Bascoul, N.; Hays, M.; Vernejoul, F.; Baudru, A. S.; Boularan, C.; Lopes-Vicente, J.; Qushair, G.; et al. Design, Synthesis, and Biological Evaluation of Novel Cyclic Adenosine-Inosine Monophosphate (cAIMP) Analogs That Activate Stimulator of Interferon Genes (STING). *J Med Chem* **2016**, *59* (22), 10253-10267. DOI: 10.1021/acs.jmedchem.6b01300.

(142) Won, S. J.; Cheung See Kit, M.; Martin, B. R. Protein depalmitoylases. *Crit Rev Biochem Mol Biol* **2018**, *53* (1), 83-98. DOI: 10.1080/10409238.2017.1409191 From NLM Medline.

(143) Hirano, T.; Kishi, M.; Sugimoto, H.; Taguchi, R.; Obinata, H.; Ohshima, N.; Tatei, K.; Izumi, T. Thioesterase activity and subcellular localization of acylprotein thioesterase 1/lysophospholipase 1. *Biochim Biophys Acta* **2009**, *1791* (8), 797-805. DOI: 10.1016/j.bbalip.2009.05.001 From NLM Medline.

(144) Burger, M.; Zimmermann, T. J.; Kondoh, Y.; Stege, P.; Watanabe, N.; Osada, H.; Waldmann, H.; Vetter, I. R. Crystal structure of the predicted phospholipase LYPLAL1 reveals unexpected functional plasticity despite close relationship to acyl protein thioesterases. *J Lipid Res* **2012**, *53* (1), 43-50. DOI: 10.1194/jlr.M019851 From NLM Medline.

(145) Tian, L.; McClafferty, H.; Knaus, H. G.; Ruth, P.; Shipston, M. J. Distinct acyl protein transferases and thioesterases control surface expression of calcium-activated potassium channels. *J Biol Chem* **2012**, *287* (18), 14718-14725. DOI: 10.1074/jbc.M111.335547 From NLM Medline.

(146) Kok, B. P.; Ghimire, S.; Kim, W.; Chatterjee, S.; Johns, T.; Kitamura, S.; Eberhardt, J.; Ogasawara, D.; Xu, J.; Sukiasyan, A.; et al. Discovery of small-molecule enzyme activators by activity-based protein profiling. *Nat Chem Biol* **2020**, *16* (9), 997-1005. DOI: 10.1038/s41589-020-0555-4.

Literature

(147) Cravatt, B. F.; Wright, A. T.; Kozarich, J. W. Activity-based protein profiling: from enzyme chemistry to proteomic chemistry. *Annu Rev Biochem* **2008**, *77*, 383-414. DOI: 10.1146/annurev.biochem.75.101304.124125 From NLM.

(148) Uetrecht, J. Idiosyncratic drug reactions: past, present, and future. *Chem Res Toxicol* **2008**, *21* (1), 84-92. DOI: 10.1021/tx700186p From NLM.

(149) Cheng, A. C.; Coleman, R. G.; Smyth, K. T.; Cao, Q.; Soulard, P.; Caffrey, D. R.; Salzberg, A. C.; Huang, E. S. Structure-based maximal affinity model predicts small-molecule druggability. *Nature Biotechnology* **2007**, *25* (1), 71-75. DOI: 10.1038/nbt1273.

(150) Lin, H. Protein cysteine palmitoylation in immunity and inflammation. *FEBS J* **2021**, *288* (24), 7043-7059. DOI: 10.1111/febs.15728.

(151) Troup, R. I.; Fallan, C.; Baud, M. G. J. Current strategies for the design of PROTAC linkers: a critical review. *Exploration of Targeted Anti-tumor Therapy* **2020**, *1* (5), 273-312. DOI: 10.37349/etat.2020.00018.

(152) Rostovtsev, V. V.; Green, L. G.; Fokin, V. V.; Sharpless, K. B. A Stepwise Huisgen Cycloaddition Process: Copper(I)-Catalyzed Regioselective "Ligation" of Azides and Terminal Alkynes. *Angewandte Chemie International Edition* **2002**, *41* (14), 2596-2599. DOI: https://doi.org/10.1002/1521-3773(20020715)41:14<2596::AID-ANIE2596>3.0.CO;2-4.

(153) Krishna, H.; Caruthers, M. H. Alkynyl Phosphonate DNA: A Versatile "Click"able Backbone for DNA-Based Biological Applications. *JACS* **2012**, *134* (28), 11618-11631. DOI: 10.1021/ja3026714.

(154) Liu, J.; Yuan, L.; Ruan, Y.; Deng, B.; Yang, Z.; Ren, Y.; Li, L.; Liu, T.; Zhao, H.; Mai, R.; et al. Novel CRBN-Recruiting Proteolysis-Targeting Chimeras as Degraders of Stimulator of Interferon Genes with In Vivo Anti-Inflammatory Efficacy. *J Med Chem* **2022**, *65* (9), 6593-6611. DOI: 10.1021/acs.jmedchem.1c01948 From NLM Medline.

(155) Liu, K.; Lan, Y.; Li, X.; Li, M.; Cui, L.; Luo, H.; Luo, L. Development of small molecule inhibitors/agonists targeting STING for disease. *Biomed Pharmacother* **2020**, *132*, 110945. DOI: 10.1016/j.biopha.2020.110945 From NLM Medline.

(156) Hou, Z.; Matherly, L. H. Biology of the major facilitative folate transporters SLC19A1 and SLC46A1. *Curr Top Membr* **2014**, *73*, 175-204. DOI: 10.1016/b978-0-12-800223-0.00004-9 From NLM.

(157) Zhao, R.; Diop-Bove, N.; Visentin, M.; Goldman, I. D. Mechanisms of membrane transport of folates into cells and across epithelia. *Annu Rev Nutr* **2011**, *31*, 177-201. DOI: 10.1146/annurev-nutr-072610-145133 From NLM.

(158) Zhao, R.; Matherly, L. H.; Goldman, I. D. Membrane transporters and folate homeostasis: intestinal absorption and transport into systemic compartments and tissues. *Expert Rev Mol Med* **2009**, *11*, e4. DOI: 10.1017/s1462399409000969 From NLM.

(159) Willibald, J.; Harder, J.; Sparrer, K.; Conzelmann, K. K.; Carell, T. Click-modified anandamide siRNA enables delivery and gene silencing in neuronal and immune cells. *J Am Chem Soc* **2012**, *134* (30), 12330-12333. DOI: 10.1021/ja303251f From NLM Medline.

(160) Zhu, Z.; Johnson, R. L.; Zhang, Z.; Herring, L. E.; Jiang, G.; Damania, B.; James, L. I.; Liu, P. Development of VHL-recruiting STING PROTACs that suppress innate immunity. *Cellular and Molecular Life Sciences* **2023**, *80* (6), 149. DOI: 10.1007/s00018-023-04796-7.

(161) Su, W.; Tan, M.; Wang, Z.; Zhang, J.; Huang, W.; Song, H.; Wang, X.; Ran, H.; Gao, Y.; Nie, G.; et al. Targeted Degradation of PD-L1 and Activation of the STING Pathway by Carbon-Dot-Based PROTACs for Cancer Immunotherapy. *Angew Chem Int Ed Engl* **2023**, *62* (11), e202218128. DOI: 10.1002/anie.202218128 From NLM Medline.

Literature

(162) Ahn, G.; Banik, S. M.; Miller, C. L.; Riley, N. M.; Cochran, J. R.; Bertozzi, C. R. LYTACs that engage the asialoglycoprotein receptor for targeted protein degradation. *Nat Chem Biol* **2021**, *17* (9), 937-946. DOI: 10.1038/s41589-021-00770-1.

(163) Takahashi, D.; Ora, T.; Sasaki, S.; Ishii, N.; Tanaka, T.; Matsuda, T.; Ikeda, M.; Moriyama, J.; Cho, N.; Nara, H.; et al. Second-Generation AUTACs for Targeted Autophagic Degradation. *J Med Chem* **2023**, *66* (17), 12342-12372. DOI: 10.1021/acs.jmedchem.3c00861.

(164) Fan, Y.; Gao, Y.; Nie, L.; Hou, T.; Dan, W.; Wang, Z.; Liu, T.; Wei, Y.; Wang, Y.; Liu, B.; et al. Targeting LYPLAL1-mediated cGAS depalmitoylation enhances the response to anti-tumor immunotherapy. *Mol Cell* **2023**, *83* (19), 3520-3532.e3527. DOI: 10.1016/j.molcel.2023.09.007 From NLM.

(165) Su, C.; Cheng, T.; Huang, J.; Zhang, T.; Yin, H. 4-Octyl itaconate restricts STING activation by blocking its palmitoylation. *Cell Reports* **2023**, *42* (9), 113040. DOI: https://doi.org/10.1016/j.celrep.2023.113040.

(166) Zhu, X.-F.; Williams, H. J.; Ian Scott, A. An Improved Transient Method for the Synthesis of N-Benzoylated Nucleosides. *Synthetic Communications* **2003**, *33* (7), 1233-1243. DOI: 10.1081/SCC-120017200.

(167) Meynier, V.; Iannazzo, L.; Catala, M.; Oerum, S.; Braud, E.; Atdjian, C.; Barraud, P.; Fonvielle, M.; Tisné, C.; Ethève-Quelquejeu, M. Synthesis of RNA-cofactor conjugates and structural exploration of RNA recognition by an m6A RNA methyltransferase. *Nucleic Acids Res* **2022**, *50* (10), 5793-5806. DOI: 10.1093/nar/gkac354 From NLM.

(168) Leung, M. K. M.; Such, G. K.; Johnston, A. P. R.; Biswas, D. P.; Zhu, Z.; Yan, Y.; Lutz, J.-F.; Caruso, F. Assembly and Degradation of Low-Fouling Click-Functionalized Poly(ethylene glycol)-Based Multilayer Films and Capsules. *Small* **2011**, *7* (8), 1075-1085. DOI: https://doi.org/10.1002/smll.201002258.